Synthesis of manganese tricarbonyl PhotoCORM conjugates – from small molecules to peptides and dendrimers

Dissertation zur Erlangung des naturwissenschaftlichen Doktorgrades
der
Julius-Maximilians-Universität Würzburg

vorgelegt von

Sandesh Pai

aus Sirsi, Indien

Würzburg 2014

Eingereicht bei der Fakultät für Chemie und Pharmazie am

Gutachter der schriftlichen Arbeit

1. Gutachter: Prof. Dr. U. Schatzschneider

2. Gutachter: Prof. Dr. Todd B. Marder

Prüfer des öffentlichen Promotionskolloquiums

1. Prüfer: Prof. Dr. U. Schatzschneider

2. Prüfer: Prof. Dr. Todd B. Marder

3. Prüfer:

Datum des öffentlichen Promotionskolloquiums

Doktorurkunde ausgehändigt am

"No, our science is no illusion. But an illusion it would be to suppose that what science cannot give us we can get elsewhere"

Sigmund Freud

Acknowledgements

The quest for knowledge has taken me into a journey filled with interesting challenges and given me an opportunity to work with the intellectuals who made this experience commendable. At this juncture I feel duty bound to thank everyone for playing an important role in making my efforts a success.

I would like to express my deepest gratitude to my supervisor Prof. Dr. Ulrich Schatzschneider for his guidance and encouragement. I am deeply indebted to him for introducing and providing me the opportunity to work in this interesting research theme. I am also grateful to him for his understanding, patience and moral support during my doctoral research.

I specially would like to thank Prof. Dr. Todd B. Marder and Prof. Dr. Dr. Lorenz Meinel for their willingness to review my doctoral thesis during their busy schedule.

Furthermore, I would like to thank Prof. Dr. Benito Yard for performing the biological testing of the compounds at UMM Universitätsmedizin Mannheim.

I also take this opportunity to thank everyone who has contributed and been part of this success: Dr. Krzysztof Radacki and Christoph Nagel for measuring and solving the crystal structures; all the scientific and non-scientific employees of the Institut für Anorganische Chemie of the Julius-Maximilians-Universität Würzburg. The alumni of the Schatzschneider group - Johanna, Hendrik, and Wanning.

I enjoyed working here and thus would like to extend my sense of gratitude to Thomas, Christoph, and Luisa. Apart from being a good friend, I wish to express my warm thanks to Pete for sharing his knowledge of chemistry, teaching new techinques. I thank my friends Shubhankar, Geetha, Sakya, Arun and Joachim who made the last couple of years memorable.

My chain of gratitude would be incomplete without the mention of my family members. So, I thank my parents, sister and brother for their support directly or indirectly. A very special thanks to Perpeth for sharing my success and failures equally and for her indubitable support and motivation that kept me going to date. I wish to thank all whose help I have taken knowingly or unknowingly.

The publications listed in the table below are partly reproduced in this dissertation. The table itemizes to what extent the different sections of the papers have been reused at which position in this work. For the figures, it is noted in the respective captions whether it is a reproduction or an adaptation from the corresponding publication.

<table>
<tr><td colspan="3">S. Pai, M. Hafftlang, G. Atongo, C. Nagel, J. Niesel, S. Botov, H.-G. Schmalz, B. Yard, U. Schatzschneider, Dalton Trans. 2014, 43, 8664-8678.</td></tr>
<tr><td>thesis p. 36 - 37</td><td colspan="2">Table 3.1, Fig. 3.1, Text mainly reproduced, modified and extended from the paper</td></tr>
<tr><td>thesis p. 40 - 44</td><td colspan="2">Table 3.3, Fig. 3.3- 3.4, Fig. 3.6-3.7, Text mainly reproduced, modified and extended from the paper</td></tr>
<tr><td>thesis p. 45 - 46</td><td colspan="2">Table 3.5, Fig. 3.8, Text reproduced, modified and extended from the paper</td></tr>
<tr><td>thesis p. 48 - 50</td><td colspan="2">Table 3.6, Fig. 3.11-3.12, Text mainly reproduced, modified and extended from the paper</td></tr>
<tr><td>thesis p. 51 - 52</td><td colspan="2">Fig. 3.13, Text mainly reproduced, modified and extended from the paper</td></tr>
<tr><td>Contributions</td><td>S. Pai

M. Hafftlang, B. Yard
C. Nagel
G. Atongo, J. Niesel
S. Botov, H. –G. Schmalz
U. Schatzschneider</td><td>Synthesis, characterization, CO release measurements, manuscript writing
Biological data
X-ray structure analysis
Part of ligand synthesis
COP-1 probe synthesis
DFT calculations, manuscript proof reading</td></tr>
<tr><td colspan="3">S. Pai, K. Radacki, U. Schatzschneider, Eur. J. Inorg. Chem. 2014, 2886-2895.</td></tr>
<tr><td>thesis p. 55 - 58</td><td colspan="2">Scheme 3.3, Fig. 3.16, Text mainly reproduced, modified and extended from the paper</td></tr>
<tr><td>thesis p. 59 - 61</td><td colspan="2">Scheme 3.4-3.5, Fig. 3.17, Text mainly reproduced, modified and extended from the paper</td></tr>
<tr><td>thesis p. 62 - 64</td><td colspan="2">Fig. 3.19-3.21, Text mainly reproduced, modified and extended from the paper</td></tr>
<tr><td>thesis p. 65 - 67</td><td colspan="2">Table 3.7, Fig. 3.23-3.25, Text mainly reproduced, modified and extended from the paper</td></tr>
<tr><td>Contributions</td><td>S. Pai

K. Radacki
U. Schatzschneider</td><td>Synthesis, characterization, peptide synthesis, CO release measurements, manuscript writing
X-ray structure analysis
Manuscript proof reading</td></tr>
</table>

Table of Contents

Abbreviations **III**

1. Introduction **1**

1.1 Medicinal organometallic chemistry 1

1.2 Luminescent transition metal complexes for biomedical applications 7

1.3 Metal-based radiopharmaceuticals 9

1.4 Organometal-peptide conjugates and their medicinal applications 11

1.5 Biological generation and activity of carbon monoxide 13

1.6 Carbon monoxide-releasing molecules (CORMs) 16

1.7 Mechanisms of CO release from CORMs 18

1.7.1 CO release triggered by ligand exchange reactions 18

1.7.2 Enzyme-triggered CO-releasing molecules 19

1.7.3 Photoactivated CO-releasing molecules 20

1.8 PhotoCORM conjugation to delivery vectors 23

1.9 *In vitro*/*in vivo* detection of carbon monoxide 25

1.10 Solid-phase peptide synthesis 27

1.11 Bioorthogonal click reactions 29

2. Motivation **33**

3. Results and discussion **35**

3.1 Manganese(I) tricarbonyl complexes as PhotoCORMs 35

3.1.1 Synthesis and characterization of *fac*-[Mn(N-N-N)$(CO)_3]^+$ complexes 35

3.1.2 X-ray structure analysis 40

3.1.3 Photolysis and stability studies 43

3.1.4 CO release studies and quantum yield measurements 45

3.1.5 CO release monitored by solution IR spectroscopy 47

3.1.6 *In vitro* detection of photoinduced CO release using COP-1 as a fluorogenic switch-on probe 50

3.1.7 Discussion 53

3.2 Manganese(I) tricarbonyl PhotoCORM peptide conjugates 55
3.2.1 Synthesis of peptide conjugates by CuAAC "click" reaction and oxime ligation 55
3.2.2 Photolysis and stability studies in DMSO and water 65
3.2.3 CO release and quantum yield measurements 66
3.2.4 Discussion 68
3.3 Manganese(I) tricarbonyl DAB-G1-PPI and PAMAM-G0 dendrimer conjugates 69
3.3.1 Synthesis of diaminobutane (DAB) and polyamidoamine (PAMAM) conjugates 69
3.3.2 Photolysis and stability studies in phosphate buffered solution (PBS) 75
3.3.3 Photoinducible CO release experiments with the myoglobin assay 77
3.3.4 Discussion 79
4. Summary **81**
5. Experimental section **89**
5.1 General procedures and instrumentation 89
5.1.1 Single crystal X-ray diffraction 90
5.1.2 Myoglobin assay 91
5.1.3 High-pressure liquid chromatography (HPLC) 92
5.1.4 Solid-phase peptide synthesis (SPPS) 92
5.1.5 Photolysis experiments monitored by solution IR spectroscopy 93
5.1.6 Ferrioxalate actinometry 93
5.1.7 Cell culture experiments 94
5.1.8 Density functional theory calculations 95
5.2 Synthetic procedures 96
6. References **139**
7. Appendices **149**

Abbreviations

Aoa	aminoxyacetic acid
Asn	asparagine
ATP	adenosine triphosphate
ATR	attenuated total reflection
Cp	cyclopentadienyl
BODIPY	dipyrromethene**b**oron difluoride
bpea	2,2′-bis(pyrazolyl)ethylamine
bpy	2,2′-bipyridine
HbCO	carboxy haemoglobin
COP-1	carbon monoxide probe-1
CORM	CO-releasing molecule
CPP	cell-penetrating peptide
CQ	chloroquine
2-CT	2-chlorotrityl
CuAAC	copper-catalyzed azide-alkyne cycloaddition
DAB	diaminobutane
DAT	dopamine transporter
DCC	*N*,*N*-dicyclohexylcarbodiimide
DIEA	*N*,*N*-diisopropylethylamine
DMF	*N*,*N*-dimethylformamide
DMSO	dimethylsulfoxide
DNA	deoxyribonucleic acid
dppn	benzo[*i*]dipyrido[3,2-*a*:2′,3′-*c*]phenazine
dppz	dipyrido[3,2-*a*:2′,3′-*c*]phenazine
EDTA	ethylenediaminetetraacetic acid
Enk	enkephalin
EPR	enhanced permeability and retention

ESI	electrospray ionisation
ET-CORM	enzyme-triggered CO-releasing molecule
FAB	fast atom bombardment
Fmoc	9-fluorenylmethyloxycarbonyl
FQ	ferroquine
FTIR	fourier transform infrared spectroscopy
5-FU	5-fluoro uracil
Gly	glycine
GMP	guanosine monophosphate
GOF	goodness of fit
GTP	guanosine triphosphate
Hb	haemoglobin
HBTU	*O*-(tenzotriazol-1-yl)-*N*,*N*,*N*′,*N*′-tetramethyluronium hexafluorophosphate
His	histidine
HO	heme oxygenase
HOBt	1-hydroxybenzotriazole
HPLC	high-performance liquid chromatography
HUVEC	human umbilical vein endothelial cell
IC	inhibitory concentration
iCORM	inactivated CO-releasing molecule
IL	intraligand
Leu	leucine
Mb	myoglobin
MbCO	carbonmonoxy myoglobin
MLCT	metal-to-ligand charge transfer
NAD	nicotinamide adenine dinucleotide
3-NBA	3-nitrobenzylalcohol
NIR	near infrared

NMR	nuclear magnetic resonance
NOS	nitric oxide synthase
PAMAM	polyamidoamine
PBS	phosphate-buffered saline
PDE	phosphodiesterases
PET	positron emission tomography
phen	1,10-phenanthroline
PNA	peptide nucleic acid
Pro	proline
PTA	1,3,4-triaza-7-phosphatricyclo[3.3.1.1]decane
pz	pyrazol
ROS	reactive oxygen species
Ser	serine
sGC	soluble guanylyl cyclase
SPECT	single photon emission computed tomography
SPPS	solid-phase peptide synthesis
t-BOC	tert-butoxycarbonyl
TFA	trifluoroacetic acid
TGF	transforming growth factor
TIS	tri(isopropyl)silane
TMS	tetramethylsilane
tpm	tris(1-pyrazolyl)methane
Trt	trityl
UV	ultraviolet

1 Introduction

1.1 Medicinal organometallic chemistry

Organometallic chemistry provides a very wide range of compounds for homogenous catalysis[1] as well as precursors for the synthesis of advanced materials. In 1985, the term '*bioorganometallic chemistry*' was introduced by G. Jaouen to indicate a rapidly expanding new field of research. It is focused on the synthesis of compounds with at least one metal-carbon bond for biological and medicinal applications.[2-3] The most prominent example of a naturally occurring bioorganometallic compound is Vitamin B12, which incorporates a stable cobalt-carbon bond between the carbon atom of a methyl or 5'-deoxyadenosyl moiety and the cobalt center of cobalamin. Among the many facets of bioorganometallic chemistry, medicinal applications have potential in the chemotherapy of cancer[4-6] but might also serve as antimalarial, antimicrobial and diagnostic agents.[7] For example, due to the toxic side effects of anticancer drug cisplatin, *cis*-[$PtCl_2(NH_3)_2$], and its congeners (Fig. 1.1), Ru(III) ammines like [$RuCl_3(NH_3)_3$] have been explored for their anticancer activity by Clarke.[8]

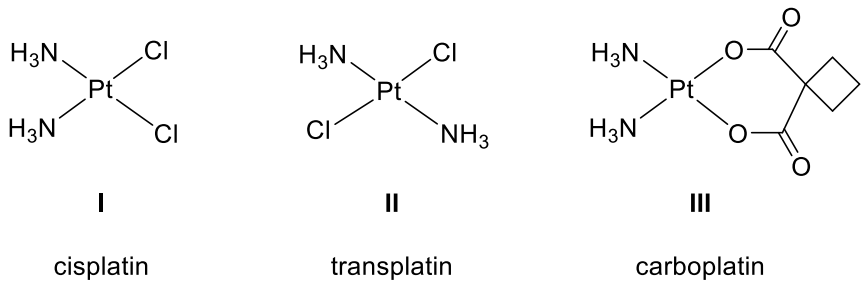

Fig. 1.1: Platinum(II) diam(m)ine complexes in clinical use as anticancer drugs.

Unlike the platinum-based drugs, ruthenium compounds are active towards cisplatin-resistant cell lines and generally less toxic. Two coordination compounds based on Ru(III), namely KP1019, indazolium *trans*-[tetrachlorobis(1*H*-indazole)-ruthenate(III)] and NAMI-A, which shows antimetastatic activity, are currently in advanced clinical trials.[9-10] The activity of these compounds is thought to be based on the *in vivo* reduction of Ru(III) to labile and more reactive Ru(II) species.[11-12] As a result, in particular Sadler and Dyson have extensively studied organometallic half-sandwich

"piano-stool" complexes based on ruthenium (Fig. 1.2) as novel anticancer drug candidates.[13-15]

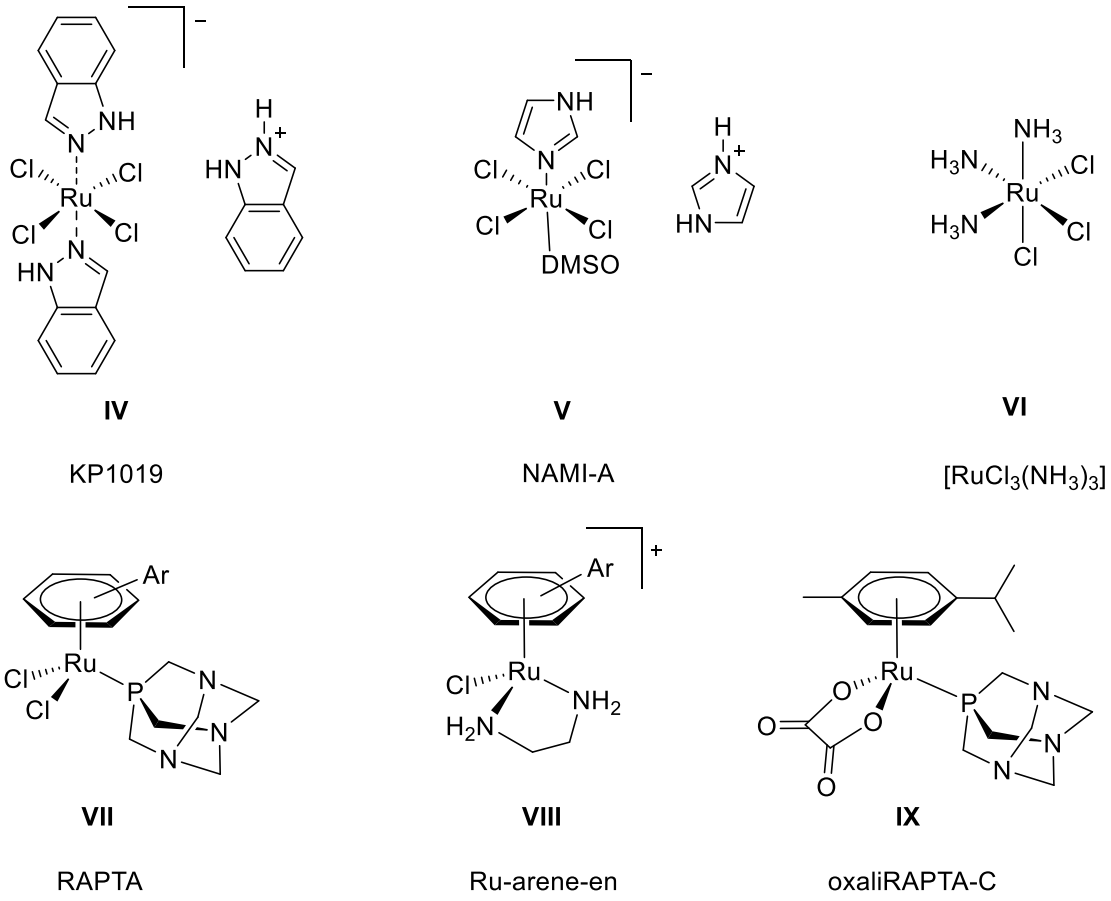

Fig. 1.2: Ruthenium coordination compounds (top) and organometal half-sandwich compounds (bottom) explored as anticancer drug candidates.

Furthermore, both *in vitro* and *in vivo* studies have revealed that the mode of action of Ru-arene complexes, for example $[RuCl(\eta^6\text{-arene})(en)]^+$, is analogous to that of cisplatin. The substitution of the chloride ligand by water results in a reactive aqua species, a transformation which is more pronounced in the nucleus due to the lower chloride concentration (4 mM) compared to blood (~100 mM).[16] Such species appear to target nuclear DNA with an affinity towards the N7 of guanine nucleobases, forming monoadducts with DNA in contrast to bifunctional adducts formed by cisplatin.[17-18] On the other hand, the water-soluble RAPTA complexes (with the ampiphilic PTA ligand) do not target DNA, but instead exert their cytotoxic activity due to the ligand exchange mechanism with water. This is also supported by the synthesis of derivatives of RAPTA compounds in which the chloride ligands are

replaced by chelating dicarboxylato ligands as in oxaliRAPTA-C, which resists hydrolysis. Such robust organometallic compounds show high affinity towards serum proteins, in particular the sulfur atoms of enzyme targets.[19-20] Although NAMI-A is known to selectively reduce the growth of lung metastasis in tumors such as MCa mammary carcinoma, the exact mechanism of its action has not been elucidated so far.

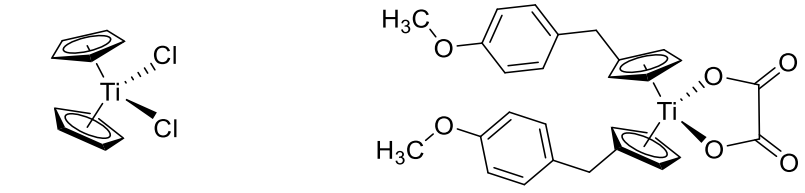

X titanocene dichloride

XI oxali-titanocene Y

Fig. 1.3: Titanocene dichloride and one of its derivatives.

In the late 1970s, Köpf and Köpf-Maier investigated the *in vitro* antitumor activity of metallocene dichlorides such as titanocene dichloride, $[TiCl_2(\eta\text{-}C_5H_5)_2]$. Titanocene dichloride, a dicyclopentadienyl Ti(IV) complex, has a *cis*-arrangement of the halide ligands and forms a bifunctional cross-link with DNA due to its affinity towards the phosphate backbone.[21] The hydrolysis of this compound as a result of chloride ligand replacement by water/hydroxide leads to a solvated Ti(IV) ion, which binds to transferrin (Tf), an iron transport protein, under loss of both Cp ligands.[22] Apart from its complex solution chemistry, there is continuing interest in preparing analogues of such metallocenes due to their selective delivery to cancer cells. However, clinical phase II trials were abandoned due to its instability in aqueous medium and the failure of certain treatment improvement. In search for a better stability under physiological conditions, several derivatives have been developed based on the titanocene dichloride core (Fig. 1.3). In particular, oxali-titanocene Y compounds were synthesized, with the two chloride ligands replaced by a chelating oxalato ligand. Although the presence of a chelating ligand provides stability towards hydrolysis, the water solubility of the complex still remained elusive.[23]

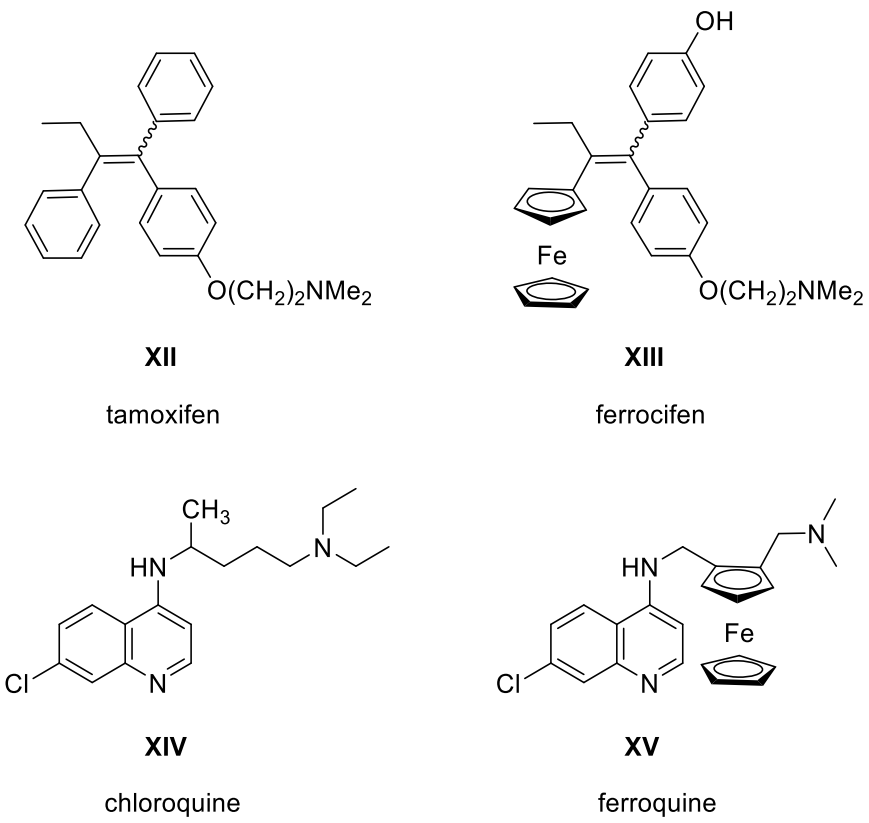

Fig. 1.4: Tamoxifen and ferrocene based anticancer agent ferrocifen (top). Antimalarial chloroquine and ferroquine drug candidate (bottom).

Modified sandwich complexes based on ferrocene are of particular interest due to their redox activity, and can show cytotoxic effects due to the formation of reactive oxygen species (ROS). The redox potential of ferrocene derivatives lie in the biologically accessible range and might be beneficial for their medicinal activity. For example, estrogen induces the growth of breast tumors due to the overexpression of the targeted receptor ERα. A selective design of estrogen-receptor targeting motifs has led to novel anticancer drug candidates.[24] Jaouen and co-workers have developed such a class of oxidatively activated ferrocenyl prodrugs called ferrocifens (Fig. 1.4).[25] The β-phenyl ring of the organic drug tamoxifen was replaced by a ferrocenyl moiety, which leads to higher lipophilicity and a stronger cytotoxic effect. Furthermore, the biological activity is correlated with quinone methide formation after electron transfer from the conjugated Ferrocene group.[26] This work also inspired bioorganometallic modification of the antimalarial drug chloroquine (CQ). Ferroquine (FQ) is the result of a screening over 50 ferrocene compounds and is highly active against CQ-resistant

strains of the malaria parasite *P. falciparum*. Based on the *in vitro* and *in vivo* activities of FQ, several structural modifications of the latter have also been evaluated.

These works show that organometallic compounds can be developed as highly active and specific drugs by careful ligand design. Meanwhile, inspired by the natural product staurosporine, Meggers and coworkers have developed a series of effective kinase inhibitors based on an organometallic structural motif (Fig. 1.5). Staurosporin is a protein kinase Pim-1 inhibitor that prevents the binding of ATP to the active site of the enzyme.[5] The 3D structure of biomolecules makes the targeting of proteins difficult since detailed structural information is required on the conformation and spatial orientation. However, organometallic chemistry provides an easy access to structures able to occupy the enzyme active sites due to their rigid shape.

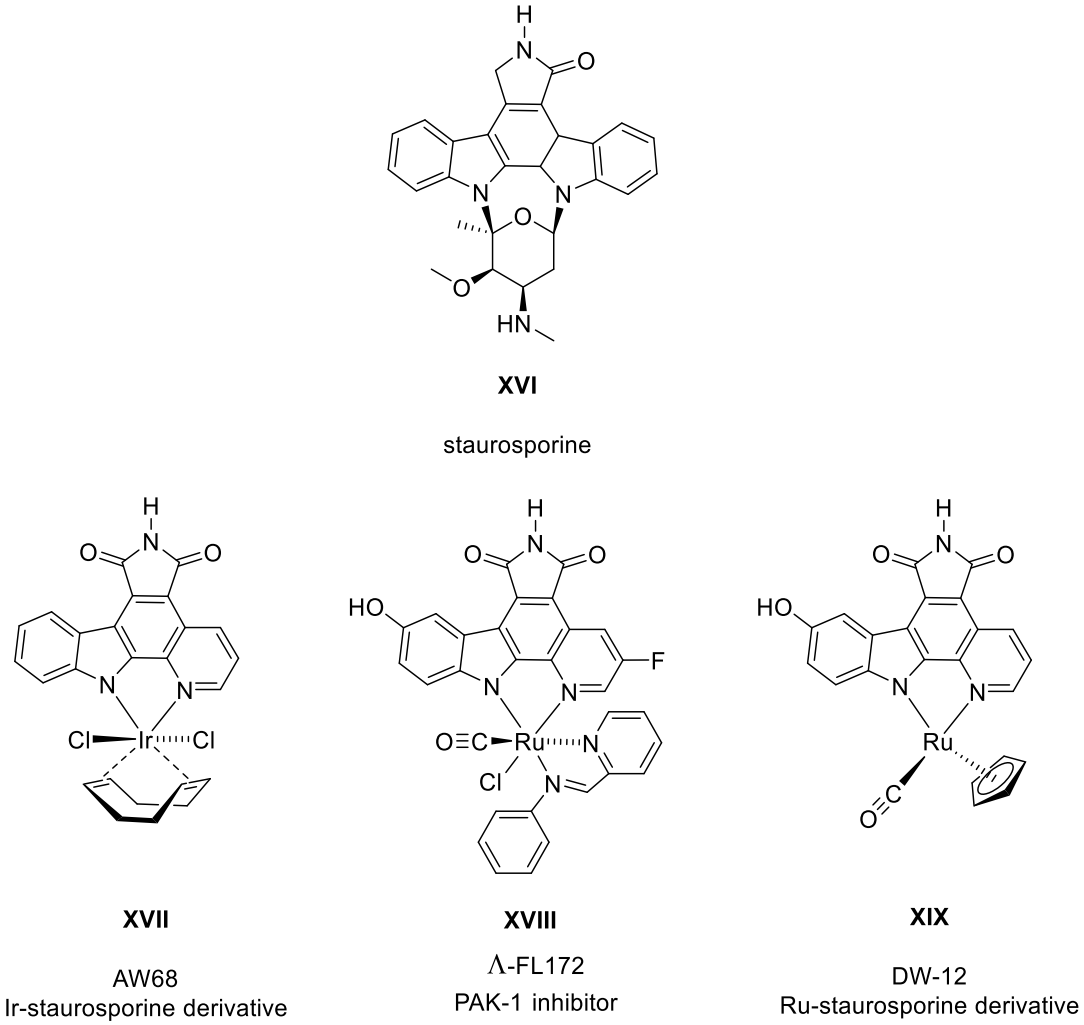

Fig. 1.5: Natural product staurosporine (top) and derived organometallic protein kinase inhibitors based on ruthenium and iridium (bottom).

In the organometallic kinase inhibitors, the carbohydrate moiety of staurosporine was replaced by a metal-coligand scaffold, leading to high affinity in the nM to pM range to specific kinases *in vitro*.[27-28] The non-toxic organometallic iridium complex AW68 was also inhibits the development of blood vessels in a zebrafish angiogenesis model. Thus, careful molecular design can pave the way for new developments in medicinal organometallic chemistry.

1.2 Luminescent transition metal complexes for biomedical applications

Transition metal complexes possess intense and long-lived triplet charge transfer and intraligand transition emissions which makes them suitable as luminescent probes for biomolecules. They also display interesting photophysical properties such as phosphorescence due to large Stokes shifts, which distinguishes them from most organic fluorophores. Furthermore, the emission properties of luminescent metal complexes can be tuned by the choice of metal center and auxiliary ligands and might also respond to the biological environment.[29] They exhibit long-lived and intense emission at room temperature allowing the imaging of biological events.

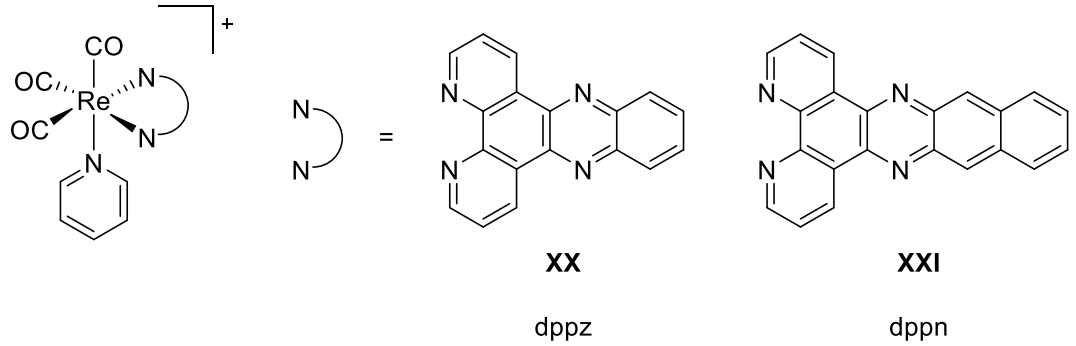

Fig. 1.6: Luminescent Re(I) metallointercalators.

For example, the group of Schanze studied *fac*-$[Re(CO)_3(dppz)(4\text{-}Mepy)]^+$ as a luminescent switch-on probe for duplex DNA, whereas Yam reported on $[Re(CO)_3(dppz)(py)]^+$ and $[Re(CO)_3(dppn)(py)]^+$ as luminescent metallointercalators (Fig. 1.6).[30-31] Interestingly, the dppz complexes exhibit a ^{3}IL ($\pi \rightarrow \pi^*$) (dppz) emissive state while the dppn analogues have a substantial ^{3}MLCT ($d\pi(Re) \rightarrow \pi^*(dppn)$) character. Absorption and emission titrations demonstrated the intercalative binding mode of these complexes. While the excited dppz complex oxidises DNA, the dppn compound causes DNA strand scissions due to the production of superoxide and hydroxyl radicals upon photoexcitation.

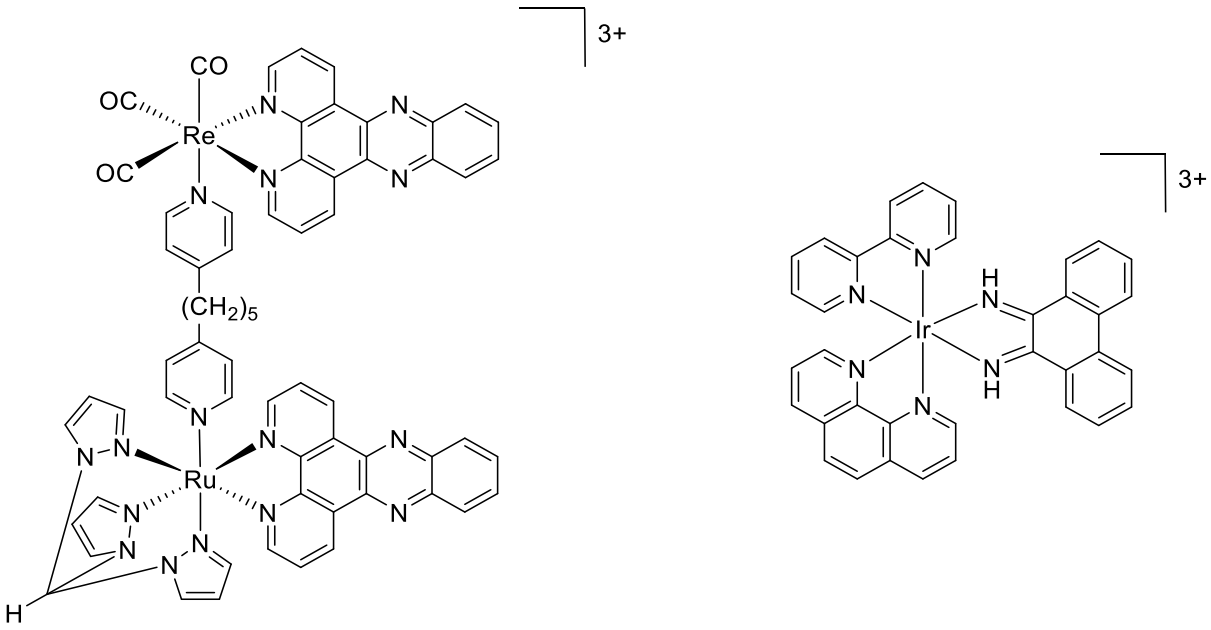

Fig. 1.7: Luminescent heterobimetallic polypyridyl complex with DNA-light switch properties (left) and iridium-based DNA-binding probe (right).

A heterobimetallic ruthenium/rhenium (Fig. 1.7) was developed by Thomas and co-workers showing dual DNA-light switch and photocleavage properties.[32] The dinuclear compound is non-emissive in aqueous solutions but becomes brightly emissive in the presence of DNA with a binding constant K_b of 6 x 10^5 M^{-1}. Upon photoexcitation, it is able to cleave the DNA as well.

Iridium(III) polypyridine complexes, on the other hand, have attracted much attention due to their luminescence properties since the emissive studies on *cis*-$[IrCl_2(bpy)_2]^+$.[33] Barton *et al*. synthesised a tris(heteroleptic) iridium(III) phenanthrenequinone diimine complex $[Ir(bpy)(phen)(phi)]^{3+}$ (Fig. 1.7) and extensively studied its DNA binding properties by electrochemistry.[34] With the aid of a DNA-modified electrode, a binding affinity of K_b = 1.1 x 10^6 M^{-1} was determined and demonstrated a concerted two-electron reduction to a diradical species.

1.3 Metal-based radiopharmaceuticals

Radiopharmaceutical chemistry involves the potential utility of radiometals in the fields of radiochemistry, nuclear medicine, and molecular imaging.[35] It is basically performed in the nM to pM range without compromising with the accessibility of the radionuclide and high target localisation.[36-37] Positron emission tomography (PET) and single-photon emission computed tomography (SPECT) are the two most important radioisotope-based methods in nuclear medicine. The first organometallic compound for SPECT to enter clinical use was $[^{99m}Tc(CNR)_6]^+$ (R = $CH_2C(CH_3)_2OCH_3$) (Fig. 1.8), which is a technetium-essential agent and is sold under the trade name Cardiolite due to its application in myocardial perfusion with a favorable decay half-life of ^{99m}Tc of 6.02 h.

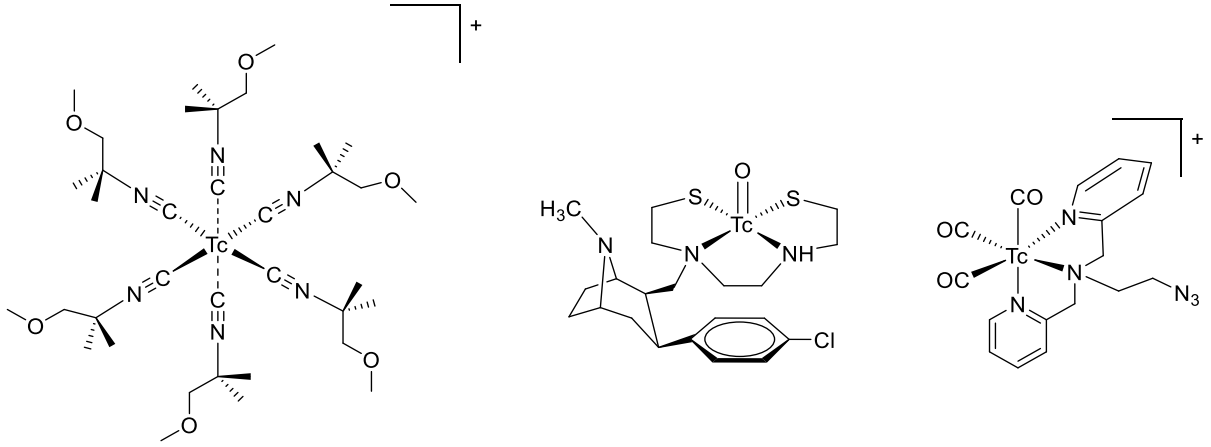

Fig. 1.8: ^{99m}Technetium radiopharmaceuticals for molecular imaging.

The second class of SPECT imaging agents are the technetium non-essential agents. The biodistribution of such compounds is often determined by enzymatic processes associated with the carrier molecule. For example, the tropane analogue [^{99m}TcO(TRODAT)] binds to the dopamine transporter (DAT) and is used in the diagnosis of Parkinson's disease (Fig. 1.8).[38-40] On the other hand, the organometallic nature of the *fac*-$[Tc(CO)_3]^+$ core provides a wide range of options for the design of technetium tricarbonyl-based radiopharmaceuticals.[41-44] It is easily prepared from the water-soluble precursor $[^{99m}Tc(CO)_3(H_2O)_3]^+$ as developed by Alberto *et al*. and is

chemically robust due to its low spin $4d^6$ configuration. Many different donor atoms can be used in chelators to prepare complexes that are most likely retained in the liver and kidney.[45] Some tridentate chelators have even been modified by introduction of additional functional groups such as azides (Fig. 1.8, right) to give ^{99m}Tc-labelled PNA oligomer conjugates by the CuAAC click reaction.[46]

1.4 Organometal-peptide conjugates and their medicinal applications

The study of cellular uptake of metal complexes and its intra-cellular localization is well studied by group of Nolte, by using the concept of organometallic peptide conjugates. Peptides are attractive targeting vectors for the delivery of metal-based compounds. Solid-phase peptide synthesis (SPPS) is the method of choice for the synthesis of small to medium sized peptides. The labeling of such peptides with robust organometallics can be carried out during the SPPS. However, only selected organometallic groups withstand the strong acid used during peptide cleavage from the solid support. As a result, a post-labeling strategy is usually utilized in solution. For a detailed SPPS scheme see: Nolte *et al*.[47]

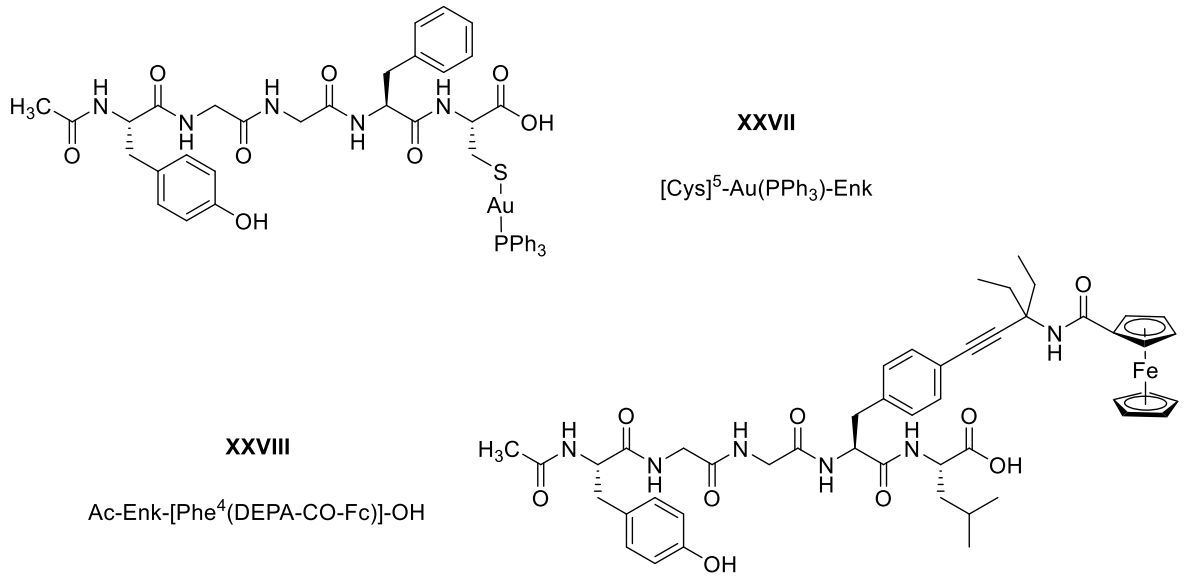

Fig. 1.9: Organometallic-enkephalin conjugates synthesized by SPPS.

For example, a gold(I)-thiolate peptide conjugate (Fig. 1.9 top) was isolated by the selective deprotection of cysteine in [Cys^5]-Enk, a derivative of naturally occurring enkephalin and further complexation of $Au(PPh)_3$ to the thiol group, demonstrating the stability of the gold(I) moiety under the conditions of SPPS.[48] As an alternative post-labeling method, the same research group also used the Sonogashira coupling reaction of ferrocenyl alkyne with a *p*-iodo-phenylalanine functionalized Enk-peptide.[49]

Additionally, the group of Neundorf investigated the cellular uptake of cymantrene and cymantrene peptide conjugates in MCF-7 human breast cancer and HT-29 human colon carcinoma cells by coupling the organometallic moiety with cell penetrating peptide sC18 via different carboxylic acid linkers.[50] The cymantrene-sC18 conjugates incorporating a protease-cleavable GFLG linker are recognised by endopeptidase cathepsin B, resulting in low IC_{50} values of only 15 μM compared to other conjugates. In summary, organometal-peptide conjugates are a unique method for the targeted delivery of metal complexes of biological significance.

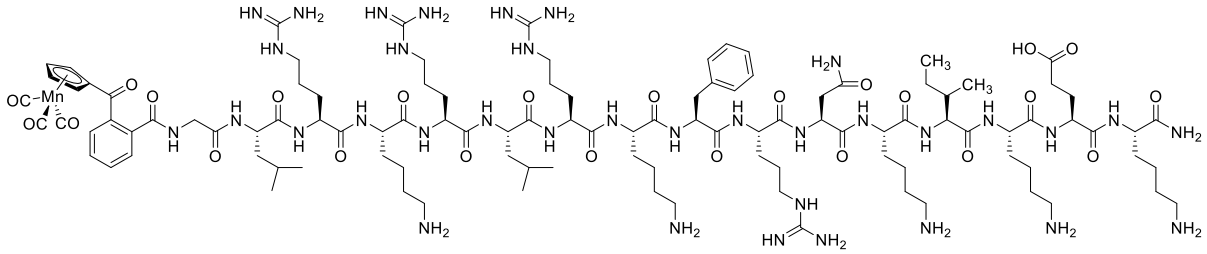

XXIX

Fig. 1.10: Cymantrene-sC18 conjugate incorporating 1,2-phenylene linker from group of Neundorf.

1.5 Biological generation and activity of carbon monoxide

Carbon monoxide (CO) has a reputation in the general public as a "deadly molecule" due to its chronic health hazards. CO intoxication mainly results due to the prolonged exposure to environmentally generated CO resulting from incomplete combustion of carbon fuels. An elevated concentration of CO in the bloodstream results in binding of CO to haemoglobin (Hb), forming carbonmonoxy haemoglobin (HbCO). This impairs both the oxygen storage capacity of Hb and oxygen transportation function of COHb to the tissues. As a result, organs such as brain and heart become more vulnerable to CO induced acute hypoxia.[51] However, in 1895, Haldane showed the antagonistic effect of a high partial pressure of oxygen on CO binding to haemoglobin[52] and the first experimental evidence for the endogenous production of CO was provided by Sjöstrand.[53-55] Today, it is well established that CO is endogenously generated by the enzymatic degradation of heme to biliverdin and ferrous iron catalyzed by heme oxygenase (HO) (Scheme. 1.1). There are two HO isoforms, inducible HO-1,[56-57] a ubiquitous stress response protein which becomes highly abundant during oxidative stress and inflammation, and acts as an antioxidant.[58-60] The HO-2 isoform on the other hand is constitutively expressed in neurons controlled by post-translational modification.[61]

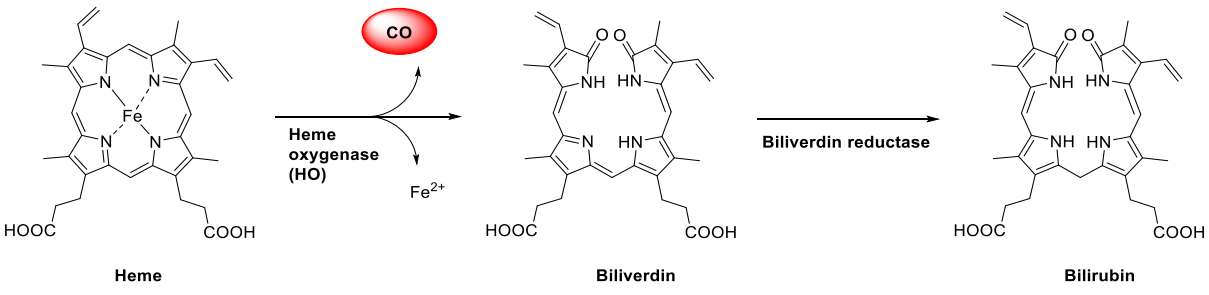

Scheme 1.1: Heme oxygenase (HO)-catalyzed degradation of heme to biliverdin with the release of a molecule of carbon monoxide (CO) as well as ferrous iron.

Carbon monoxide is thought to be able to freely diffuse through cellular membranes and exert its physiological effects on cellular targets such as ion channels,[62] surface inhibition NADPH oxidase,[63] MAP kinases,[64] and to some extent on *soluble guanylyl cyclase* (sGC) leading to the cellular generation of cGMP.[65]

Soluble guanylate cyclase (sGC) is a heme protein in which the heme as a prosthetic group is coordinated by the histidine residue of the β subunit and is able to bind either NO or CO.[66-68] Thus the binding of CO to heme protein marginally increases the production of cyclic GMP from GTP (Fig. 1.11) and modulates vasodilatory effects, as in the case of NO. YC-1, an activator of sGC on the other hand works synergistically in the presence of CO. The possible explanation is that YC-1 cleaves the His-Fe bond and as a result CO becomes a good activator in the presence of YC-1.[66] Soluble guanylate cyclase is now very questionable as a target for CO, since its activation without YC-1 is rather extremely low and no natural YC-1 analogue has been found so far.

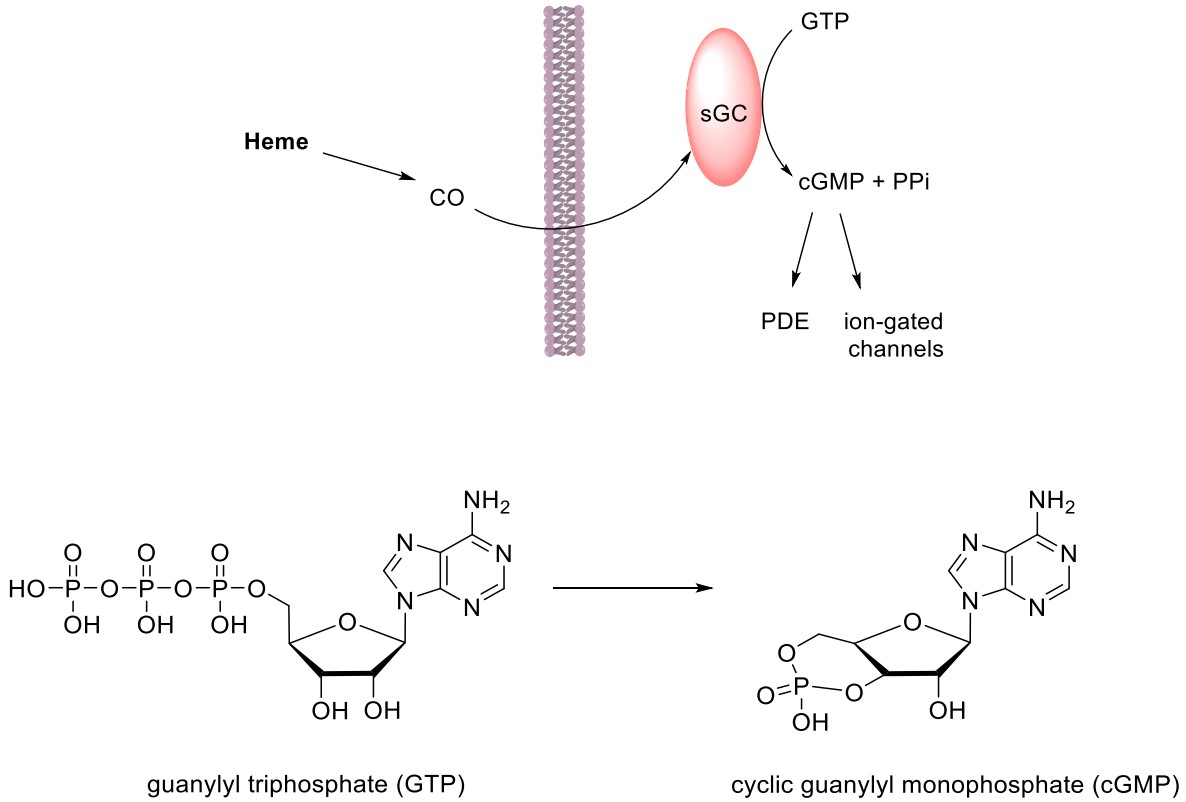

Fig. 1.11: Endogenously generated CO activates sGC producing cGMP which in turn activates phosphodiesterases (PDE) and ion-gated channels (above). Conversion of guanylyl triphosphate to cyclic guanylyl monophosphate (below).

The cross-talk between CO and NO mediated signalling pathways arises from the binding of carbon monoxide to nitric oxide synthase (NOS) in the NO pathways of cerebral and renal circulation. Additionally, it was shown that CO can increase the activity of NOS in the liver, leading to increased levels of NO, which in turn activates HO-1.[69] As a result, CO and NO signalling are interrelated, which can be utilized to trigger NO production in remote tissues. Large conductance Ca^{2+} and voltage activated K^+ channels (BK_{Ca}) are expressed in variety of tissues and take part in the critical functions such as modulating neurotransmitter release and signal processing in neurons. It was demonstrated that CO modulates BK_{Ca} channels, which is accompanied by an increase in cGMP production.[70] Electrophysiological studies suggest that the CO-stimulated activation of BK_{Ca} channel delivers them as gas sensor systems.[71] Although the physiological relevance of CO and ion-channel interactions still remain elusive, the knowledge obtained from such reports contributes and direct towards the beneficial effects of small signalling molecule CO.

1.6 Carbon monoxide-releasing molecules (CORMs)

There is steadily growing interest in potential therapeutic applications of carbon monoxide ever since its discovery as a small-molecule messenger in the 1950s.[72] For an exogenous delivery of CO, the Covox DS device (http://www.ikaria.com) is commercially available, which specifically delivers pharmacological-grade CO for inhalation. However, a drawback of such inhalative CO application is the high general toxicity when overdosed. As a result, there is a need for molecules that can deliver CO in a safer way. In this context, Motterlini and coworkers introduced the term *CO-releasing molecules* (CORMs) for metal carbonyl complexes which can be used to carry and release carbon monoxide to biological systems.[73] The first compound to be studied in this context was dimanganese decacarbonyl [$Mn_2(CO)_{10}$] also called CORM-1.

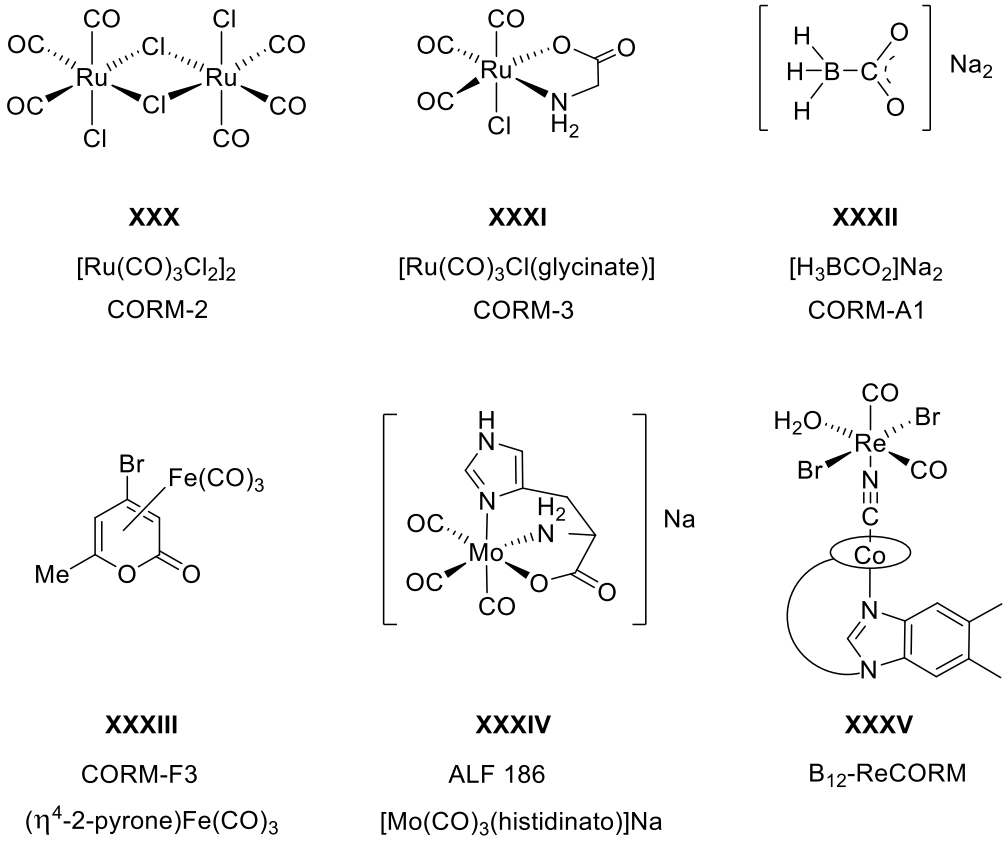

Fig. 1.12: Selected lead structures of CO-releasing molecules (CORMs) activated by ligand exchange reactions with medium.

Additionally, a number of main group compounds such as CORM-A1 ($Na_2[H_3BCO_2]$), were also studied by the group of Alberto.[74-77] CORM-A1 releases CO under

physiological conditions with a half-life of 21 min and promotes hypotension and vasorelaxation. However, one of the most widely used CO-releasing molecules is [RuCl(glycinate)$(CO)_3$] (CORM-3) which has a half-life of 98 h in water. However, in blood plasma, this is reduced to just 3.6 min, probably due to the coordination of *trans*-labilising thiol groups of glutathione to the metal centre.[78] CORM-3 protects myocardial cells against ischemia-reperfusion injury and the kidney from cisplatin-induced toxic effects.[79] The initial work of Motterlini showed that carbon monoxide release from the metal centre mainly occurs via a ligand exchange mechanism with medium, which will be discussed comprehensively in the next chapter. The CO release inevitably leaves behind a metal-coligand fragment which might have a biological activity of its own, which is however often not fully characterized. This inactivated CORM is called 'iCORM' and needs to be explored more broadly since many ruthenium compounds are known for their cytotoxic properties.[80-81] Another set of CORMs based on iron(0) carbonyl complexes bearing a 2-pyrone ligand was prepared by Fairlamb *et al*. since 2-pyrone compounds exhibit biological activity due to the carbonyl ring opening.[82-83] A closer look into the literature also shows a family of 17-electron Re(II) dicarbonyl CORMs, one of which has been attached to the naturally occurring carrier molecule cobalamin.[84] A particular emphasis was laid on the stability of such CORMs in aqueous aerobic media to achieve good biocompatibility.

In another approach, Romao *et al*. synthesized a series of Mo(0) tricarbonyl compounds with different ancillary ligands. Extensive screening revealed that the complexes with isocyanide ligands showed high *in vivo* activity towards acute liver failure. A better tissue specificity was achieved by selection of much simpler ancillary ligand in the coordination sphere as highlighted by Romao *et al*.[85] The interaction with lysozyme was studied using Na[Mo(histidinate)$(CO)_3$], ALF-186. A crystal structure analysis of the protein adduct revealed the formation of polyoxomolybdate $[PMo_{12}O_{40}]^{3-}$ as a result of CO release and further decomposition of the complex in the acidic crystallization medium.[86] A number of recent review articles have stressed the need for a better molecular design for potential therapeutic applications of CO releasing molecules.[72-75-85-87-90]

1.7 Mechanisms of CO release from CORMs

1.7.1 CO release triggered by ligand exchange reactions

Since CO gas itself is difficult to administer due to its general toxicity, CO-releasing molecules might serve as prodrugs for the delivery of carbon monoxide to utilize its physiological effects for medicinal applications. One of the mechanism which triggers the CO release from transition metal centers is the ligand exchange reaction with medium. CO-releasing molecules such as CORM-2, CORM-3, CORM-A1, ALF-186 and several others release CO upon dissolution in medium due to the ligand exchange reactions with the medium. Although CORM-3, [RuCl(glycinate)$(CO)_3$] is well-soluble in water, it has a complicated solution chemistry. Addition of one equivalent of aqueous hydrochloric acid results in the conversion of [RuCl$(CO)_3(NH_2CH_2CO_2)$] to [$RuCl_2(CO)_3(NH_2CH_2CO_2H)$], in which the glycine is now coordinated to ruthenium in a monodentate fashion via the nitrogen atom. A pH-dependent speciation showed the presence of different isomers (Fig. 1.14) which was further supported by ^{13}C and ^{15}N NMR spectroscopy.

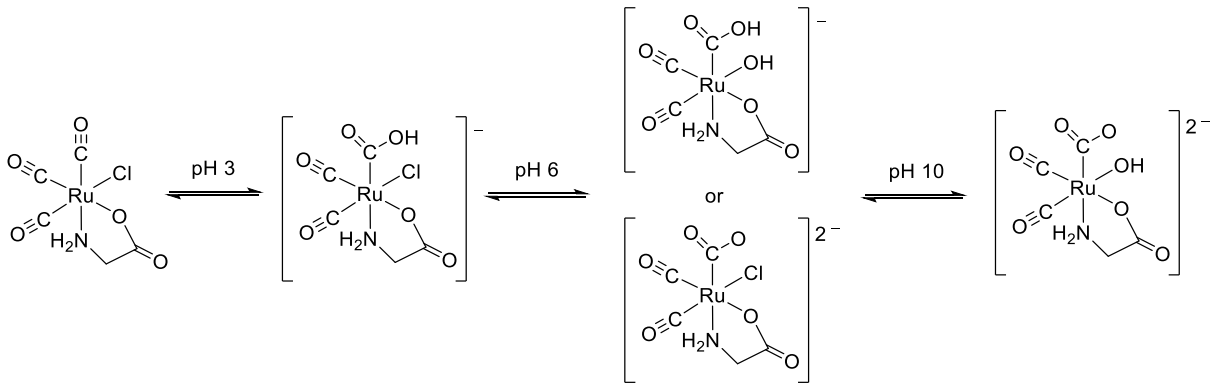

Scheme 1.2: pH-dependent speciation of [RuCl(glycinate)$(CO)_3$].[78]

CORM-A1, Na[H_3BCO_2H], on the other hand, releases CO slowly at physiological pH *via* an unknown mechanism. The half-life of these complexes sets the limit for *in vivo* application since the desired physiological effect of CO should be exerted before a significant amount of CORM has decayed.

1.7.2 Enzyme-triggered CO-releasing molecules

Very recently, the group of Schmalz introduced a new concept called enzyme-triggered CO-releasing molecules (ET-CORMs). This is based on the enzymatic hydrolysis of ester derivatives of dienol-iron tricarbonyl complexes by esterases/phosphatases, resulting in the formation of an intermediate labile enol complex. This intermediate which is a 16-VE species undergoes further decomposition under oxidative conditions and subsequently releases CO as well as ferric iron and the enone ligand (Scheme 1.3).[91]

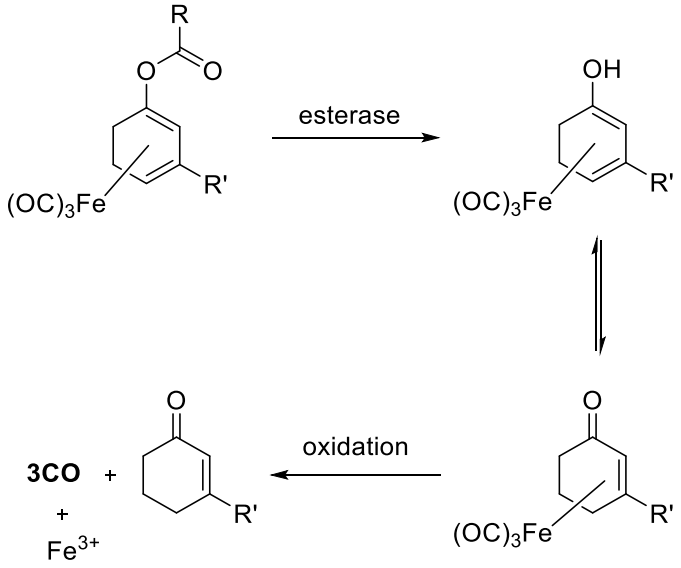

Scheme 1.3: Proposed mechanism for enzyme-triggered CO-release from iron tricarbonyl ET-CORMs.[92]

Further investigation of the effect of ET-CORMs on nitric oxide production by iNOS showed a 30% NO inhibition at 5 μM. CO is thought to bind to the iron center of the heme protein and actively suppresses the iNOS activity by the generation of inactive carbonmonoxy-iNOS. These iron tricarbonyl ET-CORMs also offer promising new ways to synthesize CO-releasing molecules for the CO-release of tissue specificity.[93]

1.7.3 Photoactivated CO-releasing molecules

Photoactivation is currently extensively explored by several research groups to trigger the CO release from CORMs since it allows for a precise spatial and temporal control of biological action of CO upon illumination.[81-94] Light as an external trigger does not only allow one to control the dosage of the CO release but also to define its location and timing. Due to the spontaneous release of CO from ligand exchange-triggered CORMs, the half-life of such compounds is a limiting factor to address a specific target in the body. PhotoCORM on the other hand release CO only when externally stimulated with light. Additionally, a PhotoCORM should show good solubility in aqueous solution or at least in aqueous dimethylsulfoxide (DMSO), as this is commonly used in drug delivery.

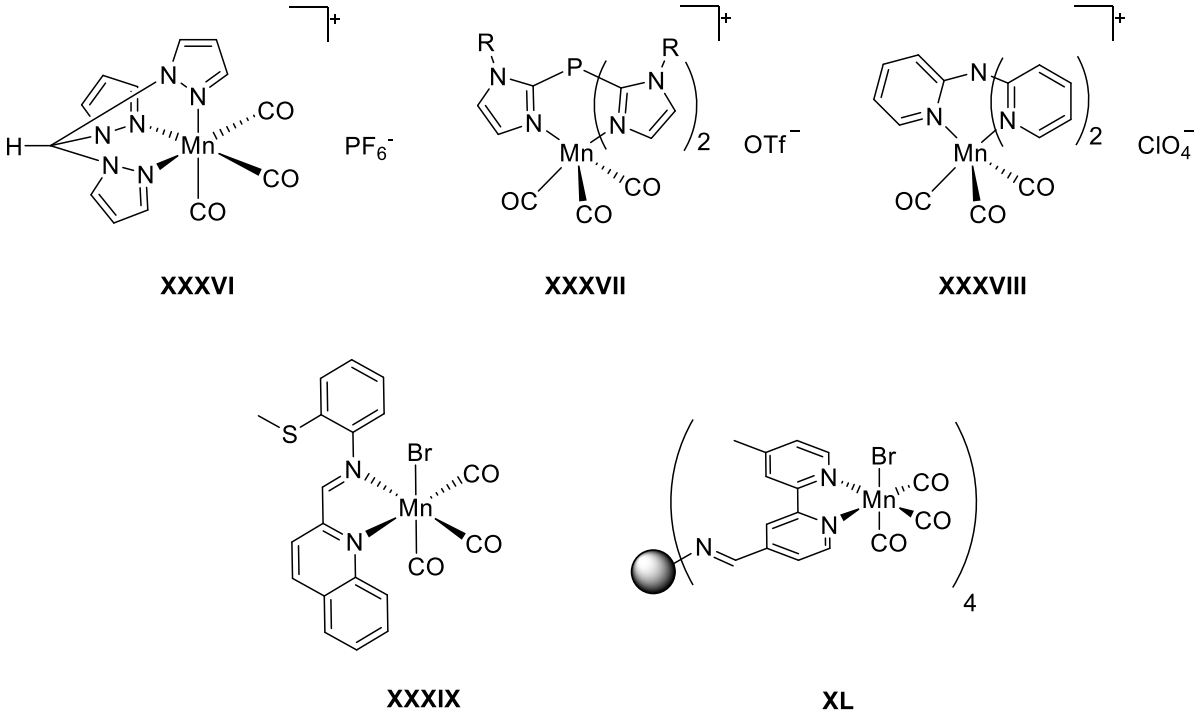

Fig. 1.13: Manganese tricarbonyl complexes explored as PhotoCORMs.

The initial introduction of dimanganese decacarbonyl $Mn_2(CO)_{10}$ as a PhotoCORM[73] led to the search for novel photoactivated CO-releasing molecules. Some of the well-known PhotoCORMs based on manganese(I) are shown in Figure 1.13. The biocompatibility of **XXXVI** $[Mn(CO)_3(tpm)]^+$ (tpm = trispyrazolylmethane) was demonstrated both in cell uptake studies and cytotoxicity assays on HT29 human colon cancer cells.[95] The cationic complex showed a significant photoinduced

cytotoxicity with the loss of cell biomass to a value comparable to that of organic cytotoxic agent 5-fluorouracil (5-FU). The inherent C≡O stretching vibrations of the complex appear between 1800 and 2200 cm^{-1}, where the vibrational background signal of cell constituents is negligible. As a result, the cellular distribution of this complex was also investigated by live cell imaging using Raman microspectroscopy.[96] In compound **XXXVII**, the effect of substitution of the imidazolylphosphane ligand on the CO release behavior of the complex was studied.[97] The substituted imidazolylphosphane complexes release only one equivalent of CO per mole of complex compared to the non-substituted imidazolylphosphane, which releases two moles of CO. In an attempt to increase the absorption of the complex and induce the CO release in the visible light region, compound **XXXVIII** and its quinoline derivatives were synthesized.[98] The number of pyridine groups was increased and extended conjugation in the ligand frame was introduced. The efficacy of light-induced CO-release lead to an induced vasorelaxation in mouse aortic muscle rings. Additionally, the group of Mascharak introduced compound **XXXIX** and its derivatives incorporating conjugated aromatic nitrogen donors in the ligand system. Apart from conjugation, an improved CO donating behavior was observed due to the influence of both electron rich thioether group and the inclusion of ancillary bromide ligand in the coordination sphere.[99] These structural design principles led to CO release by visible light activation with the aim of photoreactivity at wavelengths where the tissue penetration depth of light is optimal.

In addition to the manganese-based PhotoCORMs mentioned above, several other systems based on iron and tungsten have also been reported (Fig. 1.14). The water-soluble dicarbonyl iron(cysteamine) PhotoCORM, compound **XLII** releases CO upon illumination at 470 nm under physiological conditions, as demonstrated by a membrane patch clamp experiment; since carbon monoxide can modulate the potassium channels as explained in Chapter 1.5.[100] A 365 nm photoexcitation of complex **XLIII** induced cytotoxicity in PC-3 human prostate cancer cells reportedly due to the CO release. However, it was also found that the loss of cell viability was probably due to the cytotoxicity of $Fe(N4Py)^{2+}$ generated after photolysis.[101]

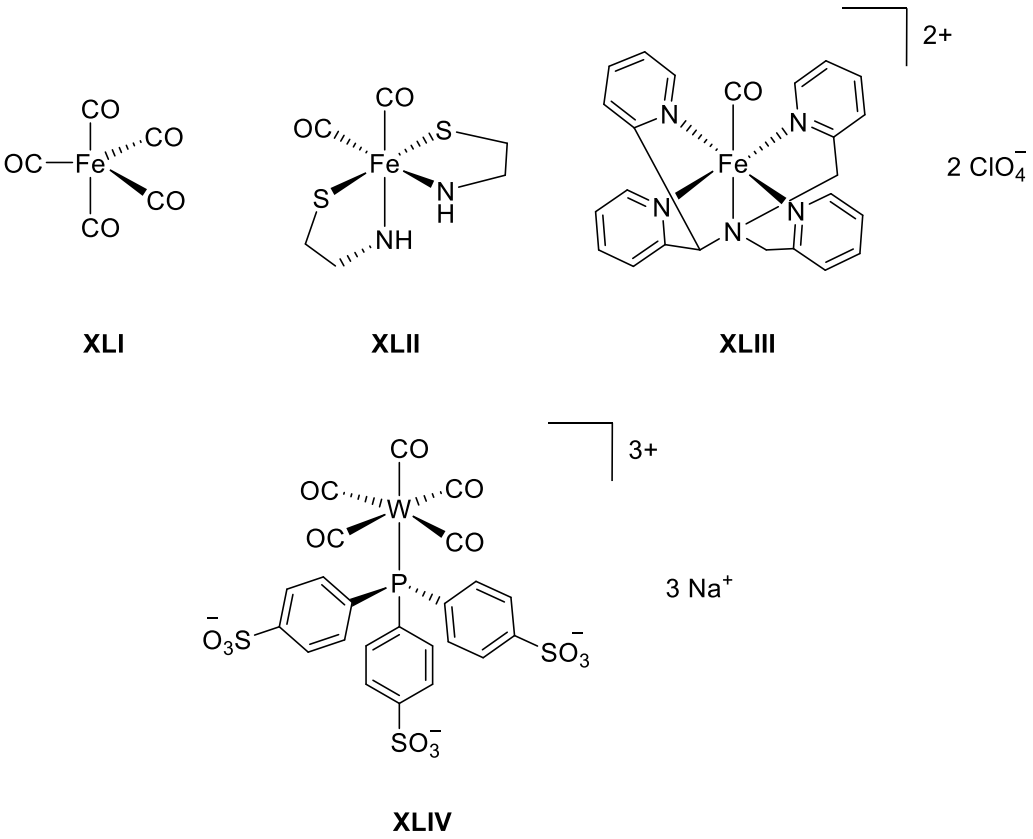

XLI **XLII** **XLIII**

XLIV

Fig. 1.14: PhotoCORMs based on iron and tungsten.

A water-soluble tungsten(0) carbonyl complex **XLIV**, $[W(CO)_5(tppts)]^{3-}$ (tppts = tris(sulfonatophenyl)phosphine) releases CO upon UV-light activation, as confirmed by FTIR analysis and ^{31}P NMR spectroscopy. The initial product $[W(CO)_4(H_2O)(tppts)]^{3-}$ upon photolysis in air further degrades *via* a slow secondary reaction leading to the release of an additional equivalent of CO.[101] Since the tissue penetration depth of light is wavelength-dependent,[102-104] it is difficult to target deeper tissues with light of shorter wavelength. Photoactivation at longer wavelengths such as the near infrared (NIR) region would be optimal also due to minimal photodamage. Thus photoactivation with low energy light should be a key property for the future design of the photoCORMs. Photoactivation at longer wavelengths can be achieved by conjugation of PhotoCORMs to photosensitizers with high extinction coefficient, two-photon excitation and the use of upconverting nanoparticles (UCNPs).

1.8 PhotoCORM conjugation to delivery vectors

In order to facilitate the selective delivery of PhotoCORMs to specific cells and tissues, it was envisioned that the conjugation of such CORMs to peptides as a targeting moiety might enable a selective uptake. In this context, Schatzschneider *et al*. attached $[Mn(CO)_3(tpm)]^+$ to a 5mer carrier peptide, either *N*-terminally or in the side-chain, using an azido or an iodoarene group (Fig. 1.15). With the Sonogashira or CuAAC click reaction, the PhotoCORM was successfully coupled to the peptide in a post-labeling strategy due to the sensitivity of the manganese tricarbonyl moiety towards the strongly acidic conditions employed during the peptide cleavage from the solid support.[105]

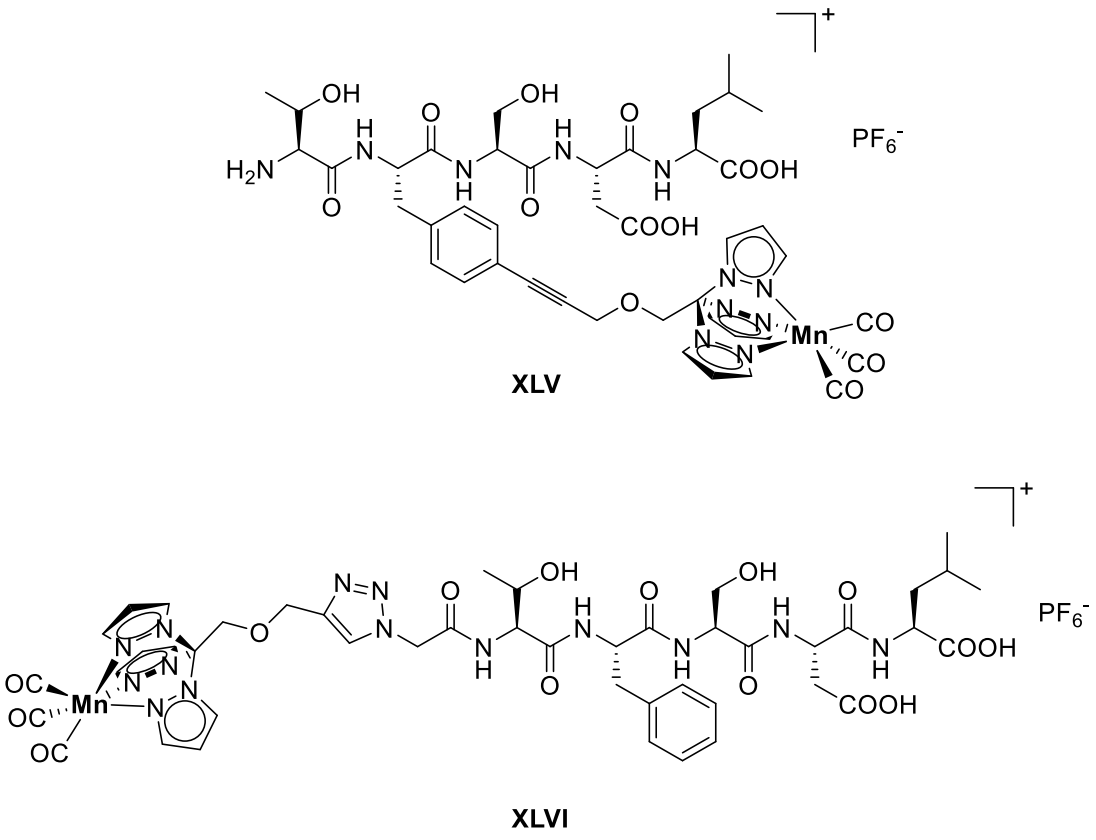

Fig. 1.15: $[Mn(CO)_3(tpm)]^+$-functionalized PhotoCORM peptide bioconjugates prepared by Sonogashira (above) or CuAAC click reaction (below).

In another strategy, the same group employed an ethoxypropargyl-functionalized $[Mn(CO)_3(tpm)]^+$ complex to couple it to azido-modified silica nanoparticles *via* a copper-catalyzed 1,3-dipolar azide-alkyne cycloaddition (CuAAC) reaction.[106] Since nanoparticles are known to passively accumulate in tumour tissues due to the

enhanced permeability and retention (EPR) effect, they are also promising delivery vehicles.[107-110] In that work, the PhotoCORM was covalently attached to silica nanoparticles with an average diameter of 20 nm and the conjugates were characterized by FTIR, electron-dispersive X-ray spectroscopy and atomic absorption spectroscopy. Dendrimers are another class of macromolecules that can be functionalized with organometallic complexes for cellular delivery.[111] Interest in such systems is stimulated due to their facile preparation and accumulation in tumor tissue, also as a result of the EPR effect. Thus, Smith *et al*. have synthesized first- and second generation tricarbonylmanganese(I)-functionalized polypyridyl metallodendrimers (Fig. 1.16). Upon photoactivation at 410 nm, the total amount of CO equivalents released was shown to increase from about 7 to 15 moles of CO per dendrimer molecule for the first and second generation conjugates.[112] Furthermore, it was shown that the $Mn(CO)_3$ groups in the dendrimers behave independently during light-activated CO release resulting in a linear scaling effect.

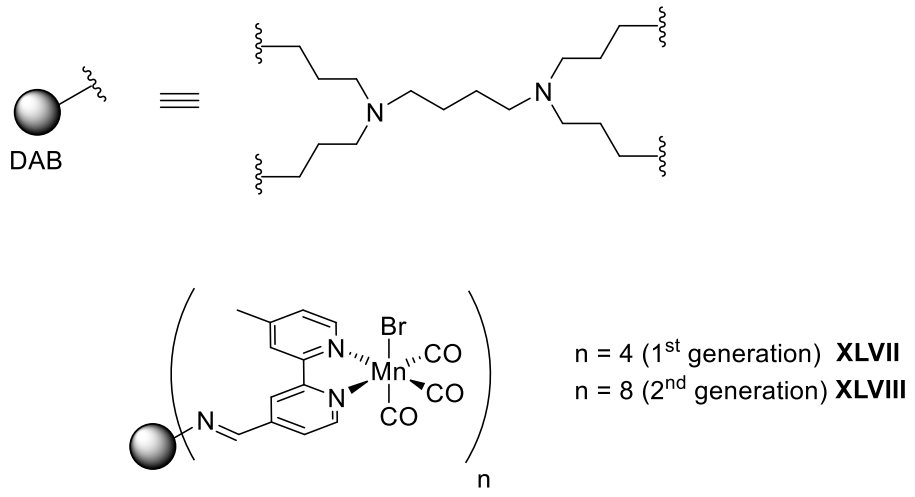

Fig. 1.16: First and second generation diaminobutane (DAB) CORM dendrimer conjugates.

1.9 *In vitro*/*in vivo* detection of carbon monoxide

Although the field of CO-releasing molecules is growing rapidly, the speciation of CO in a complex biological environment is still unknown due to the lack of methods that can selectively detect CO in an intact biological system. Some of the techniques used so far for CO detection are gas chromatography and electrochemical sensors, which however are limited for applications on living systems.[113-114] However, recently, two fluorescent probes capable of selectively detecting CO in living cells were reported. A genetically encoded fluorescent probe named COSer was designed by He *et al*. that is based on CooA, a CO-sensing dimeric heme protein. The fluorescent probe called COSer was then constructed by the fusion of cpVenus, a circularly permuted variant of the yellow fluorescent protein with the heme protein CooA.[115] The resulting probe gives a selective fluorescence response with a low detection limit of 0.5 μM and up to 1-2 μM of CO over other ligands such as NO, O_2, and CN^-.

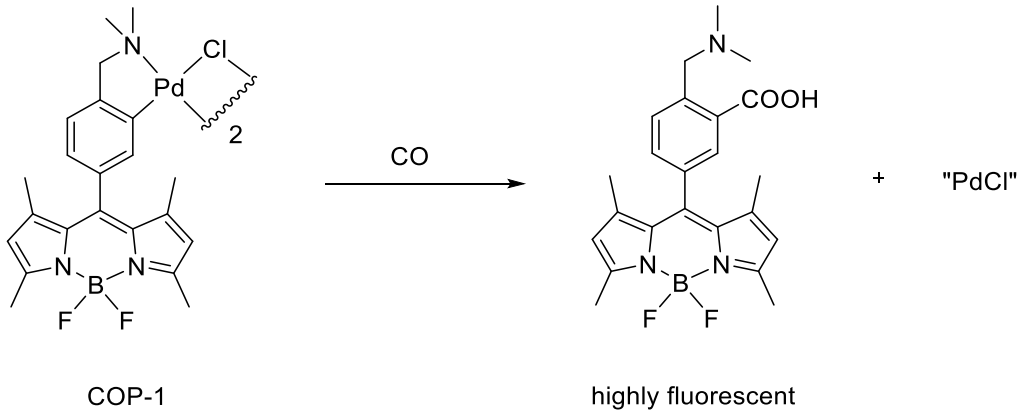

Scheme 1.4: Reactivity of COP-1 towards carbon monoxide, generating the fluorescent BODIPY species together with a "PdCl" fragment.

In another approach, Chang *et al*. designed CO-Probe 1 (COP-1) based on palladium-mediated carbonyl chemistry.[116] This compound is non-fluorescent in the absence of carbon monoxide but shows a strong fluorescence signal upon insertion of CO in the Pd-C bond, leading to the release of Pd metal and a BODIPY fluorescent dye (Scheme 1.4). An intracellular fluorescence signal was detected by confocal microscopy on HEK293T cells at a concentration of COP-1 of 1 μM against 50 μM of CORM-3 as the CO source. However, apart from its general suitability for CO detection, the "PdCl"

fragment is also generated and might have a biological activity of its own making it difficult in terms of future application.

An interesting and biocompatible water-soluble PhotoCORM $[Re(bpy)(CO)_3(PR_3)]^+$ (R = CH_2OH) was recently reported by the group of Ford.[117] Exhaustive photolysis at 405 nm in water results in the liberation of the CO *trans* to the phosphine ligand, producing an aqua compound (Scheme 1.5). Interestingly, both the PhotoCORM and the aqua compound formed are luminescent with emission wavelengths of 465-495 nm and 660 nm, respectively. This bifunctional photoactivated CO-releasing molecule can release CO upon light activation and at the same time act as a luminescent reporter of the site of its CO release.

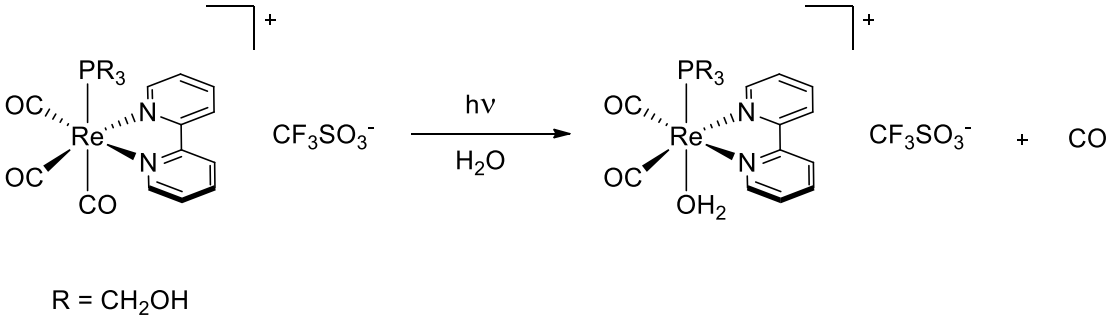

Scheme 1.5: Photolysis of $[Re(bpy)(CO)_3(thp)]^+$ (thp=tris(hydroxymethyl)phosphine) at 405 nm leads to formation of $[Re(bpy)(CO)_2(H_2O)(thp)]^+$.

1.10 Solid-phase peptide synthesis

Solid-phase peptide synthesis (SPPS) was developed by Merrifield in the early 1960s.[118] As depicted in Scheme 1.6, this method is based on the covalent attachment of the first amino acid which is *N*-protected *via* a carboxyl group to a solid polymer usually polystyrene [poly(phenylethene)] called as resin. The resin should be insoluble in the solvents used during peptide synthesis and is functionalized with the group to which the amino acid is linked by a covalent bond. A number of amino-protective groups are available, among which 9-fluorenylmethyloxycarbonyl (Fmoc) is the most preferred one due to the ease of deprotection under mild conditions using an organic base such as 30% piperidine in DMF.[119] Carboxyl group protection is usually carried out using either a benzyl ester or *tert*–butoxycarbonyl ester (*t*-Boc), which is further deprotected under harsh acidic conditions using hydrofluoric acid (HF) and trifluoroacetic acid (TFA), respectively. The successive coupling of amino acids involves repeated cycles of removal of the *N*-terminal protective group of the previous amino acid in the chain and coupling of the next amino acid using coupling reagents such as DIEA, HOBt, and HBTU. The activation of amino acid is performed with a base *N,N'*-diisopropylethylamine (DIEA) which initiates the active ester formation between the *N*-protected amino acid to be attached and uranium salts such as 1-hydroxybenzotriazole (HOBT).[120]

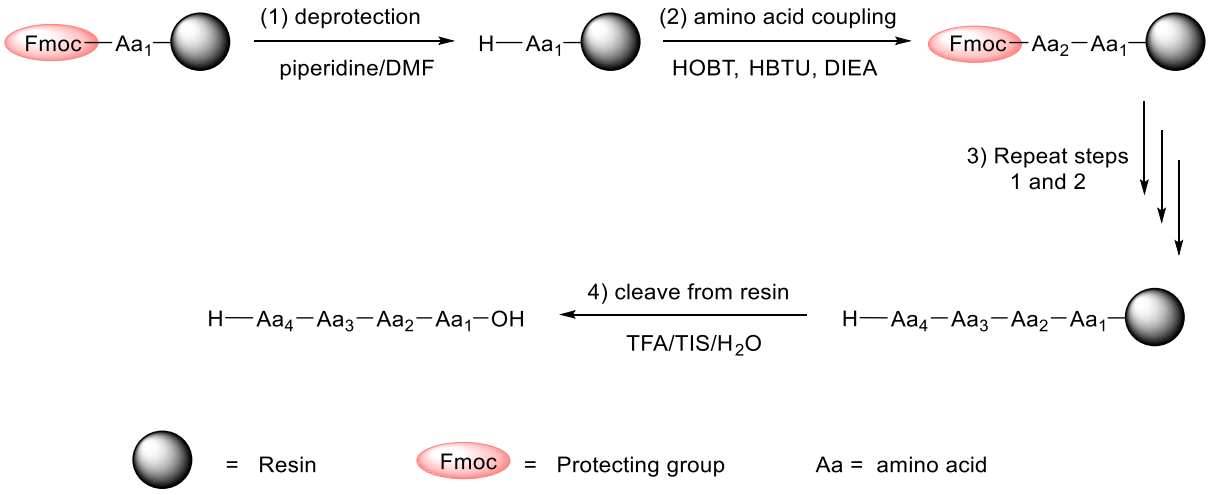

Scheme 1.6: Synthesis of peptides by solid-phase peptide synthesis (SPPS).

The final step involves the cleavage of the peptide from the solid support under strongly acidic conditions and is typically done using 90% trifluoroacetic acid (TFA), 5% water and 5% tri(isopropyl)silane (TIS). The latter is added to trap the carbocations and undesired radicals formed during the cleavage procedure.[121] However, it can also be replaced by other reagents such as thiols and phenols. Final purification of the peptide is usually necessary to analyse the purity of peptide and to remove the side products formed during amino acid side chain modification and peptide cleavage steps. The purification of peptides is usually carried out by preparative reverse-phase high performance liquid chromatography (HPLC) and the final confirmation of purity is done by analytical HPLC using different solvent mixture as an eluent.

1.11 Bioorthogonal click reactions

In 2001, Sharpless, Kolb and Finn introduced the concept of "click" reactions for the rapid assembly of molecular building blocks intended to give a high-yield product with little or no byproducts, which works under diverse reaction conditions.[122] In their original work, the reaction of organic azides with alkynes and olefins was studied. However, due to the low reaction rate, the groups of Fokin and Sharpless[123] as well as Meldal[124] independently reported the use of copper(I) as a catalyst for click reactions which is now well known as the copper-catalyzed azide-alkyne cycloaddition or simply CuAAC "click" reaction. The reaction is highly selective and transforms the organic azides and terminal alkynes into the corresponding 1,4-disubstituted 1,2,3-triazoles, whereas the uncatalyzed reaction works at higher temperature and give rise to a mixture of 1,4- and 1,5-triazole regioisomers (Scheme 1.7).

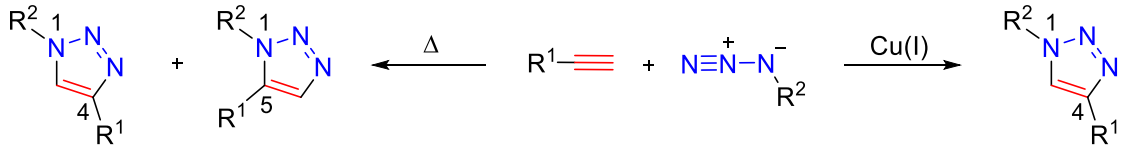

Scheme 1.7: Huisgen 1,3-dipolar cycloaddition (left) and copper(I) catalyzed azide-alkyne cycloaddition (CuAAC, right).

The first step in the mechanism of the CuAAC click reaction is the π-coordination of the alkyne to the copper resulting in the formation of a copper(I) acetylide followed by the activation of the azide. As a result, the azide becomes more electrophilic and a strained copper metallacycle is formed in the next step. Subsequently, a reductive elimination of copper species from an energetically favourable copper triazolide complex results in 1,4-disubstituted 1,2,3-triazole as shown in Scheme 1.8. The most commonly used source for Cu(I) is copper(II) sulfate and is generated by the use of an in situ reducing agent like sodium ascorbate. This is the preferred reductant due to its effectiveness in generating catalytically active Cu(I).[125] Furthermore, in order to maintain copper in its +1 oxidation state and reduce reactive oxygen species generated by ascorbate, the tris(benzyltriazole)methyl amine (TBTA) ligand is widely employed. The ligand also significantly accelerates the reaction as well. However, other triazolyl

amine ligands have also been studied due to the poor solubility of TBTA in water.[126] Despite the wide applicability of the CuAAC reaction, the combination of copper and sodium ascorbate is known to generate reactive oxygen species, which is deleterious to biological system. Hence, there is an interest to perform the click reaction under catalyst-free conditions.

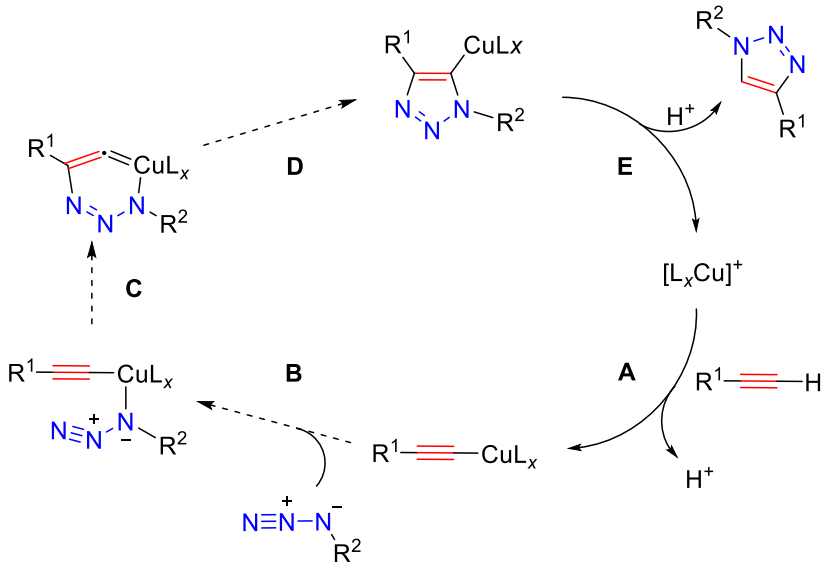

Scheme 1.8: Proposed mechanism for the CuAAC click reaction.

Chemoselective ligation on the other hand, has become an essential tool for chemical modification of biomolecules. Further, both aldehydes and ketones are known to have history in modification of proteins and can be introduced in biomolecules.[127-128] There are mainly two steps involved in the chemical modification of a biomolecule. First, the biomolecule is tagged with a metabolic chemical reporter which is then treated in the second step with a probe molecule with an orthogonal functionality.[128] For example, in a typical imine-based reaction, a carbonyl group reacts under acidic condition with primary amines. However, the equilibrium of this reversible imine is susceptible towards the formation of free carbonyl group under hydrolytic conditions. Compared to imines, oximes have a higher stability due to the α-effect of the oxygen atom adjacent to the nitrogen in groups such as aminoxy (Scheme 1.9). The formation of the oxime bond is much faster at acidic pH but only proceeds poorly at pH 7.[129] However, when aniline is used as a nucleophilic catalyst, a 400-fold accelerated ligation rate was reported in aqueous solution at pH 4.5 and still, a 40-fold acceleration was achieved

at pH 7 which extends the applicability of the oxime ligation to submillimolar concentration.[130]

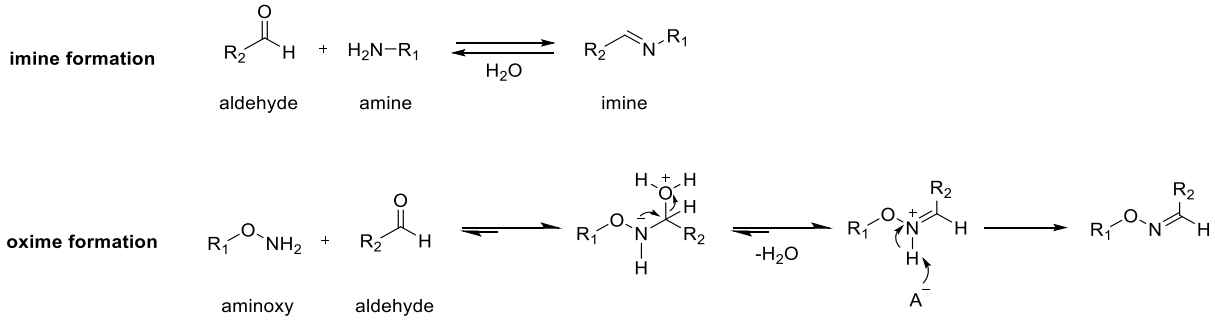

Scheme 1.9: Formation of hydrolytically unstable imine (top) and stable oxime-bonds (bottom).

Thus, the oxime ligation has been used to attach metal complexes to biomolecules under catalyst-free conditions.[131] A large number of glycoconjugates, labeled bioconjugates, and cyclic peptides have also been synthesized by the oxime ligation, either *via* introduction of aldehyde tags or aminoxy groups.[132-134]

2 Motivation

Carbon monoxide is endogenously generated by enzymatic processes in higher organisms, including humans, and shows a wide range of physiological effects. To utilize these for biomedical applications, metal-carbonyl complexes are a promising choice as a solid storage and delivery agent for carbon monoxide. Many of the initial complexes investigated in the context of *CO-releasing molecules* (CORMs) released CO under physiological conditions through ligand exchange reactions with medium on a short time scale. Release of CO *via* photoactivation, however, allows the precise control of the location, timing, and dosage of CO released. Thus, PhotoCORMs are a subject of intense research and might be useful for the treatment of skin cancer, for example.

Thus, the aim of this work is to investigate manganese(I) tricarbonyl complexes as potential photoinducible CO-releasing molecules (PhotoCORMs), and also their potential conjugation to bio(macro)molecules for the targeted cellular delivery of CO. This choice was guided by the fact that *fac*-Mn(I) tricarbonyl complexes are oxidatively stable and allow the introduction of tridentate ligands which stabilize the complex. Thus, the first section of the present work deals with the synthesis of manganese(I) tricarbonyl complexes with a tridentate ligand based on the bis(pyrazolyl)ethylamine (bpea) moiety with a pendant *para*-substituted phenyl group. This allows the introduction of different functional groups for bioconjugation *via* Sonogashira coupling or CuAAC "click" reactions. The study of photoinduced CO release from the complexes and identification of possible intermediates was carried out using solution IR spectroscopy and DFT calculations. The myoglobin assay was used to determine the CO release rate and stoichiometry. Finally, the light-induced CO release was further studied in living cells using the small-molecule fluorescent switch-on carbon monoxide probe COP-1.

Since peptides are attractive targeting vectors for the delivery of metal-based compounds, the conjugation of $[Mn(bpea)(CO)_3]^+$ complexes to a TGF-β_1 binding peptide was explored based on Sonogashira coupling or CuAAC click reactions. As an alternative conjugation strategy, the bioorthogonal and catalyst-free oxime ligation

was also explored. A comparative study of the stability of the oxime *vs*. the triazole linkage was done by HPLC analysis and the photoactivated CO release from the peptide conjugate to be compared to the parent compound.

In the final section of this work, the carrier function of dendrimers was explored since they are known to accumulate in tumour tissue due to the enhanced permeability and retention (EPR) effect. The functionalization of dendrimers based on different core structures with the Mn(I) tricarbonyl complexes was studied and the effect of photoactivation at different excitation wavelengths explored.

3 Results and discussion

3.1 Manganese(I) tricarbonyl complexes as PhotoCORMs

3.1.1 Synthesis and characterization of *fac*-[Mn(N-N-N)(CO)$_3$]$^+$ complexes

The introduction of tris(pyrazolyl) (tp) scorpionate ligand by Trofimenko[135] has led to the search of new *N-N-N* chelators for complexes with possible biomedical applications. In this direction, several new tridentate ligands such as tris(pyrazolyl)methane[136] and tris(pyrazolyl)phosphanes were reported in recent years.[97] Furthermore, their corresponding *fac*-Mn(CO)$_3$ complexes were shown to exhibit photoinduced cytotoxicity against HT29 colon cancer cells.[95] However, such tridentate ligands do not allow for the facile introduction of different functional groups for coupling reactions with carrier molecules such as nanoparticles, peptides and proteins. As a result, one of the aims of this work was to synthesize new bis(pyrazolyl)ethylamine (bpea) ligands and their corresponding manganese tricarbonyl complexes as CO-releasing molecules (CORMs). The bpea ligand allows a modular and flexible introduction of functional groups for bioorthogonal coupling by condensation of the amine with different *para*-substituted benzaldehydes. In this context, the desired functionalized tridentate ligands **9-14** were synthesized by the condensation reaction of bpea **5** with para-substituted benzaldehydes **6-8** (Scheme 3.1).

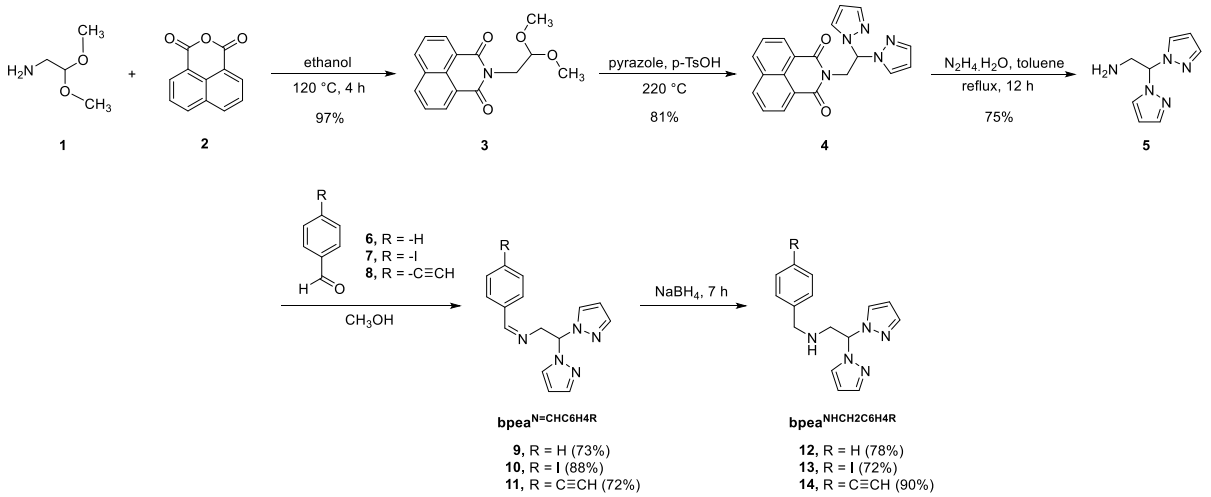

Scheme 3.1: Synthesis of bpea-based ligands **9-14**.

The three ligands **9-11** contain an imine backbone with a *para*-substituted phenyl group where R = H, I, or C≡C-H. Due to the known instability of the imines towards hydrolysis, further reduction of imines **9-11** with sodium borohydride gave the corresponding reduced stable amine ligands **12-14**. The iodo and alkynyl functional groups at the *para*-position further offer options for bioconjugation *via* a Sonogashira or CuAAC "click" reaction. All ligands were obtained in good purity without the need for further purification by column chromatography. The ligands **9-14** were reacted with manganese pentacarbonyl bromide in refluxing acetone in the dark. The resulting complexes **15-20** were obtained as yellow solids after precipitation with potassium hexafluorophosphate (Scheme 3.2) and are soluble in polar solvents such as acetone, dimethylsulfoxide, methanol, and acetonitrile, but insoluble in water.

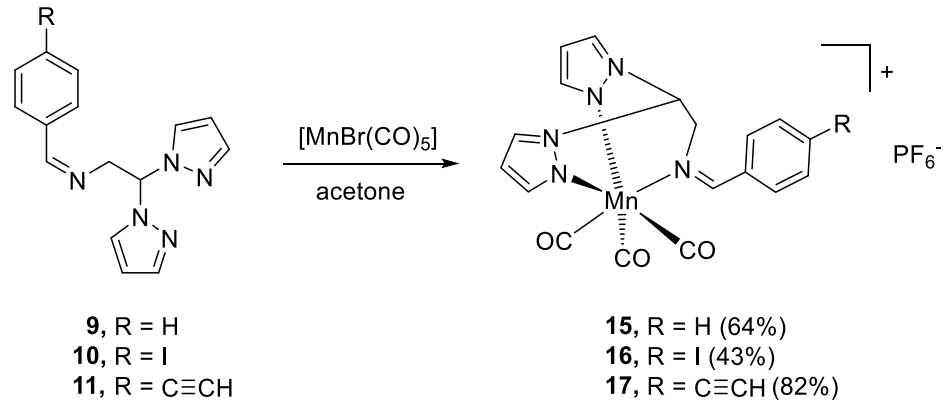

9, R = H
10, R = I
11, R = C≡CH

15, R = H (64%)
16, R = I (43%)
17, R = C≡CH (82%)

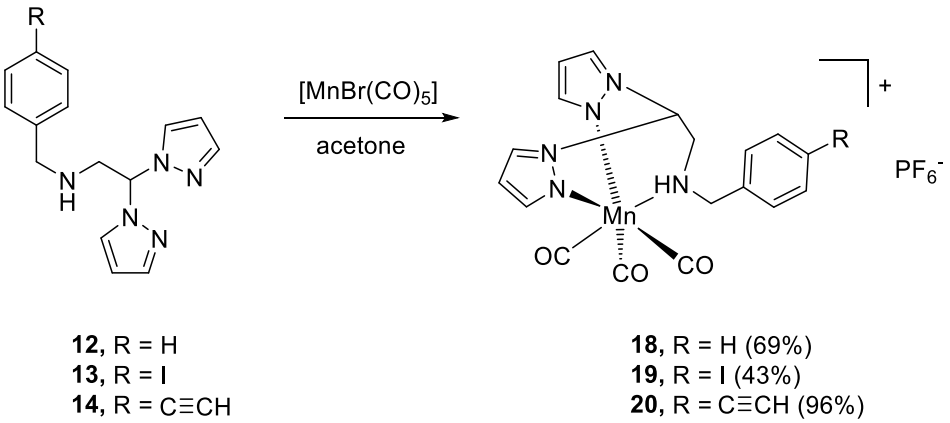

12, R = H
13, R = I
14, R = C≡CH

18, R = H (69%)
19, R = I (43%)
20, R = C≡CH (96%)

Scheme. 3.2: Synthesis of *fac*-[Mn(bpea)(CO)$_3$]$^+$ complexes **15-20**.

Table 3.1: IR vibrational band positions (cm^{-1}) of ligands (**9-14**) and complexes (**15-20**).

Ligands	$\tilde{\upsilon}$ (C=N)	Complexes	$\tilde{\upsilon}$ (C=N)	$\tilde{\upsilon}_{asymm}$ (C≡O)	$\tilde{\upsilon}_{symm}$ (C≡O)
9	1649	**15**	1625	1932	2040
10	1644	**16**	1624	1931	2043
11	1641	**17**	1633	1930	2041
12	-	**18**	-	1939	2045
13	-	**19**	-	1928	2041
14	-	**20**	-	1928	2040

The ATR IR spectra of all complexes show two intense vibrational bands at around 1930 and 2040 cm^{-1}, which are assigned to the asymmetric and symmetric C≡O stretching vibrations (Figure 3.1). Additionally, complexes **15-17** show a band at around 1630 cm^{-1} and is assigned to the C=N stretching vibration. Whereas, in ligands **9-11** they appear at around 1640 cm^{-1}. The C=N stretching vibrations of the complexes **15-17** show a shift of 20 cm^{-1} towards the lower wavenumbers compared to the free ligands **9-11** due to its coordination to the metal center. However, no prominent effects were observed due to the different substituents in the *para*-position (Table 3.1).

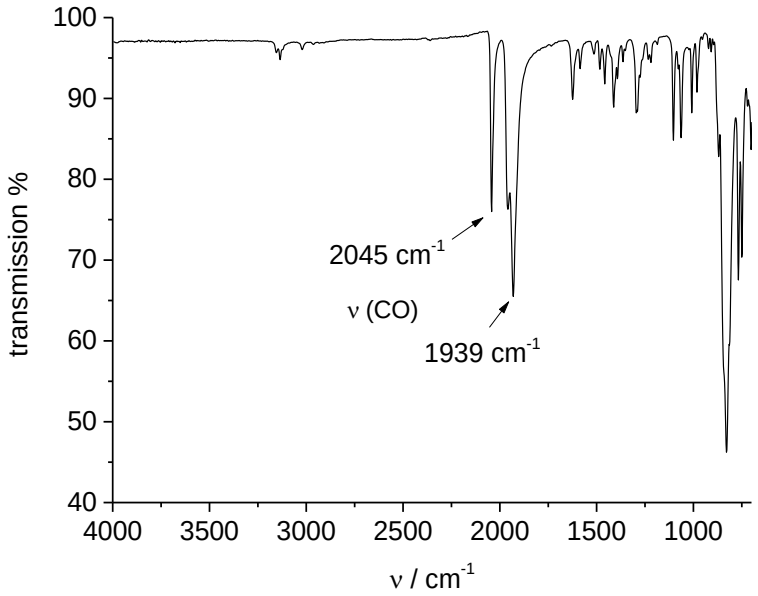

Fig. 3.1: ATR-IR spectrum of $[Mn(bpea^{NHCH2C6H5})(CO)_3]PF_6$ **18**.

The ^{1}H-NMR spectrum of ligands **9-11** shows a signal at around 8.2 ppm that is assigned to the imine proton, whereas, in complexes **15-17** it appears at about 9.4 ppm. This signal for imine proton shows a downfield shift for **15-17** compared to the ligands **9-11** due to its coordination to the Mn(I) center. A triplet at 6.8 ppm with an integral of one is assigned to the methine proton of the imine ligands **9-11**. In case of complexes **15-17**, it appears downfield at around 7.7 ppm. In both the ligands **9-11** and complexes **15-17**, a doublet at 4.6 ppm with an intensity of two belongs to the methylene protons. Two doublets at 7.6 and 7.5 ppm with an intensity of two are assigned to the $H_{3,3'}$ and $H_{5,5'}$ protons of the pyrazole ring, respectively, for ligands **9-11**. In complexes **15-17**, they also appear as a doublet at 8.3 and 8.4 ppm, respectively. Furthermore, a doublet of doublet appears at 6.2 ppm for **9-11** which is assigned to the remaining $H_{4,4'}$ protons of the pyrazole. In case of **15-17**, they further appear at 6.75 ppm. In complexes **18-20**, a broad singlet appears at 5.6 ppm which is now assigned to the amine (N*H*) proton. In case of amine ligands **12-14**, a signal at 6.5 ppm is observed and is assigned to the methine proton, whereas, in its corresponding complexes **18-20**, the same signal now appear at 7.4 ppm. A doublet appears between 3.7 – 3.5 ppm for amine ligands **12-14**, which belongs to the methylene protons next to the methine proton. However upon coordination to the Mn(I) center, in complexes **18-20**, these methylene protons show a diastereotopic splitting pattern and appear as individual signals at 3.5 and 3.1 ppm, respectively, due to the splitting by ^{3}J coupling with the neighbouring C*H* and N*H* potons (Table 3.2 and Figure 3.2). The ligands **12-14** shows a singlet with an integral of two which is assigned to the other methylene protons alpha to the phenyl ring. They also show a diastereotopic splitting in complexes **18-20**, and now appear as individual signals at 4.6 and 4.2 ppm, respectively. Additionally, for **18-20**, four doublets with an integral of one each appear between 8.5 – 8.4 ppm and are assigned to the H_3, $H_{3'}$, H_5, and $H_{5'}$ protons of the coordinated pyrazole rings. Similarly, two doublets with an integral of one each between 6.7 – 6.6 ppm belongs to the H_4, and $H_{4'}$ protons of the pyrazole. Whereas, in amine ligands **12-14**, the pyrazole protons appear as doublets at 7.6, 7.5 and 6.2 ppm. The complete NMR spectra of the complexes **15-20** are shown in appendix.

Table 3.2: ^{1}H-NMR chemical shifts of (i) imine ligands (**9-11**) and its corresponding Mn complexes (**15-17**) and (ii) amine ligands (**12-14**) and its corresponding Mn complexes (**18-20**). The chemical shifts δ are reported in ppm.

(i)

compound	C***H***	C***H***$_2$	N=C***H***	***H***$_{3,3'}$-pz	***H***$_{4,4'}$-pz	***H***$_{5,5'}$-pz
9	6.80	4.66	8.20	7.67	6.25	7.56
10	6.77	4.64	8.11	7.65	6.25	7.55
11	6.78	4.67	8.17	7.66	6.25	7.55
15	7.81	4.67	9.41	8.38	6.75	8.45
16	7.76	4.63	9.34	8.38	6.75	8.43
17	7.73	4.63	9.39	8.37	6.74	8.43

(ii)

compound	C***H***	C***H***$_2$	N***H***	C***H***$_2$-Ph	***H***$_{3,3'}$-pz	***H***$_{4,4'}$-pz	***H***$_{5,5'}$-pz
12	6.54	3.70	nd	3.83	7.58	6.27	7.50
13	6.52	3.66	nd	3.76	7.57	6.27	7.55
14	6.37	3.49	nd	3.69	7.92	6.28	7.49
18	7.41	3.52, 3.12	5.59, br	4.69, 4.20	8.51, 8.39	6.74, 6.66	8.33, 8.27
19	7.43	3.55, 3.12	5.60, br	4.68, 4.21	8.51, 8.40	6.74, 6.67	8.32, 8.27
20	7.24	3.03, 2.73	5.92, br	4.35, 3.96	8.49, 8.42	6.68, 6.63	8.26, 8.18

nd – not detected.

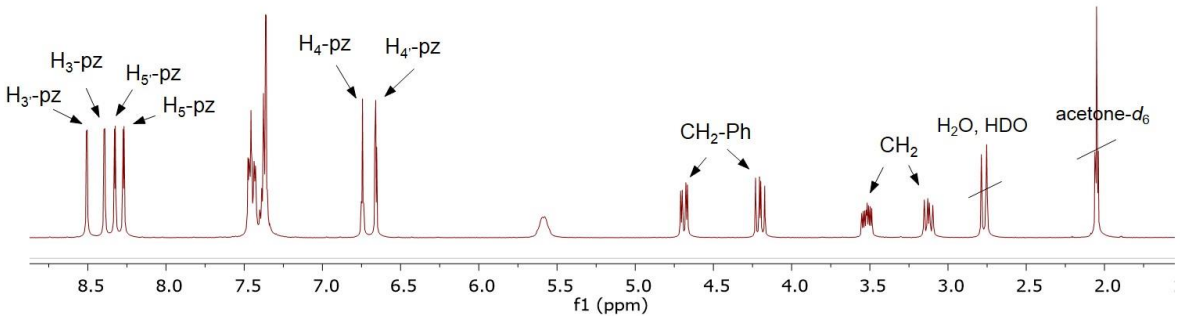

Fig. 3.2: 400 MHz ^{1}H-NMR spectrum of [Mn(bpea^{NHCH2C6H5})(CO)$_3$]PF$_6$ **18** in acetone-d_6.

3.1.2 X-ray structure analysis

Single crystals suitable for X-ray diffraction were obtained either by slow diffusion of *n*-hexane into acetone (for **16** and **19**) or *n*-pentane into dichloromethane for **20** (Figures 3.3 - 3.5; crystallographic parameters are summarized in the appendix). Compounds **16** and **19** crystallized in the monoclinic space group *P*2(1)*n* and triclinic space group *P*-1, respectively.

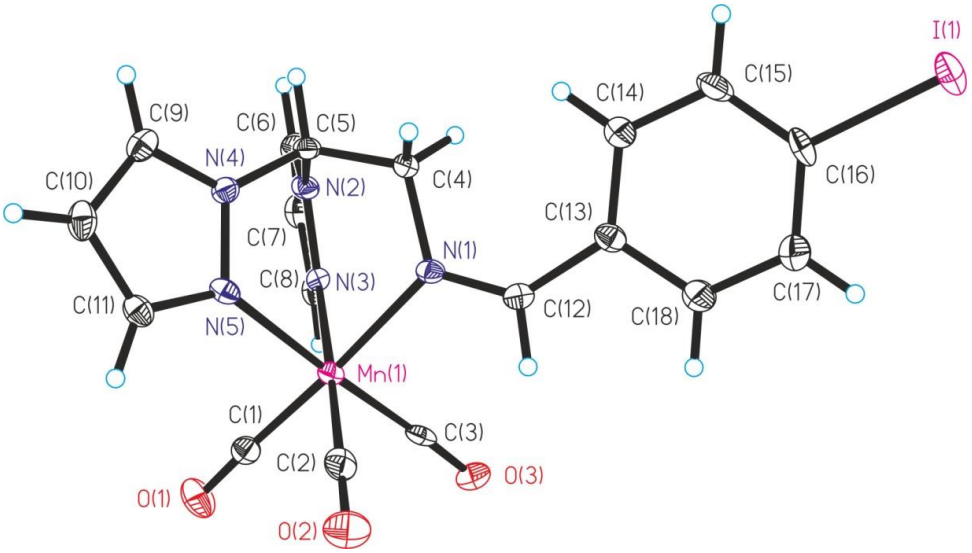

Fig. 3.3: Molecular structure of the cation of **16** in the solid state determined by single crystal X-ray diffraction. Thermal ellipsoids are drawn at the 50% probability level. The hexafluorophosphate counterion has been omitted for clarity. Selected bond distances (Å) and bond angles (°): Mn1-C1 1.812(3), Mn1-C2 1.822(4), Mn1-C3 1.804(4), Mn1-N1 2.091(2), Mn1-N3 2.042(3), Mn1-N5 2.042(3), C1-O1 1.144(4), C2-O2 1.141(4), C3-O3 1.147(4), C1-Mn1-N1 175.09(13), C2-Mn1-N3 178.48(13), C3-Mn1-N5 176.86(12), N1-Mn1-N5 84.56(10), N1-Mn1-N3 84.58(10), N5-Mn1-N3 85.81(10), C1-Mn1-C3 87.30(14), C1-Mn1-C2 89.34(14), C3-Mn1-C2 89.93(15).

The three nitrogen atoms of the tridentate bpea ligand, two from the pyrazole group and one from the imine, are located opposite to the carbonyl ligands to give an approximately C_{2v} symmetry. The three CO ligands are coordinated to the Mn(I) center in a facial manner. Furthermore, the imine *vs*. amine coordination to the Mn(I) center affects the Mn1-N1 bond distance, which is 2.091(2) Å in **16** but is extended to 2.133(2) Å in **19**. The Mn-C and C≡O bond distances show less variations of about 0.01-0.02 Å from **16** to **19**, indicating that the imine *vs*. amine ligation do not significantly affect the $Mn(CO)_3$ core. The bond angles around the Mn(I) center are close to 90° and 180°, respectively, as expected for a near-octahedral coordination environment.

However, the orientation of the phenyl ring relative to the bis(pyrazolyl) core differs from **16** to **19** due to the sp^2 *vs*. sp^3 nature of the nitrogen atoms, respectively. In **16**, the phenyl ring is located in the mean plane intersecting the N3-Mn1-N5 and C2-Mn1-C3 angles, defined by Mn1, N1, C4, and C5 and is slightly distorted relative to the C=N group, with a (Mn1-N1-C4-C5)-(N1-C12-C13) angle of 8.1° and a (N1-C12-C13)-phenyl angle of 9.7°. In **19**, the sp^3 nature of N1 leads to significantly expanded dihedral angles of 48.7° and 93.7° for the orientation of these atoms, respectively.

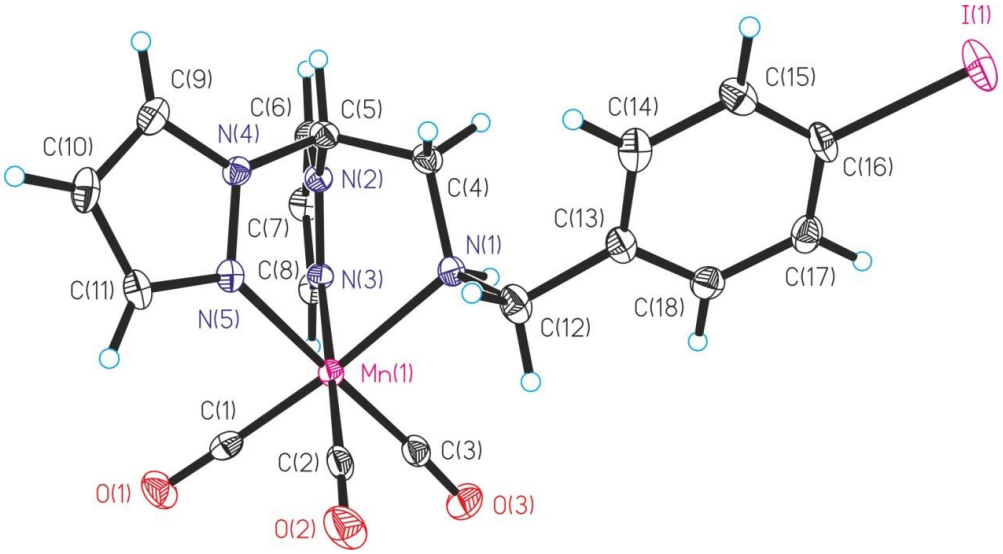

Fig. 3.4: Molecular structure of the cation of **19** in the solid state determined by single crystal X-ray diffraction. Thermal ellipsoids are drawn at the 50% probability level. The hexafluorophosphate counterion has been omitted for clarity. Selected bond distances (Å) and bond angles (°): Mn1-C1 1.805(2), Mn1-C2 1.801(2), Mn1-C3 1.818(2), Mn1-N1 2.133(2), Mn1-N3 2.036(2), Mn1-N5 2.035(2), C1-O1 1.153(3), C2-O2 1.151(3), C3-O3 1.146(3), C1-Mn1-N1 174.30(8), C2-Mn1-N3 177.90(9), C3-Mn1-N5 178.03(9), N1-Mn1-N5 86.73(7), N1-Mn1-N3 82.87(7), N5-Mn1-N3 85.70(7), C1-Mn1-C3 90.18(10), C1-Mn1-C2 88.85(9), C3-Mn1-C2 89.50(10).

Compound **20** crystallizes in monoclinic space group *P*1 21/*c*1. The tridentate bpea ligand is facially coordinated to the Mn(I) center with three carbonyl ligands opposite to each of the nitrogen donor atoms. The Mn-C bond distances range from 1.794(3) to 1.812(3) Å and the Mn-N bond distances from 2.041(3) to 2.128(2) Å. These are very similar to the amine complex **19**. The bond angle C2-Mn1-N1 which is 92.68(9) in **19**, is reduced by about 1.34 Å to 91.34(11) Å in **20**. The C≡C bond distance is 1.183(5). This alkyne slightly extends the carbon-carbon bond distances of the phenyl ring from 1.378(3) to about 1.390(4), in comparison to **19** which has an iodo group.

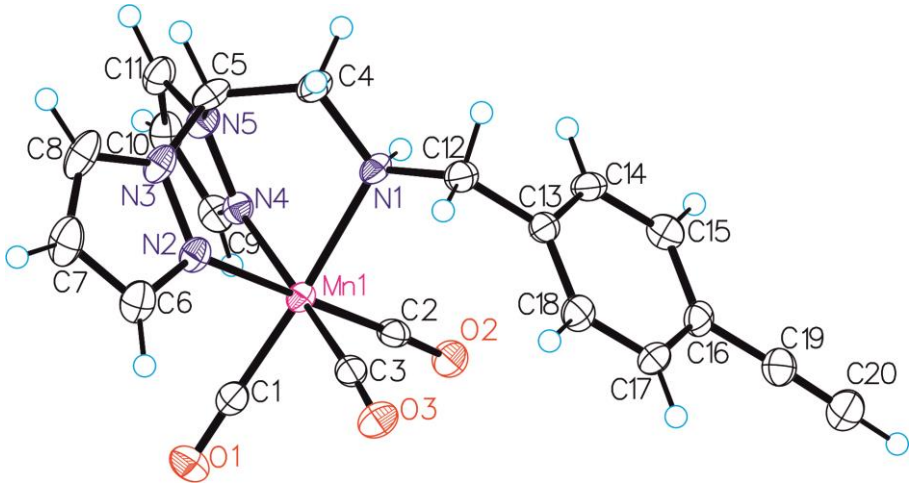

Fig. 3.5: Molecular structure of the cation of **20** in the solid state determined by single crystal X-ray diffraction. Thermal ellipsoids are drawn at the 50% probability level. The hexafluorophosphate counterion has been omitted for clarity. Selected bond distances (Å) and bond angles (°): Mn1-C1 1.794(3), Mn1-C2 1.812(3), Mn1-C3 1.812(3), Mn1-N1 2.128(2), Mn1-N2 2.048(2), Mn1-N4 2.041(3), C1-O1 1.147(4), C2-O2 1.141(3), C3-O3 1.146(4), C1-Mn1-N1 173.56(12), C2-Mn1-N2 178.89(12), C3-Mn1-N4 175.17(11), N1-Mn1-N2 88.39(10), N1-Mn1-N4 80.97(10), N2-Mn1-N4 86.15(10), C1-Mn1-C3 88.90(14), C1-Mn1-C2 88.08(13), C3-Mn1-C2 91.88(13).

3.1.3 Photolysis and stability studies

The electronic absorption spectra of complexes **15-20** were measured in dimethylsulfoxide (Figure 3.6). All complexes show a broad maximum centered at around 350 nm which is assigned to a metal-to-ligand charge transfer (MLCT) transition. The extinction coefficients of the complexes are collected in Table 3.3. They are smaller for the amine complexes due to the decreased electronic communication with the manganese center. The *para*-substituents on the phenyl ring do not show any notable effect on the extinction coefficients of the complexes.

Table 3.3: Absorption maxima and molar extinction coefficient of complexes **15-20**.

Complex	λ_{max} [nm]	ε_{λ} [M^{-1} cm^{-1}]	$\varepsilon_{365\ nm}$ [M^{-1} cm^{-1}]
15	341	3457 ± 58	3005 ± 54
16	348	4412 ± 57	3547 ± 39
17	347	5500 ± 308	5496 ± 95
18	355	2136 ± 78	2017 ± 85
19	356	2276 ± 78	2155 ± 64
20	355	2154 ± 23	2395 ± 87

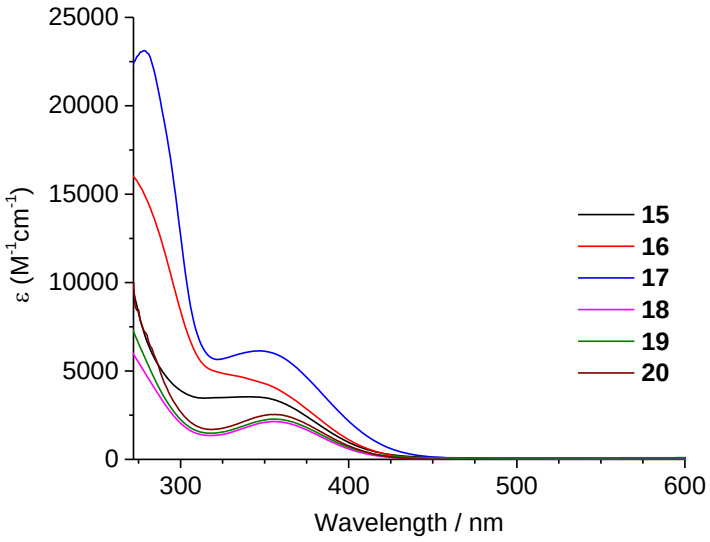

Fig. 3.6: Electronic absorption spectra of complexes **15-20** in DMSO.

The stability of complexes **15-20** was studied in aerated dimethylsulfoxide due to their poor solubility in water. Upon incubation in the dark, the complexes showed no change in absorbance for up to 14 h. However, upon illumination at 365 nm using a UV lamp, a decrease in intensity of the MLCT band centered at around 350 nm was observed, and reached a plateau value after 5-10 min. The dark stability and photolysis of complex **18** is shown in Figure 3.7 (for complexes **15-17** and **19-20** see appendix). The half-life ($t_{1/2}$) and the rate constant (k_{CO}) of all the complexes upon exhaustive photolysis in DMSO are collected in Table 3.4. The imine complexes **15-17** tend to release CO at a slightly faster rate, by a factor of about two, compared to the amine complexes **18-20**.

Table 3.4: Half-life and rate-constant values of CO release as determined in DMSO solution.

Compound	**15**	**16**	**17**	**18**	**19**	**20**
Half-life, $t_{1/2}$ (min)	1.8	1.1	1.0	1.5	1.6	2.5
Rate constant, k_{CO} (10^{-3} s^{-1})	6.4	10.6	12.1	7.8	7.4	4.6

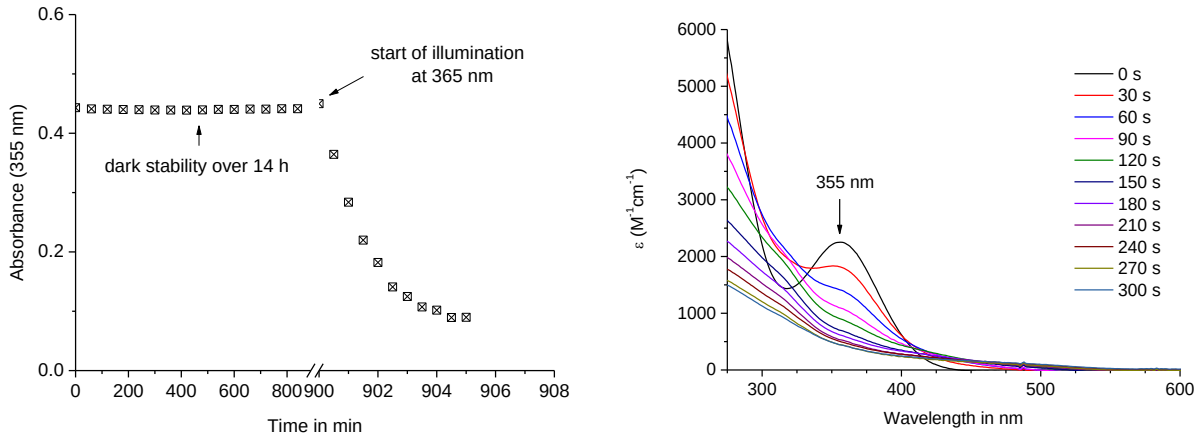

Fig. 3.7: Absorption changes at 355 nm of **18** in DMSO upon incubation in the dark for 14 h and subsequent photolysis with an UV lamp at 365 nm (left). UV/Vis spectral changes of **18** (0.2 mM) upon photolysis with increasing illumination time, 0-300 s. (right).

3.1.4 CO release studies and quantum yield measurements

The photoinduced CO release from complexes **15-20**, was investigated using the myoglobin assay.[137-138] In a typical experiment, a 15 μM solution of the metal complex in dimethylsulfoxide was added to 60 μM of freshly prepared horse skeletal muscle myoglobin MbFe(II) in phosphate-buffered solution (PBS) at pH 7.4, which was then reduced with an excess of sodium dithionite under an inert atmosphere in the dark. The addition of sodium dithionite prevents the oxidation of Fe(II) to Fe(III), which has a low binding affinity for CO. The conversion of MbFe(II) to MbFe(II)CO upon illumination was monitored by UV/Vis spectroscopy as described in Chapter 5.1.2. Initially, the stability of the complexes was assessed in the dark under the conditions of the myoglobin assay. In the dark, **15-20** showed no spectral changes in the Q-band region of myoglobin as shown in Figure 3.8 for complex **18**. This was followed immediately by illumination at 365 nm using a UV lamp which lead to a decrease in absorption of MbFe(II) at 557 nm while the peaks for MbFe(II)CO at 540 and 577 nm increased in intensity with illumination time (Figure 3.9). The amount of MbCO formed was then calculated using the molar extinction coefficient of MbCO [$\lambda_{540\ nm}$ = 15.4 $(mM)^{-1}\ L^{-1}$].[73]

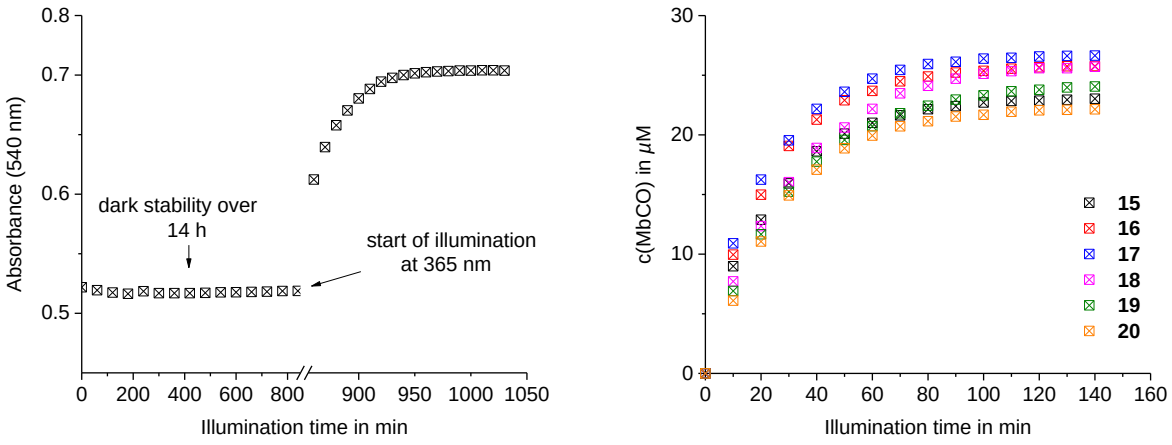

Fig. 3.8: Change in absorption at 540 nm of complex **18** (10 μM) in the dark over a period of 14 h and upon illumination at 365 nm in the presence of myoglobin (60 μM) and sodium dithionite (10 mM) under dinitrogen (left). Amount of MbCO (in μM) formed with increasing illumination time of a solution of complex **15-20** in 0.1 M PBS pH 7.4 (right).

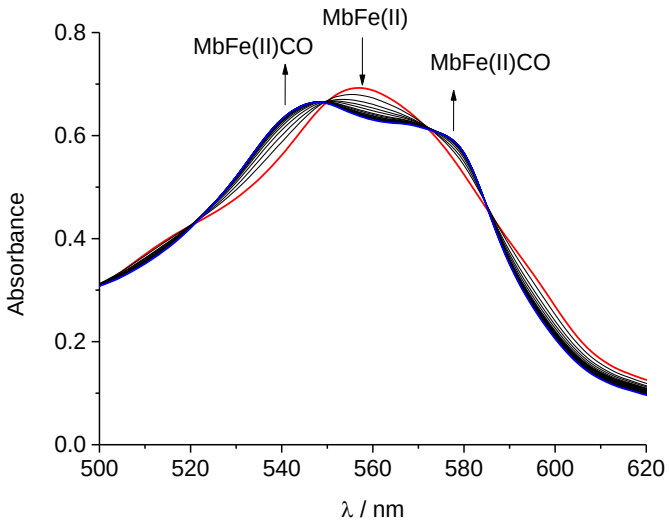

Fig. 3.9: UV/Vis spectral changes in the Q-band region of myoglobin (60 μM in 0.1 M PBS pH 7.4) with complex **18** (10 μM solution in DMSO) with increasing illumination time at 365 nm.

Complexes **15-20** release two equivalent of CO under the conditions of the myoglobin assay upon illumination at 365 nm. The CO release results from the myoglobin assay for complexes **15-20** are summarized in Table 3.5. The half-lives of the imine complexes **15-17** are slightly shorter than those of the amine complexes **18-20**, which could be due to the slightly higher rate constants of imine *vs* amine complexes, and thus a faster CO release rate (see Table 3.4 for rate constants). Thus, these Mn(I) tricarbonyl complexes have been established as photoactivatable CO-releasing molecules (PhotoCORMs) and prodrugs with good dark stability.

Table 3.5: CO-release data and reaction quantum yield values at 365 nm of **15-20**.

Compound	Conc. of MbCO (μM)	Equiv. of CO released	Half-life, $t_{1/2}$ [a](min)	Reaction quantum yield ($Ø_{365\ nm}$)[b]
15	22.5 ± 0.3	2.3 ± 0.1	21.6 ± 0.3	(5.9 ± 0.2) x 10^{-3}
16	24.8 ± 0.8	2.5 ± 0.1	21.3 ± 0.5	(6.3 ± 0.4) x 10^{-3}
17	23.2 ± 0.2	2.3 ± 0.1	18.5 ± 0.2	(6.6 ± 0.1) x 10^{-3}
18	20.7 ± 0.3	2.1 ± 0.1	25.8 ± 0.2	(4.4 ± 0.2) x 10^{-3}
19	21.3 ± 0.3	2.1 ± 0.1	28.7 ± 0.8	(4.3 ± 0.2) x 10^{-3}
20	21.7 ± 0.4	2.1 ± 0.1	19.3 ± 0.2	n.d

[a] Under the conditions of myoglobin assay. [b] Calculated using a photon flux of the UV lamp of (2.82 ± 0.05) x 10^{-8} Einstein s^{-1}. n.d - not determined

The reaction quantum yield of complexes **15-20** was determined by ferrioxalate actinometry as explained in Chapter 5.1.6.[139] For the imine complexes **15-17** they are slightly higher than that of the amine complexes **18-19**. The quantum yield values are much lower than those reported for $[Mn(tpa)(CO)_3]ClO_4$ and $[Mn(dpa)(CO)_3]Br$ at similar wavelengths and are in the order of 10^{-3}.[98] The lower quantum yield values of the present system is due to the internal shielding effect caused by the horse skeletal muscle myoglobin which shows significant absorption at the excitation wavelength of 365 nm.

3.1.5 CO release monitored by solution IR spectroscopy

In addition to the myoglobin assay, the CO release from **15** and **18** upon photoactivation at 365 nm was investigated by IR spectroscopy in DMSO. To achieve a signal intensity greater than 0.1 for the symmetrical vibrational band at 2045 cm^{-1}, the concentration of the complexes was set to 9 mM, which is 5 times higher than the concentration used in the UV/Vis experiments (0.2 mM). The liquid IR cell was filled with the sample solution and was illuminated at 365 nm for fixed time intervals followed by the recording of the IR spectra. The spectral changes in the solution IR of **15** and **18** are displayed in Figure 3.10.

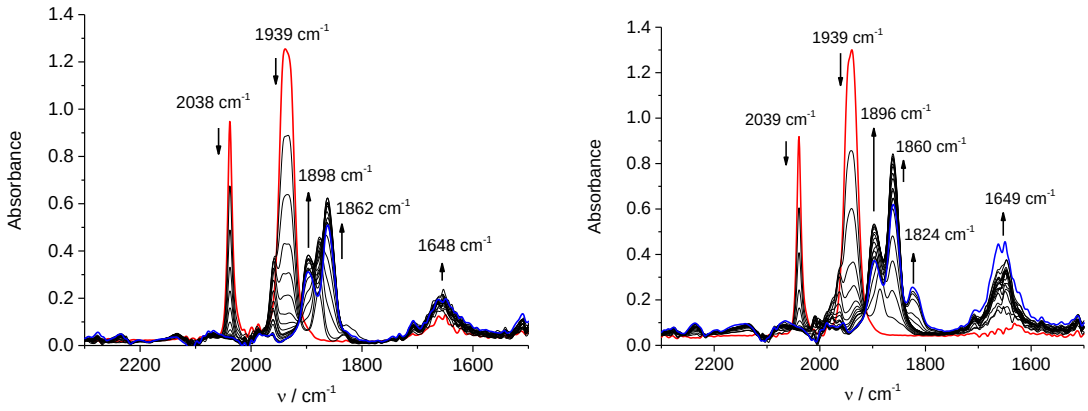

Fig. 3.10: Spectral change in the solution IR of **15** (left, 9 mM solution in DMSO) and **18** (right, 9 mM solution in DMSO) upon illumination at 365 nm for 22 and 36 min, respectively.

The intensity of the symmetric and antisymmetric bands at 2038 and 1939 cm^{-1} decreases upon illumination, while three new bands appear in the region between 1640 and 1900 cm^{-1}. The two new bands at 1898 and 1860 cm^{-1} grow in intensity with increase in illumination time for **18**. These two bands are presumably due to the formation of *cis*-$Mn(CO)_2$ species after the release of the first equivalent of CO. Free CO was not detected at around 2140 cm^{-1} due to it having a very weak IR signal below the detection limit of the instrument.

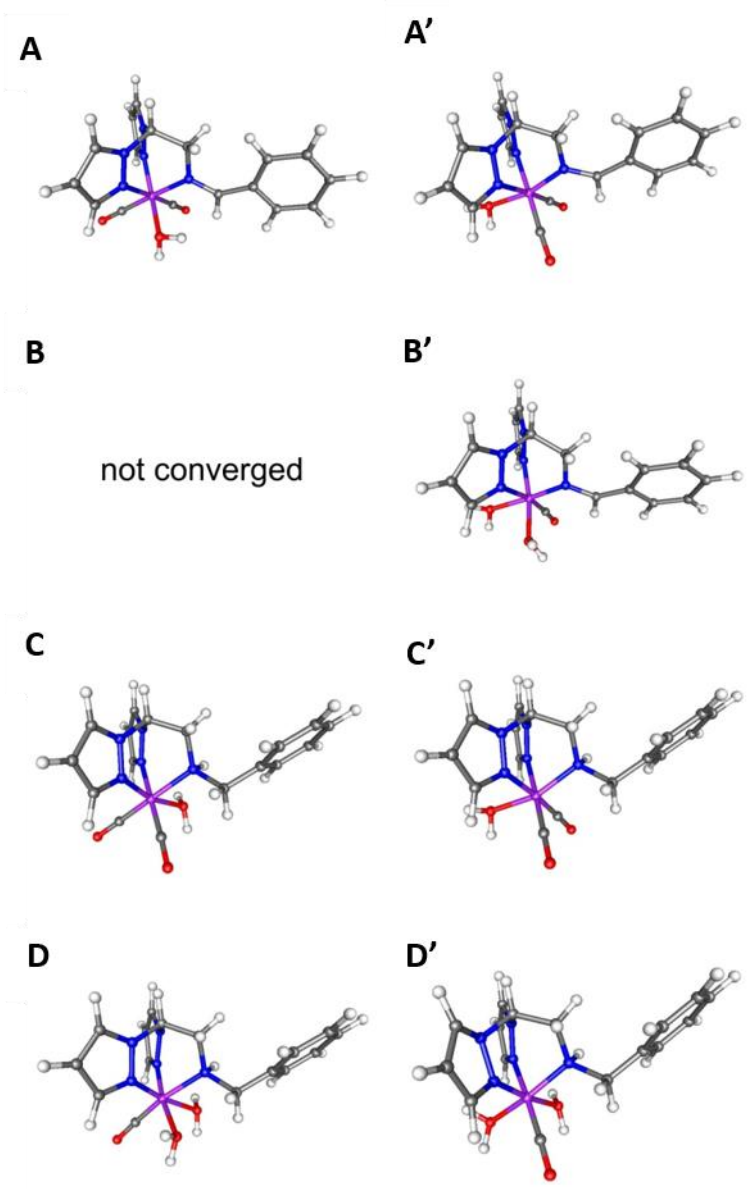

Fig. 3.11: DFT-optimized structures of the cationic unit of iCORM intermediates **A-D** obtained with the BP86 functional after subsequent removal of carbonyl ligands and replacement with one or two solvent water molecules. Figure adapted from Ref. [168] with permission from The Royal Society of Chemistry.

In order to obtain an insight into the potential photoproducts and intermediates, DFT calculations were carried out to assign these species. Two isomers were studied for each of the CO release steps, depending on whether the CO was removed either from a position *trans* to the pyrazole (**A**, **C**, **D**) or *trans* to the amine/imine group (**A'**, **B'**, **C'** and **D'**) as shown in Figure 3.11. As listed in Table 3.6, the scaled calculated vibrational frequencies were in good agreement with the experimental values, in absolute terms, less than 40 cm^{-1}. The broad antisymmetrical and the symmetrical C≡O stretches are overestimated by a maximum of about +2 and +40, respectively, compared to the experimental band positions for imine complex **15**. On the other hand, the antisymmetrical C≡O stretches are underestimated by a maximum of about +30 and the symmetrical C≡O stretches are overestimated by +40 compared to the experimental bands for complex **18**. However, upon illumination, the release of first CO was followed by the coordination of DMSO solvent molecule and the subsequent coordination of second DMSO molecule would result in the release of second equivalent of CO. However, the DMSO solvent molecule was replaced by water molecule as model for solvent. Although the first intermediate is identified as a *cis*-$Mn(CO)_2$ species, further ligand substitution could result in the formation of monocarbonyl species (**D**, **D'**) upon exhaustive photolysis.

Table 3.6: Scaled calculated vibrational frequencies for potential products **A** – **D** resulting from the exhaustive photolysis of **15** and **18** at 365 nm. The deviations from the experimental values are given in parentheses (in cm^{-1}).

Mode	A	A'	B[a]	B'
$\tilde{\upsilon}$ (CH=N)	1560 (-89)	1554 (-95)	—	1629 (-20)
$\tilde{\upsilon}_{antisym}$ (C≡O)	1862 (+2)	1863 (-2)	—	—
$\tilde{\upsilon}_{sym}$ (C≡O)	1935 (+39)	1940 (+44)	—	1848 (+24)[b]

Mode	C	C'	D	D'
$\tilde{\upsilon}_{antisym}$ (C≡O)	1846 (-16)	1835 (-27)	—	—
$\tilde{\upsilon}_{sym}$ (C≡O)	1935 (+37)	1919 (+21)	1825[b,c]	1826[b,c]

[a] Could not be converged in the low-spin state. [b] Monocarbonyl species, only one C≡O vibrational mode. [C] Not observed.

3.1.6 *In vitro* detection of photoinduced CO release using COP-1 as a fluorogenic switch-on probe

As described in Chapter 1.9, Chang *et al*. reported a small-molecule system composed of a BODIPY switch-on fluorescent dye coupled to a cyclometalated dimeric palladium metal called as COP-1, which is cleaved upon reaction with carbon monoxide. Due to its general suitability for CO detection, the photoinduced CO-release from **18** was assessed using COP-1 both in buffered solution and in living cells. Initially, the response of COP-1 fluorescence to the increasing concentrations of **18** was investigated in PBS buffer both in presence and absence of UV light. Upon addition of different concentrations of **18** (0-100 μM) to COP-1 (10 μM in PBS) followed by photoactivation at 365 nm for 30 min, a non-linear increase of COP-1 fluorescence was observed. Whereas, the non-illuminated sample with exactly same conditions showed no fluorescence intensity (Figure 3.12).

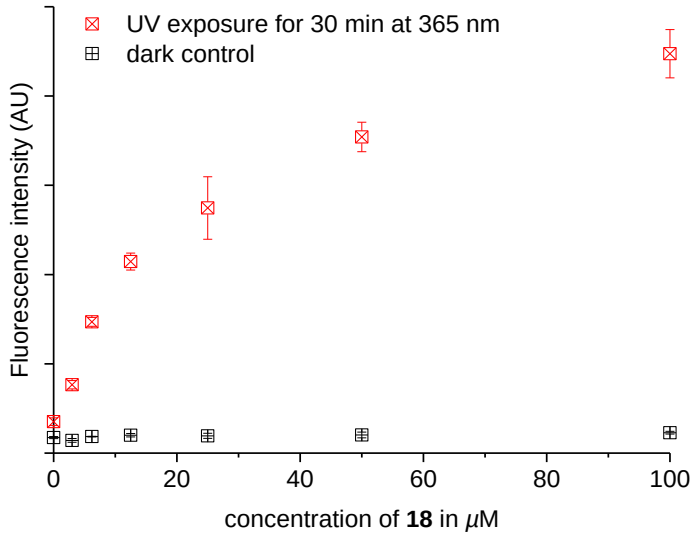

Fig. 3.12: Dose-dependent fluorescence response of COP-1 (10 μM) in PBS to photoinduced release of CO at increasing concentrations of **18** (data points are shown at 0, 3, 6, 12.5, 25, 50, and 100 μM). Fluorescence intensity was measured at an emission wavelength, λ_{em} = 510 nm with λ_{ex} = 475 nm. The experiments were performed in quadruplicate with data expressed as mean fluorescence intensity ± SD. Figure adapted from Ref. [168] with permission from The Royal Society of Chemistry.

A fluorescence response of 1 : 10 molar ratio of COP-1 to **18** was studied in order to achieve complete saturation of the fluorescence signal. However, a non-linear response of COP-1 fluorescence was observed and the signal was not fully saturated. Nonetheless, the COP-1 system validates a response to photoinduced carbon monoxide release from the PhotoCORM in the PBS buffer.

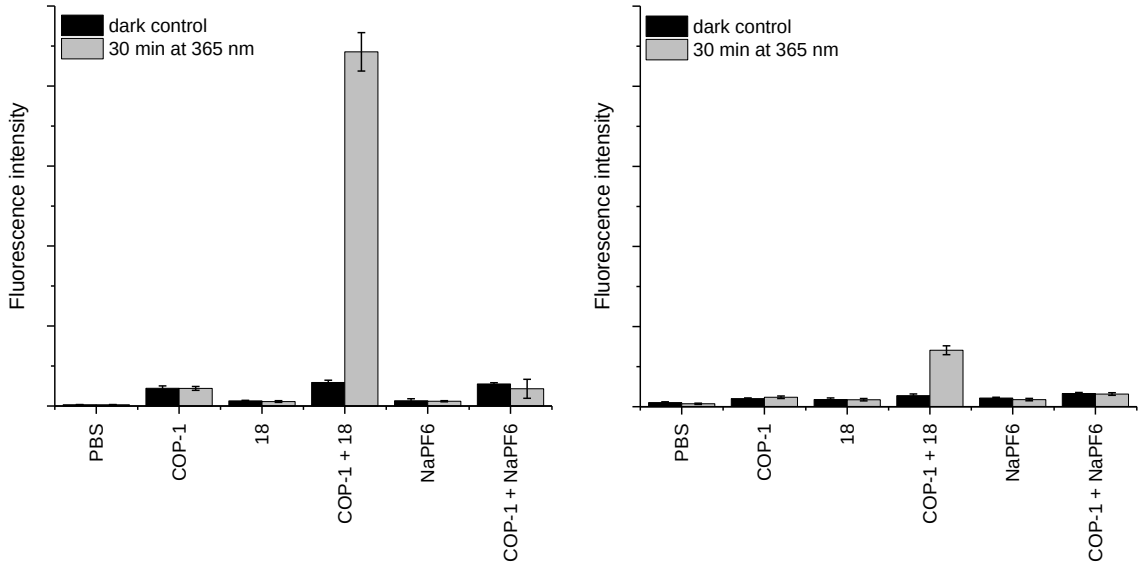

Fig. 3.13: Fluorescence intensity (λ_{ex} = 475 nm, λ_{em} = 510 nm) observed upon incubation of human umbilical vein endothelial cells (HUVECs) with **18** (100 μM) in either the supernatant (left) or the cell-containing fraction (right). Black bars: dark control; grey bars: illuminated for 30 min at 365 nm. COP-1 (10 μM) in PBS, $NaPF_6$ (100 μM) in PBS were used as controls. Data are expressed as mean fluorescence intensity ± SD with experiments performed in quadruplicate. Figure adapted from Ref. [168] with permission from The Royal Society of Chemistry.

Additionally, the light-induced CO release from **18** was investigated in human umbilical vein endothelial cells (HUVECs) using the COP-1 fluoregenic probe. The cells were incubated in microtiter plates with 10 μM COP-1 in PBS followed by the addition of **18** (100 μM) in the dark. The cells were then illuminated with 365 nm light for 30 min while a control experiment was performed under the same conditions but without illumination. Additionally, PBS, COP-1, and sodium hexafluorophosphate in PBS served as controls, both in the presence and absence of light. Both the cell-containing fraction and the supernatant were assessed for their individual fluorescence signal. Initially, the signal for the supernatant consisting the controls

$NaPF_6$ which is the source of counter ion, PBS, COP-1, **18** and mixture of COP-1 and $NaPF_6$ were assessed. Negligible fluorescence was detected for all the controls both in the dark and upon illumination at 365 nm for 30 min. A mixture of COP-1 (10 μM) and **18** (100 μM) in PBS showed no signal when placed in the dark, however upon illumination for 30 min at 365 nm a 15-fold increase in fluorescence intensity was observed (Figure 3.13 left). Similarly, the controls of the cell-containing fractions were also assessed for the fluorescence signal and remained especially non-emissive or at the basal level both in the dark and upon illumination. Further, the mixture of COP-1 and **18** from the cell containing fraction showed only a 5-fold increase in fluorescence intensity for the illuminated *vs* non-illuminated. The 3-fold difference in the fluorescence intensity between the cell containing fraction and the supernatant could be explained due to the improper cellular uptake of either the COP-1 probe or **18**, or both, although the diffusion of CO into the atmosphere cannot be ruled out. Nonetheless, it was demonstrated that COP-1 can serve as an *in-vitro* probe for the detection of light-induced CO release from PhotoCORMs.

3.1.7 Discussion

A series of six manganese(I) tricarbonyl complexes based on the bis(pyrazolyl)ethylamine (bpea) moiety with a pendant *para*-substituted phenyl group, in which R = H, I, or C≡C-H, were synthesized. All the complexes were obtained in good yield and fully characterized, including X-ray structure analysis for three compounds. The iodo and alkyne functional groups offer a handle for bioconjugation *via* a Sonogashira or CuAAC "click" reactions (see next chapter). All six compounds are stable in dimethylsulfoxide solution in the dark for a period of up to 14 h. Exhaustive photolysis of the imine complexes release CO at a slightly faster rate compared to the amine compounds, with half-lives in the range of 1-2 min. Furthermore, under the conditions of myoglobin assay, all compounds (**15-20**) show a rapid release of two equivalents of CO upon illumination at 365 nm with half-lives in the range of 20-30 min.

Solution IR spectroscopy showed the formation of two new bands between the region 1640 and 1900 cm^{-1}, which are assigned as *cis*-$Mn(CO)_2$ intermediates. This was further supported by DFT calculations with the possibility of formation of monocarbonyl species upon exhaustive photolysis. Further, in order to detect the CO release under physiological conditions, a small-molecule fluoregenic switch-on carbon monoxide probe COP-1 was used. Initially, a dose-dependent behaviour of COP-1 with 10-fold excess of **18** in PBS was investigated. In the dark, no fluorescence signal was detected, however, upon illumination a non-linear fluorescence response was observed with the concentration of **18**. Further, a light induced release of carbon monoxide from **18** was studied in HUVEC cells. When placed in the dark no fluorescence signal was observed for the additives and for the complex **18**. Upon illumination at 365 nm, COP-1 showed a significant response to the complex **18** both in the supernatant and the cell-containing fraction. A 15-fold increase in the fluorescence signal was observed for the supernatant compared to a 5-fold increase for the cell containing fraction, which could be due to the impaired cellular uptake of either the COP-1 probe or compound **18**, or both. Therefore, further investigations are needed to address a well-defined cellular uptake of both COP-1 and PhotoCORMs.

3.2 Manganese(I) tricarbonyl PhotoCORM peptide conjugates

3.2.1 Synthesis of peptide conjugates by CuAAC "click" reaction and oxime ligation

Solid-phase peptide synthesis (SPPS) allows the facile synthesis of peptides of variable amino acid sequences, and has also been used in the conjugation of robust organometallic half-sandwich complexes to peptide chains by amide bond formation.[140-142] Peptides are attractive targeting vectors for the cellular delivery of metal-based compounds. Most metal complexes, however, are not stable under the strong acidic conditions used to cleave the peptide from the solid support. Thus, a post-labeling strategy usually needs to be followed using bioorthogonal coupling reactions.[128-143] In this work, the synthesis of PhotoCORM-peptide conjugates by the palladium-mediated Sonogashira coupling, copper-catalyzed azide-alkyne cycloaddition (CuAAC) reactions, and catalyst-free oxime ligation were explored. For the Sonogashira coupling and CuAAC click reaction, **16** and **17** functionalized with iodo and alkynyl groups were used. The synthesis and CO release properties of these compounds are described in chapter 3.1. In order to explore the catalyst-free oxime ligation, a novel aldehyde-functionalized tridentate ligand bpea^{NHCH2C6H4CHO}, **25** was synthesized starting from 2,2-bis(pyrazolyl)ethylamine, **5**. This was condensed with 4-(diethoxymethyl)benzaldehyde **22** and then, without the isolation of imine **23** was reduced with sodium borohydride in methanol to give **24** as shown in Scheme 3.3.

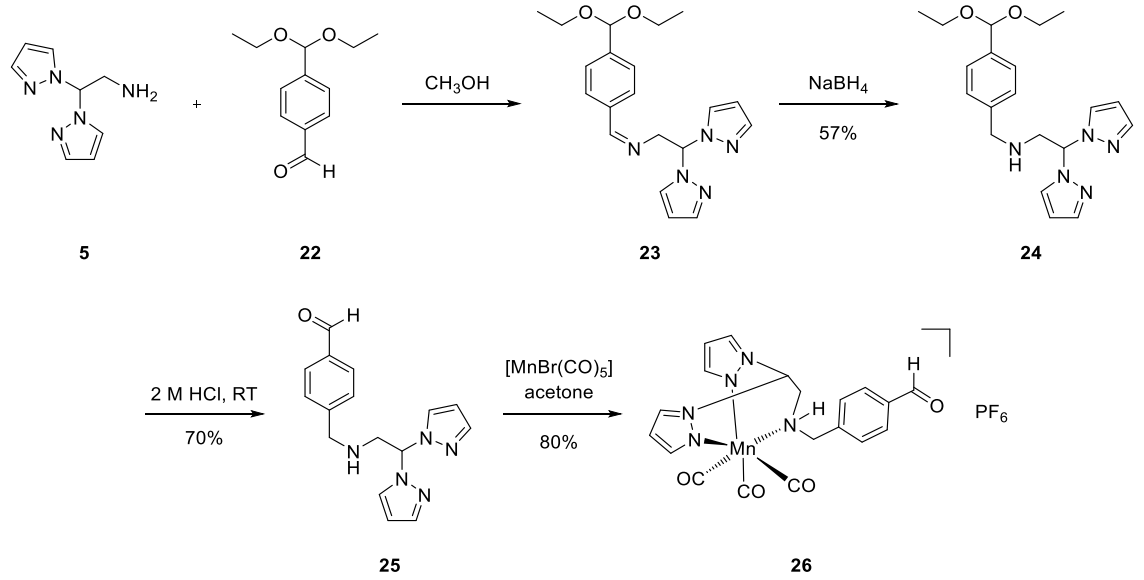

Scheme 3.3: Synthesis of [Mn(bpea^{NHCH2C6H4CHO})(CO)$_3$]PF$_6$ **26** for oxime ligation.

The acetal group was deprotected with 2 M hydrochloric acid to give the aldehyde-functionalized ligand **25**. The reaction of **25** with manganese pentacarbonyl bromide in acetone at reflux under dinitrogen and exclusion of light afforded the corresponding *fac*-[Mn(bpea^{NHCH2C6H4CHO})(CO)$_3$]$^+$ complex **26** in good yield. The compound is soluble in polar solvents such as acetone, dimethylsulfoxide, methanol, and acetonitrile but insoluble in water. The IR spectrum of the complex shows two prominent bands at 2036 and 1928 cm^{-1}, which are assigned to the symmetrical and antisymmetrical C≡O stretching vibrations, respectively (Figure 3.14). Additionally, a peak at 1691 cm^{-1} is assigned to the C=O vibration of the aldehyde functional group.

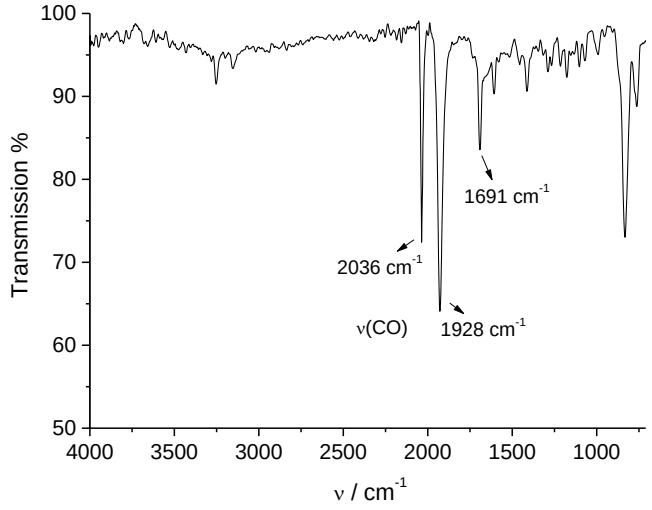

Fig. 3.14: ATR-IR spectrum of [Mn(CO)$_3$(bpea^{NHCH2C6H4CHO})]PF$_6$ **26**.

The ^{1}H NMR spectrum of **26** shows a signal at 10.0 ppm and is assigned to the aldehyde proton. Four doublets with an integral of one each appear between 8.5 – 8.3 ppm and are assigned to the H$_3$, H$_{3'}$, H$_5$, and H$_{5'}$ protons of the coordinated pyrazole rings. However, in ligand **25** these protons appear as doublets with an integral of two each at 7.6 and 7.5 ppm. Two doublets at 7.9 and 7.7 ppm belongs to the four phenyl protons of **26**. Furthermore, a singlet at 7.5 ppm is assigned to the methine proton of the complex **26** and in case of the ligand **25** it appears more upfield at 6.5 ppm. A broad singlet at 5.8 ppm belongs to the N*H* proton of **26** as a result of coordination to the metal center. Additionally, two doublets with an integral of one each appear between 6.6 – 6.8 ppm and are assigned to the H$_4$, and H$_{4'}$ protons of the pyrazole of **26**, which

however, appear as a doublet at 6.3 ppm for **25**. A singlet at 3.9 ppm belongs to the methylene protons at the alpha position with respect to the coordinated amine group of the ligand **25**, however, show a diastereotopic splitting in complex **26** and now appear as individual signals at 4.8 and 4.3 ppm, respectively. Furthermore, a doublet at 3.7 ppm for ligand **25** belongs to the methylene protons next to the methine. However, upon coordination to the Mn(I) center, in complex **26**, they appear as a doublet at 3.6 and 3.2 ppm with ^{2}J coupling constants of 13.2 and 13.8 Hz, respectively, due to the diastereotopic environment generated by metal coordination. These signals are further split by coupling with the neighbouring methine and N*H* protons (Figure 3.15). The positive-mode ESI mass spectrum only shows one signal at m/z = 434.08, which is assigned to the cationic $[M\text{-}PF_6]^+$ unit of complex **26**. An additional peak at m/z = 350.09 was also observed due to the $[M\text{-}3CO\text{-}PF_6]^+$ species.

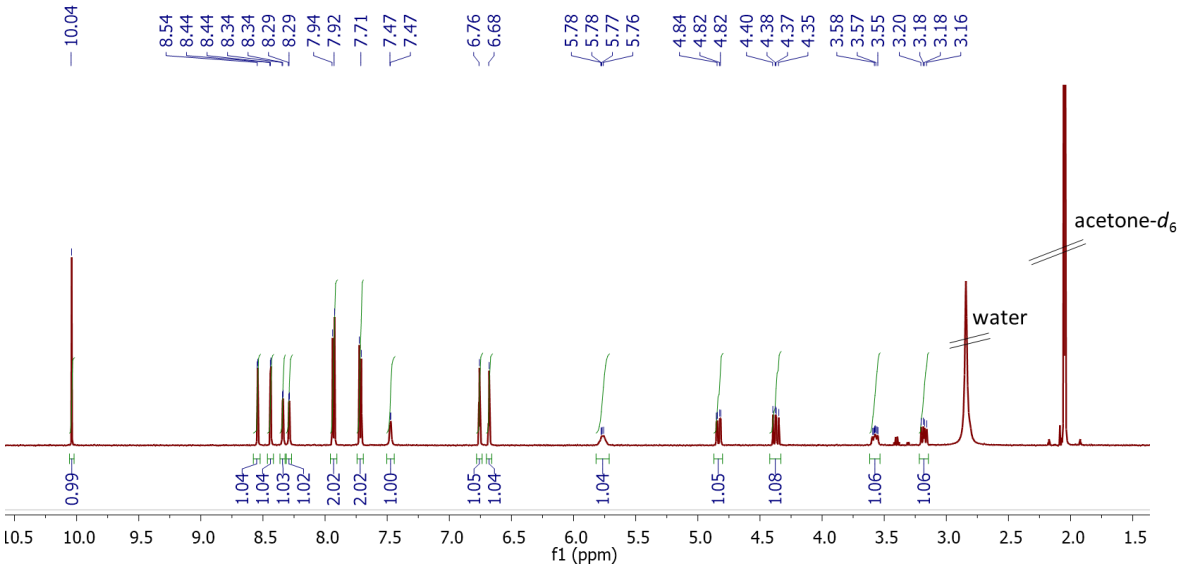

Fig. 3.15: 300 MHz ^{1}H-NMR spectrum of **26** in acetone-d_6.

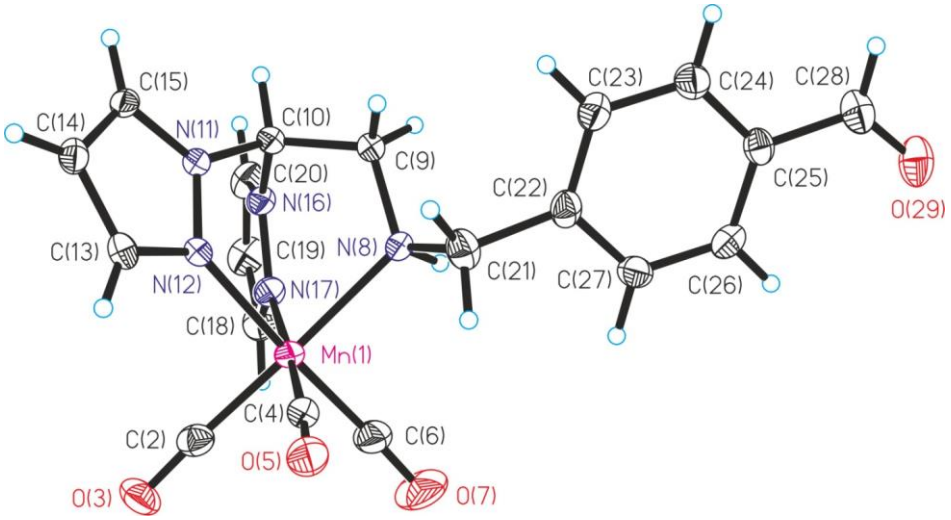

Fig. 3.16: Molecular structure of the cation of **26** in the solid state determined by single crystal X-ray diffraction. Thermal ellipsoids are drawn at the 50% probability level. The hexafluorophosphate counterion has been omitted for clarity. Selected bond distances (Å) and bond angles (°): Mn-C2 1.813(3), Mn-C4 1.817(3), Mn-C6 1.811(3), Mn-N8 2.151(2), Mn-N12 2.032(2), Mn-N17 2.047(2), C2-O3 1.147(4), C4-O5 1.146(4), C6-O7 1.141(4), C28-O29 1.219(4), C2-Mn-C6 88.22(14), C4-Mn-C6 90.24(14), C2-Mn-C4 87.87(13), N12-Mn-N17 87.29(9), N8-Mn-N12 84.95(9), N8-Mn-N17 82.70(9), C6-Mn-N8 91.68(12), C2-Mn-N8 174.31(12), C4-Mn-N8 97.82(12), C6-Mn-N12 176.57(12), C2-Mn-N12 95.20(11), C4-Mn-N12 89.63(11), C6-Mn-N17 92.89(13), C2-Mn-N17 91.62(12), C4-Mn-N17 176.82(11).

Crystals suitable for X-ray structure analysis were obtained by slow diffusion of diethylether into a solution of **26** in dichloromethane at room temperature. The crystallographic parameters are summarized in appendix and the molecular structure is displayed in Figure 3.16. The compound crystallizes in the monoclinic space group *P*2(1)/*n*. The three carbonyl ligands are coordinated to the manganese(I) center in a facial manner with two of the nitrogen donor atoms from each of the bpea pyrazole rings and the amine nitrogen completing the octahedral geometry. The bond distances between the Mn center and the two pyrazolyl nitrogen donor atoms, Mn-N12 and Mn-N17 are 2.032(2) and 2.047(2) Å. While the manganese-amine Mn-N8 bond distance at 2.151(2) Å is longer by about 0.11 Å. The Mn-C and C≡O bond distances show no variations relative to the *trans* N ligand.

The Sonogashira coupling and copper-catalyzed azide-alkyne cycloaddition CuAAC "click" reactions were evaluated for the synthesis of PhotoCORM peptide conjugates. The amino acid sequence R'-LPLGNSH-OH was used which is derived from a TGF-β_1 binding peptide, where R' is either 5-hexynoic or azido acetic for the coupling with the bpea ligand bearing the complimentary coupling partner.[144] The transforming growth factor (TGF-β) family of cytokines is ubiquitous and multifunctional.[145] It shows pleiotropic effects on cell proliferation, differentiation, migration and regulates immune responses.[146] Despite these effects, TGF-β also shows opposing function like tumour promotion due to its dysfunction in some signalling pathway. As a result, the tumour cells gain resistance towards growth suppression and induction of apoptosis by TGF-β.[147-148] Such a TGF-β binding peptide sequence has been selected as a carrier for the PhotoCORM. Compounds **16** and **17** with an iodobenzyl and alkyne functional group were used in a Sonogashira coupling and CuAAC reaction, whereas **26** was to be employed for oxime ligation with the peptide. The peptide was synthesized by solid-phase peptide synthesis (SPPS) on a preloaded H-L-His(Trt)-2CT resin by using standard Fmoc methodology (Scheme 3.4). The *N*-terminal functionalization with 5-hexynoic acid and 2-azido acetic acid was carried out on the resin using same methodology. The final cleavage of the peptides from solid resin was performed using a cocktail of TFA/TIS/H_2O (90:5:5, v/v/v) with further purification by preparative HPLC to give peptides **27-29**, as described in Chapter 5.1.3.

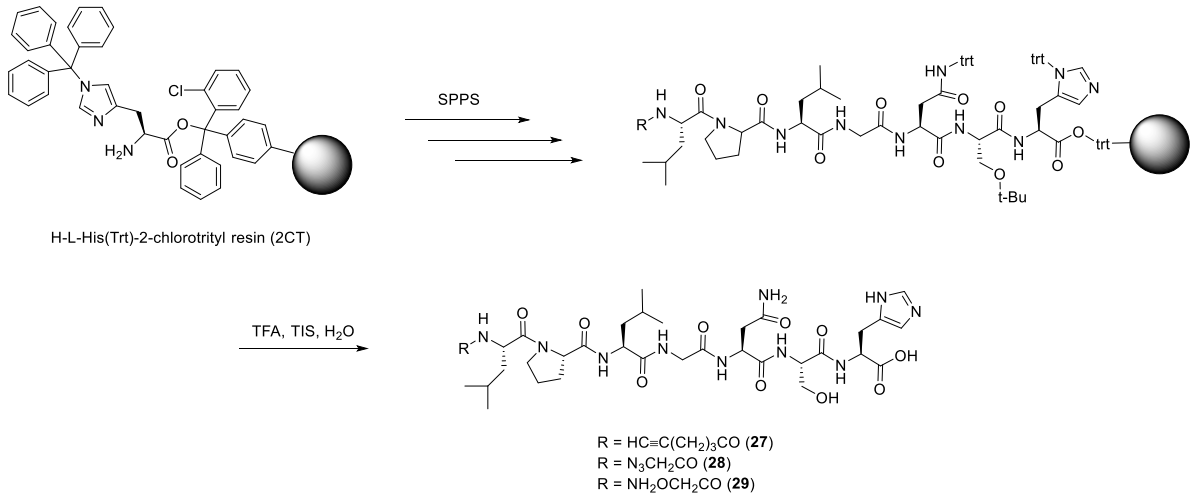

Scheme 3.4: Solid-phase peptide synthesis of R'-LPLGNSH-OH peptide sequence with R' = 5-hexynoic **27**, azido acetic **28** or aminoxyacetic **29**.

The Sonogashira coupling of **16** with the hexynoic acid-terminated peptide **27** was investigated under different reaction conditions using $PdCl_2(PPh_3)_2$ as the catalyst and copper(I) iodide as the co-catalyst. However, despite repetitive attempts with catalyst modifications in the reaction conditions, no conjugate **30** could be detected in any case as monitored by ESI mass spectrometry and HPLC. As a result, a CuAAC click reaction between the azido acetic-terminated peptide **28** and compound **17** was carried out in a mixture of *N*,*N*-dimethylformamide/water (1:1, v/v) using copper(II) sulfate as a catalyst and sodium ascorbate as the *in situ* reductant to generate the active copper(I) species as shown in Scheme 3.5.

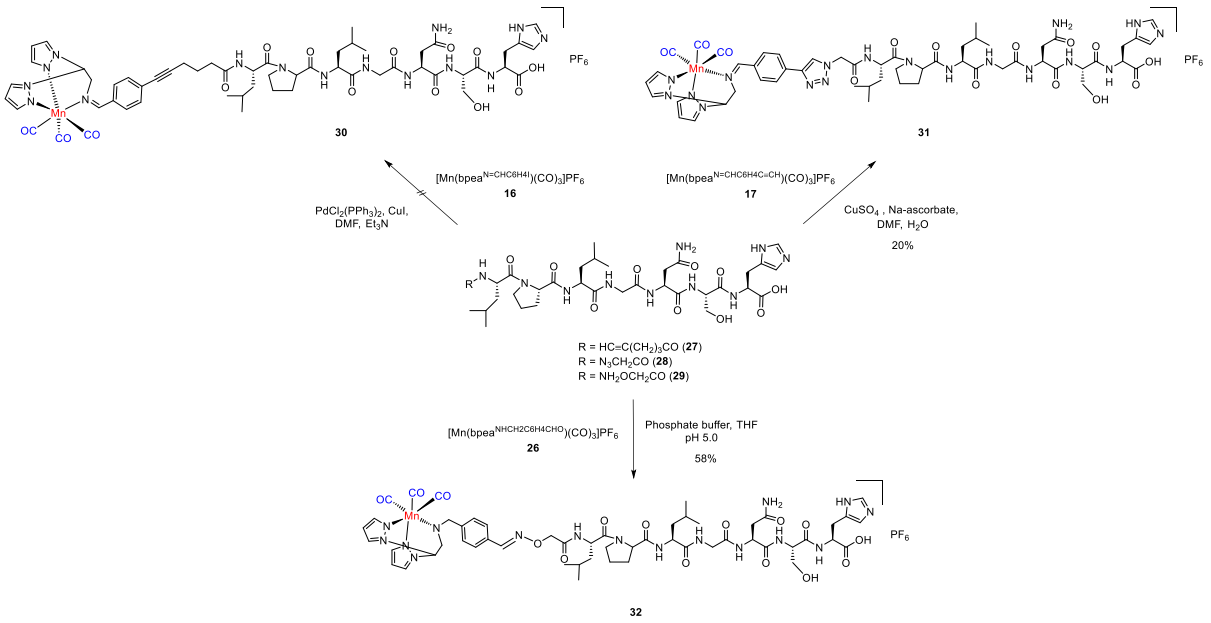

Scheme 3.5: Synthesis of peptide conjugates **31** and **32** by CuAAC and catalyst-free oxime ligation.

The formation of peptide conjugate **31** was monitored by RP-HPLC both at 220 nm and at 350 nm, the latter corresponding to the MLCT transition of the metal complex. The RP-HPLC chromatogram showed a single peak with a retention time of 30.1 min, which is significantly longer compared to the peptide itself which has t_r = 22.9 min (Figure 3.17). The ATR-IR spectrum of conjugate **31** shows two signals at 2040 and 1932 cm^{-1} and are assigned to the symmetric and asymmetric C≡O stretching vibrations, indicating the successful conjugation of the metal tricarbonyl moiety to the peptide and the conservation of its C_{3v} symmetry (Figure 3.18). This is also supported by the disappearance of the azide vibrational band at 2109 cm^{-1}.

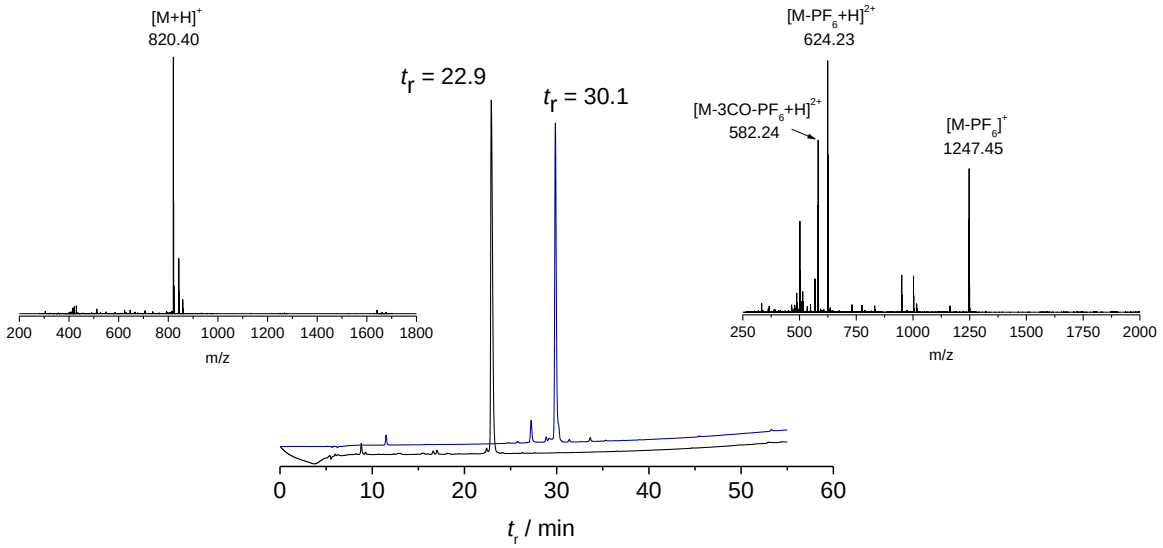

Fig. 3.17: Analytical HPLC chromatogram of peptide **28** (black, 220 nm) and conjugate **31** (blue, 350 nm). ESI^+ mass spectrum of peptide **28** (inset left) and conjugate **31** (inset right).

Additional proof for the successful CuAAC coupling comes from ESI-MS analysis. Conjugate **31** shows a peak at *m/z* = 1247.45, which is assigned to the monocationic species $[M\text{-}PF_6]^+$. In addition, two additional peaks are observed at *m/z* = 624.23 and 582.24 which are assigned to the dicationic species $[M\text{-}PF_6+H]^{2+}$ and $[M\text{-}3CO\text{-}PF_6+H]^{2+}$, respectively. On the other hand, peptide **28** showed only one major peak at *m/z* = 820.40 due to $[M+H]^+$.

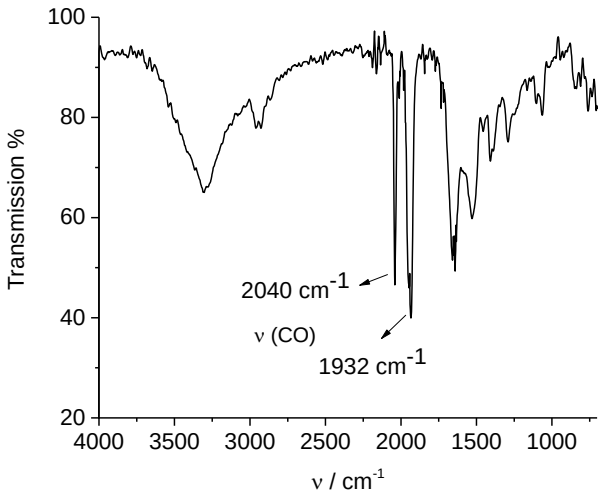

Fig. 3.18: ATR-IR spectrum of peptide conjugate **31**.

However, even after repeated cycles preparative HPLC, the peptide conjugate **31** could not be obtained in pure form due to the presence of an additional peak with a smaller retention time of 27.6 min. As a result, the stability of the conjugate was assessed by analytical HPLC in an acetonitrile/water mixture (10:90, v/v). The peak at t_r = 27.6 min gradually grew and reached an intensity of 30% relative to the major peak after 39 h (Figure 3.19). This is thought to be mainly due to the decomposition of the conjugate resulting from the hydrolysis of the imine bond in the complex under the aqueous conditions. Thus, a more stable amine bond should lead to a better stability of such conjugates.

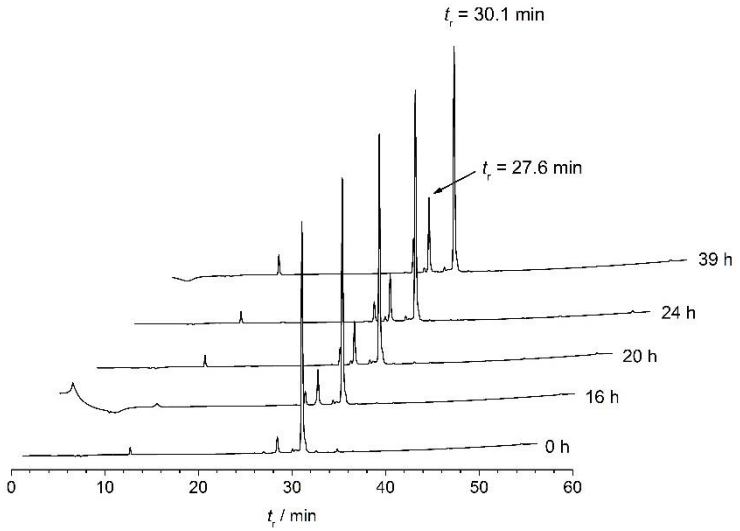

Fig. 3.19: Normalized HPLC traces (350 nm) showing the decomposition of conjugate **31** in acetonitrile/water (10:90, v/v) over a period of 39 h. The peak at t_r = 27.6 min is the decomposition product. Intensities of all traces are normalized to major peak at retention time 30.1 min.

Sonogashira coupling and CuAAC click reaction provide a possibility for modification of biomolecules, however, are limited in scope due to the use of transition-metal catalyst which can have potential toxic effects. Thus, a more mild and catalyst-free conjugation method was employed as an alternative. Therefore, the aldehyde-functionalized tricarbonylmanganese(I) complex **26** and an aminoxy-functionalized TGF-β_1 binding peptide were coupled in an oxime ligation. First, Fmoc-Aoa-OH (Aoa = aminoxyacetic acid) was synthesized by acid hydrolysis of dimethylketoxime to give aminoxyacetic acid as the hemi-hydrochloride which was subsequently protected as the 9-fluorenyl-methoxycarbonyl (Scheme 3.6).[149] Fmoc-Aoa-OH was then coupled to

the *N*-terminus of peptide through solid-phase peptide synthesis (Scheme 3.4). Two repeated couplings using 10 equiv. of Fmoc-Aoa-OH were required as indicated by a negative Kaiser test as described in Chapter 5.1.4. Peptide **29** was obtained as a white solid in 60% yield after purification by preparative HPLC with a high purity of 97% as determined by analytical HPLC and had a retention time of 15.6 min. Additionally, ESI-MS showed a single major peak at *m/z* = 810.41, assigned to $[M+H]^+$ (Figure 3.20).

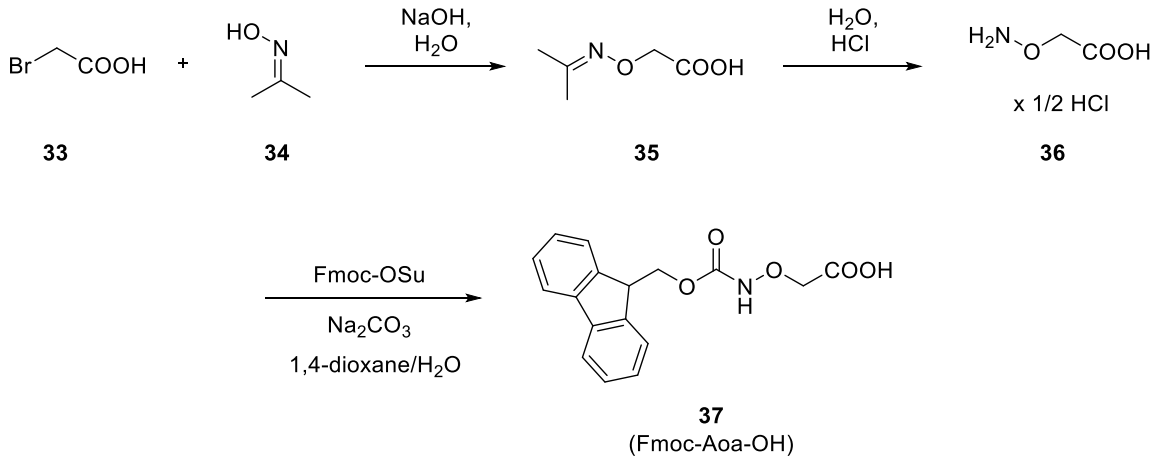

Scheme 3.6: Synthesis of Fmoc-protected aminoxyacetic acid.[149]

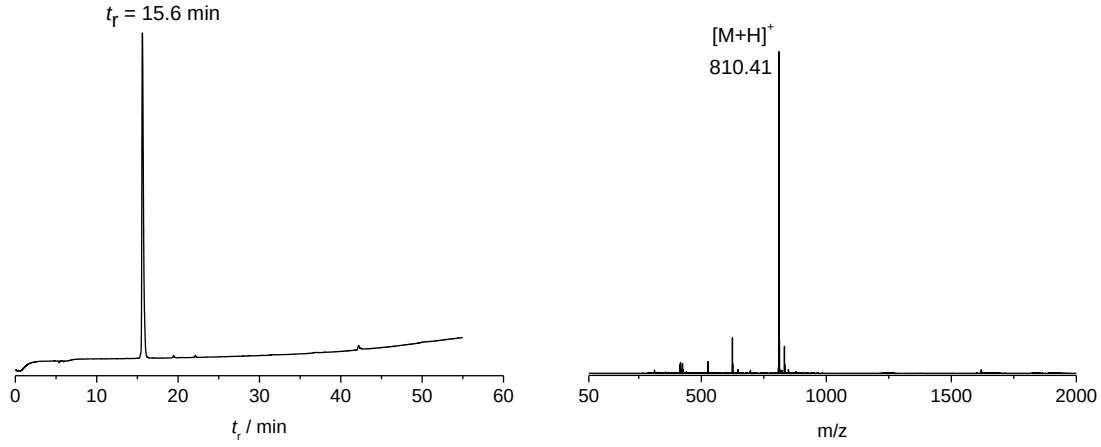

Fig. 3.20: Analytical HPLC chromatogram (220 nm detection, left) and ESI^+ mass spectrum (right) of peptide **29**.

In a post-labeling strategy, the Aoa-functionalized peptide **29** was reacted with $[Mn(bpea^{NHCH2C6H4CHO})(CO)_3]PF_6$ **26** in tetrahydrofuran/phosphate buffer (1:1, v/v) at pH 5.0 at room temperature for 3 h (Scheme 3.5). The conversion was monitored by TLC using silica as a solid phase and dichloromethane as an eluent. The mixture was desalted on a short reversed-phase column (C_{18}-SepPak) and subsequently purified by

preparative HPLC to give the corresponding peptide conjugate **32** in a yield of 58% and an excellent purity of 98%. Analytical HPLC of peptide conjugate **32** showed a significantly longer retention time, t_R = 28.3 min, in comparison to the peptide alone. Furthermore, the ESI mass spectrum displayed two main signals at *m/z* = 1225.45 and 435.65, which correspond to the monocationic species $[M\text{-}PF_6]^+$ and $[Mn(bpea^{CHO})(CO)_3+H]^+$, respectively. The latter is possibly a fragment peak resulting from the cleavage of the oxime bond (Figure 3.21).

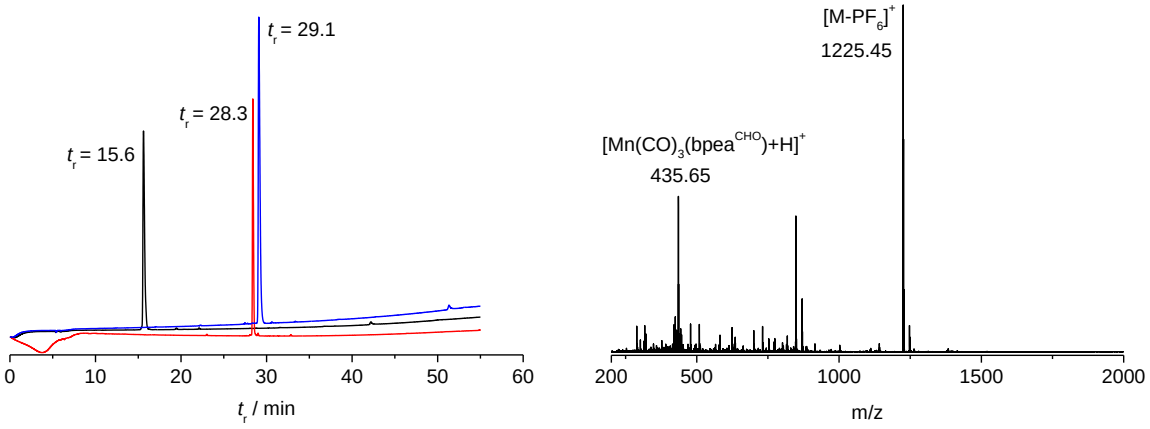

Fig. 3.21: Analytical HPLC chromatograms (left) of peptide **29** (black, 220 nm), peptide conjugate **32** (red, 350 nm), and metal complex **26** (blue, 350 nm). ESI^+ mass spectrum of conjugate **32** (right).

The successful conjugation of the complex to the peptide was also evident from the ATR IR spectrum of **32** which showed two intense vibrational bands at around 1935 and 2042 cm^{-1}, which are assigned to the asymmetric and symmetric C≡O stretching vibrations (Figure 3.22). Furthermore, disappearance of the C=O band at 1691 cm^{-1} from **26** also confirmed the successful oxime ligation.

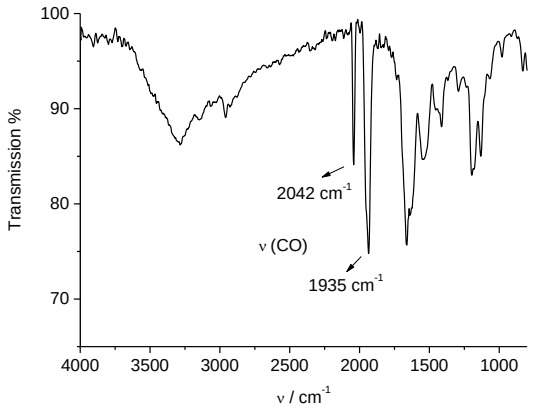

Fig. 3.22: ATR IR spectrum of peptide conjugate **32**.

3.2.2 Photolysis and stability studies in DMSO and water

In order to gain an insight into the stability of the compound **26** and its corresponding peptide conjugate **32**, UV/Vis spectroscopy studies were carried out. The stability of **26** was studied in dimethylsulfoxide solution due to its poor water solubility. Upon incubation in the dark for 16 h, the compound showed no spectral changes. However, illumination at 365 nm using a UV lamp in the MLCT absorption maximum of the Mn(bpea^{CHO})(CO)$_3$ moiety, lead to a decrease in intensity of the band at 357 nm (Figure 3.23).

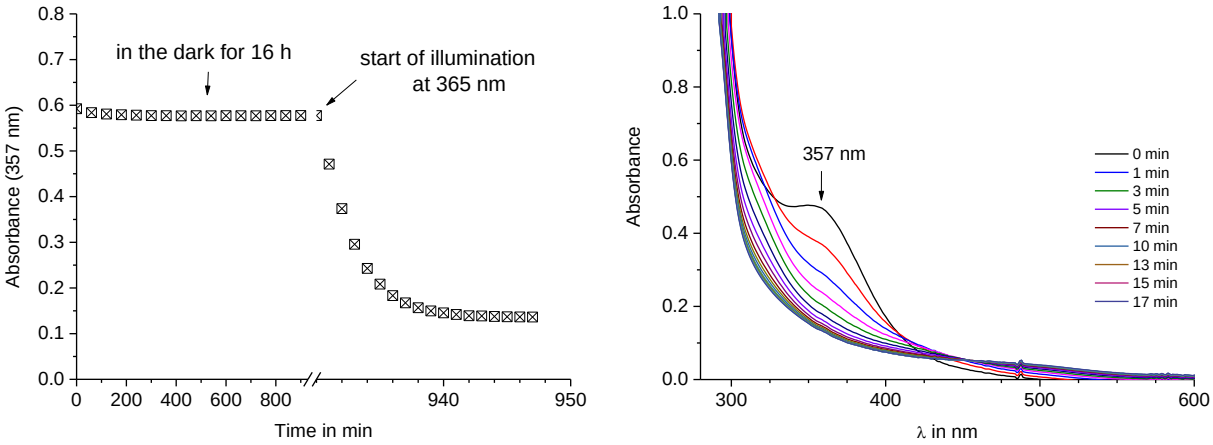

Fig. 3.23: Absorption changes at 357 nm of **26** in DMSO upon incubation in the dark for 16 h and subsequent photolysis with an UV lamp at 365 nm (left). UV/Vis spectral changes of **26** (0.3 mM) upon photolysis with increasing illumination time, 0-17 min (right).

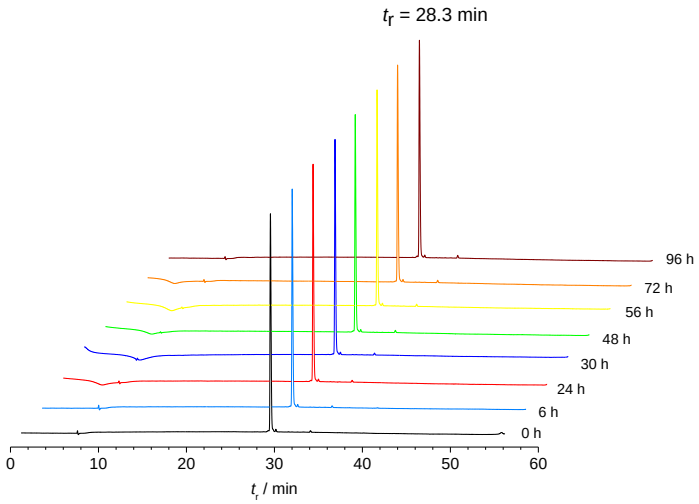

Fig. 3.24: Normalized HPLC traces (350 nm detection) of peptide conjugate **32** upon incubation in water for a period of up to 96 h. The HPLC traces were recorded after repeated freeze-thaw cycles.

The stability of peptide conjugate **32**, was also investigated with the aid of RP-HPLC in pure water. The analytical HPLC traces after repeated freeze-thaw cycles (-25 °C to room temperature) under the exclusion of light showed no additional species apart from the major peak of the conjugate at t_r = 28.3 min over a period of 4 d (Figure 3.24). These investigations reveal the excellent dark stability of the conjugate due to the stable oxime linkage between the metal complex and the peptide.

3.2.3 CO release and quantum yield measurements

The CO release behaviour of **26** and its corresponding peptide conjugate **32** were investigated using the myoglobin assay by the conversion of deoxy-Mb to carbonmonoxy-Mb. Initially, the dark stability of the complex and the conjugate was assessed under the conditions of myoglobin assay for a period of 16 h. The Q-band region of the UV/Vis spectrum remained unaltered but upon illumination at 365 nm, noticeable changes in the UV/Vis spectra were observed, indicating the conversion of $MbFe^{II}$ with λ_{max} = 557 nm into $MbFe^{II}CO$ with λ_{max} = 540 and 577 nm. The calculation of $MbFe^{II}CO$ concentration during the course of illumination showed an approximate release of 2 equivalents of CO per mole of the complex **26** or the conjugate **32** (Figure 3.25).

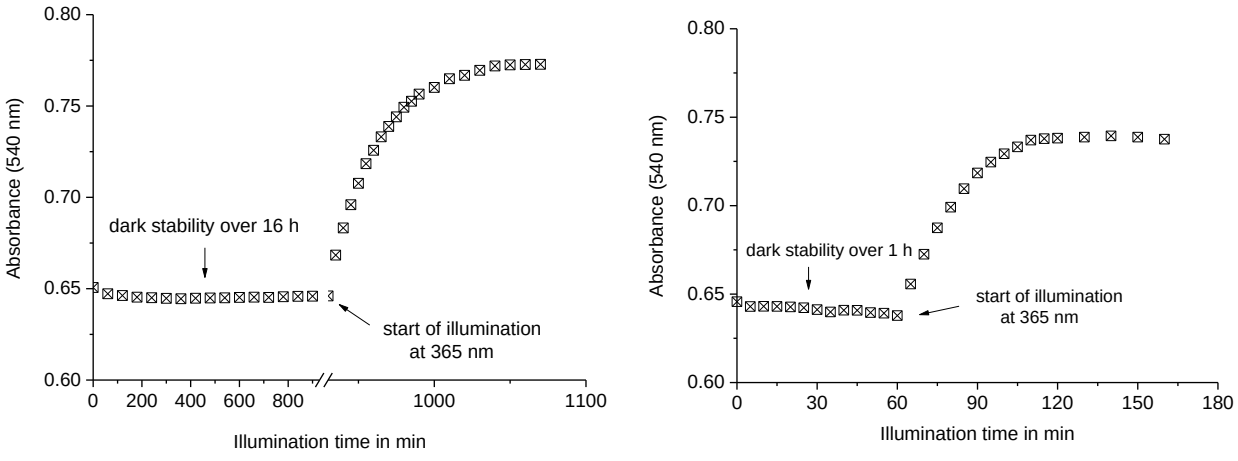

Fig. 3.25: Change in absorption at 540 nm of **26** (15 μM, left) and conjugate **32** (15 μM, right) in the dark over a period of 16 and 1 h, respectively, and further formation of MbCO upon illumination at 365 nm in presence of myoglobin (60 μM) in 0.1 M PBS at pH 7.4 under dinitrogen.

Quantum yield measurements were performed with an aid of standard ferrioxalate actinometry and the Ø values for both complex **26** and conjugate **32** are tabulated in Table 3.7. They were calculated from the initial spectral changes, thus avoiding the saturation of MbCO formed and are in the order of 10^{-4}. They are considerably lower than other known metal carbonyl complexes such as $Na_3[W(CO)_5(TPPTS)]$[150] and $[Mn(tpa)(CO)_3]ClO_4$[99] due to the internal shielding effect caused by the horse skeletal muscle myoglobin which shows significant absorption at the excitation wavelength of 365 nm.

Table 3.7: CO-release data and kinetic data of compounds **26** and **32**.

Compound	Conc. of MbCO (μM)	Equiv. of CO released	Half-life, $t_{1/2}$ [a] (min)	$Ø_{365\ nm}$ [b]	k_{CO} [c] (10^{-4} s^{-1})
26	30.7 ± 0.4	2.1 ± 0.1	22.6 ± 0.3	(4.4 ± 0.1) x 10^{-4}	5.5
32	25.1 ± 0.1	1.7 ± 0.1	15.5 ± 0.5	(4.5 ± 0.1) x 10^{-4}	7.4

[a] Under the conditions of myoglobin assay. [b] Calculated using a photon flux of the UV lamp of (2.82 ± 0.05) x 10^{-8} Einstein s^{-1}. [c] In DMSO solution from UV/Vis spectra.

3.2.4 Discussion

The synthesis of novel PhotoCORM peptide conjugates **30-32** and its CO release properties were investigated either by Sonogashira coupling, CuAAC click reaction or oxime ligation. As a model, TGF-β binding peptide sequence R'-Leu-Pro-Leu-Gly-Asn-Ser-His-OH was synthesized by solid-phase peptide synthesis, in which R' is the reactive group complimentary to the metal complex functionality **27**, **28** and **29**. All the peptides were synthesized in moderate to good yields but with high purity of 95-98%. Despite repeated attempts with different modifications in the reaction conditions, no coupling product was obtained by the Sonogashira reaction with **16**. CuAAC click reaction between the azido acetic-terminated peptide **28** and compound **17** contributed to the desired peptide conjugate. However, this led to the decomposition of the conjugate resulted by the hydrolysis of imine bond in the complex under the aqueous conditions indicating the need for a stable amine bpea ligand structure together with a good bioorthogonal coupling method.

The use of mild and catalyst-free oxime ligation between the complex **26** and the aminoxy-functionalized TGF-β binding peptide sequence **29** gave the most stable conjugate **32** without any decomposition product as analyzed by RP-HPLC over a period of 96 h. Moreover, both the parent complex and the conjugate are stable in the dark indicating the accessibility of these compounds as CO prodrugs. Further investigation of the CO release properties by myoglobin assay showed a release of two equivalents of CO upon photoactivation. Thus, an excellent conjugate accessibility and stability can be achieved by using a catalyst-free oxime ligation together with the facile preparation of CORM-peptide conjugates for the targeted delivery of carbon monoxide to biological systems.

3.3 Manganese(I) tricarbonyl DAB-G1-PPI and PAMAM-G0 dendrimer conjugates

3.3.1 Synthesis of diaminobutane (DAB) and polyamidoamine (PAMAM) conjugates

Dendrimers are branched, star-shaped macromolecules with particle size in the range of nanometers. They are an attractive choice in biomedical applications due to their easy conjugation with targeting molecules and drugs.[151] They are often highly water soluble and thus promise a good bioavailability and high drug loading capacity.[152] Additionally, dendrimers tend to accumulate in tumour tissues due to the enhanced permeability and retention (EPR) effect.[153] CO-releasing molecules generate a metal-coligand fragment upon liberation of CO which might have a biological activity of its own. Since dendrimers are easily cleared through the kidneys owing to their small size of <10 nm, covalent attachment of CORMs to the dendrimers might render the metal-coligand fragment bound to the macromolecular carrier. In the previous chapter, the conjugation of CORMs with peptides was achieved either by Sonogashira coupling or copper-catalyzed azide-alkyne cycloaddition (CuAAC) reaction, which are, however, limited in scope due to the use of exogenous metals like palladium, copper and can have potential toxic effects. Thus, tetranuclear $Mn(CO)_3$-functionalized DAB-PPI (diaminobutane-polypropyleneimine) and PAMAM (polyamidoamine) dendrimer conjugates **40** and **41** were targeted. The terminally decorated $Mn(CO)_3$-functionalized tetranuclear dendrimer conjugates **40** and **41** were prepared by a Schiff-base condensation reaction of either DAB-G1-PPI-$(NH_2)_4$ **38** or PAMAM-G0-$(NH_2)_4$ **39** with $[Mn(CO)_3(bpea^{NHCH2C6H4CHO})]PF_6$ **26**, under exclusion of light and were reduced *in situ* with sodium borohydride in methanol to give the corresponding conjugates (Scheme 3.7). The dendrimer conjugates **40** and **41** were obtained as yellow solids and purified by preparative RP-HPLC using a gradient of 5-70% acetonitrile/water with 0.1% TFA. The IR spectra of **40** and **41** show two strong bands at about 2040 and 1930 cm^{-1}, which are assigned to the asymmetrical and symmetrical C≡O stretching vibrations of the metal-tricarbonyl moiety, respectively (Figure 3.26). An additional peak at 1669 cm^{-1} in the IR spectrum of conjugate **41** is assigned to the C=O vibration of the polyamidoamine backbone.

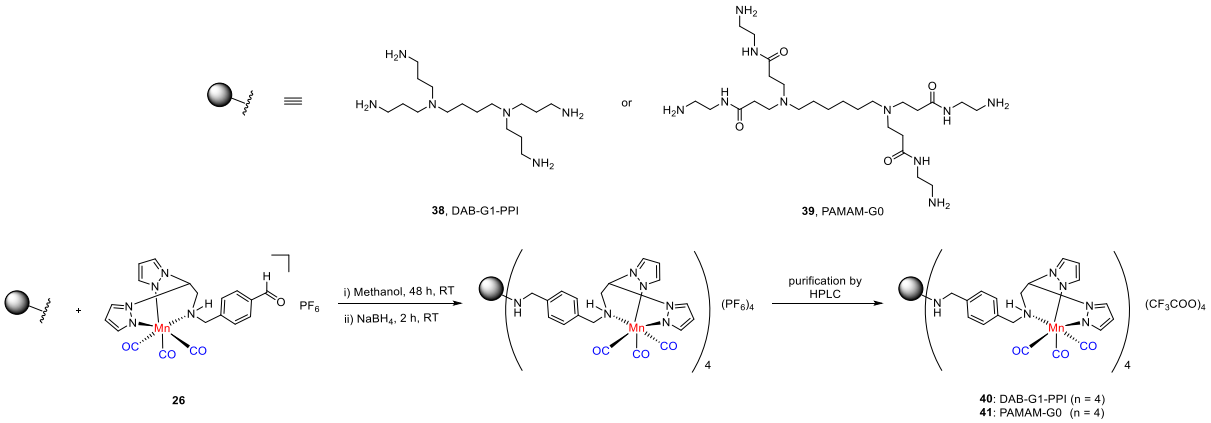

Scheme 3.7: Synthesis of tetranuclear DAB-G1-PPI **40** and PAMAM-G0 **41** dendrimer conjugates.

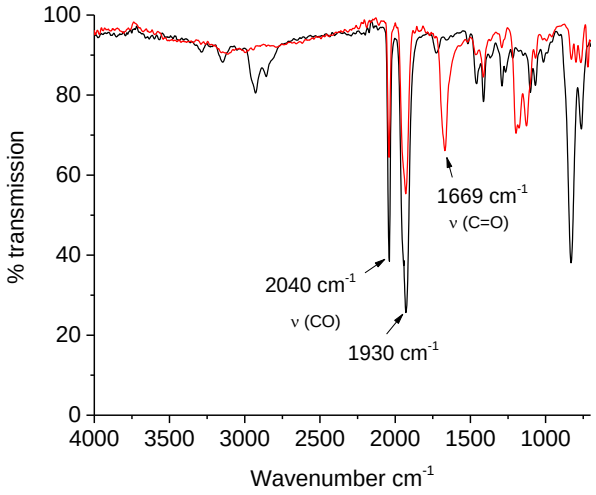

Figure 3.26: ATR-IR spectra of tetranuclear DAB-G1-PPI and PAMAM-G0 dendrimer conjugates **40** (black) and **41** (red).

The conjugation of metal complex **26** to the DAB-G1-PPI dendrimer was analyzed by ^{1}H NMR. The absence of an aldehyde peak at around 10 ppm for **40** demonstrates the successful coupling (Figure 3.27). Four doublets at 8.35, 8.26, 8.18 and 8.14 ppm appear with an integral of four each. These signals are assigned to the $H_{3'}$, H_3, $H_{5'}$ and H_5 protons of the pyrazole rings of the terminal Mn(bpea)(CO)$_3$ moieties. A singlet at 7.53 ppm with an integral of 16H belongs to the protons of the phenyl groups, indicating the functionalization of all four arms of the dendrimers with the metal complex *via* the reduced amine group. A broad doublet at 7.21 ppm appear with an integral of four is assigned to the methine proton of the terminal bpea moiety. Two triplets at 6.68 and

6.62 ppm with an integral of four each are assigned to the H_4, $H_{4'}$ of the pyrazole rings. A broad singlet at 5.69 ppm belongs to the coordinating amine proton (N*H*). Two doublet of doublets at 4.44 and 3.97 ppm with an integral of 4H each belongs to the methylene protons at the alpha position with respect to the coordinated amine group and show a diastereotopic splitting pattern similar to the complex **26**. A singlet at 4.23 ppm is assigned to the proximal methylene protons generated due to the in situ reduction of the intermediate schiff base. Three peaks at 3.27 (broad), 3.16 (triplet) and 2.22 (broad) ppm with an integral ratio of 8:8:8 are assigned to the protons of the four polypropyleneimine arms attached to the DAB core. Additional two broad peaks at 3.22 and 1.81 ppm each with an integral of four correspond to the signals of the dendrimer core. The presence of trifouoroacetate counter ion was confirmed by ^{19}F NMR and appear as a singlet at -76.89 ppm.

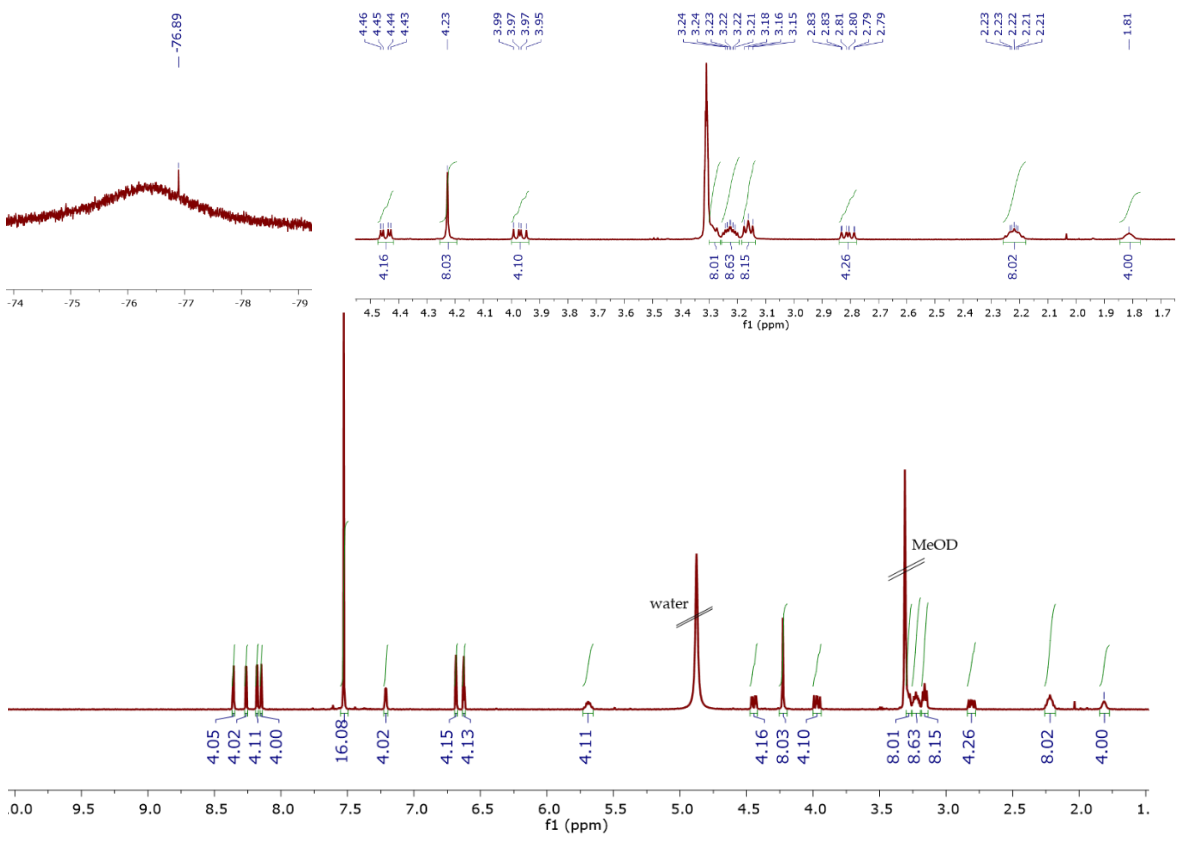

Figure 3.27: 500 MHz ^1H NMR spectrum of [DAB-G1-PPI-(Mn(bpea^{NHCH2C6H4CH2NH})$(CO)_3)_4$]$(CF_3COO)_4$ **40** in MeOD (bottom). An enlarged view of the aliphatic region showing the ^1H NMR signals of dendrimer core and the arms (inset right); and 200 MHz ^{19}F NMR spectrum (inset left).

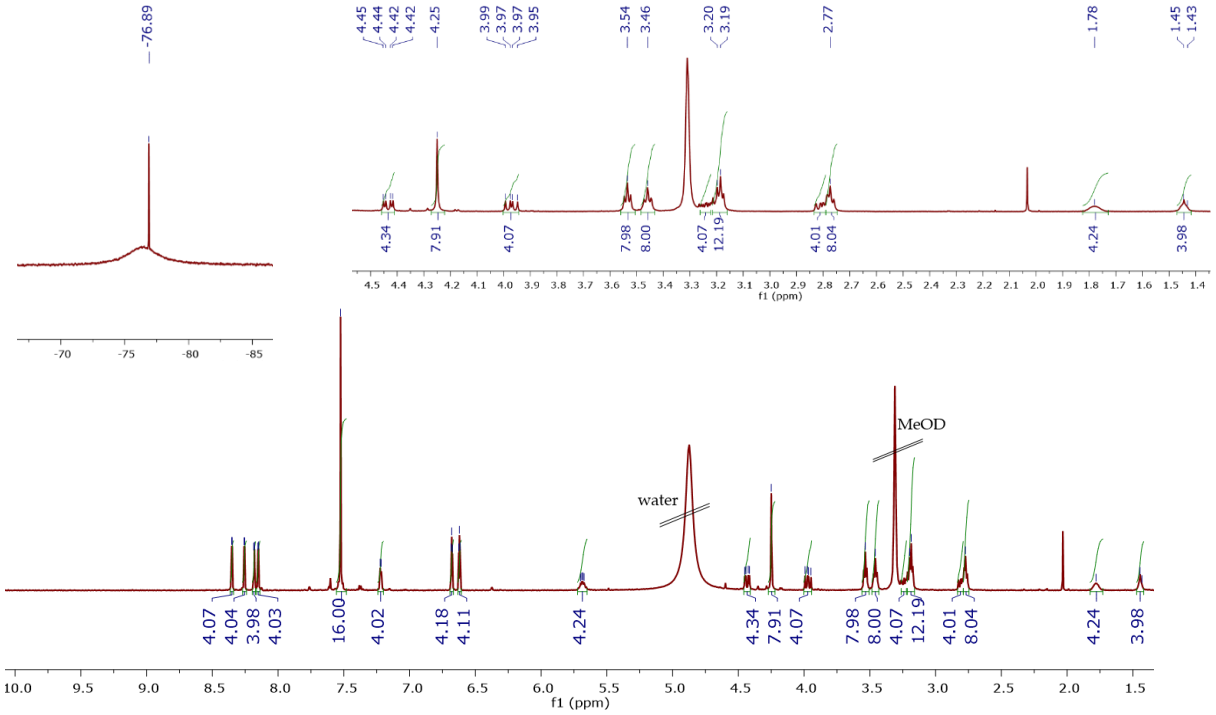

Figure 3.28: 500 MHz ^{1}H NMR spectrum of [PAMAM-G0-(Mn(bpea^{NHCH2C6H4CH2NH})(CO)$_3$)$_4$](CF$_3$COO)$_4$ **41** in MeOD (bottom). An enlarged view of the aliphatic region showing the ^{1}H NMR signals of dendrimer core and the arms (inset right); and 200 MHz ^{19}F NMR spectrum (inset left).

The ^{1}H NMR spectrum of **41** (Figure 3.28), also showed an absence of an aldehyde peak around 10 ppm and instead display a singlet at 4.25 ppm with an integral of eight which is assigned to the methylene protons due to the in situ reduction of the intermediate schiff base. Four doublets appear between 8.35 – 8.15 ppm with an integral of four each and coupling constants of ^{3}J = 2.2 and 3.3 Hz, respectively. They are assigned to the H$_{3'}$, H$_3$, H$_{5'}$ and H$_5$ protons of the pyrazole rings of the terminal Mn(bpea)(CO)$_3$ moieties. A singlet at 7.52 ppm belongs to the protons of the phenyl groups. The methine proton of the terminal bpea units appear as a broad doublet at 7.22 ppm. Two triplets at 6.68 and 6.62 ppm are due to the H$_4$, H$_{4'}$ protons of the pyrazole rings. A broad peak at 5.68 ppm is assigned to the coordinating N*H* proton. Two doublet of doublets at 4.43 and 3.97 ppm with an integral of four each belongs to the methylene protons at the alpha position with respect to the coordinated amine group and show a diastereotopic splitting pattern similar to the complex **26**. Four peaks at 3.54 (triplet), 3.45 (triplet), 3.18 (triplet) and 2.77 ppm (broad multiplet) with an integral ratio of 8:8:12:8 correspond to the protons of the PAMAM dendrimer arms.

Furthermore, the dendrimer core protons appear as two broad multiplets at 1.78 and 1.44 ppm with an integral ratio of four each. Additionally, the integrity of the $Mn(CO)_3$ group is also confirmed by the presence of two singlets in the ^{13}C-NMR spectrum at about 220 and 221 ppm. The hexafluorophosphate counter ion was exchanged to trifouoroacetate anion during the preparative HPLC purification, and the presence of which was confirmed by ^{19}F NMR which appear as a singlet at -76.89 ppm.

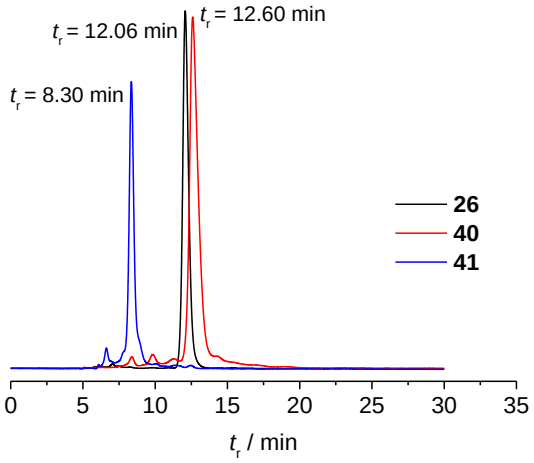

Fig. 3.29: Analytical HPLC chromatograms of compound **26** (black, 350 nm detection), dendrimer conjugates **40** (red, 350 nm detection), and **41** (blue, 350 nm detection).

The formation of dendrimer conjugates **40** and **41** was monitored by RP-HPLC both at 350 nm due to the MLCT absorption of the metal complex **26**. The analytical HPLC chromatograms of **40** and **41** each showed single peaks with retention times of 12.60 and 8.30 minutes respectively, while complex **26** had a retention time of 12.06 minutes (Figure 3.29). Apparently conjugate **40** displayed a longer retention time compared to **41** due to the decreased surface polarity of DAB-PPI than the PAMAM. Additional proof for the successful conjugation of the DAB-G1-PPI and PAMAM-G1 dendrimers with the metal complex **26** was confirmed by ESI-MS analysis. The dendrimer conjugate **40** shows two peaks at *m/z* = 1107.79 and 2328.57, which are assigned to the dicationic $[M\text{-}CF_3COO]^{2+}$ and monocationic species $[M\text{-}CF_3COO{+}H]^{+}$, respectively. Similarly, for conjugate **41** two peaks were also observed at *m/z* = 1235.85 and 2584.68,

and correspond to $[M\text{-}CF_3COO]^{2+}$ and $[M\text{-}CF_3COO+H]^{+}$, respectively. The ESI-MS data of the conjugates are shown in Figure 3.30.

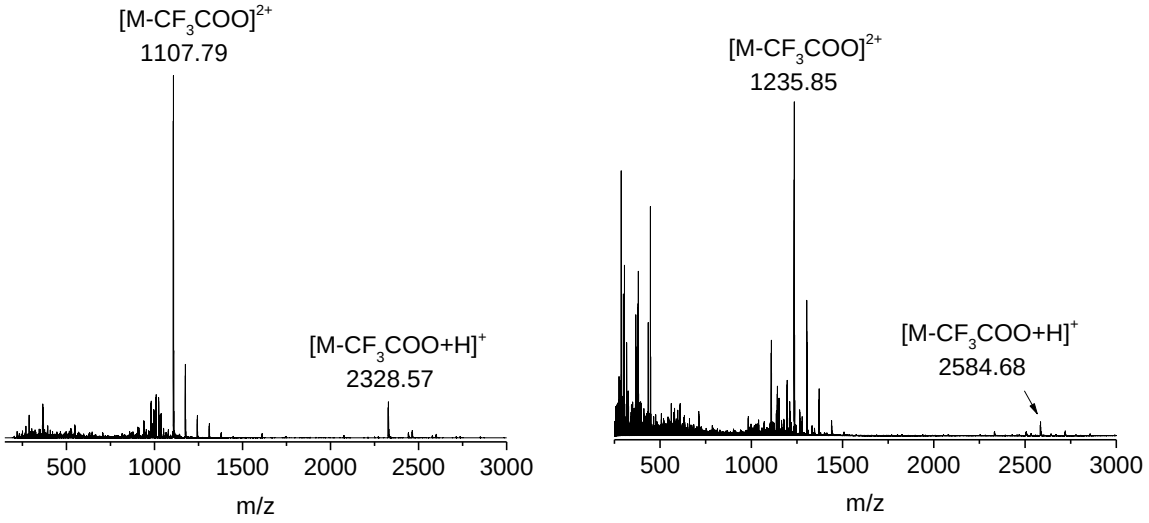

Fig. 3.30: ESI^+ mass spectrum of conjugates **40** (left) and **41** (right).

3.3.2 Photolysis and stability studies in phosphate buffered solution (PBS)

The absorption spectra of the metal complex **26**, DAB-G1-PPI **40** and PAMAM-G0 conjugate **41** were recorded in dimethylsulfoxide and are shown in Figure 3.31. All three compounds display a broad absorption maxima at around 350 nm which is assigned to a metal-to-ligand charge transfer transition. The molar extinction coefficients of dendrimer conjugates **40** and **41** are about 3-fold higher than that observed for **26** (Table 3.8). This is due to the increase in the number of $[Mn(CO)_3]$ moieties in the dendritic compounds.

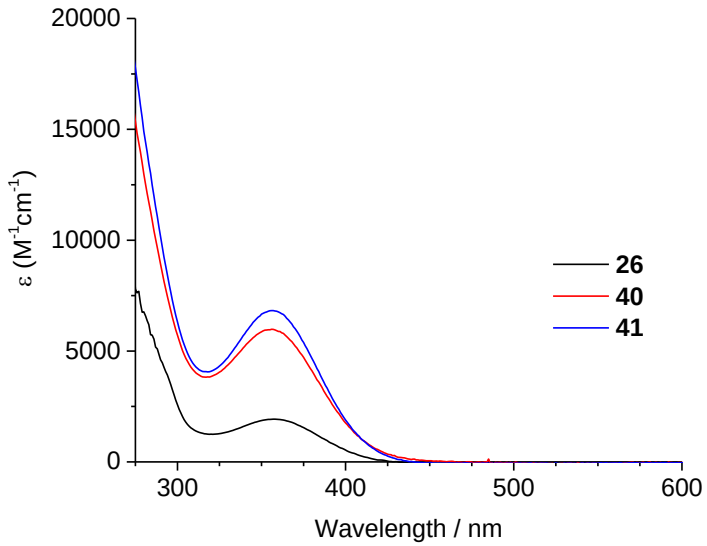

Fig. 3.31: Electronic absorption spectra of **26**, **40**, and **41** in DMSO.

Table 3.8: Absorption maxima and molar extinction coefficient of **26**, **40**, and **41**.

Compound	λ_{max} [nm]	$\varepsilon_{\lambda max}$ [M^{-1} cm^{-1}]	$\varepsilon_{365\ nm}$ [M^{-1} cm^{-1}]	$\varepsilon_{410\ nm}$ [M^{-1} cm^{-1}]
26	357	2070 ± 133	1850 ± 89	—
40	356	6056 ± 33	5651 ± 35	731 ± 86
41	357	7107 ± 81	6476 ± 57	1649 ± 25

The dark stability of the dendrimer conjugates **40** and **41** was studied in dimethylsulfoxide/PBS (10:90, v/v) solution for a period of 14 h. Essentially no spectral changes were observed in the UV/Vis. Then, illumination of the solutions was carried out either with the UV lamp at 365 nm or a custom built LED cluster at 410 nm to investigate the effect of photoactivation wavelength (Figure 3.32 and appendix). This led to the decrease in intensity of the MLCT band at 356 nm and the rate of CO release from compounds **40** and **41** was determined. The half-life ($t_{1/2}$) and the rate constants of CO release for **40** and **41** are summarized in Table 3.9. Upon photoactivation at 365 nm, a faster CO release rate with a half-life of 2.1 min was observed for **40** compared to **41**. However, a slightly longer half-life of 2.6 min was displayed by **41**. Furthermore, photoactivation at 410 nm led to a 13-fold increase in half-lives and a 13-fold decrease in CO release rates for both the compounds due to the lower extinction coefficient at this particular wavelength (Table 3.8 5th column).

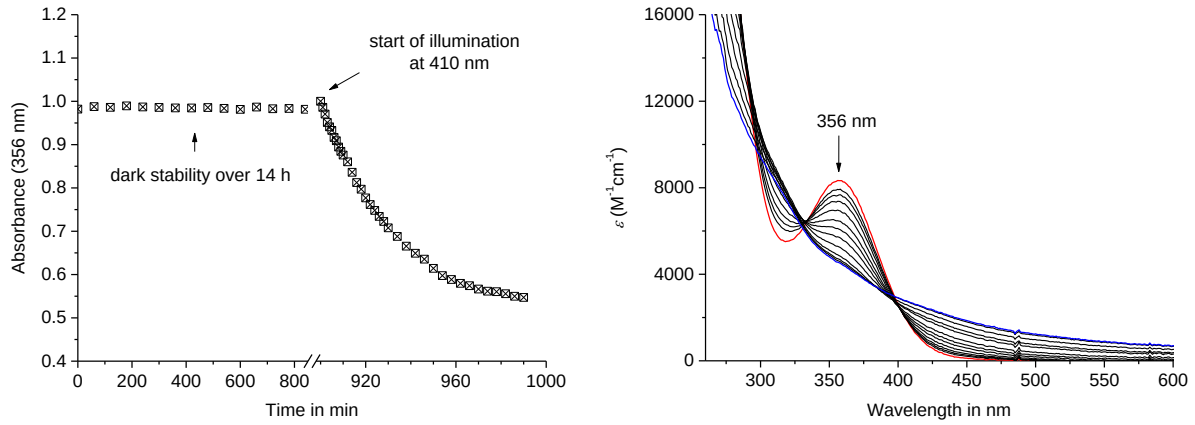

Fig. 3.32: Absorption changes at 356 nm of **40** in DMSO/PBS (10:90, v/v) upon incubation in the dark for 14 h and subsequent illumination with a LED cluster at 410 nm (left). UV/Vis spectral changes of **40** (0.12 mM) upon photolysis with increasing illumination time, 0-90 min (right).

Table 3.9: Half-life and rate-constants of CO release as determined in DMSO/PBS (10:90, v/v) solution using either 365 nm UV lamp or 410 nm LED cluster.

Compound	Half-life, $t_{1/2}$ (min)		Rate constant, k_{CO} (10^{-4} s^{-1})	
	365 nm	410 nm	365 nm	410 nm
40	2.1	28.9	54.1	4.1
41	2.6	33.3	44.2	3.5

3.3.3 Photoinducible CO release experiments with the myoglobin assay

The light-induced CO release from metallodendrimers **40** and **41** was studied with the aid of the myoglobin assay by monitoring the conversion of deoxy-MbFe(II) into carbonmonoxy-MbFe(II). In order to assess the dark stability of **40** and **41** under these conditions, a freshly prepared solution of compound in dimethylsulfoxide was added to 60 μM of freshly prepared horse skeletal muscle myoglobin MbFe(II) in to 0.1 M phosphate buffered solution (PBS, pH 7.4). This was further reduced with excess of sodium dithionite under dinitrogen and incubated in the dark for up to 14 h. Both metallodendrimers showed no spectral changes at four different wavelengths in the Q-band region of myoglobin, between 500 and 600 nm (Figure 3.33).

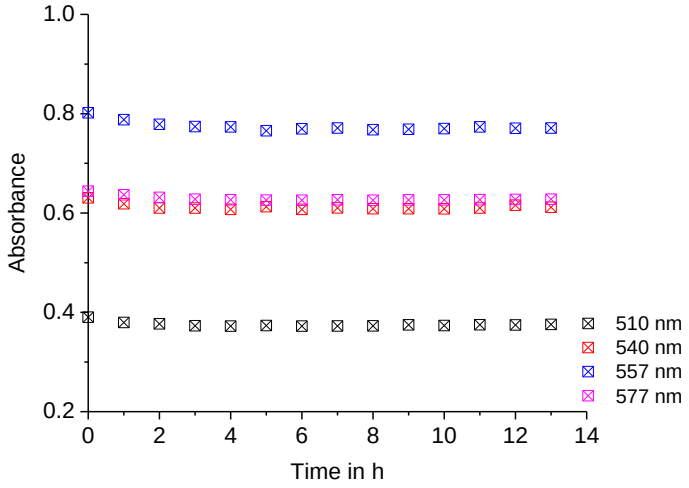

Fig. 3.33: Plot of absorption over wavelength in the Q-band region upon incubation of **41** (4 μM) in 0.1 M PBS at pH 7.4 in presence of myoglobin (60 μM) and sodium dithionite (10 mM) in the dark for 14 h under a dinitrogen atmosphere as monitored by UV/Vis spectroscopy.

Upon illumination at 365 nm, noticeable changes were observed in the Q-band region of the myoglobin absorption. The band at 557 nm, typical for deoxyMb slowly decreased in intensity while two new peaks at 540 and 577 nm slowly grow with increasing illumination time. These are characteristic for the conversion of deoxyMb to MbCO. The concentration of MbCO formed at the plateau level was determined using a molar extinction coefficient of MbCO [$\lambda_{540\,nm}$ = 15.4 $(mM)^{-1}L^{-1}$] (Figure 3.34).[154] Upon photoactivation of a solution containing either **40** or **41** (4 μM) and deoxyMb (60 μM), the CO release profile showed a release of about seven CO ligands per mole

of **40** or **41**. The half-lives of CO release of compounds **40** and **41** are listed in Table 3.10.

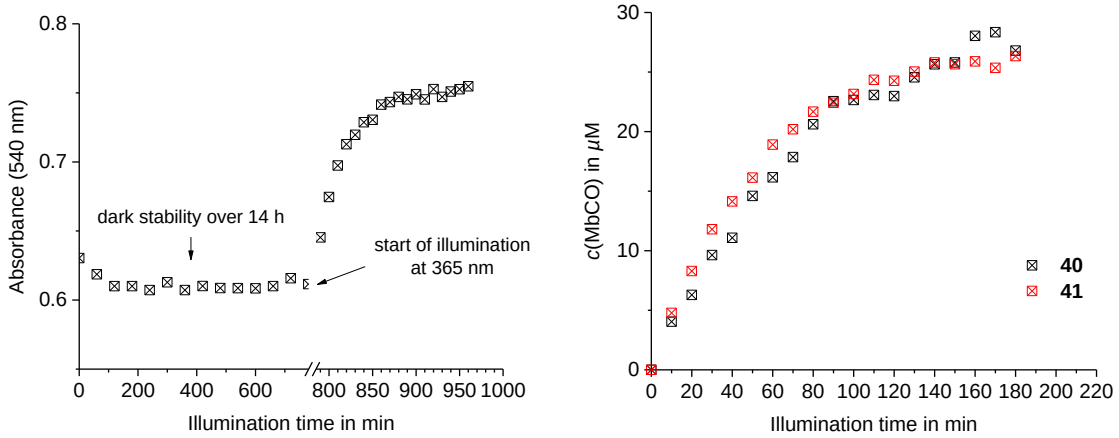

Fig. 3.34: Change in absorption at 540 nm showing the stability of **41** (4 μM) in the dark (over a period of 14 h) and the formation of MbCO upon illumination at 365 nm in presence of myoglobin (60 μM) and sodium dithionite (10 mM) under dinitrogen (left). Amount of MbCO (in μM) formed with the increasing illumination time of a solution of **40** and **41** (right).

Table 3.10: CO release data from myoglobin assay of **40** and **41**.

Compound	Conc. of MbCO (μM)	Equiv. of CO released	Half-life, $t_{1/2}$ (min)	CO released (%)
26	30.7 ± 0.4	2.0 ± 0.1	22.6 ± 0.3	66.7
40	24.9 ± 3.3	6.2 ± 0.8	63.1 ± 7.5	51.6
41	26.6 ± 0.2	6.8 ± 0.2	34.5 ± 6.0	56.6

Both metallodendrimers **40** and **41** release about 50-55% of the total amount of CO under the conditions of myoglobin assay. The metal complex **26** show a release of two equivalents of CO with a half-life of 23 min. When compared to the parent complex **26**, both conjugates **40** and **41** tend to release nearly seven equivalents of CO per mole of the compounds with a half-life of 64 and 35 min, respectively. Furthermore, the half-life of CO release for **41** is almost twice the half-life of **40**. However, in both metallodendrimers, it is still not clear whether the CO release from different $Mn(CO)_3$ moieties is an associative process or an independent release mechanism.

3.3.4 Discussion

Two dendrimers diaminobutane-polypropyleneimine (DAB-PPI) and polyamidoamine (PAMAM) were successfully functionalized with [Mn(bpea^{NHCH2C6H4CHO})$(CO)_3$]PF_6 **26**. The integrity of the $Mn(CO)_3$ moiety was confirmed by ^{1}H and ^{13}C NMR, IR spectroscopy and mass spectrometry. The dark stability of both the conjugates was studied in dimethylsulfoxide/PBS (10:90, v/v) solution for a period of 14 h and essentially showed no spectral changes in the UV/Vis. Following the photoactivation at 365 nm led to a faster CO release from **40** with a diaminobutane dendritic core compared to **41** with an ethylenediamine core. Photoactivation at 410 nm showed a 13-fold decrease in CO release rates for both the conjugates. The photoinduced CO release behaviour of **40** and **41** was examined using the myoglobin assay and they showed a release of an approximate seven equivalents of CO. This was further accounted for a release of nearly 50-55% of total amount of CO. Additionally, the half-life of CO release for conjugate **40** was significantly longer compared to conjugate **41** (64 *vs.* 35 min). However, the parent complex **26** display a shorter half-life with a release of two equivalents of CO per mole of the compound.

Although an increased amount of CO release was observed from both the compounds **40** and **41** compared to the parent complex **26**, however, it is not clear whether the CO release mechanism from the $Mn(CO)_3$ moieties of the dendrimer arms is an independent or a cooperative process. Furthermore, the assessment of biological activity of these compounds in cellular systems is very much needed to verify its bioavailability.

4 Summary

The aim of this thesis was to explore manganese(I) tricarbonyl complexes as novel photoactivatable CO-releasing molecules (PhotoCORMs) as well as their conjugation to peptide and dendrimer carrier systems to synthesize organometal conjugates for the targeted delivery of CO.

Thus, a series of six Mn(I) tricarbonyl complexes based on the tridentate bis(pyrazolyl)ethylamine (bpea) ligand was synthesized containing a pendant *para*-substituted phenyl group with an iodo or alkyne functionality. These groups were introduced to enable further bioconjugation by a Sonogashira or CuAAC "click" reaction. All complexes were obtained in good yield with high purity. The X-ray crystal structures of the compounds with the iodo and alkyne substituents showed the expected facial coordination of the tridentate bpea ligand to the $Mn(CO)_3$ moiety. All complexes have an excellent dark stability in dimethylsulfoxide solution for up to 14 h, but release two equivalents of CO upon photoactivation at 365 nm, as detected by the myoglobin assay. Although their MLCT bands are centered at around 350 nm, photoactivation can also be achieved at 410 nm, which is more suitable for biological applications. The CO release process was also studied using solution IR spectroscopy, which allowed the assignment of new bands from possible reaction intermediates with the aid of DFT calculations. These are indicative of the formation of *cis*-$Mn(CO)_2$ species after the release of initial one equivalent of CO. A dose-dependent increase in fluorescence signal was observed only upon photoactivation of the CORM, while in the dark, no response was observed even at a 10:1 ratio of CORM *vs*. COP-1. The light-induced CO release was also studied in HUVEC cells with one of the complexes. A significant increase in COP-1 fluorescence relative to the background (15-fold) was observed in the supernatant compared to the cell-containing fraction (5-fold). This might be due to an impaired cellular uptake of either the COP-1 probe or the complex or both. Nonetheless, these compounds have been established as novel photoactivatable CO-releasing molecules (PhotoCORMs).

Peptides are attractive targeting vectors for the cellular delivery of metal complexes. As a model for carrier system, a transforming growth factor β-recognizing (TGF-β) peptide was synthesized by solid-phase peptide synthesis. The conjugation of a $[Mn(bpea)(CO)_3]^+$ complex to the peptide *via* peripheral ligand functionalities was investigated by Sonogashira coupling and CuAAC "click" reactions in a post-labeling strategy. However, a successful construct was not obtained by the Sonogashira coupling under different reaction conditions. On the other hand, the CuAAC click reaction between an alkyne-functionalized metal complex and an azide-modified peptide provided the desired conjugate *N*-terminally linked through a triazole group. Still, a major decomposition product resulted from the hydrolysis of the imine bond in the bpea ligand under aqueous conditions. As a result, a bioorthogonal coupling strategy was employed utilizing the mild and catalyst-free oxime ligation and a more stable amine ligand. The coupling between an aminoxy acetic acid-terminated TGF-β_1-binding peptide and an aldehyde-functionalized metal complex gave the corresponding conjugate in good yield with excellent stability for up to 96 h even when exposed to repeated freeze-thaw cycles. The CO release behaviour of the parent complex and the conjugate were identical, with release of two equivalents of CO upon photoactivation at 365 nm on a 1-1.5 h time-scale. Thus, the catalyst-free oxime ligation offers a facile preparation of CORM-peptide conjugates with excellent stability.

Dendrimers are tree-like molecules with functional groups mostly in the periphery which allow modification with metal complexes for biological application. Due to the enhanced permeability and retention (EPR) effect, the conjugation of CO-releasing molecules to dendrimers might enable their enrichment in tumour tissue for anticancer chemotherapy. Thus, $Mn(CO)_3$-functionalized G1 diaminobutane (DAB) and polyamidoamine (PAMAM) dendrimer conjugates with four terminal amine groups each were synthesized by a Schiff-base condensation with an aldehyde-functionalized metal complex. Both dendrimer conjugates showed good dark stability in aqueous DMSO solution for up to 14 h. Photolysis studies in dimethylsulfoxide/phosphate buffered saline solution showed a slightly faster CO-release rates for DAB-G1 compared to the PAMAM-G0 conjugate. The photoactivation at 410 nm was 13-fold slower compared to 365 nm illumination which

is due to the lower extinction coefficient at higher wavelength. The CO release studies using the myoglobin assay showed a release of 50-55% of total CO from both conjugates. Also, the CO release profile of both conjugates were identical with a release of seven equivalents of CO.

In summary, novel manganese(I) tricarbonyl complexes based on the tridentate bis(pyrazolyl)ethylamine (bpea) ligand with pendant functionalized phenyl groups were synthesized and conjugated to biological carrier systems like peptides and dendrimers. Their dark stability establishes them as CORM prodrugs. The monomers show a faster CO-release compared to the peptide and dendrimer conjugates. However, both monomers and peptide conjugates release two equivalents of CO upon photoactivation at 365 nm. The dendrimer conjugates can deliver up to seven equivalents of CO due to the higher number of $Mn(CO)_3$ moieties per molecular unit. In the future, the biological activity of the conjugates needs to be further explored to establish the targeted delivery of CO to cells and tissues.

Zusammenfassung

Das Ziel dieser Doktorarbeit war die Synthese von Mangan(I)-Tricarbonylkomplexen als neuartige photoaktivierbare *CO-releasing molecules* (PhotoCORMs) und ihrer Peptid- und Dendrimer-Konjugate als Trägersysteme für das *targeted delivery* von Kohlenstoffmonoxid in biologischen Systemen.

Dafür wurde eine Serie von sechs Mn(I)-Tricarbonylkomplexen basierend auf dem Bis(pyrazolyl)ethylamin-Liganden (bpea) hergestellt welche einen *para*-substituierten Phenylring mit einer peripheren Iod- oder Alkin-Gruppe enthalten. Diese sollten eine Konjugation an Biomoleküle mittels Sonogashira- oder CuAAC-"click"-Reaktion ermöglichen. Alle Verbindungen wurden in guter Ausbeute mit hoher Reinheit erhalten. Die Einkristall-Röntgenstrukturen der Verbindungen mit Iod- und Alkin-Substituenten belegen die faciale Koordination des tridentaten bpea-Liganden an die $Mn(CO)_3$-Gruppe. Alle Komplexe zeigen bei Lichtausschluß eine sehr gute Stabilität in Dimethylsulfoxid-Lösung über bis zu 14 h, die Photoaktivierung bei 365 nm führt dagegen zur Freisetzung von zwei Äquivalenten Kohlenstoffmonoxid pro Mol Komplex. Obwohl die Verbindungen MLCT-Banden um 350 nm ausweisen, können sie auch noch bei 410 nm stimuliert werden, was für biologische Anwendungen vorteilhaft ist. Die photoinduzierte CO-Freisetzung wurde auch mittels IR-Spektroskopie in Lösung verfolgt. Die Banden neu auftretender Intermediate konnten dabei mit Hilfe von DFT-Rechnungen zugeordnet werden und belegen die Bildung von *cis*-$Mn(CO)_2$-Spezies nach der Freisetzung eines ersten Äquivalents Kohlenstoffmonoxid.

Die CO-Freisetzung wurde auch mit Hilfe eines des fluoreszenten CO-Indikators COP-1 untersucht. Während bei Inkubation im Dunkeln auch bei einem 10:1-Verhältnis von CORM zu COP-1 kein Signal beobachtet werden konnte, führt die lichtinduzierte CO-Freisetzung zu einem konzentrationsabhängigen Anstieg der Fluoreszenz. Die photoaktivierte CO-Freisetzung wurde auch in lebenden HUVEC-Zellen untersucht. In der überstehenden Lösung konnte ein Ansteig der COP-1-Fluoreszenz relativ zum Hintergrund um einen Faktor von 15 beobachtet werden während die Intensititäszunahme für die Zellfraktion nur bei etwa 5-fach lag. Dies

könnte auf eine nur geringe Zellaufnahme von COP-1 oder CORM oder beider Moleküle zurückzuführen sein. Die Untersuchungen etablieren die bpea-Komplexe aber eindeutig als photoaktivierbare *CO-releasing molecules* (PhotoCORMs).

Peptide sind attraktive Trägersysteme für das *cellular delivery* von Metallkomplexen. Als Modell für solche Trägerpeptide wurde die *transforming growth factor β*-bindende (TGF-β) Sequenz durch Festphase-Peptidsynthese hergestellt. Die Anknüpfung von $[Mn(bpea)(CO)_3]^+$ an das Peptid über eine periphere Funktionalität des Liganden über eine Sonogashira-Kreuzkupplung bzw. CuAAC-"Click"-Reaktion sollte in einer Postlabelling-Strategie erfolgen. Obwohl verschiedene Bedingungen getestet wurden führte erstere Reaktion jedoch nicht zum Erfolg. Die CuAAC-Reaktion zwischen einem Alkin-funktionalisierten Metallkomplex und einem Azid-terminierten Peptid führt dagegen zu dem gewünschten *N*-terminal funktionalisierten Konstrukt, welches über eine Triazolgruppe zusammengehalten wird. Trotzdem zeigte das Konjugat auf Grund einer Imin-Bindung im bpea-Liganden eine Tendenz zur Hydrolyse in wässrigem Medium. Als Alternative wurde daher die milde und katalysatorfreie Oxim-Ligation in Verbindung mit einem stabileren, Amin- anstatt Imin-basierten Liganden untersucht. Die Kupplung zwischen einem Aminoxyessigsäure-terminierten TGF-β_1-bindenden Peptid und einem Aldehyde-funktionalisierten Metallkomplex ergab das gewünschte Konjugat in guter Ausbeute mit höher Stabilität. Für bis zu 96 h konnte selbst bei wiederholten *freeze-thaw*-Zyklen keinerlei Zersetzung beobachtet werden. Das CO-Freisetzungsverhalten von Konjugat und Stammverbindung war identisch, die Photoaktivierung bei 365 nm führt für beide innerhalb von 1–1.5 h zur Freisetzung von zwei Äquivalenten CO pro Mol Komplex. Die Oxim-Ligation konnte so als milder Zugang zu CORM-Peptidkonjugaten etabliert werden.

Dendrimere sind Baum-artige Moleküle mit einer Vielzahl von Funktionalitäten in der Peripherie, die eine Modifikation mit Metallkomplexen für biologische Anwendungen erlauben. Von besonderem Interesse ist hierbei die Anreicherung in Tumorgewebe auf Grund des *enhanced permeability and retention*(EPR)-Effekts. Diaminobutan(DAB)- und Polyamidoamin(PAMAM)-Dendrimere der Generation 1

mit vier terminalen Amingruppen wurden daher in einer Schiff-Base-Kondensation mit Aldehyd-funktionalisierten Mn(bpea)$(CO)_3$-Komplexen umgesetzt. Die erhaltenten Metallkomplex-Dendrimer-Konjugate waren in wässriger DMSO-Lösung im Dunkeln für bis zu 14 h stabil. Die Photolyse zeigte eine geringfügig schnellere CO-Freisetzung für das DAB- vs. dem PAMAM-Dendrimer. Eine Anregung bei 410 nm führte zu einer deutlich langsameren CO-Freisetzung gegenüber der 365 nm-Belichtung. Mit Hilfe des Myoglobin-Assays konnte gezeigt werden daß auf diese Weise 50–55% der Gesamtzahl an CO-Liganden aus dem System freigesetzt werden kann.

Im Rahmen der vorliegenden Arbeit wurden neue Mangan(I)tricarbonyl-Komplexe auf der Basis des tridentaten Bis(pyrazolyl)ethylamin(bpea)-Liganden hergestellt, die in der Peripherie funktionalisierte Phenylgruppen tragen, welche die Anknüpfung an biologische Trägersysteme auf der Basis von Peptiden und Dendrimeren erlauben. Auf Grund ihrer Stabilität unter Lichtausschluß sind diese Verbindungen als CORM-Prodrugs geeignet. Die Photoaktivierung bei 365 nm führt zur Freisetzung von zwei Äquivalenten CO pro Mol CORM, wobei die Stammverbindungen eine etwas schnellere Kinetik aufweisen als die Konjugate. Insbesondere die Dendrimer-basierten Systeme können auf Grund der hohen Anzahl von Mn$(CO)_3$-Gruppen bis zu sieben CO pro Mol Konjugat liefern.

Für die Zukunft bleibt zu zeigen ob diese Konjugate eine zelluläre Anreicherung für biologische Anwendungen erlauben wird.

(übersetzt aus der englischen Originalfassung der Doktorarbeit von Prof. Dr. Ulrich Schatzschneider)

5 Experimental Section

5.1 General procedures and instrumentation

General

Reactions were carried out in oven-dried Schlenk glassware under an atmosphere of pure dinitrogen when necessary. Solvents such as methanol, acetone, and acetonitrile were dried over 3 Å molecular sieves and degassed with pure dinitrogen prior to use. All reactions involving manganese carbonyl complexes were protected from light by wrapping the apparatus in aluminium foil. Fmoc-Aoa-OH (**37**) and azidoacetic acid were synthesized according to the literature procedures.[105-149] All reagents were obtained from commercial sources and used without further purification.

NMR spectroscopy

NMR spectra were recorded on Bruker Avance 200, DPX 200, DRX 300, DRX 400 and Avance 500 spectrometers (^{1}H: 200.13, 300.13, 400.13, and 500.13 MHz, respectively; ^{13}C: 50.33, 75.47, 100.62, and 125.75 MHz; ^{19}F: 188.09 MHz, ^{11}B: 96.30, and 160.47 MHz) at ambient temperature. Chemical shifts δ in ppm indicate a downfield shift relative to tetramethylsilane (TMS) and were referenced relative to the signal of the solvent.[155] ^{11}B NMR signals are quoted relative to $BF_3 \cdot OEt_2$; and ^{19}F NMR signals relative to $CFCl_3$. Coupling constants *J* are given in Hz. Individual peaks are marked as singlet (s), doublet (d), doublet-of-doublet (dd), triplet (t), quartet (q), or multiplet (m). Spectra were analysed with MestReNova (V 5.2.5) or TopSpin (V 3.2).

Mass spectrometry

Mass spectra were measured on VG Autospec (EI, FAB), Bruker Esquire 6000 (ESI) and Bruker MicroTOF (ESI) instruments. Only characteristic fragments are given for the most abundant isotope peak. The solvent flow rate for the ESI measurements was 4 μL min^{-1} with a nebulizer pressure of 5 psi and a dry gas flow rate of 4 L min^{-1} at a dry gas temperature of 180 °C. 3-Nitrobenzylalcohol (3-NBA) was used as the matrix in the FAB measurements. Data were recorded in positive ion mode.

IR spectroscopy

Infrared spectra were recorded on pure solid samples using a Bruker Tensor 27 IR spectrometer equipped with a Pike MIRacle Micro ATR accessory or a Nicolet 380 FT-IR spectrometer equipped with a SMART iTR ATR unit. IR spectra of liquid samples were recorded with a Jasco FT/IR-4100 spectrometer using a flow-cell holder equipped with calcium fluoride windows (d = 4 mm) and a Teflon spacer (d = 0.5 mm).

Microanalysis

The elemental composition (C, H, N) of the compounds was determined with a VarioEL instrument from Elementar Analysensysteme GmbH, Hanau. The elemental composition of halogenated compounds was determined with an EA 3000 Elemental Analyser from HEKAtech GmbH, Wegberg.

UV/Vis spectroscopy

UV/Vis spectra were recorded on an Agilent 8453 diode array spectrophotometer in quartz cuvette (d = 1 cm) with Teflon caps. Absorption maxima and the molar extinction coefficient ε_{max} are given in nm and $L \cdot mol^{-1} \cdot cm^{-1}$, respectively.

5.1.1 Single crystal X-ray diffraction

The X-ray crystal structure determination of **16, 19,** and **20** was carried out by Christoph Nagel. The crystal structure of **26** was solved by Dr. Krzysztof Radacki, Institut für Anorganische Chemie, Universität Würzburg. Crystal and refinement data are summarized in the appendix. For the crystal structure determination, the diffraction data was collected on an Oxford Diffraction system using a Sapphire 2-CCD detector for **16** and **19**, a Bruker Apex-II CCD diffractometer for **20** and, a Bruker D8 Quest diffractometer for **26** using graphite-monochromated Mo-$K\alpha$ radiation (λ = 0.71073 Å). Final cell constants were obtained from a least square fit of a subset of a few thousand strong reflections. For crystal structures **16** and **19**, the programs CrysAlis RED and CrysAlis CCD, for **20**, the Olex2 software, and for **26**, the SAINT-PLUS software (ver. 8.18C, Bruker AXS), were used for cell refinement and data reduction. The SADABS program was used to account for the absorption, and SHELXL-97 as well as Olex2 for refinement and drawing of the structures.[156-158]

5.1.2 Myoglobin assay

Horse skeletal muscle myoglobin (10 mg) was dissolved in 0.1 M phosphate buffer (2 mL, pH 7.4) and filtered off to get a clear solution. The concentration of myoglobin solution was determined using $\varepsilon_{560nm}(MbFe^{II})$ = 13.8 L·mmol^{-1}·cm^{-1}.[73] In a quartz cuvette, a solution of horse skeletal muscle myoglobin in 0.1 M phosphate buffer (PBS, pH 7.4) was degassed by bubbling with dinitrogen and reduced by addition of sodium dithionite (100 mM, 100 μL) in PBS buffer (0.1 M, pH 7.4). To this mixture, 10 μL of either metal complex or peptide conjugate in pure dimethylsulfoxide was added to give a total volume of 1000 μL with final concentrations of 10 μM of CORM, 10 mM of sodium dithionite, and 60 μM of myoglobin with $A_{557} < 1$. The solution was illuminated under dinitrogen either using a UV/Vis hand lamp (365 nm, UVIlite LF-206LS, 6 W, UVITEC, UK) or a custom-built LED light source (410 nm, 5 mm round type UV-LEDs, model YDG-504VC, Kingbright Elec. Co., Taipei, Taiwan, part no. 181000-05) positioned perpendicular to the cuvette at a distance of 3 cm. The illumination was interrupted in regular intervals to take UV/Vis spectra on an Agilent 8453 UV/Vis diode array spectrophotometer. As a dark control, measurements were carried out by using the automated spectrophotometer software for a pre-defined period of time (16 h). The concentration of MbCO was calculated from changes in the absorption of the Q-band region at 540 nm according to Eq. 1 using $\varepsilon_{540nm}(MbCO)$ = 15.4 L·mmol^{-1}·cm^{-1}.[73] The number of CO equivalents and the half-life time of the CO release were determined by a first-order exponential fit from a plot of c(MbCO) vs illumination time. All experiments were carried out in triplicate.

$$c(MbCO) = \left[\frac{A(t)}{l} - \frac{A(t=0)}{l}\right] \cdot \frac{1}{\varepsilon 540\text{nm}(MbCO) - \frac{A(t=0)}{c_0(Mb) \cdot l}} \qquad (\mathbf{1})$$

5.1.3 High-pressure liquid chromatography (HPLC)

The analytical and preparative HPLC was performed with a DIONEX Ultimate 3000 instrument equipped with a diode array detector and a ReproSil 100 column (C18, 5 µm, 4.6 mm diameter for analytical and 10 mm diameter for preparative HPLC, 250 mm column length) using either an isocratic gradient of 40% acetonitrile/water over 30 min at a flow rate of 0.6 mL min^{-1} or a linear gradient of 5-90% acetonitrile/water containing 0.1% TFA as the eluent over 50 min at a flow rate of 0.6 mL min^{-1} for analytical and 3.0 mL min^{-1} for preparative chromatography, respectively.

5.1.4 Solid-phase peptide synthesis (SPPS)

The peptides were synthesized manually in a filter syringe according to the method described by Kirin *et al*. using the Fmoc strategy on a preloaded H-L-His(Trt)-2CT resin as the solid support.[159] All the amino acids were used in the L-configuration. The Fmoc-protected amino acids were deprotected on the resin with a solution of piperidine in *N*,*N*-dimethylformamide (30%, v/v). For each coupling step, Fmoc-amino acids (5 equiv., 0.97 M in DMF) and coupling reagent (HOBT/HBTU, 0.97 M in DMF each) were used. Ten equivalents of diisopropylethylamine (DIEA) were used as the activator base. The completeness of each coupling step was monitored with the Kaiser test.[160] For a typical Kaiser test, a few resin beads were incubated for 5 min at 90 °C with two drops of each of the following reagents: i) a solution of ninhydrin in ethanol (5%, w/v), ii) a solution of phenol in ethanol (80%, w/v) and iii) a mixture of an aqueous potassium cyanide solution (1 mM) and pyridine (2% v/v). The peptide was cleaved from the solid support manually in a filter syringe at room temperature using a cleavage cocktail of TFA/TIS/H_2O (90:5:5, v/v). The peptide was isolated by precipitation with cold diethyl ether (-25 °C) and repeated cycles of washing, centrifuging, and decanting. The residue was then dissolved in acetonitrile/water (1:1, v/v) and lyophilized to yield the peptides as white solids.

5.1.5 Photolysis experiments monitored by solution IR spectroscopy

The photolysis experiments were monitored by IR spectroscopy with solutions of the complexes in pure DMSO on a Jasco FT/IR-4100 spectrometer. An IR flow-cell holder equipped with calcium fluoride windows and a Teflon spacer was filled with a freshly prepared solution of metal complex in DMSO (9 mM). Background corrections were made against the pure solvent. Illuminations were carried out using an UV/Vis hand lamp (365 nm, UVIlite LF-206LS, 6 W, UK) with the flow cell positioned at a distance of 3 cm. The illumination was interrupted at a regular intervals and IR spectra were recorded.

5.1.6 Ferrioxalate actinometry

In a 1 cm quartz cuvette, 0.006 M potassium ferrioxalate (3 mL) in 0.05 M sulfuric acid (3 mL) as the chemical actinometer was illuminated with a 365 nm UV hand lamp under efficient stirring. 1 mL of this solution was then mixed with 1,10-phenanthroline in water (0.1% w/v) and 1 M aqueous sodium acetate buffer (0.5 mL, pH 3.5) and further diluted to 10 mL with water. A reference sample was prepared the same way but without illumination. Both solutions were placed in the dark for 1 h to allow the complexation to complete. The absorbance was then measured at 510 nm (ε = 11,100 L·mmol^{-1}·cm^{-1}). A_{510} was kept within the range of 0.4 - 1.0. The photon flux of the 365 nm UV hand lamp was then calculated according to Eq. 2 using $\Phi_{365\,nm}$ = 1.21.[161]

$$\emptyset_p = \frac{\Delta A \cdot V_1 \cdot 10^{-3} \cdot V_3}{\emptyset_\lambda \cdot \varepsilon_{510} \cdot V_2 \cdot t} \qquad (\mathbf{2})$$

Here, V_1 = volume of potassium ferrioxalate solution illuminated, V_2 = volume of V_1 used for complexation with 1,10-phenanthroline, V_3 = total volume. The value of Φp obtained was (2.82 ± 0.05) x 10^{-8} Einstein s^{-1}.

5.1.7 Cell culture experiments

Cell culture experiments were performed by Prof. Dr. Benito Yard, V. Medizinische Klinik, Universitätsmedizin Mannheim. Human umbilical vein endothelial cells (HUVECs) were received in collaboration with the Institute of Transfusion Medicine and Immunology, Medical Faculty Mannheim, University of Heidelberg. Permission for isolation and propagation of endothelial cells from umbilical cords for research purposes was granted by the local ethics committee of the clinical faculty Mannheim, University of Heidelberg with informed consent in writing. HUVECs were isolated from fresh umbilical cords as described previously.[162] The cells were cultured in endothelial cell growth medium (EGM) (Promocell, Heidelberg, Germany) in T25 flasks (Greiner, Frickenhausen, Germany) coated with gelatine (1%). Confluent monolayers were passaged by Trypsin/EDTA (Sigma-Aldrich, St. Louis, MO). Characterization of endothelial cells were performed on the basis of a positive uptake of acetylated LDL, Factor VIII related antigen, and PECAM (CD31) expression, and a negative staining for alpha smooth muscle actin.

***In vitro* detection of CO release using the COP-1 fluorogenic switch-on probe**

(a) In phosphate-buffered saline: To a 96-well microtiter plate, phosphate-buffered saline (PBS, 100 μL) containing different concentrations of compound (3–100 μM) dissolved in DMSO was added to each well followed by the addition of COP-1 dissolved in PBS to a final concentration of 10 μM. The plate was subsequently exposed for 30 min to UV light at 365 nm using a 6 W UV hand lamp (UVITEC Cambridge, UK) positioned parallel to the plate at a distance of 3 cm. Meanwhile, another plate was prepared under the same experimental conditions but kept in the dark for 30 min. The fluorescence was measured immediately afterwards on an Infinite M200 reader (Tecan, Crailsheim, Germany) using the I-control v9 software. The fluorescence intensity was assessed at excitation and emission wavelengths of 475 and 510 nm, respectively. The experiments along with the controls were performed in quadruplicate and the data are expressed as mean fluorescence intensity ± SD.

(b) In cell culture: HUVEC cells were seeded in 96-well plates (Greiner, Frickenhausen, Germany) at a concentration of 10^5 cells/well. After 1 d of seeding, the supernatant was aspirated and replaced by a freshly prepared solution of compound in DMSO diluted with PBS to a final concentration of 100 μM of metal carbonyl compound. Then, COP-1 dissolved in PBS was added to a final concentration of 10 μM. As negative controls, pure PBS buffer, COP-1 (10 μM), metal complex (100 μM) and sodium hexafluorophosphate (100 μM) were also included in the experiments. One plate was subsequently exposed for 30 min to UV light at 365 nm using a 6 W UV hand lamp (LF-206-LS, UVITEC, Cambridge, UK) positioned parallel to the plate at a distance of 3 cm. Meanwhile, another plate was prepared under the same experimental conditions but kept in the dark for 30 min. After exposure, the whole supernatant was transferred to a fresh plate to measure the fluorescence intensity in the medium. The cell-containing plates were washed twice with PBS and after the last wash, 100 μL of PBS was added to each well and the fluorescence intensity measured on an Infinite M200 reader (Tecan, Crailsheim, Germany) using the I-control v9 software. The fluorescence intensity was assessed at excitation and emission wavelengths of 475 and 510 nm, respectively. The experiments along with the controls were performed in quadruplicate and the data are expressed as mean fluorescence intensity ± SD.

5.1.8 Density functional theory calculations

DFT calculations were carried out by Prof. Dr. Ulrich Schatzschneider on the Linux cluster of the Leibniz-Rechenzentrum (LRZ) in Munich with ORCA version 2.8,[163] using the BP86 functional with the resolution-of-the-identity (RI) approximation, a def2-TZVP/def2-TZVP/J basis set,[164-165] the tightcf and grid4 options, and the COSMO solvation model with dimethylsulfoxide as the solvent for geometry optimizations and subsequent calculation of vibrational frequencies to characterize the structures obtained as minima by inspection for the absence of imaginary modes. Reported vibrational modes are scaled with a factor of 1.036 relative to the calculated values.

5.2 Synthetic procedures

5.2.1 Synthesis of *N*-[2,2-(dimethoxy)ethane]-1,8-naphthalimide[166-167]

USC-SP-001-01

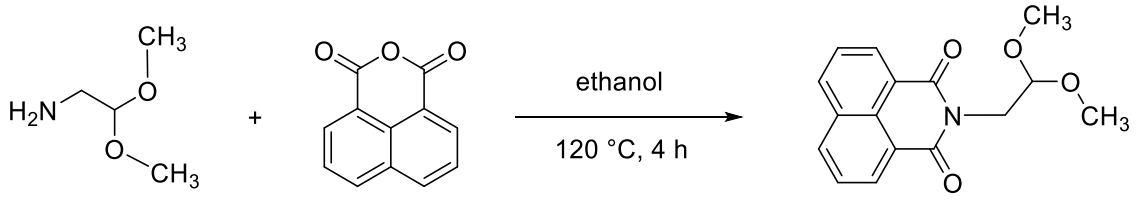

1 $C_4H_{11}NO_2$ 105 g/mol

2 $C_{12}H_6O_8$ 198 g/mol

3 $C_{16}H_{15}NO_4$ 285 g/mol

1,8-Naphthalic anhydride (19.82 g, 0.10 mol) and 2,2-dimethoxyethaneamine (12.49 g, 0.12 mol) were completely dissolved in ethanol (500 mL) and heated to 120 °C for 4 h. The reaction mixture was then allowed to cool to room temperature whereupon the compound precipitated as a crystalline white solid which was filtered off and dried in the air. A second crop was isolated by removing the solvent under vacuum and also air dried.

Yield: 97% (27.73 g, 0.10 mol). IR (ATR, $\tilde{\upsilon}/cm^{-1}$) 2922, 1697 ($\nu_{C=O}$), 1655, 1584, 1437, 1121 (ν_{C-O}). MS (FAB+): *m/z* 285 $[M]^+$. ^{1}H-NMR (200 MHz, $CDCl_3$, ppm): δ 8.61 (d, 2H, ^3J = 8.4 Hz, $H_{2,7}$-*napth*), 8.22 (d, 2H, ^3J = 7.3 Hz, $H_{3,6}$-*napth*), 7.75 (dd, 2H, ^3J = 8.24, 7.29 Hz, $H_{4,5}$-*napth*), 4.92 (t, 1H, C*H*$(OCH_3)_2$), 4.39 (d, 2H, ^3J = 5.7 Hz, N-CH_2), 3.42 (s, 6H, -OCH_3). ^{13}C-NMR (50.33 MHz, $CDCl_3$, ppm) δ 41.06 (*C*H_2), 53.63 (OCH_3), 100.83 (*C*H), 122.77 ($C_{1,8}$-*napth*), 127.09 (C_9-*napth*), 128.47 ($C_{3,6}$-*napth*), 131.57 (C_{10}-*napth*), 131.78 ($C_{4,5}$-*napth*), 134.14 ($C_{2,7}$-*napth*), 164.42 (*C*=O).

5.2.2 Synthesis of *N*-[2,2-bis(pyrazolyl)ethane]-1,8-naphthalimide[166-167]

USC-SP-002-01

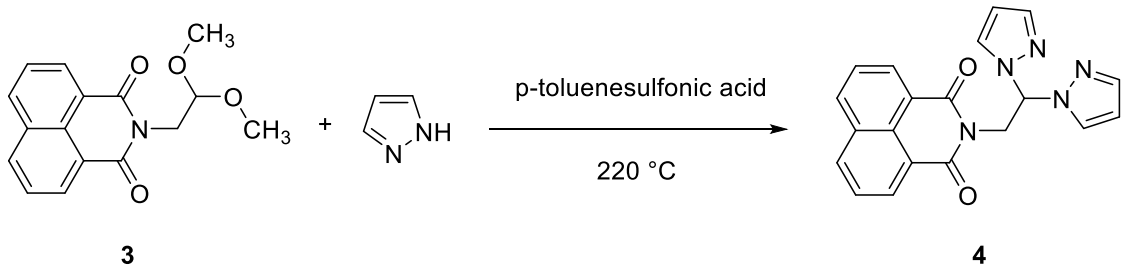

3 **4**

$C_{16}H_{15}NO_4$	$C_3H_4N_2$	$C_{20}H_{15}N_5O_2$
285 g/mol	68 g/mol	357 g/mol

Pyrazole (19.06 g, 0.28 mol), *N*-[2,2-(dimethoxy)ethane]-1,8-naphthalimide (**3**) (26.49 g, 0.09 mol) and *p*-toluenesulfonic acid (500 mg) were placed in a 500 mL round bottom flask. A distillation head equipped with a volumetric liquid trap was attached to the flask. The setup was evacuated, backfilled with dinitrogen and heated to 220 °C. The mixture was kept at this temperature until 5 mL of methanol were collected. The molten product was then carefully added to boiling dichloromethane (500 mL). Precautions were taken since the addition of the molten product caused splattering of solvent and product. The solution was allowed to cool to room temperature, and the solvent was reduced to half of its volume under vacuum. The solution was then shaken in a separating funnel against aqueous potassium carbonate solution. The organic layer was separated, dried over magnesium sulfate and filtered. Removal of the solvent under vacuum gave a pale brown solid product.

Yield: 81% (26.82 g, 0.07 mol). IR (ATR, $\tilde{\nu}/cm^{-1}$) 3124, 2162, 1699 ($\nu_{C=O}$), 1658 ($\nu_{C=N}$), 1587, 1436, 1386. MS (FAB+): *m/z* 358 $[M+H]^+$, 380 $[M+Na]^+$. ^{1}H-NMR (200 MHz, $CDCl_3$, ppm): δ 8.55 (d, 2H, ^3J = 7.3 Hz, $H_{2,7}$-*napth*), 8.20 (d, 2H, ^3J = 8.3 Hz, $H_{4,5}$-*napth*), 7.82 (d, 2H, ^3J = 2.2 Hz, H_5-pz), 7.72 (dd, 2H, ^3J = 8.1, 7.2 Hz, $H_{3,6}$-*napth*), 7.46 (d, 2H, ^3J = 1.4 Hz, H_3-pz), 7.13 (t, 1H, ^3J = 7.3 Hz, C*H*(pz)$_2$), 6.25 (m, 2H, H_4-pz), 5.29 (d, 2H, ^3J = 7.3 Hz, CH_2). ^{13}C-NMR (50.33 MHz, $CDCl_3$, ppm) δ 42.61 (CH_2), 72.32 (CH), 106.83 (C_4-pz), 122.18 ($C_{1,8}$-*napth*), 127.09 (C_9-*napth*), 128.42 ($C_{3,6}$-*napth*), 129.60 (C_5-pz), 131.64 ($C_{4,5}$-*napth*), 131.76 (C_{10}-*napth*), 134.43 ($C_{2,7}$-*napth*), 140.48 (C_3-pz.), 164.11 (*C*=O).

5.2.3 Synthesis of 2,2'-bis(pyrazolyl)ethylamine (bpea)[166-167]

USC-SP-003-01

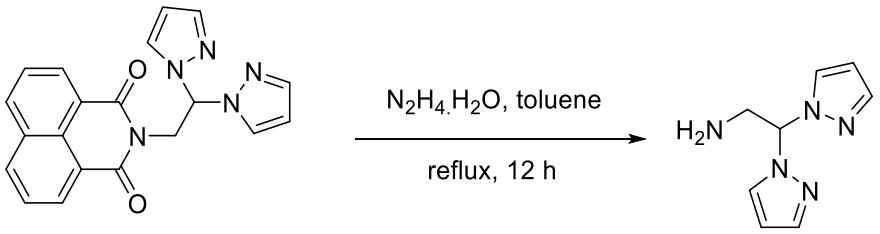

4

$C_{20}H_{15}N_5O_2$
357 g/mol

5

$C_8H_{11}N_5$
177 g/mol

N-[2,2-bis(pyrazolyl)ethane]-1,8-naphthalimide (**4**) (20.00 g, 0.06 mol) was completely dissolved in warm toluene (300 mL). Hydrazine monohydrate (20.34 mL, 0.42 mol) was added and the mixture heated to reflux for 12 h. After cooling to room temperature, the toluene and excess of hydrazine were removed under vacuum and the product was dried at reduced pressure. The solid was dissolved in water (2×100 mL) and the combined solutions were filtered. The water was removed under vacuum to give the product as a sticky brown solid.

Yield: 75% (7.46 g, 0.04 mol). IR (ATR, $\tilde{\nu}/cm^{-1}$): 3353 ($\nu_{N\text{-}H}$), 3103, 2956 ($\nu_{C\text{-}H}$), 1590. MS (FAB+): *m/z* 178 $[M+H]^+$. ^{1}H-NMR (200 MHz, $CDCl_3$, ppm): δ 7.6 (d, 2H, ^3J = 1 Hz, H_3-pz), 7.57 (d, 2H, ^3J = 2 Hz, H_5-pz), 6.39 (t, 1H, ^3J = 7 Hz, C*H*(pz)$_2$), 6.29 (dd, 2H, ^3J = 2, 1 Hz, H_4-pz), 3.77 (d, 2H, ^3J = 6.9 Hz, CH_2), 2.53 (br s, 2H, NH_2). ^{13}C-NMR (50.33 MHz, $CDCl_3$, ppm) δ 44.94 (N-CH_2), 105.28 (*C*(pz)$_2$), 106.84 (C_4-pz), 129.15 (C_5-pz), 140.54 (C_3-pz).

5.2.4 Synthesis of benzylidene(2,2-bis(pyrazolyl)ethyl)amine

USC-SP-004-01

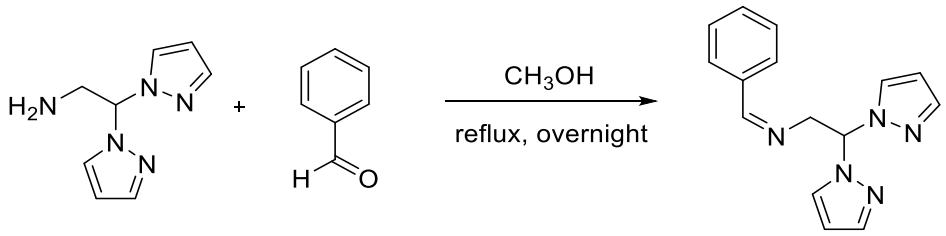

5 $C_8H_{11}N_5$ 177 g/mol

6 C_7H_6O 106 g/mol

9 $C_{15}H_{15}N_5$ 265 g/mol

Bis-2,2-(pyrazol-1-yl)ethylamine (**5**) (2.00 g, 0.01 mol) was dissolved in methanol (75 mL). Once completely dissolved, benzaldehyde (1.12 mL, 0.01 mol) was added and the mixture was heated to reflux overnight. The solvent was removed under vacuum to give a pale yellow solid product.

Yield: 73% (2.12 g, 0.01 mol). Elemental analysis (%): calc. for $C_{15}H_{15}N_5$: C 67.90, H 5.69, N 26.39; found: C 67.75, H 5.88, N 26.74. MS (FAB+): *m/z* 266 $[M+H]^+$. IR (ATR, $\tilde{\upsilon}/cm^{-1}$): 3108 ($\nu_{C\text{-}H}$), 2852, 1649 ($\nu_{C=N}$), 1514, 1434. ^{1}H-NMR (200 MHz, $CDCl_3$, ppm): δ8.20 (s, 1H, C*H*-C_6H_5), 7.67 (d, 2H, ^3J = 2.4 Hz, H_3-pz), 7.56 (d, 2H, ^3J = 1.5 Hz, H_5-pz), 7.39 (m, 5H, C_6H_5), 6.80 (t, 1H, ^3J = 7 Hz, C*H*(pz)$_2$), 6.25 (t, 2H, H_4-pz), 4.66 (d, 2H, ^3J = 6.8 Hz, CH_2). ^{13}C-NMR (50.33 MHz, $CDCl_3$, ppm) δ62.99 (CH_2), 75.24 (C(pz)$_2$), 106.55 (C_4-pz), 128.41 ($C_{3,5}$-C_6H_5), 128.69 ($C_{2,6}$-C_6H_5), 129.22 (C_4-C_6H_5), 131.26 (C_5-pz), 135.79 (C_1-C_6H_5), 140.49 (C_3-Pz), 164.93 (*C*=N).

5.2.5 Synthesis of 2,2-bis(pyrazolyl)ethyl(4-iodobenzylidene)amine

USC-SP-009-01

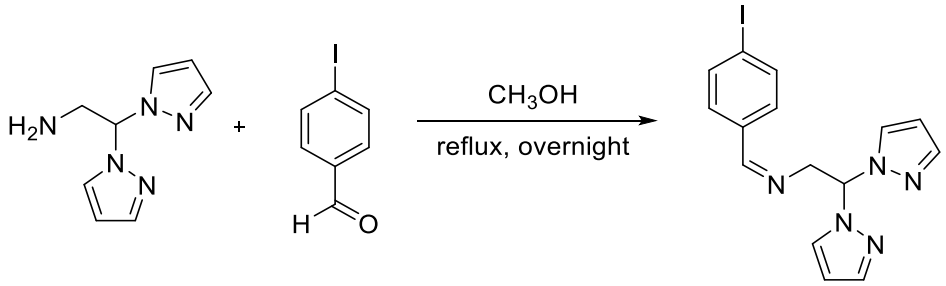

5 $C_8H_{11}N_5$ 177 g/mol

7 C_7H_5IO 232 g/mol

10 $C_{15}H_{14}N_5I$ 391 g/mol

Bis-2,2-(pyrazol-1-yl)ethylamine (**5**) (600 mg, 3.38 mmol) was completely dissolved in methanol (40 mL). *p*-Iodobenzaldehyde (800 mg, 3.38 mmol) was added and the reaction mixture was heated to reflux overnight. After cooling the solution to -20 °C, a colorless crystalline precipitate formed which was filtered off and dried under vacuum.

Yield: 87.8% (1.17 g, 2.99 mmol). Elemental analysis (%): calc. for $C_{15}H_{14}N_5I$: C 46.05, H 3.60, N 17.90; found: C 46.14, H 3.69, N 17.82. MS (FAB+): *m/z* 392 $[M+H]^+$, 414 $[M+Na]^+$. IR (ATR, $\tilde{\upsilon}/cm^{-1}$): 3100 ($\nu_{Ar.C-H}$), 1644 ($\nu_{C=N}$), 1586, 1510, 1436, 1387. ^{1}H-NMR (200 MHz, $CDCl_3$, ppm): δ 8.11 (s, 1H, C*H*=N), 7.71 (d, 2H, ^3J = 8.4 Hz, $H_{3,5}$-C_6H_4), 7.65 (d, 2H, ^3J = 2.3 Hz, H_3-pz), 7.55 (d, 2H, ^3J = 1.5 Hz, H_5-pz), 7.34 (d, 2H, ^3J = 8.4 Hz, $H_{2,6}$-C_6H_4), 6.77 (t, 1H, ^3J = 6.8 Hz, C*H*(pz)$_2$), 6.25 (m, 2H, H_4-pz), 4.64 (dd, 2H, ^3J = 6.8, 1.2 Hz, CH_2). ^{13}C-NMR (100.62 MHz, $CDCl_3$, ppm) δ 62.95 (CH_2), 75.14 (*C*(pz)$_2$), 98.06 (C_4-C_6H_4), 106.61 (C_4-pz), 129.19 (C_5-pz), 129.84 ($C_{2,6}$-C_6H_4), 135.19 (C_1-C_6H_4), 137.95 ($C_{3,5}$-C_6H_4), 140.51 (C_3-pz), 163.88 (*C*=N).

5.2.6 Synthesis of 2,2-bis(pyrazolyl)ethyl(4-ethynylbenzylidene)amine

USC-SP-012-01

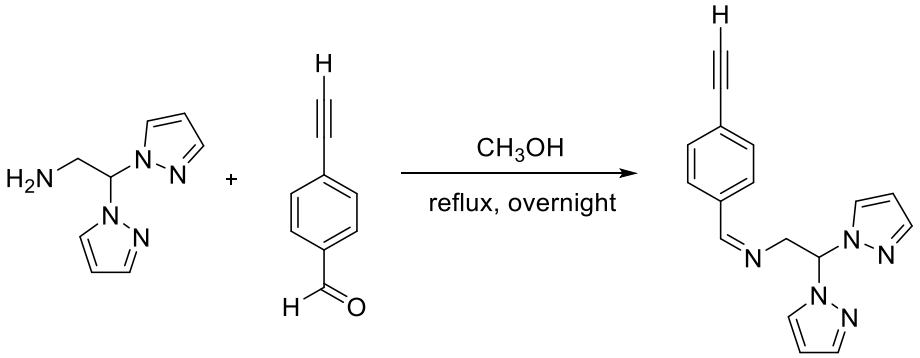

5
$C_8H_{11}N_5$
177 g/mol

8
C_9H_6O
130 g/mol

11
$C_{17}H_{15}N_5$
289 g/mol

Bis-2,2-(pyrazol-1-yl)ethylamine (**5**) (500 mg, 2.82 mmol) was completely dissolved in methanol (100 mL). 4-Ethynylbenzaldehyde (365 mg, 2.83 mmol) was added and the reaction mixture was heated to reflux overnight. After cooling to -20 °C, a colorless crystalline precipitate formed which was filtered off and dried under vacuum.

Yield: 72% (585 mg, 2.02 mmol). Elemental analysis (%): calc. for $C_{17}H_{15}N_5$: C 70.57, H 5.22, N 24.20; found: C 70.49, H 5.31, N 24.27. MS (FAB+): *m/z* 290 $[M+H]^+$, 312 $[M+Na]^+$. IR (ATR, $\tilde{\nu}/cm^{-1}$): 3254 ($\nu_{C\equiv C\text{-}H}$), 3137 ($\nu_{C\text{-}H}$), 2917 ($\nu_{Ar.C\text{-}H}$), 2105 ($\nu_{C\equiv C}$), 1641, 1556, 1433. ^{1}H-NMR (400 MHz, $CDCl_3$, ppm): δ 8.17 (s, C*H*-C_6H_5), 7.66 (d, 2H, ^3J = 2.4 Hz, *H*$_3$-pz), 7.57 (d, 2H, ^3J = 8.4 Hz, *H*$_{3,5}$-C_6H_4), 7.55 (d, 2H, ^3J = 1.6 Hz, *H*$_5$-pz), 7.47 (d, 2H, ^3J = 8.4 Hz, *H*$_{2,6}$-C_6H_4), 6.78 (t, 1H, ^3J = 6.8 Hz, C*H*(pz)$_2$), 6.25 (m, 2H, *H*$_4$-pz), 4.67 (dd, 2H, ^3J = 6.8, 1.2 Hz, C*H*$_2$), 3.16 (s, 1H, Alkynyl-*H*). ^{13}C-NMR (100.62 MHz, $CDCl_3$, ppm) δ 62.99 (*C*H$_2$), 75.20 (*C*$_8$-Alkynyl), 79.34 (*C*(pz)$_2$), 83.29 (*C*$_7$-Alkynyl), 106.59 (*C*$_4$-pz), 124.98 (*C*$_4$-C_6H_4), 128.23 (*C*$_{2,6}$-C_6H_4), 129.23 (*C*$_5$-pz), 132.43 (*C*$_{3,5}$-C_6H_4), 135.87 (*C*$_1$-C_6H_4), 140.5 (*C*$_3$-pz), 164.0 (*C*=N).

5.2.7 Synthesis of benzyl-(2,2-bis(pyrazolyl)ethyl)amine

USC-SP-010-01

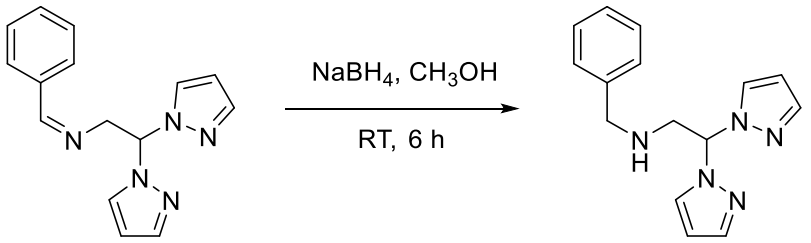

9

$C_{15}H_{15}N_5$
265 g/mol

12

$C_{15}H_{17}N_5$
267 g/mol

Benzylidene-(2,2-bis(pyrazolyl)ethyl)amine (**9**) (230 mg, 0.86 mmol) was completely dissolved in methanol (10 mL). An excess of solid sodium borohydride (65.46 mg, 1.72 mmol) was added in portions and the mixture stirred for 6 h at room temperature. The solvent was then removed under vacuum and the residue was dissolved in ethyl acetate (40 mL). The organic layer was washed with water (3×100 mL), dried over anhydrous sodium sulfate, filtered and then the solvent was removed under vacuum to give a pale yellow solid.

Yield: 78% (177.8 mg, 0.66 mmol). Elemental analysis (%): calc. for $C_{15}H_{17}N_5$: C 67.39, H 6.40, N 26.19; found: C 67.12, H 6.35, N 26.61. MS (FAB+): *m/z* 268 $[M+H]^+$, 290 $[M+Na]^+$. IR (ATR, $\tilde{\upsilon}/cm^{-1}$): 3341 ($\nu_{N\text{-}H}$), 3137 ($\nu_{Ar.C\text{-}H}$), 2830 ($\nu_{C\text{-}H}$), 1599, 1493, 1367. ^{1}H-NMR (400 MHz, $CDCl_3$, ppm): δ7.58 (d, 2H, ^3J = 2.4 Hz, *H*$_3$-pz), 7.55 (d, 2H, ^3J = 1.7 Hz, *H*$_5$-pz), 7.28 (m, 5H, C$_6$*H*$_5$), 6.54 (t, 1H, ^3J = 7 Hz, C*H*(pz)$_2$), 6.27 (m, 2H, *H*$_4$-pz), 3.83 (s, 2H, C*H*$_2$-C$_6$H$_5$), 3.70 (d, 2H, ^3J = 7.0 Hz, C*H*$_2$-NH). ^{13}C-NMR (100.62 MHz, $CDCl_3$, ppm) δ51.19 (*C*H$_2$NH), 53.44 (*C*H$_2$-C$_6$H$_5$), 75.20 (*C*(pz)$_2$), 106.78 (*C*$_4$-pz), 127.33 (*C*$_4$-C$_6$H$_5$), 128.17 (*C*$_{3,5}$-C$_6$H$_5$), 128.65 (*C*$_{2,6}$-C$_6$H$_5$), 129.13 (*C*$_5$-pz), 139.82 (*C*$_1$-C$_6$H$_5$), 140.44 (*C*$_3$-pz).

5.2.8 Synthesis of 2,2-bis(pyrazolyl)ethyl(4-iodobenzyl)amine

USC-SP-011-01

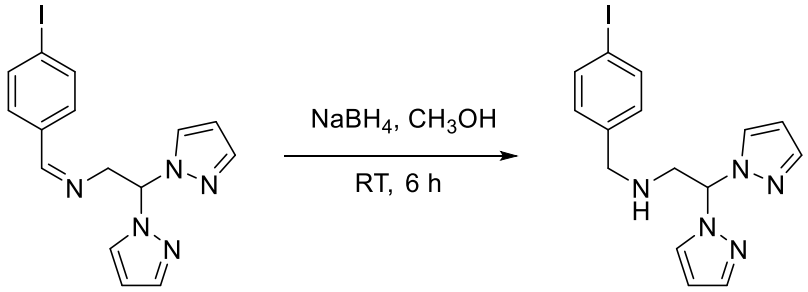

10

$C_{15}H_{14}N_5I$
391 g/mol

13

$C_{15}H_{16}N_5I$
393 g/mol

2,2-bis(pyrazolyl)ethyl(4-iodobenzylidene)amine (**10**) (160 mg, 0.41 mmol) was completely dissolved in methanol (10 mL) and an excess of solid sodium borohydride (38.58 mg, 1.02 mmol) was added in portions with stirring. The mixture was stirred for 6 h at room temperature. The solvent was removed under vacuum and the residue was dissolved in ethyl acetate (40 mL). The organic layer washed with water (3×100 mL), dried over anhydrous sodium sulfate, filtered and then the solvent was removed under vacuum to give a colorless solid.

Yield: 72% (115 mg, 0.29 mmol). Elemental analysis (%): calc. for $C_{15}H_{16}N_5I$: C 45.81, H 4.10, N 17.80; found: C 45.66, H 4.23, N 17.69. MS (FAB+): *m/z* 394 $[M+H]^+$, 416 $[M+Na]^+$. IR (ATR, $\tilde{\upsilon}/cm^{-1}$): 3327 ($\nu_{N\text{-}H}$), 3090 ($\nu_{C\text{-}H}$), 2928 ($\nu_{Ali.C\text{-}H}$), 1510, 1482, 1387, 1283. ^{1}H-NMR (400 MHz, $CDCl_3$, ppm): δ 7.62 (d, 2H, ^3J = 8.3 Hz, $H_{3,5}$-C_6H_4), 7.57 (d, 2H, ^3J = 2.4 Hz, H_3-pz), 7.55 (d, 2H, ^3J = 1.5 Hz, H_5-pz), 7.02 (d, 2H, ^3J = 8.3 Hz, $H_{2,6}$-C_6H_4), 6.52 (t, 1H, ^3J = 7 Hz, C*H*(pz)$_2$), 6.27 (m, 2H, H_4-pz), 3.76 (s, 2H, CH_2-C_6H_4), 3.66 (d, 2H, ^3J = 6.9 Hz, CH_2). ^{13}C-NMR (100.62 MHz, $CDCl_3$, ppm) δ 51.12 (*C*H$_2$), 52.78 (*C*H$_2$-C_6H_4), 75.19 (*C*(pz)$_2$), 92.56 (C_4-C_6H_4), 106.85 (C_4-pz), 129.12 ($C_{3,5}$-C_6H_4), 120.13 ($C_{2,6}$-C_6H_4), 137.69 (C_5-pz), 139.55 (C_1-C_6H_4), 140.46 (C_3-pz).

5.2.9 Synthesis of 2,2-bis(pyrazolyl)ethyl(4-ethynylbenzyl)amine

USC-SP-120-01

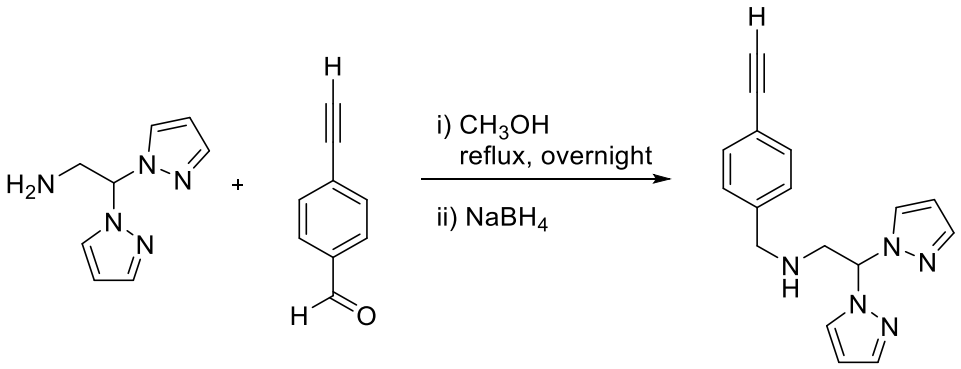

5
$C_8H_{11}N_5$
177 g/mol

8
C_9H_6O
130 g/mol

14
$C_{17}H_{17}N_5$
291 g/mol

Bis-2,2-(pyrazolyl)ethylamine (**5**) (645 mg, 3.85 mmol) was completely dissolved in methanol (100 mL). 4-Ethynylbenzaldehyde (474 mg, 3.84 mmol) was added and the reaction mixture was heated to reflux overnight. After cooling to room temperature, solid sodium borohydride (291.3 mg, 7.70 mmol) was added slowly under stirring and the reaction mixture was further stirred for 7 h at room temperature. Water (20 mL) was added and the product was extracted with dichloromethane (3x100 mL), The organic layer was separated, dried over magnesium sulfate (~10 g), and filtered. The solvent was then removed under reduced pressure to give the product as a light brown oil and dried under vacuum.

Yield: 90% (1.00 g, 3.43 mmol). Elemental analysis (%): calc. for $C_{17}H_{17}N_5$: calc. for C 70.08, H 5.88, N 24.03; found: C 69.73, H 5.74, N 24.32. MS (FAB+): *m/z* 292 $[M+H]^+$. IR (ATR, $\tilde{\nu}/cm^{-1}$): 3284 ($\nu_{C\equiv C\text{-}H}$), 3137 ($\nu_{C\text{-}H}$), 2928 ($\nu_{Ar.C\text{-}H}$), 1510, 1390, 1289, 1092, 1044, 752. ^{1}H-NMR (200 MHz, DMSO-d_6, ppm): δ7.92 (d, 2H, ^3J = 2.2 Hz, H_3-pz), 7.49 (d, 2H, ^3J = 1.1 Hz, H_5-pz), 7.39 (d, 2H, ^3J = 7.9 Hz, $H_{2,6}$-C_6H_4), 7.24 (d, 2H, ^3J = 8.1 Hz, $H_{3,5}$-C_6H_4), 6.37 (t, 1H, ^3J = 7.1 Hz, C*H*(pz)$_2$), 6.28 (dd, 2H, ^3J = 3.9 Hz, 2.0 Hz, H_4-pz), 4.12 (s, 1H, C≡C*H*), 3.69 (s, 2H, CH_2-C_6H_4), 3.49 (d, 2H, ^3J = 6.9 Hz, CH_2-CH). ^{13}C-NMR (50.33 MHz, DMSO-d_6, ppm) δ50.28 (*C*H$_2$), 51.64 (*C*H$_2$- C_6H_4), 73.96 (*C*(pz)$_2$), 80.34 (C_8-Alkynyl), 83.55 (C_7-Alkynyl), 105.87 (C_4-pz), 119.96 (C_4-C_6H_4), 128.07 ($C_{2,6}$-C_6H_4), 129.45 (C_5-pz), 131.54 ($C_{3,5}$-C_6H_4), 139.43 (C_3-pz), 141.65 (C_1-C_6H_4).

5.2.10 Synthesis of [Mn(bpea$^{N=CHC_6H_5}$)(CO)$_3$]PF$_6$

USC-SP-008-01

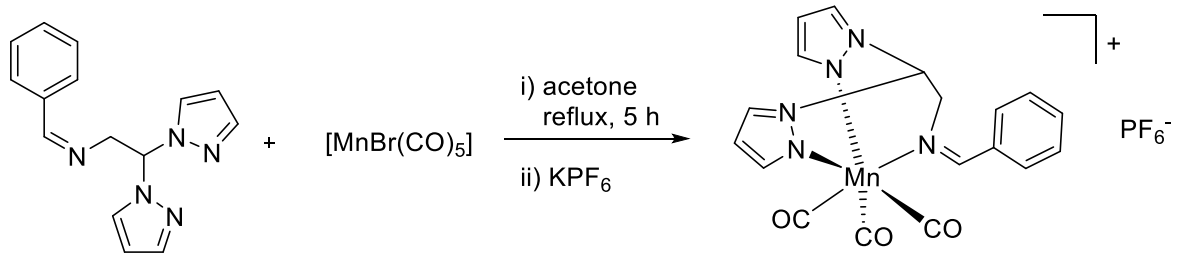

9

$C_{15}H_{15}N_5$
265 g/mol

15

$C_{18}H_{15}F_6MnN_5O_3P$
549 g/mol

Manganese pentacarbonyl bromide (206.17 mg, 0.75 mmol) and benzylidene(2,2-bis(pyrazolyl)ethyl)amine (**9**) (200 mg, 0.75 mmol) were completely dissolved in anhydrous acetone (20 mL) and heated to reflux under a dinitrogen atmosphere for 5 h with exclusion of light. The solvent was then removed under vacuum. The yellow residue was washed with diethylether (10 mL) and then redissolved in methanol (10 mL). Potassium hexafluorophosphate (207.07 mg, 1.12 mmol) was added to precipitate a yellow product, which was filtered off, washed with water (10 mL) and diethylether (10 mL) and dried under vacuum.

Yield: 64% (263 mg, 0.48 mmol). Elemental analysis (%): calc. for $C_{18}H_{15}F_6MnN_5O_3P{\cdot}H_2O$: C 38.11, H 3.02, N 12.35; found: C 38.36, H 2.83, N 11.99. MS (ESI$^+$, CH_3OH): *m/z* 403.82 $[M\text{-}PF_6]^+$. UV-Vis (DMSO): λ_{max} (ε) = 341 nm (3460 l·mol^{-1}·cm^{-1}). IR (ATR, $\tilde{\upsilon}$/cm^{-1}): 3135 (w), 2962 (w), 2040 (s, $\nu_{C\equiv O}$), 1932 (s, $\nu_{C\equiv O}$), 1625 (s, $\nu_{C=N}$), 1414, 1261, 1102, 1065. ^{1}H-NMR (400 MHz, acetone-d_6, ppm): δ9.41 (s, 1H, C*H*=N), 8.45 (dd, 2H, ^3J = 2.7, 0.6 Hz, *H*$_5$-pz), 8.38 (d, 2H, ^3J = 2.3 Hz, *H*$_3$-pz), 7.81 (t, 1H, ^3J = 2.5 Hz, C*H*(pz)$_2$), 7.66 (m, 5H, C$_6$*H*$_5$), 6.75 (m, 2H, *H*$_4$-pz), 4.67 (dd, 2H, ^3J = 2.6, 2.1 Hz, C*H*$_2$). ^{13}C-NMR (100.62 MHz, actone-d_6, ppm) δ62.98 (*C*H$_2$), 69.67 (*C*(pz)$_2$), 109.55 (*C*$_4$-pz), 129.02 (*C*$_4$-C$_6$H$_5$), 129.69 (*C*$_{3,5}$-C$_6$H$_5$), 132.26 (*C*$_{2,6}$-C$_6$H$_5$), 135.76 (*C*$_5$-pz), 136.88 (*C*$_1$-C$_6$H$_5$), 146.83 (*C*$_3$-pz), 181.64 (*C*=N).

5.2.11 Synthesis of [Mn(bpea$^{N=CHC_6H_4I}$)(CO)$_3$]PF$_6$

USC-SP-014-01

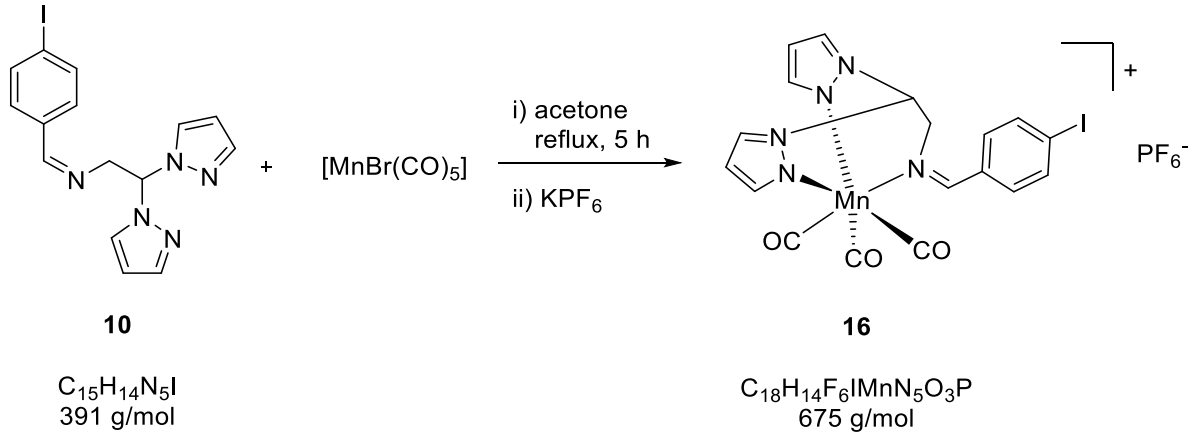

10

$C_{15}H_{14}N_5I$
391 g/mol

16

$C_{18}H_{14}F_6IMnN_5O_3P$
675 g/mol

Manganese pentacarbonyl bromide (140.19 mg, 0.51 mmol) and 2,2-bis(pyrazolyl)ethyl(4-iodobenzylidene)amine (**10**) (200 mg, 0.51 mmol) were completely dissolved in anhydrous acetone (20 mL) and heated to reflux under a dinitrogen atmosphere for 5 h with exclusion of light. The solvent was then removed under vacuum. The yellow residue was washed with diethylether (10 mL) and redissolved in methanol (10 mL). Potassium hexafluorophosphate (140.8 mg, 0.76 mmol) was added to precipitate the yellow product which was filtered off, washed with water (10 mL) and diethylether (10 mL) and dried under vacuum.

Yield: 43% (148 mg, 0.22 mmol). Elemental analysis (%): calc. for $C_{18}H_{14}F_6IMnN_5O_3P$: C 32.02, H 2.09, N 10.37; found: C 31.83, H 1.91, N 10.26. MS (ESI$^+$, CH_3OH): *m/z* 529.74 [M-PF$_6$]$^+$. UV-Vis (DMSO): λ_{max} (ε) = 348 nm (4410 l·mol^{-1}·cm^{-1}). IR (ATR, $\tilde{\upsilon}$/cm^{-1}): 3135 (w), 3021 (w), 2043 (s, $\nu_{C\equiv O}$), 1931 (s, $\nu_{C\equiv O}$), 1624 (s, $\nu_{C=N}$), 1412, 1295, 1103. ^{1}H-NMR (400 MHz, acetone-d_6, ppm): δ 9.34 (s, 1H, C*H*=N), 8.43 (dd, 2H, ^3J = 2.7, 0.6 Hz, *H*$_5$-pz), 8.38 (d, 2H, ^3J = 2.2 Hz, *H*$_3$-pz), 8.03 (d, 2H, ^3J = 4.7 Hz, *H*$_{3,5}$-C$_6$H$_4$), 7.76 (t, 1H, ^3J = 2.7 Hz, C*H*(pz)$_2$), 7.52 (d, 2H, ^3J = 8.1 Hz, *H*$_{2,6}$-C$_6$H$_4$), 6.75 (m, 2H, *H*$_4$-pz), 4.63 (m, 2H, C*H*$_2$). ^{13}C-NMR (100.62 MHz, acetone-d_6, ppm) δ 51.42 (*C*H$_2$), 57.99 (*C*(pz)$_2$), 88.69 (*C*$_4$-C$_6$H$_4$), 98.76 (*C*$_4$-pz), 120.04, 123.03, 125.23, 127.75, 127.97, 137.01 (*C*$_3$-pz), 164.85, 171.11 (*C*=N), 209.46 (*C*≡O), 210.15 (*C*≡O).

5.2.12 Synthesis of [Mn(bpea$^{N=CHC_6H_4C\equiv CH}$)(CO)$_3$]PF$_6$

USC-SP-015-01

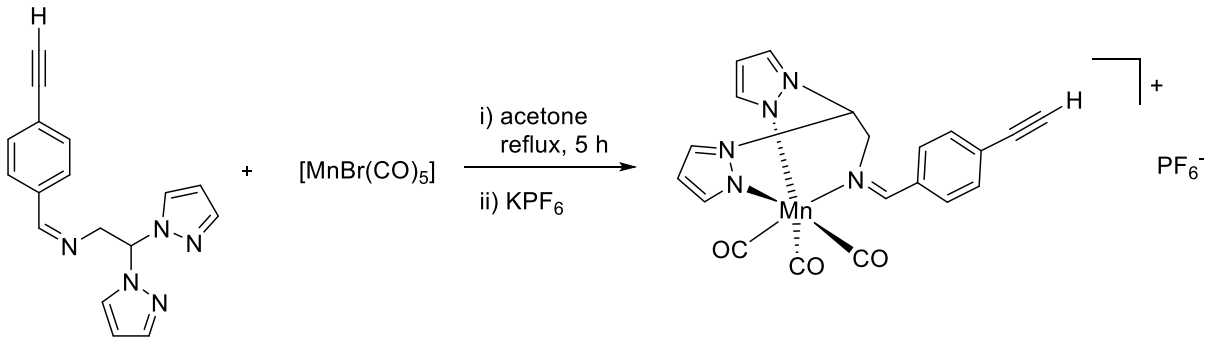

11

$C_{17}H_{15}N_5$
289 g/mol

17

$C_{20}H_{15}F_6MnN_5O_3P$
573 g/mol

Manganese pentacarbonyl bromide (189.68 mg, 0.69 mmol) and 2,2-bis(pyrazolyl)ethyl(4-ethynylbenzylidene)amine (**11**) (200 mg, 0.69 mmol) were completely dissolved in anhydrous acetone (20 mL) and heated to reflux under a dinitrogen atmosphere for 5 h with exclusion of light. The solvent was then removed under vacuum. The yellow residue was washed with diethylether (10 mL) and was redissolved in methanol (10 mL). Potassium hexafluorophosphate (381.02 mg, 2.07 mmol) was added to precipitate the yellow product which was filtered off, washed with water (10 mL) and diethylether (10 mL) and dried under vacuum.

Yield: 82% (325 mg, 0.57 mmol). Elemental analysis (%): calc. for $C_{20}H_{15}F_6MnN_5O_3P$: C 41.90, H 2.64, N 12.22; found: C 41.98, H 2.54, N 12.28. MS (ESI$^+$, CH_3OH): *m/z* 427.84 [M-PF$_6$]$^+$. UV-Vis (DMSO): λ_{max} (ε) = 347 nm (5500 l·mol^{-1}·cm^{-1}). IR (ATR, $\tilde{\upsilon}$/cm^{-1}): 3277 (m, ν_{N-H}), 3138 (w), 3021 (w), 2041 (s, $\nu_{C\equiv O}$), 1930 (s, $\nu_{C\equiv O}$), 1633 (s, $\nu_{C=N}$), 1458, 1365, 1262, 1019. ^{1}H-NMR (400 MHz, acetone-d_6, ppm): δ 9.39 (t, 1H, ^3J = 1.7 Hz, C*H*=N), 8.43 (dd, 2H, ^3J = 2.7, 0.5 Hz, *H*$_5$-pz), 8.37 (d, 2H, ^3J = 2.2 Hz, *H*$_3$-pz), 7.73 (m, 5H, C*H*(pz)$_2$, C$_6$*H*$_4$), 6.74 (m, 2H, *H*$_4$-pz), 4.63 (m, 2H, C*H*$_2$), 3.88 (s, 1H, *H*-alkynyl). ^{13}C-NMR (100.62 MHz, acetone-d_6, ppm) δ 62.88 (*C*H$_2$), 69.63 (*C*$_8$-Alkynyl), 81.70 (*C*H), 83.33 (*C*$_7$-Alkynyl), 109.58 (*C*$_4$-pz), 126.17 (*C*$_4$-C$_6$H$_4$), 129.34 (*C*$_{2,6}$-C$_6$H$_4$), 133.11 (*C*$_{3,5}$-C$_6$H$_4$), 135.72 (*C*$_5$-pz), 136.97 (*C*$_1$-C$_6$H$_4$), 147.83 (*C*$_3$-pz) 181.93 (*C*=N) 220.31 (*C*≡O).

5.2.13 Synthesis of $[Mn(bpea^{NHCH_2C_6H_5})(CO)_3]PF_6$

USC-SP-016-01

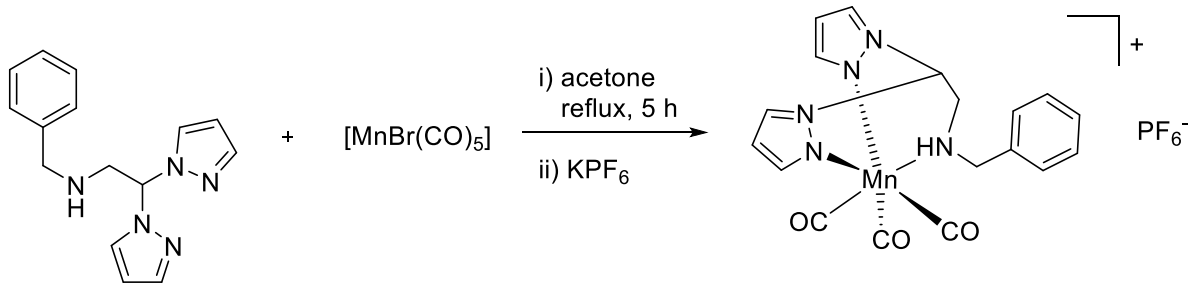

12

$C_{15}H_{17}N_5$
267 g/mol

18

$C_{18}H_{17}F_6MnN_5O_3P$
551 g/mol

Manganese pentacarbonyl bromide (205.6 mg, 0.75 mmol) and benzyl-(2,2-bis(pyrazolyl)ethyl)amine (**12**) (200 mg, 0.75 mmol) were completely dissolved in anhydrous acetone (20 mL) and heated to reflux under a dinitrogen atmosphere for 5 h with exclusion of light. The solvent was then removed under vacuum. The yellow residue was washed with diethylether (10 mL) and was redissolved in methanol (10 mL). Potassium hexafluorophosphate (409.37 mg, 2.22 mmol) was added to precipitate the yellow product which was filtered off, washed with water (5 mL) and diethylether (10 mL) and dried under vacuum.

Yield: 69% (283 mg, 0.51 mmol). Elemental analysis (%): calc. for $C_{18}H_{17}F_6MnN_5O_3P$: C 39.22, H 3.11, N 12.70; found: C 39.21, H 3.27, N 12.76. MS (ESI^+, CH_3OH): *m/z* 405.92 $[M\text{-}PF_6]^+$. UV-Vis (DMSO): λ_{max} (ε) = 355 nm (2135 $l \cdot mol^{-1} \cdot cm^{-1}$). IR (ATR, $\tilde{\upsilon}/cm^{-1}$): 3307 (m, $\nu_{N\text{-}H}$), 2045 (s, $\nu_{C\equiv O}$), 1939 (s, $\nu_{C\equiv O}$), 1604, 1519, 1450, 1315. ^{1}H-NMR (400 MHz, acetone-d_6, ppm): δ 8.51 (d, 1H, ^3J = 2.2 Hz, $H_{3'}$-pz), 8.39 (d, 1H, ^3J = 2.2 Hz, H_3-pz), 8.33 (dd, 1H, ^3J = 2.7, 0.6 Hz, $H_{5'}$-pz), 8.27 (dd, 1H, ^3J = 2.7, 0.5 Hz, H_5-pz), 7.41 (m, 6H, C*H*(pz)$_2$, C$_6$*H*$_5$), 6.74 (m, 1H, H_4-pz), 6.66 (m, 1H, $H_{4'}$-pz), 5.59 (s, br, 1H, NH), 4.69 (dd, 1H, ^3J = 13.4, 4.1 Hz, $H_{b'}$-C*H*$_2$-C$_6$H$_5$), 4.20 (dd, 1H, ^3J = 13.4, 10.1 Hz, H_b-C*H*$_2$-C$_6$H$_5$), 3.52 (ddd, 1H, ^3J = 13.9, 7.8, 4.0 Hz, $H_{a'}$- NC*H*$_2$), 3.12 (ddd, 1H, ^3J = 13.9, 8.9, 1.1 Hz, H_a-NC*H*$_2$). ^{13}C-NMR (100.62 MHz, acetone-d_6, ppm) δ 50.33 (*C*H$_2$-N), 62.32 (*C*H$_2$-C$_6$H$_5$), 68.71 (*C*(pz)$_2$), 108.34 (C_4-pz), 108.38 ($C_{4'}$-pz), 128.51, 128.65, 129.55 , 134.26 (C_5-pz), 134.74 ($C_{5'}$-pz), 135.83 (C_1-C$_6$H$_5$), 147.00 (C_3-pz), 147.13 ($C_{3'}$-pz).

5.2.14 Synthesis of [Mn(bpea^{NHCH2C6H4I})(CO)$_3$]PF$_6$

USC-SP-017-01

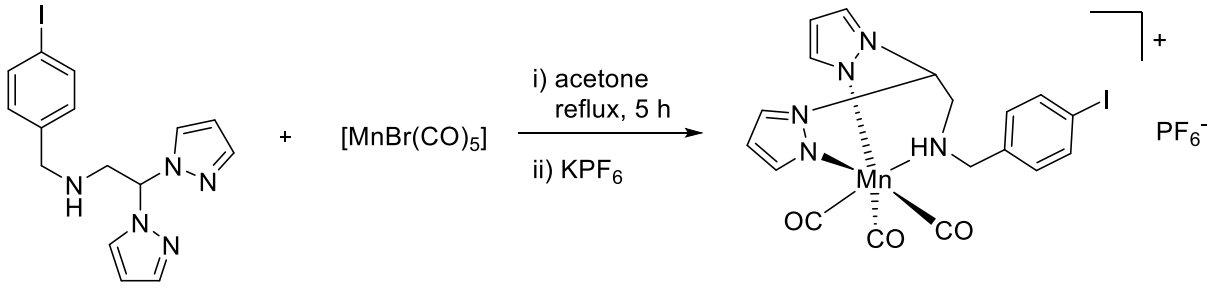

13

$C_{15}H_{16}N_5I$
393 g/mol

19

$C_{18}H_{16}F_6IMnN_5O_3P$
677 g/mol

Manganese pentacarbonyl bromide (68.72 mg, 0.25 mmol) and 2,2-bis(pyrazolyl)ethyl(4-iodobenzyl)amine (**13**) (100 mg, 0.25 mmol) were completely dissolved in anhydrous acetone (20 mL) and heated to reflux under a dinitrogen atmosphere for 5 h with exclusion of light. The solvent was then removed under vacuum. The yellow residue was washed with diethylether (10 mL) and was redissolved in methanol (10 mL). Potassium hexafluorophosphate (115.04 mg, 0.62 mmol) was added to precipitate the yellow product which was filtered off, washed with water (5 mL) and diethylether (10 mL) and dried under vacuum.

Yield: 43% (72.4 mg, 0.11 mmol). Elemental analysis (%): calc. for $C_{18}H_{17}F_6MnN_5O_3P$: C 31.93, H 2.38, N 10.34; found: C 32.01, H 2.31, N 10.46. MS (ESI$^+$, CH_3OH): *m/z* 531.77 $[M\text{-}PF_6]^+$. UV-Vis (DMSO): λ_{max} (ε) = 356 nm (2275 l·mol^{-1}·cm^{-1}). IR (ATR, $\tilde{\upsilon}$/cm^{-1}): 3275 (m, $\nu_{N\text{-}H}$), 3139 (w), 2962 (w), 2041 (s, $\nu_{C\equiv O}$), 1928 (s, $\nu_{C\equiv O}$), 1520, 1443, 1307, 1261, 1148, 1065. ^{1}H-NMR (400 MHz, acetone-d_6, ppm): δ8.51 (d, 1H, ^3J = 2.2 Hz, $H_{3'}$-pz), 8.40 (d, 1H, ^3J = 2.2 Hz, H_3-pz), 8.32 (d, 1H, ^3J = 2.3 Hz, $H_{5'}$-pz), 8.27 (d, 1H, ^3J = 2.4 Hz, H_5-pz), 7.76 (d, 2H, ^3J = 8.4 Hz, $H_{2,6}$-C_6H_4), 7.43 (d, 1H, ^3J = 3.1 Hz, C*H*(pz)$_2$), 7.30 (d, 2H, ^3J = 8.3 Hz, $H_{3,5}$-C_6H_4), 6.74 (t, 1H, ^3J = 2.5 Hz, $H_{4'}$-pz), 6.67 (t, 1H, ^3J = 2.5 Hz, H_4-pz), 5.60 (s, 1H, NH), 4.68 (dd, 1H, ^3J = 13.5, 4.0 Hz, $H_{b'}$-C*H*$_2$-C_6H_4), 4.21 (dd, 1H, ^3J = 13.5, 10.2 Hz, H_b-C*H*$_2$-C_6H_4), 3.55 (ddd, 1H, ^3J = 13.7, 7.8, 3.8 Hz, $H_{a'}$-NC*H*$_2$), 3.12 (dd, 1H, ^3J = 13.7, 8.9 Hz, H_a- NC*H*$_2$). ^{13}C-NMR (100.62 MHz, acetone-d_6, ppm) δ51.20 (*C*H$_2$-N), 62.4 (*C*H$_2$-

C_6H_4), 69.61 (C(pz)$_2$), 94.77 (C_4-C_6H_4), 109.31 (C_4-pz), 132.68 (C_3-C_6H_4), 135.22 (C_5-pz), 135.72 ($C_{5'}$-pz), 136.60 (C_1-C_6H_4), 138.70 ($C_{2,6}$-C_6H_4), 147.97 (C_3-pz), 148.09 ($C_{3'}$-pz).

5.2.15 Synthesis of [Mn(bpea$^{NHCH_2C_6H_4C\equiv CH}$)(CO)$_3$]PF$_6$

USC-SP-121-01

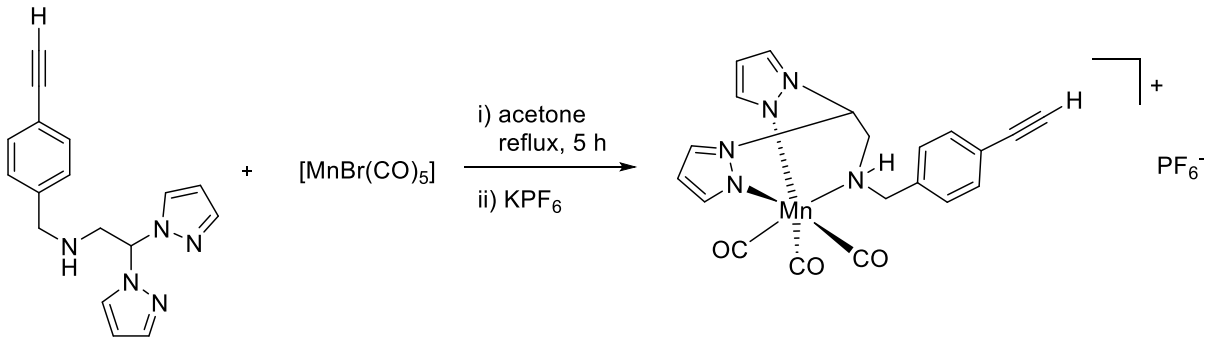

14

$C_{17}H_{17}N_5$
291 g/mol

20

$C_{20}H_{17}F_6MnN_5O_3P$
575 g/mol

Manganese pentacarbonyl bromide (380 mg, 1.38 mmol) and 2,2-bis(pyrazolyl)ethyl(4-ethynylbenzyl)amine (**14**) (400 mg, 1.37 mmol) were dissolved in anhydrous acetone (80 mL) and heated to reflux for 5 h under a dinitrogen atmosphere with exclusion of light. The solvent was then removed under reduced pressure. The yellow residue was redissolved in methanol (10 mL) and an aqueous solution of potassium hexafluorophosphate (445 mg, 2.41 mmol) was added. The yellow product which precipitated was filtered off, washed with water (5 mL), and diethylether (10 mL) and dried under vacuum.

Yield: 96% (691 mg, 1.20 mmol). Elemental analysis (%): calc. for $C_{20}H_{17}F_6MnN_5O_3P$: C 41.75, H 2.97, N 12.17; found: C 41.63, H 2.81, N 12.05. MS (ESI$^+$, CH_3CN): *m/z* 430.06 $[M\text{-}PF_6]^+$, 346.08 $[M\text{-}3CO\text{-}PF_6]^+$. UV-Vis (DMSO): λ_{max} (ε) = 355 nm (2154 L·mol^{-1}·cm^{-1}). IR (ATR, $\tilde{\upsilon}$/cm^{-1}): 3270 (s, $\nu_{N\text{-}H}$), 3140 (m), 2040 (s, $\nu_{C\equiv O}$), 1951 (s, $\nu_{C\equiv O}$), 1928 (s, $\nu_{C\equiv O}$), 1458, 1365, 1289, 1013, 822, 769. ^{1}H-NMR (500 MHz, DMSO-d_6, ppm): δ 8.49 (d, 1H, ^3J = 2.2 Hz, $H_{3'}$-pz), 8.42 (d, 1H, ^3J = 2.3 Hz, H_3-pz), 8.26 (dd, 1H, ^3J = 3.4, 2.7 Hz, $H_{5'}$-pz), 8.18 (dd, 1H, ^3J = 3.4, 2.7 Hz, H_5-pz), 7.48 (d, 4H, ^3J = 8.0 Hz, C_6H_4), 7.24 (d, 1H, ^3J = 3.0 Hz, C*H*(pz)$_2$), 6.68, (t, 1H, ^3J = 2.4 Hz, $H_{4'}$-pz), 6.63 (t, 1H, ^3J = 2.4 Hz, H_4-pz), 5.92 (s, 1H, N*H*), 4.35 (dd, 1H, ^3J = 13.4, 4.0 Hz, $H_{b'}$-CH_2-C_6H_4), 4.23 (s, 1H, C≡C*H*), 3.96 (dd, 1H, ^3J = 13.5, 10.2 Hz, H_b-CH_2-C_6H_4), 3.03 (ddd, 1H, ^3J = 13.6, 7.7, 4.2 Hz, $H_{a'}$-NCH_2),

2.73 (ddd, 1H, ^{3}J = 13.4, 9.5 Hz, H_a-NCH_2).^{13}C-NMR (125.75 MHz, DMSO-d_6, ppm) δ49.52 (NCH$_2$), 61.00 (*C*H$_2$-C$_6$H$_4$), 67.75 (*C*(pz)$_2$), 81.33 (*C*$_8$-Alkynyl), 83.15 (*C*$_7$-Alkynyl), 108.03 (*C*$_4$-pz), 108.12 (*C*$_{4'}$-pz), 121.51 (*C*$_4$-C$_6$H$_4$), 130.19 (*C*$_{3,5}$-C$_6$H$_4$), 131.53 (*C*$_{2,6}$-C$_6$H$_4$), 134.29 (*C*$_{5'}$-pz), 134.59 (*C*$_5$-pz), 136.69 (*C*$_1$-C$_6$H$_4$), 146.71 (*C*$_3$-pz), 146.84 (*C*$_{3'}$-pz), 216.26 (*C*≡O).

5.2.16 Synthesis of [Mn(bpea$^{NHCH2C6H4C\equiv CH}$)(CO)$_3$]Cl

USC-SP-122-01

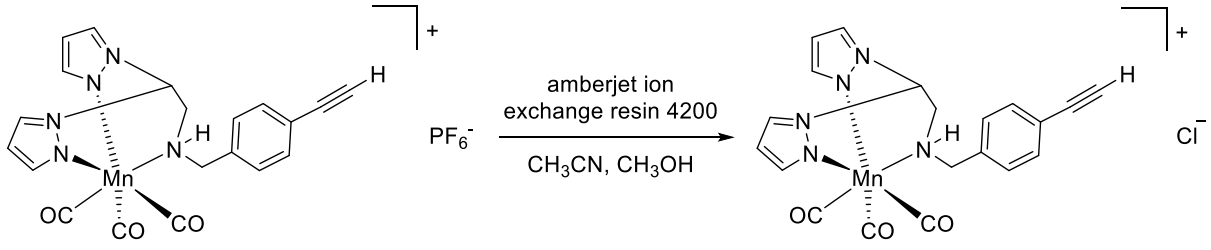

20

$C_{20}H_{17}F_6MnN_5O_3P$
575 g/mol

21

$C_{20}H_{17}ClMnN_5O_3$
466 g/mol

[Mn(bpea$^{NHCH2C6H4C\equiv CH}$)(CO)$_3$]PF$_6$ (**20**) (150 mg, 0.26 mmol) was dissolved in an acetonitrile/methanol (1:1, v/v) mixture and the hexafluorophosphate counterion was exchanged to chloride by ion exchange chromatography on a Amberjet ion exchange resin 4200 (Cl^- form; Acros Organics) column (dimensions: 45x3 cm) using an acetonitrile/methanol (1:1, v/v) mixture as the eluent with a flow rate of 1 drop/s. The yellow main fraction was collected and the solvent was removed under reduced pressure to give a yellow residue. The product was then dissolved in acetonitrile/water (1:1, v/v) and lyophilized to dryness to give a yellow solid.

Yield: 76% (90 mg, 0.19 mmol). Elemental analysis (%): calc. for $C_{20}H_{17}ClMnN_5O_3$: C 51.57, H 3.67, N 15.03; found: C 51.23, H 3.55, N 14.91. MS (ESI^+, CH_3CN): m/z 895.11 $[2M+Cl]^+$, 1360.14 $[3M+2Cl]^+$, 1827.18 $[4M+3Cl]^+$, 346.08 $[M-3CO]^+$. UV-Vis (DMSO): λ_{max} (ε) = 355 nm (1503 L·mol^{-1}·cm^{-1}). IR (ATR, $\tilde{\nu}$/cm^{-1}): 3298 (w), 3095 (w), 2035 (s, $\nu_{C\equiv O}$), 1916 (s, $\nu_{C\equiv O}$), 1463, 1411, 1290, 1100, 1065, 765. ^{1}H-NMR (500 MHz, DMSO-d_6, ppm): δ 8.48 (d, 1H, ^3J = 2.2 Hz, $H_{3'}$-pz), 8.41 (d, 1H, ^3J = 2.1 Hz, H_3-pz), 8.28 (d, 1H, ^3J = 2.4 Hz, $H_{5'}$-pz), 8.20 (d, 1H, ^3J = 2.6 Hz, H_5-pz), 7.48 (d, 4H, ^3J = 6.0 Hz, C_6H_4), 7.24 (s, 1H, C*H*(pz)$_2$), 6.67, (t, 1H, ^3J = 2.4 Hz, $H_{4'}$-pz), 6.63 (t, 1H, ^3J = 2.4 Hz, H_4-pz), 5.94 (s, 1H, N*H*), 4.35 (dd, 1H, ^3J = 13.5, 4.0 Hz, $H_{b'}$-CH_2-C$_6$H$_4$), 4.22 (s, 1H, C≡C*H*), 3.96 (dd, 1H, ^3J = 13.2, 9.9 Hz, H_b-CH_2-C$_6$H$_4$), 3.03 (m, 1H, $H_{a'}$-NCH_2), 2.74 (ddd, 1H, ^3J = 13.6, 8.6 Hz, H_a-NCH_2).^{13}C-NMR (125.75 MHz, DMSO-d_6, ppm) δ 49.50 (NCH$_2$), 60.99 (*C*H$_2$-C$_6$H$_4$), 67.67 (*C*(pz)$_2$), 81.30 (*C*$_8$-Alkynyl), 83.14 (*C*$_7$-Alkynyl), 108.00 (*C*$_4$-pz), 108.09 (*C*$_{4'}$-pz),

121.49 (C_4-C_6H_4), 130.17 ($C_{3,5}$-C_6H_4), 131.50 ($C_{2,6}$-C_6H_4), 134.26 ($C_{5'}$-pz), 134.57 (C_5-pz), 136.66 (C_1-C_6H_4), 146.67 (C_3-pz), 146.80 ($C_{3'}$-pz).

5.2.17 Synthesis of 4-([(2,2-bis(pyrazolyl)ethyl)amino]methyl)benzaldehyde

USC-SP-058-01

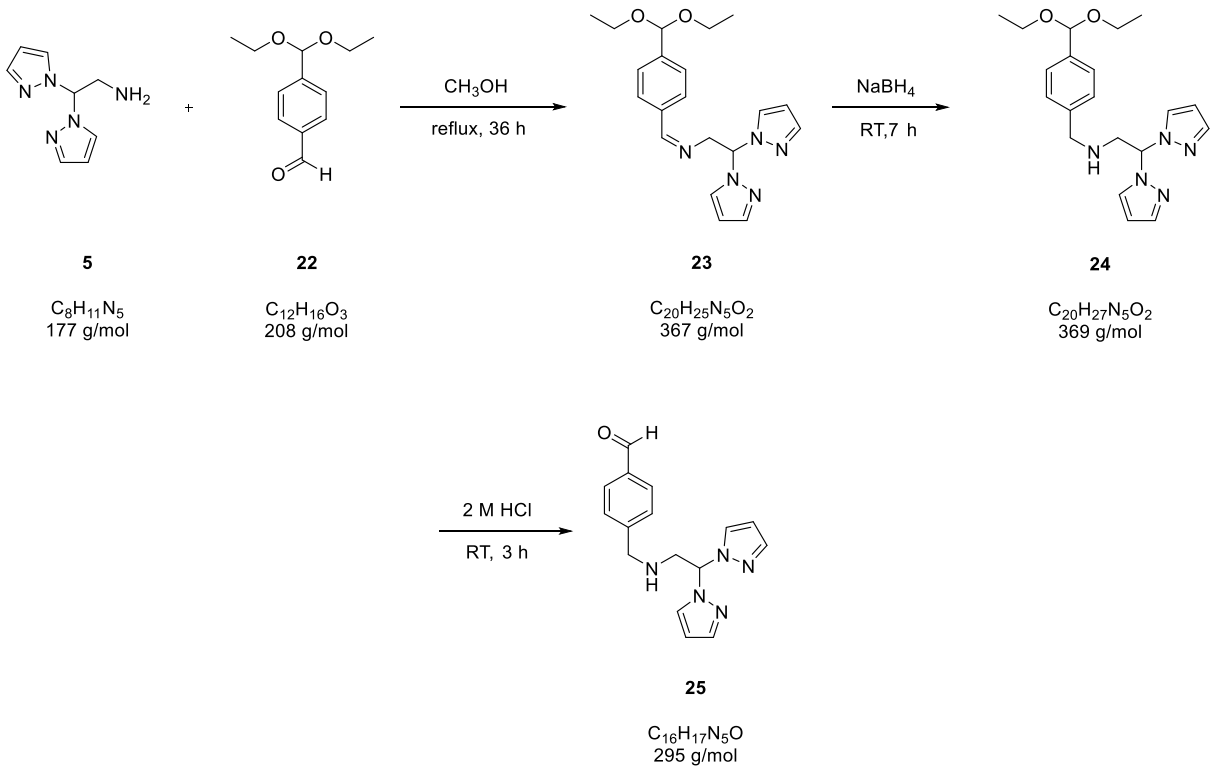

5
$C_8H_{11}N_5$
177 g/mol

22
$C_{12}H_{16}O_3$
208 g/mol

23
$C_{20}H_{25}N_5O_2$
367 g/mol

24
$C_{20}H_{27}N_5O_2$
369 g/mol

25
$C_{16}H_{17}N_5O$
295 g/mol

To a solution of 2,2'-bis(pyrazolyl)ethylamine (**5**) (0.50 g, 2.82 mmol) in anhydrous methanol (20 mL) was added 4-(diethoxymethyl)benzaldehyde (**22**) (0.58 g, 2.82 mmol). The mixture was heated to reflux in the presence of molecular sieves (4 Å) under a dinitrogen atmosphere for 36 h. The molecular sieves were then filtered off and the solution cooled to 0 °C. Solid sodium borohydride (186.70 mg, 4.94 mmol) was added to reduce the resulting intermediate imine **23** and stirring continued for 7 h at room temperature. Water (10 mL) was added to the reaction mixture and the product was extracted with dichloromethane (100 mL) and washed with brine (3 × 50 mL). The organic layer was separated, dried over magnesium sulfate (~10 g), and filtered. The solvent was then removed under reduced pressure to give a yellow oil. Yield: 57% (0.60 g, 1.60 mmol). This intermediate aminoacetal **24** (0.59 g, 1.60 mmol) was treated with 2 M hydrochloric acid (8 mL) and stirred at room temperature for 3 h. The reaction mixture turned white, was made alkaline with aqueous sodium hydroxide, and extracted with dichloromethane (3 × 50 mL). The combined organic extracts was

washed with brine (3 × 100 mL), dried over sodium sulfate (~10 g), and filtered. The solvent was then removed under reduced pressure to give the product as a yellow oil. Yield: 70% (0.33 g, 1.12 mmol). Elemental analysis (%): calc. for $C_{16}H_{17}N_5O$: C 65.06, H 5.80, N 23.71; Found: C 64.82, H 5.75, N 23.28. MS (ESI^+, MeOH): *m/z* 318.13 $[M+Na]^+$. IR (ATR, $\tilde{\upsilon}/cm^{-1}$): 3115 (m, $\nu_{N\text{-}H}$), 2844, 1691 (s, $\nu_{C=O}$), 1606, 1390, 1090. ^{1}H-NMR (300 MHz, $CDCl_3$, ppm): δ 9.98 (s, 1H, C*H*O), 7.82 (d, 2H, ^3J = 8.3 Hz, $H_{2,6}$-C_6H_4), 7.57 (d, 2H, ^3J = 2.4 Hz, H_3-pz), 7.55 (d, 2H, ^3J = 1.7 Hz, H_5-pz), 7.43 (d, 2H, ^3J = 7.9 Hz, $H_{3,5}$-C_6H_4), 6.55 (t, 1H, ^3J = 6.9 Hz, C*H*(pz)$_2$), 6.28 (dd, 2H, ^3J = 2.4 Hz, ^4J = 1.8 Hz, H_4-pz), 3.90 (s, 2H, CH_2-C_6H_4) 3.69 (d, 2H, ^3J = 6.9 Hz, CH_2-CH). ^{13}C-NMR (75.47 MHz, $CDCl_3$, ppm) δ 51.21 (*C*H_2CH), 53.03 (*C*H_2-C_6H_4), 75.12 (*C*(pz)$_2$), 106.92 (C_4-pz), 128.55 ($C_{3,5}$-C_6H_4), 129.14 ($C_{2,6}$-C_6H_4), 130.13 (C_5-pz), 135.66 (C_1-C_6H_4), 140.49 (C_3-pz), 147.04 (C_4-C_6H_4), 192.07 (*C*HO).

5.2.18 Synthesis of [Mn(bpea^{NHCH2C6H4CHO})(CO)$_3$]PF$_6$

USC-SP-060-01

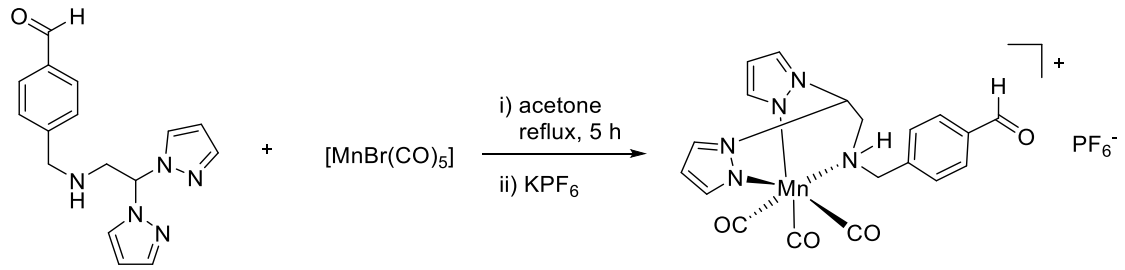

25

$C_{16}H_{17}N_5O$
295 g/mol

26

$C_{19}H_{17}F_6MnN_5O_4P$
579 g/mol

Manganese pentacarbonyl bromide (368 mg, 1.34 mmol) and 4-([(2,2-bis(pyrazolyl)ethyl)amino]methyl)benzaldehyde (**25**) (346 mg, 1.17 mmol) were dissolved in anhydrous acetone (50 mL) and heated to reflux for 5 h under a dinitrogen atmosphere with exclusion of light. The solvent was removed in vacuo. The yellow residue was redissolved in methanol (10 mL) and an aqueous solution of potassium hexafluorophosphate (430.70 mg, 2.34 mmol) was added. The yellow product which precipitated was filtered off, washed with water, diethylether and dried under vacuum.

Yield: 80% (544 mg, 0.94 mmol). Elemental analysis (%): calc. for $C_{19}H_{17}F_6MnN_5O_4P$: calc. for C 39.39, H 2.95, N 12.09; found: C 38.91, H 3.03, N 11.61. MS (ESI$^+$, MeOH): *m/z* 434.08 [M-PF$_6$]$^+$. UV-Vis (DMSO): λ_{max} (ε) = 357 nm (2070 L·mol^{-1}·cm^{-1}). IR (ATR, $\tilde{\upsilon}$/cm^{-1}): 3252 (m, $\nu_{N\text{-}H}$), 2036 (s, $\nu_{C\equiv O}$), 1928 (s, $\nu_{C\equiv O}$), 1691 (s, ν_{CHO}), 1607, 1412, 1288, 832. ^{1}H-NMR (300 MHz, acetone-*d*$_6$, ppm): δ10.04 (s, 1H, C*H*O), 8.54 (d, 1H, ^3J = 2.2 Hz, *H*$_{3'}$-pz), 8.43 (d, 1H, ^3J = 2.2 Hz, *H*$_3$-pz), 8.34 (d, 1H, ^3J = 2.6 Hz, *H*$_{5'}$-pz), 8.28 (d, 1H, ^3J = 2.7 Hz, *H*$_5$-pz), 7.93 (d, 2H, ^3J = 8.3 Hz, *H*$_{3,5}$-C$_6$H$_4$), 7.71 (d, 2H, ^3J = 8.1 Hz, *H*$_{2,6}$-C$_6$H$_4$), 7.47 (br s, 1H, C*H*(pz)$_2$), 6.75 (t, 1H, ^3J = 2.4 Hz, *H*$_4$-pz), 6.68 (t, 1H, ^3J = 2.4 Hz, *H*$_{4'}$-pz), 5.77 (br s, 1H, N*H*), 4.83 (dd, 1H, ^3J = 13.5, 4.1 Hz, H$_{b'}$-C*H*$_2$-C$_6$H$_4$), 4.38 (dd, 1H, ^3J = 13.4, 10.3 Hz, H$_b$-C*H*$_2$-C$_6$H$_4$), 3.57 (ddd, 1H, ^3J = 13.2, 7.9, 3.1 Hz, H$_{a'}$-NC*H*$_2$), 3.18 (dd, 1H, ^3J = 13.8, 8.9 Hz, H$_a$-NC*H*$_2$).^{13}C-NMR (75.47 MHz, acetone-*d*$_6$,

ppm) δ 60.93 (CH_2-N), 72.23 (CH_2-C_6H_4), 79.28 ($C(pz)_2$), 118.98 ($C_{4,4'}$-pz), 140.26 ($C_{3,5}$-C_6H_4), 140.92 ($C_{2,6}$-C_6H_4), 144.94 ($C_{5'}$-pz), 145.42 (C_5-pz), 147.30 (C_4-C_6H_4), 152.73 (C_1-C_6H_4), 157.68 (C_3-pz), 157.81 ($C_{3'}$-pz), 202.23 (CHO).

5.2.19 Synthesis of HC≡C(CH$_2$)$_3$CO-Leu-Pro-Leu-Gly-Asn-Ser-His-OH (5-hexynoic-TGFβ$_1$-OH)

USC-SP-044-01

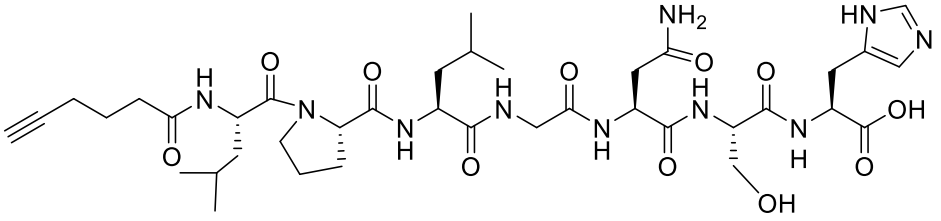

27

$C_{38}H_{58}N_{10}O_{11}$
830 g/mol

The peptide was prepared on a 0.24 mmol scale on a preloaded H-L-His(Trt)-2CT resin (300 mg, 0.78 mmol/g) using the amino acids Fmoc-L-Ser(tBu)-OH, Fmoc-L-Asn(Trt)-OH, Fmoc-L-Gly-OH, Fmoc-L-Leu-OH, Fmoc-L-Pro-OH, Fmoc-L-Leu-OH under manual solid phase peptide synthesis conditions as described above. Two repeated couplings of 5-hexynoic acid (10 eq.) were required to attain complete coupling as indicated by a negative Kaiser test. Cleavage time: 3 h (TFA/TIS/H_2O, 90:5:5, v/v/v). The peptide was obtained as a white solid after lyophilization and purified by preparative HPLC using a linear gradient of 5-90% acetonitrile/water containing 0.1% TFA as the eluent over 50 min at a flow rate of 3.0 mL min^{-1}..

Yield: 54% (106 mg, 0.13 mmol). RP-HPLC: t_r = 22.80 min; MS (ESI$^+$, MeOH): *m/z* 831.43 [M+H]$^+$. IR (ATR, $\tilde{\upsilon}$/cm^{-1}): 3290 (m), 2959 (m), 1659 (s), 1623 (s), 1538 (s), 1437 (m), 1197 (s), 1134 (s).

5.2.20 Synthesis of N_3-Ac-Leu-Pro-Leu-Gly-Asn-Ser-His-OH (N_3-Ac-TGFβ$_1$-OH)

USC-SP-053-01

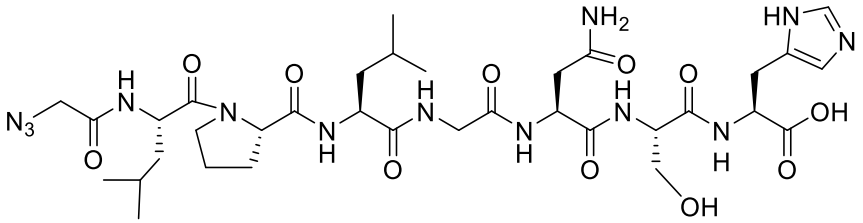

28

$C_{34}H_{53}N_{13}O_{11}$
819 g/mol

The peptide was synthesized on a 0.39 mmol scale on a preloaded H-L-His(Trt)-2CT resin (500 mg, 0.78 mmol/g) using the amino acids Fmoc-L-Ser(tBu)-OH, Fmoc-L-Asn(Trt)-OH, Fmoc-L-Gly-OH, Fmoc-L-Leu-OH, Fmoc-L-Pro-OH, Fmoc-L-Leu-OH under manual solid phase peptide synthesis conditions as described above. Two repeated couplings of azido acetic acid (10 eq.) were required to attain complete coupling as indicated by a negative Kaiser test. Cleavage time: 3 h (TFA/TIS/H_2O, 90:5:5, v/v/v). The peptide was obtained as a white solid after lyophilization and purified by preparative HPLC using a linear gradient of 5-90% acetonitrile/water containing 0.1% TFA as the eluent over 50 min at a flow rate of 3.0 mL min^{-1}.

Yield: 55% (172 mg, 0.21 mmol). RP-HPLC: t_r = 22.90 min; MS (ESI$^+$, MeOH): *m/z* 820.40 [M+H]$^+$. IR (ATR, $\tilde{\upsilon}$/cm^{-1}): 3284 (m), 2958 (m), 2109 (s, ν_{N3}) 1658 (s), 1536 (s), 1440 (m), 1200 (s), 1134 (s).

5.2.21 Synthesis of Aoa-Leu-Pro-Leu-Gly-Asn-Ser-His-OH (Aoa-TGFβ1-OH)

USC-SP-059-03

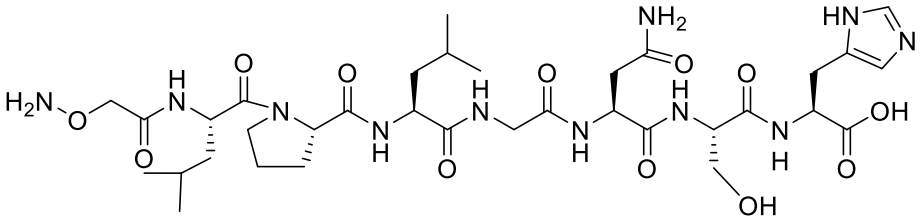

29

$C_{34}H_{55}N_{11}O_{12}$
809 g/mol

The peptide was synthesized on a 0.32 mmol scale on a preloaded H-L-His(Trt)-2CT resin (500 mg, 0.78 mmol/g) using the amino acids Fmoc-L-Ser(tBu)-OH, Fmoc-L-Asn(Trt)-OH, Fmoc-L-Gly-OH, Fmoc-L-Leu-OH, Fmoc-L-Pro-OH, Fmoc-L-Leu-OH under manual solid phase peptide synthesis conditions as described above. Two repeated couplings of Fmoc-Aoa-OH (10 eq.) were required to attain complete coupling as indicated by a negative Kaiser test. Cleavage time: 3 h (TFA/TIS/H_2O, 90:5:5, v/v/v). The peptide was obtained as a white solid after lyophilization and purified by preparative HPLC using a linear gradient of 5-30% acetonitrile/water containing 0.1% TFA as the eluent over 45 min at a flow rate of 3.0 mL min^{-1}.

Yield: 60% (185 mg, 0.23 mmol). RP-HPLC: t_r = 15.60 min; MS (ESI^+, MeOH): *m/z* 810.41 $[M+H]^+$. IR (ATR, $\tilde{\upsilon}/cm^{-1}$): 3288 (m), 2961 (m), 1658 (s), 1537 (s), 1439 (m), 1198 (s), 1133 (s).

5.2.22 Synthesis of [Mn(bpea$^{C=C(CH2)3CO\text{-}TGF\beta1\text{-}OH}$)(CO)$_3$]PF$_6$

USC-SP-046-01

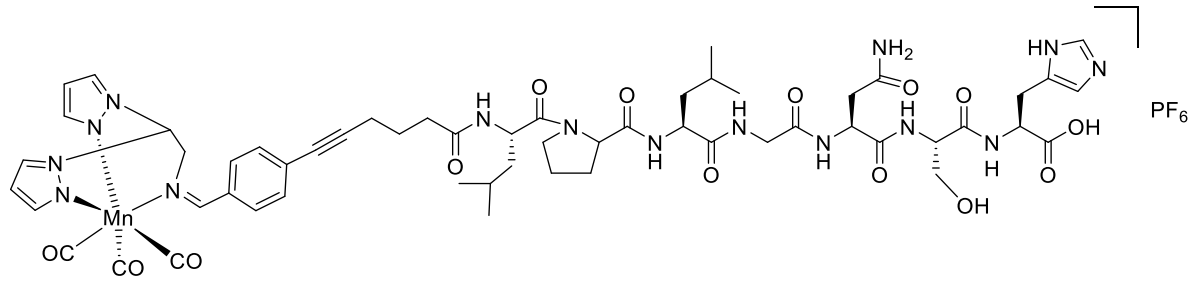

30

$C_{56}H_{71}F_6MnN_{15}O_{14}P$
1378 g/mol

[Mn(bpea$^{N=CHC6H4I}$)(CO)$_3$]PF$_6$ (**16**) (24.30 mg, 36 µmol) and 5-hexynoic-TGFβ1-OH (**27**) (30 mg, 36 µmol) were dissolved in a mixture of *N*,*N*-dimethylformamide (1 mL) and triethylamine (1.5 mL). The solution was degassed by three freeze-pump-thaw cycles. Copper(I) iodide (1 mg, 4.32 µmol, 12 mol%) and *cis*-dichlorobis(triphenylphosphine)palladium(II) (1 mg, 1.44 µmol, 4 mol%) were added under a dinitrogen, and the reaction mixture was degassed. The yellow solution was stirred at room temperature under the exclusion of light for 28 h and then loaded onto a short reversed-phase column (Waters C_{18} Sep-Pak, 5 g) washed with water (5 x 10 mL). However, no conjugate formation could be detected under these conditions as probed by HPLC and ESI-MS.

5.2.23 Synthesis of [Mn(bpea$^{C2HN3\text{-}CH2CO\text{-}TGF\beta1\text{-}OH}$)(CO)$_3$]PF$_6$

USC-SP-054-02

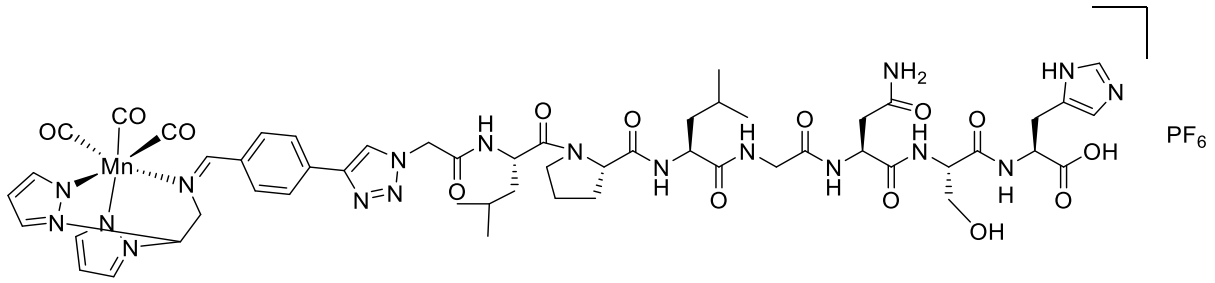

31

$C_{54}H_{68}F_6MnN_{18}O_{14}P$
1393 g/mol

[Mn(bpea$^{N=CHC6H4C\equiv CH}$)(CO)$_3$]PF$_6$ (**17**) (28.02 mg, 48.90 µmol) and N$_3$-Ac-TGFβ$_1$-OH (**28**) (40.10 mg, 48.90 µmol) were dissolved in a mixture (1:1, v/v) of *N*,*N*-dimethylformamide (1 mL) and water (1 mL). Sodium ascorbate (0.70 mg, 3.50 µmol, 25 mol%) and copper(II) sulfate pentahydrate (0.15 mg, 0.70 µmol, 5 mol%) were subsequently added and the mixture was stirred for 24 h at room temperature under exclusion of light. The yellow solution was loaded on a short reversed phase column (Waters C$_{18}$-SepPak, 5 g) and washed with water (5x10 mL). The conjugate was then eluted with pure acetonitrile as a yellow band. The solution was lyophilized to give the product as a yellow solid which was purified by preparative HPLC using a linear gradient of 5-60% acetonitrile/water containing 0.1% TFA as the eluent over 30 min at a flow rate of 3.0 mL min^{-1}.

Yield: 20% (13 mg, 0.001 mmol). RP-HPLC: t_r = 30.10 min; MS (ESI$^+$, MeOH): *m/z* 1247.45 [M-PF$_6$]$^+$. IR (ATR, $\tilde{\upsilon}$/cm^{-1}): 2958 (m), 2040 (s, $\nu_{C\equiv O}$), 1932 (s, $\nu_{C\equiv O}$), 1663 (s), 1533 (m), 1413 (m), 1132 (m).

5.2.24 Synthesis of [Mn(bpea$^{NHCH2C6H4CH=OCH2CO\text{-}TGF\beta1\text{-}OH}$)(CO)$_3$]PF$_6$

USC-SP-0062-02

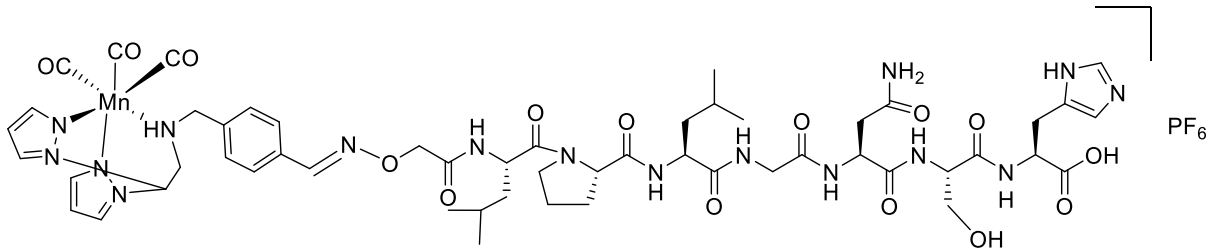

32

$C_{53}H_{70}F_6MnN_{16}O_{15}P$
1371 g/mol

[Mn(bpea^{NHCH2C6H4CHO})(CO)$_3$]PF$_6$ (**26**) (5.79 mg, 0.01 mmol) and Aoa-TGFβ$_1$-OH (**29**) (10 mg, 0.01 mmol) were dissolved in a mixture (1:1, v/v) of tetrahydrofuran (2 mL) and phosphate buffer saline (PBS) (2 mL, 100 mM, pH 5.2). The resulting yellow solution was stirred for 3 h at room temperature under exclusion of light. The solvent was removed via lyophilization and the yellow residue was dissolved in acetonitrile/water mixture (1:9, v/v) and loaded on a short reversed phase column (Waters C$_{18}$-SepPak, 5 g) and washed with water (5x10 mL) followed by pure acetonitrile (5x10 mL). The conjugate was then eluted with acetonitrile/water (1:1, v/v) as a yellow band. The solution was lyophilized to give the product as a yellow solid which was purified by preparative HPLC using a linear gradient of 5-70% acetonitrile/water containing 0.1% TFA as the eluent over 50 min at a flow rate of 3.0 mL min^{-1}.

Yield: 58% (8 mg, 0.006 mmol). RP-HPLC: t_r = 28.30 min; MS (ESI$^+$, MeOH): *m/z* 1225.45 [M-PF$_6$]$^+$. IR (ATR, $\tilde{\upsilon}$/cm^{-1}): 3284 (m), 2042 (s, $\nu_{C\equiv O}$), 1934 (s, $\nu_{C\equiv O}$), 1662 (s), 1546 (s), 1413 (m), 1195 (s), 1132 (s).

5.2.25 Synthesis of dimethylketoxime

USC-SP-077-01

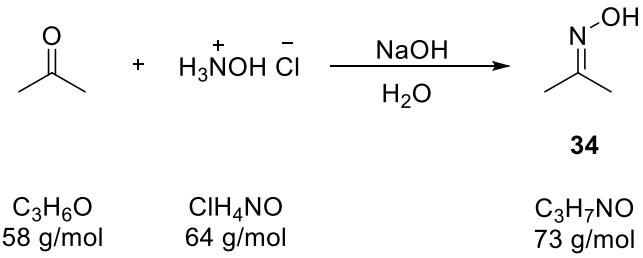

Hydroxylamine hydrochloride (30 g, 0.43 mol) was dissolved in water (60 mL) and an aqueous solution (30 mL) of sodium hydroxide (18 g, 0.46 mol) was added over a period of 15 min under cooling with an ice bath. Acetone (20 mL, 0.46 mol) was added dropwise using a dropping funnel over 30 min. A white precipitate was formed which dissolved upon further stirring. The pH of the solution was adjusted to 6 after 30 min of stirring by addition of con. hydrochloric acid. The reaction mixture was stirred for an hour (pH 7.5) and extracted with diethylether (4 x 100 mL), dried over magnesium sulfate (~ 20 g). The solvent was removed by evaporation to give a white solid which was dried *in vacuo*.

Yield: 44% (14.35 g, 19.65 mmol). IR (ATR, $\tilde{\upsilon}/cm^{-1}$): 3196 (s), 3134 (s), 2889 (s), 1678 (s, $\nu_{C=O}$), 1494 (s), 1426 (s), 1368 (s), 1268 (s), 1065 (s), 945 (s), 791 (m). ^{1}H-NMR (200 MHz, DMSO-d_6, ppm): δ 10.16 (s, 1H, O*H*), 1.76 (s, 3H, (E/Z)-CH_3), 1.73 (s, 3H, (E/Z)-CH_3). ^{13}C-NMR (50.33 MHz, DMSO-d_6, ppm): δ 14.52 ((E/Z)-CH_3), 21.36 ((E/Z)-CH_3), 152.00 (*C*=N).

5.2.26 Synthesis of dimethylketoxime-*O*-acetic acid

USC-SP-081-01

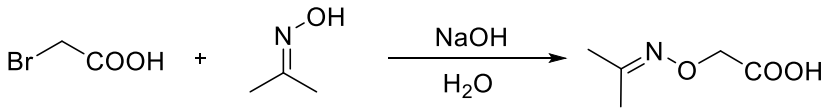

33 **34** **35**

$C_2H_3BrO_2$ 139 g/mol | C_3H_7NO 73 g/mol | $C_5H_9NO_3$ 131 g/mol

Bromoacetic acid (6.60 g, 48 mmol) was dissolved in water (15 mL) and cooled to 0 °C. An aqueous solution of sodium hydroxide (3.5 mL, 40% w/w, 50 mmol) was added dropwise while keeping the temperature below 20 °C. A solution of dimethylketoxime **34** (3.10 g, 43 mmol) in water (20 mL) was added followed by an aqueous solution of sodium hydroxide (3.0 mL, 40% w/w, 43 mmol). The reaction mixture was allowed to warm to room temperature and stirred overnight. The mixture was extracted with diethylether (1 x 100 mL), acidified to pH 1 with con. hydrochloric acid and extracted again with diethylether (4 x 75 mL). The latter extracts were combined and dried over magnesium sulfate (~ 10 g). Removal of the solvent gave the product as a white solid.

Yield: 44% (2.74 g, 20.91 mmol). IR (ATR, $\tilde{\upsilon}/cm^{-1}$): 2926 (m), 2582 (m), 1723 (s), 1406 (m), 1257 (s), 1107 (s), 1020 (m), 930 (m), 874 (m). ^{1}H-NMR (200 MHz, DMSO-d_6, ppm): δ12.58 (s, 1H, COO*H*), 4.44 (s, 2H, CH_2), 1.82 (s, 3H, (E/Z)-CH_3), 1.79 (s, 3H, (E/Z)-CH_3). ^{13}C-NMR (50.33 MHz, DMSO-d_6, ppm): δ15.44 ((E/Z)-CH_3), 21.17 ((E/Z)-CH_3), 69.52 (CH_2), 155.38 (*C*=N), 171.32 (*C*=O).

5.2.27 Synthesis of aminoxyacetic acid hemi hydrochloride

USC-SP-082-01

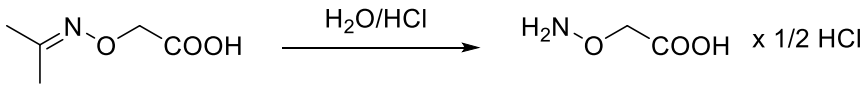

35

$C_5H_9NO_3$
131 g/mol

36

$C_2H_5NO_3$ x 1/2 HCl
109 g/mol

Dimethylketoxime-*O*-acetic acid **35** (6 g, 47 mmol) was dissolved in water (50 mL) and con. hydrochloric acid (5 mL) was added. The mixture was heated to 95 °C for 4 h in an open flask with a stream of dinitrogen passing through. The volume of the solvent was reduced to about 10 mL during the course of the reaction. After cooling to room temperature, the residue was treated with isopropanol (50 mL) followed by diethylether (150 mL) and stored at -25 °C overnight. The crystalline precipitate was formed and filtered off, washed with diethylether and dried under vacuum to give the product as a white solid in the hemi hydrochloride form.

Yield: 85% (1.92 g, 17.60 mmol). Elemental analysis (%): calc. for $C_2H_5NO_3 \cdot 1/2$ HCl: calc. for C 21.98, H 5.07, N 12.82; found: C 21.70, H 5.38, N 12.56. IR (ATR, $\tilde{\upsilon}/cm^{-1}$): 2856 (s), 2680 (s), 2017 (m), 1710 (s), 1516 (s), 1440 (s), 1398 (s), 1206 (s), 1051 (s), 1006, 855, 797. ^{1}H-NMR (200 MHz, DMSO-d_6, ppm): δ 4.56 (s, 2H, CH_2). ^{13}C-NMR (50.33 MHz, DMSO-d_6, ppm): δ 70.26 (CH_2), 169.54 (*C*=O).

5.2.28 Synthesis of *N*-(9-fluorenylmethoxycarbonyl)aminoxyacetic acid (Fmoc-Aoa-OH)

USC-SP-068-01

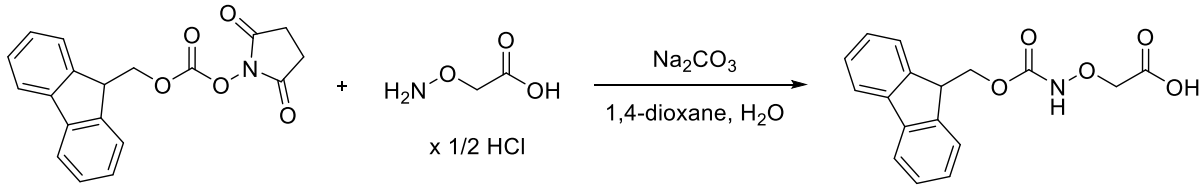

36 **37**

$C_{19}H_{15}NO_5$ 337 g/mol | $C_2H_5NO_3$ x 1/2 HCl 109 g/mol | $C_{17}H_{15}NO_5$ 313 g/mol

Aminoxyacetic acid hemi hydrochloride **36** (500 mg, 4.6 mmol) was dissolved in 1,4-dioxane/water mixture (60 mL, v/v 60:40) and sodium carbonate (1.22 g, 11.50 mmol) was added. The mixture was cooled to 0 °C and a solution of 9-fluorenylmethoxycarbonyl-*N*-succinimidyl carbonate (1.55 g, 4.60 mmol) in 1,4-dioxane (20 mL) was added while stirring. The resulting mixture was stirred for 2 h at 0 °C and the white precipitate formed was filtered off. The filtrate was concentrated under vacuum and the residue was dissolved in water (100 mL). Addition of con. hydrochloric acid gave a white precipitate which was filtered off, washed with dil. hydrochloric acid and lyophilized.

Yield: 77% (1.14 g, 3.64 mmol). Elemental analysis (%): calc. for $C_{17}H_{15}NO_5$: calc. for C 65.17, H 4.82, N 4.47; found: C 64.75, H 4.56, N 4.44. MS (ESI^+, CH_3OH): *m/z* 336.08 $[M+Na]^+$, 649.17 $[2M+Na]^+$. IR (ATR, $\tilde{\upsilon}/cm^{-1}$): 3237 (w), 3064 (w), 1727 (s), 1708 (s), 1429 (m), 1327 (s), 1247 (s), 1106 (s), 1077 (w), 758 (s). ^{1}H-NMR (300 MHz, DMSO-d_6, ppm): δ12.89 (s, 1H, COO*H*), 10.69 (s, 1H, N*H*), 7.89 (d, 2H, ^3J = 7.2 Hz, Fmoc-$H_{5,8}$), 7.69 (m, 2H, Fmoc-$H_{1,4}$), 7.42 (dt, 2H, Fmoc-$H_{7,6}$, ^3J = 7.5 Hz, ^4J = 1.2 Hz), 7.32 (dt, 2H, Fmoc-$H_{2,3}$, ^3J = 7.4 Hz, ^4J = 1.2 Hz), 4.37 (d, 2H, Fmoc-CH_2, ^3J = 7.4 Hz), 4.26 (s, 2H, Aoa-CH_2). ^{13}C-NMR (75.47 MHz, DMSO-d_6, ppm): δ46.51 (Fmoc-C_9), 66.14 (Fmoc-CH_2), 72.06 (Aoa-CH_2), 120.16 (Fmoc-$C_{1,8}$), 125.26 (Fmoc-$C_{4,5}$), 127.12 (Fmoc-$C_{2,7}$), 127.73 (Fmoc-$C_{1,8}$), 140.76 (Fmoc-$C_{4a,4b}$), 143.58 (Fmoc-$C_{9,8}$), 156.95 (Fmoc C=O), 170.10 (Aoa-*C*=O).

5.2.29 Synthesis of [DAB-G1-PPI-(Mn(bpea^{NHCH2C6H4CH2NH})(CO)$_3$)$_4$](CF$_3$COO)$_4$

USC-SP-112-02

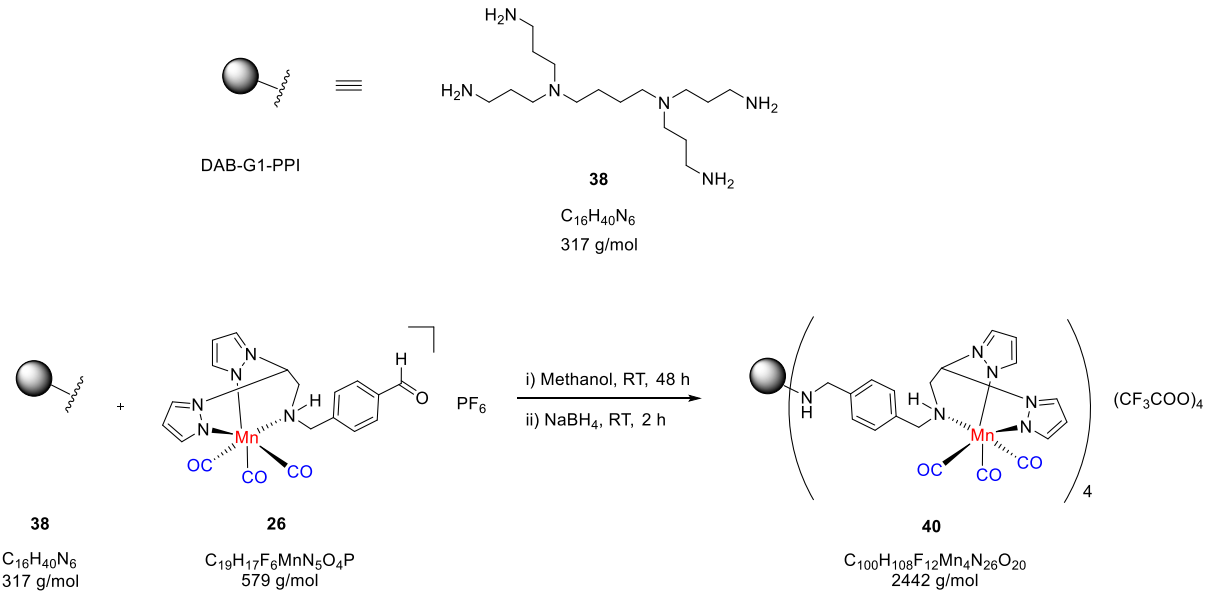

A solution of diaminobutane-G1-polypropyleneimine (DAB-G1-PPI) (**38**) (14 mg, 0.044 mmol) in anhydrous methanol (20 mL) was added dropwise to a stirred solution of [Mn(bpea^{NHCH2C6H4CHO})(CO)$_3$]PF$_6$ (**26**) (108 mg, 0.18 mmol) in anhydrous methanol (10 mL). The reaction mixture was stirred at room temperature for 48 h under a dinitrogen atmosphere with exclusion of light, after which solid sodium borohydride (16 mg, 0.40 mmol) was added slowly while stirring. The reaction mixture was stirred overnight at room temperature with exclusion of light. Water (30 mL) was added to the reaction mixture and the product was extracted with dichloromethane (100 mL). The organic layer was separated, dried over magnesium sulfate (~5 g), and filtered. The solvent was then removed under vacuum and the residue redissolved in dichloromethane (5 mL) and added dropwise to a stirred solution of *n*-hexane (25 mL). The yellow product which precipitated was filtered off, washed with *n*-hexane (10 mL) and dried under vacuum. This was further purified by preparative HPLC using a linear gradient of 5-70% acetonitrile/water containing 0.1% TFA as the eluent over 50 min at a flow rate of 3.0 mL min^{-1} to give the yellow product containing trifluoroacetate anions due to the presence of trifluoroacetic acid in the eluent.

Yield: 72% (42 mg, 0.017 mmol). Elemental analysis (%): calc. for $C_{100}H_{108}F_{12}Mn_4N_{26}O_{20}$: calc. for C 49.18, H 4.45, N 14.91; found: C 49.36, H 4.12, N 14.57. MS (ESI^+, CH_3CN): *m/z* 1107.79 $[M\text{-}CF_3COO]^{2+}$, 2328.57 $[M\text{-}CF_3COO+H]^+$. UV-Vis (DMSO): λ_{max} (ε) = 356 nm (6056 $L \cdot mol^{-1} \cdot cm^{-1}$). IR (ATR, $\tilde{\nu}/cm^{-1}$): 3146 (w), 2928, 2039 (s, $\nu_{C\equiv O}$), 1929 (s, $\nu_{C\equiv O}$), 1726 (w), 1458, 1412, 1290, 1101, 763. RP-HPLC: t_r = 12.60 min. ^{1}H-NMR (500 MHz, MeOD, ppm): δ8.35 (d, 4H, ^3J = 2.2 Hz, $H_{3'}$-pz), 8.26 (d, 4H, ^3J = 2.2 Hz, H_3-pz), 8.18 (dd, 4H, ^3J = 3.4, 2.7 Hz, $H_{5'}$-pz), 8.14 (dd, 4H, ^3J = 3.4, 2.7 Hz, H_5-pz), 7.53 (s, 16H, C_6H_4), 7.21 (d, 4H, ^3J = 3.0 Hz, $CH(pz)_2$), 6.68 (t, 4H, ^3J = 5.0, 2.4 Hz, H_4-pz), 6.62 (t, 4H, ^3J = 5.0, 2.4 Hz, $H_{4'}$-pz), 5.69 (br m, 4H, NH), 4.44 (dd, 4H, ^3J = 13.4, 4.6 Hz, $H_{b'}$-CH_2-C_6H_4), 4.23 (s, 8H, DAB-CH_2-C_6H_4), 3.97 (dd, 4H, ^3J = 13.4, 9.4 Hz, H_b-CH_2-C_6H_4), 3.27 (br m, 8H, $NCH_2CH_2CH_2N_{branch}$), 3.22 (overlapping m, 8H, H_a-$NHCH_2CH_{bpea}$, $NCH_2CH_2CH_2CH_2N_{core}$), 3.16 (t, 8H, ^3J = 7.6 Hz, $NCH_2CH_2CH_2N_{branch}$), 2.81 (ddd, 4H, ^3J = 13.8, 8.5, 1.2 Hz, $H_{a'}$- $NHCH_2CH_{bpea}$), 2.22 (br m, 8H, $NCH_2CH_2CH_2N_{branch}$), 1.81 (br m, 4H, $NCH_2CH_2CH_2CH_{2core}$). ^{13}C-NMR (125.75 MHz, MeOD, ppm) δ21.81 ($NCH_2CH_2CH_2N_{branch}$), 21.88 ($NCH_2CH_2CH_2CH_{2core}$), 45.51 ($NCH_2CH_2CH_2N_{branch}$), 51.05 ($NCH_2CH_2CH_2N_{branch}$), 51.57 ($NHCH_2CH_{bpea}$), 52.00 (DAB-CH_2-C_6H_4), 53.65 ($NCH_2CH_2CH_2CH_2N_{core}$), 63.05 ($CH_2$-$C_6H_4$), 69.75 ($CH(pz)_2$), 109.51 ($C_{4'}$-pz), 109.58 ($C_4$-pz), 131.46 ($C_{3,5}$-$C_6H_4$), 131.59 ($C_{2,6}$-$C_6H_4$), 132.84 ($C_4$-$C_6H_4$), 134.98 ($C_{5'}$-pz), 135.48 ($C_5$-pz), 138.47 ($C_1$-$C_6H_4$), 148.27 ($C_3$-pz), 148.36 ($C_{3'}$-pz), 219.68 ($C\equiv O$). ^{19}F-NMR (188.09 MHz, MeOD, ppm) δ-76.89 (s).

5.2.30 Synthesis of [PAMAM-G0-(Mn(bpea^{NHCH2C6H4CH2NH})(CO)$_3$)$_4$](CF$_3$COO)$_4$

USC-SP-118-02

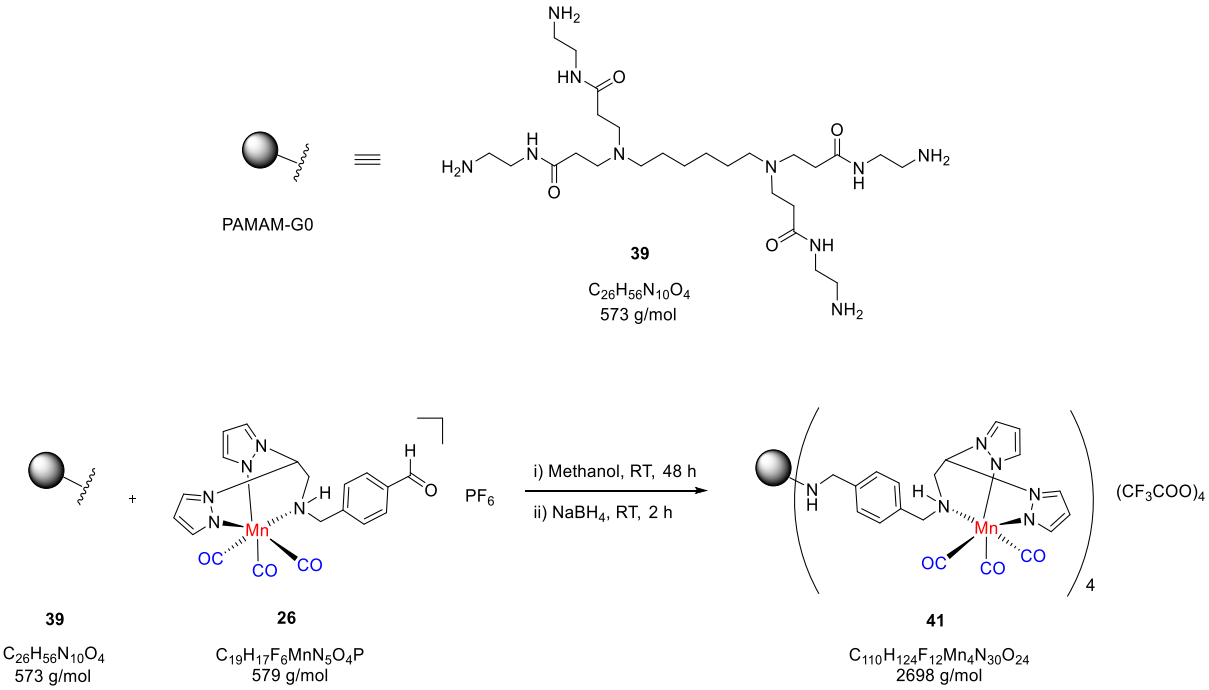

A solution of polyamidoamine-G0 (PAMAM-G0) (**39**) (25 mg, 0.044 mmol) in anhydrous methanol (20 mL) was added dropwise to a stirred solution of [Mn(bpea^{NHCH2C6H4CHO})(CO)$_3$]PF$_6$ (**26**) (105 mg, 0.18 mmol) in anhydrous methanol (10 mL). The reaction mixture was stirred at room temperature for 48 h under a dinitrogen atmosphere with exclusion of light, after which solid sodium borohydride (16 mg, 0.40 mmol) was added slowly while stirring. The reaction mixture was stirred overnight at room temperature with exclusion of light. Water (30 mL) was added to the reaction mixture and the product was extracted with dichloromethane (100 mL). The organic layer was separated, dried over magnesium sulfate (~5 g), and filtered. The solvent was then removed under vacuum and the residue was redissolved in dichloromethane (5 mL) and added dropwise to a stirred solution of *n*-hexane (20 mL). The yellow product which precipitated was filtered off, washed with *n*-hexane (10 mL) and dried under vacuum. This was further purified by preparative HPLC using a linear gradient of 5-70% acetonitrile/water containing 0.1% TFA as the eluent over 50 min at a flow rate of 3.0 mL min^{-1} to give the yellow product containing trifluoroacetate anions due to the presence of trifluoroacetic acid in the eluent.

Yield: 83% (84 mg, 0.03 mmol). Elemental analysis (%): calc. for $C_{110}H_{124}F_{12}Mn_4N_{30}O_{24}$: calc. for C 48.96, H 4.63, N 15.57; found: C 48.77, H 4.75, N 15.23. MS (ESI^+, CH_3CN): *m/z* 1235.85 $[M\text{-}CF_3COO]^{2+}$, 2584.68 $[M\text{-}CF_3COO+H]^+$. UV-Vis (DMSO): λ_{max} (ε) = 357 nm (7107 $L\cdot mol^{-1}\cdot cm^{-1}$). IR (ATR, $\tilde{\upsilon}/cm^{-1}$): 3114 (w), 2041 (s, $\nu_{C\equiv O}$), 1930 (s, $\nu_{C\equiv O}$), 1669 (s, $\nu_{C=O}$ amide), 1414, 1196, 1127, 766. RP-HPLC: t_r = 8.30 min. ^{1}H-NMR (500 MHz, MeOD, ppm): δ 8.35 (d, 4H, ^3J = 2.2 Hz, $H_{3'}$-pz), 8.25 (d, 4H, ^3J = 2.2 Hz, H_3-pz), 8.18 (dd, 4H, ^3J = 3.3, 2.7 Hz, $H_{5'}$-pz), 8.15 (dd, 4H, ^3J = 3.3, 2.7 Hz, H_5-pz), 7.52 (s, 16H, C_6H_4), 7.22 (d, 4H, ^3J = 3.3 Hz, C*H*(pz)$_2$), 6.68 (t, 4H, ^3J = 4.9, 2.5 Hz, H_4-pz), 6.62 (t, 4H, ^3J = 5.1, 2.6 Hz, $H_{4'}$-pz), 5.68 (br m, 4H, N*H*), 4.43 (dd, 4H, ^3J = 13.3, 4.6 Hz, $H_{b'}$-CH_2-C_6H_4), 4.25 (s, 8H, PAMAM-CH_2-C_6H_4), 3.97 (dd, 4H, ^3J = 13.5, 9.3 Hz, H_b-CH_2-C_6H_4), 3.54 (t, 8H, ^3J = 11.8, 5.8 Hz, $NCH_2CH_2CONH_{branch}$), 3.45 (t, 8H, ^3J = 13.5, 6.7 Hz, $NHCH_2CH_2NHCO_{branch}$), 3.24 (m, 4H, H_a-$NHCH_2CH_{bpea}$), 3.18 (t, 12H, ^3J = 11.8, 5.9 Hz, $N(CH_2)_{3\ branch}$), 2.80 (m, 4H, $H_{a'}$- $NHCH_2CH_{bpea}$), 2.77 (m, 8H, $NHCH_2CH_2NHCO_{branch}$), 1.78 (br m, 4H, $NCH_2CH_2(CH_2)_2CH_2CH_2N_{core}$), 1.44 (br m, 4H, $N(CH_2)_2CH_2CH_2(CH_2)_2N_{core}$). ^{13}C-NMR (125.75 MHz, MeOD, ppm) δ 24.44 ($NCH_2CH_2(CH_2)_2CH_2CH_2N$), 27.07 ($N(CH_2)_2CH_2CH_2(CH_2)_2N_{core}$), 29.88 ($NHCH_2CH_2NHCO_{branch}$), 36.86 ($NCH_2CH_2CONH_{branch}$), 48.03 ($N(CH_2)_{3\ branch}$), 50.50 ($NHCH_2CH_2NHCO_{branch}$), 51.59 ($NHCH_2CH_{bpea}$), 51.69 (PAMAM-$CH_2$-$C_6H_4$), 63.02 ($CH_2$-$C_6H_4$), 69.72 (*C*H(pz)$_2$), 109.49 ($C_{4'}$-pz), 109.56 ($C_4$-pz), 131.48 ($C_{3,5}$-$C_6H_4$), 131.57 ($C_{2,6}$-$C_6H_4$), 132.83 ($C_4$-$C_6H_4$), 134.95 ($C_{5'}$-pz), 135.47 ($C_5$-pz), 138.41 ($C_1$-$C_6H_4$), 148.23 ($C_3$-pz), 148.32 ($C_{3'}$-pz), 173.00 (*C*=O), 220.64 (*C*≡O), 221.31 (*C*≡O). ^{19}F-NMR (188.09 MHz, MeOD, ppm) δ -76.89 (s).

5.2.31 Synthesis of 4,4-difluoro-8-(4-chloromethyl)phenyl-1,3,5,7-tetramethyl-4-bora-3a,4a-diaza-*s*-indacene[116]

USC-SP-123-12

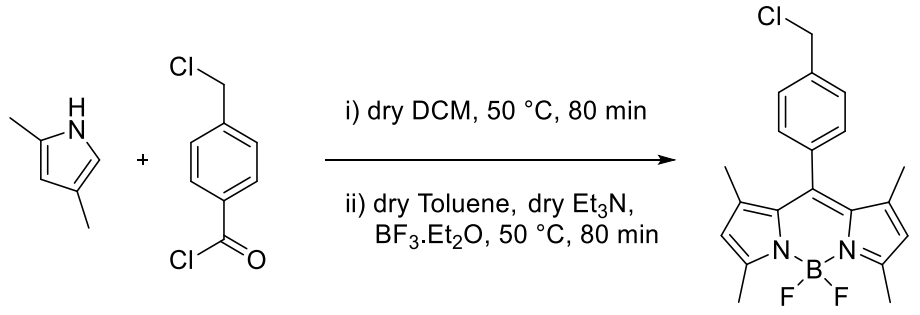

42	**43**	**44**
C_6H_9N	$C_8H_6Cl_2O$	$C_{20}H_{20}BClF_2N_2$
95 g/mol	189 g/mol	373 g/mol

A solution of 2,4-dimethylpyrrole (**42**) (3.20 mL, 31 mmol) in anhydrous dichloromethane (110 mL) was charged in an oven-dried 250 mL 3-necked round bottom flask equipped with a water condenser. 4-(Chloromethyl)benzoyl chloride (**43**) (2.90 g, 15 mmol) was added under flow of dinitrogen in approximately 100 mg portions. The solution turned yellow to orange during the course of addition. The reaction mixture was heated to 50 °C for 80-85 min and then allowed to cool to room temperature. The solution was transferred to a 500 mL one-necked Schlenk flask and the volume of solvent was reduced in vacuo to 30 mL. Subsequently, anhydrous toluene (200 mL) was added under stirring followed by the addition of anhydrous triethylamine (10 mL) under a dinitrogen atmosphere. The reaction mixture was stirred at room temperature for 30 min after which $BF_3{\cdot}Et_2O$ (9 mL) was added in a dropwise manner. The mixture was heated in an oil bath at 50 °C for 80 min. After cooling to room temperature, the solvent was removed under vacuo and the residue was dissolved in dichloromethane (200 mL), washed with water (3 x 100 mL), dried over magnesium sulfate (~20 g) and filtered. The solvent was removed under vacuo and the residue was purified by column chromatography on a silica gel 60 (0.063-0.2 mm) using dichloromethane: hexane (50:50 → 60:40 → 75:25 v/v) to give the product as orange solid.

Yield: 24% (1.34 g, 3.48 mmol). IR (ATR, $\tilde{\upsilon}/cm^{-1}$) 2925, 1536, 1502, 1466, 1303, 1183, 1047, 974. MS (ESI^+, CH_3CN): *m/z* 353.13 $[M-F]^+$, 372.13 $[M]^+$, 767.26 $[2M+Na]^+$. ^{1}H-NMR (200 MHz, $CDCl_3$, ppm): δ 7.52 (d, 2H, ^3J = 8.0 Hz, $H_{3,5}$-C_6H_4), 7.29 (d, 2H, ^3J = 8.7 Hz, $H_{2,6}$-C_6H_4), 5.98 (s, 2H, $H_{2,6}$-BODIPY), 4.66 (s, 2H, CH_2Cl), 2.55 (s, 6H, $(CH_3)_2$), 1.38 (s, 6H, $(CH_3)_2$). ^{13}C-NMR (50.33 MHz, $CDCl_3$, ppm) δ 14.68, 14.80, 45.81, 121.57, 128.63, 129.46, 131.58, 135.30, 138.81, 141.17, 143.24, 155.87. ^{11}B-NMR (160.47 MHz, $CDCl_3$, ppm) δ -0.19 (t, 1B, J_{B-F} = 33.0 Hz). ^{19}F-NMR (188.09 MHz, $CDCl_3$, ppm) δ -146.35 (q, 2F, J_{F-B} = 32.6 Hz).

5.2.32 Synthesis of 4,4-difluoro-8-(4-(*N*,*N*-dimethylmethamine))phenyl-1,3,5,7-tetramethyl-4-bora-3a,4a-diaza-*s*-indacene[116]

USC-SP-124-01

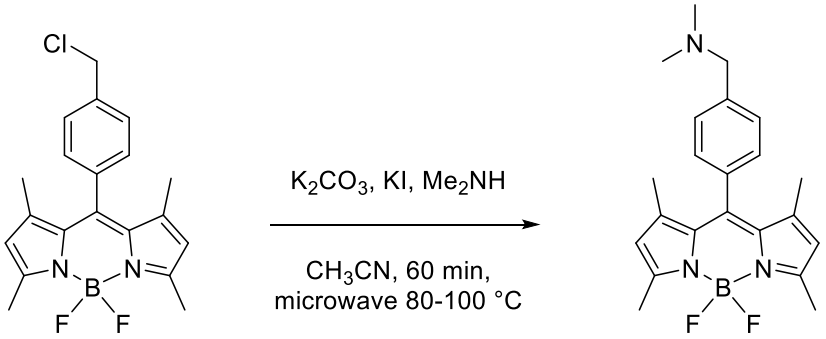

44

$C_{20}H_{20}BClF_2N_2$

373 g/mol

45

$C_{22}H_{26}BF_2N_3$

381 g/mol

A 10 mL microwave vial (Biotage Initiator$^+$) was charged with compound **44** (150 mg, 0.40 mmol), potassium carbonate (111 mg, 0.81 mmol) and potassium iodide (135 mg, 0.81 mmol) together with acetonitrile (4 mL). Dimethylamine (0.9 mL, aq. 40 wt%, 8.04 mmol) was added and the microwave vial was capped, and the reaction mixture was placed in a Biotage® Initiator$^+$ microwave reactor and heated to 80 °C for 40 min followed by an additional heating of 20 min at 100 °C. After cooling the vial to room temperature, dichloromethane (50 mL) was added and the diluted solution was washed with water (2 x 50 mL), brine (1 x 30 mL) and dried over anhydrous magnesium sulfate (~10 g). The organic phase was filtered and the solvent was removed under vacuo to give the product as an orange solid.

Yield: 88% (135 mg, 0.35 mmol). IR (ATR, $\tilde{\upsilon}/cm^{-1}$) 2937, 2761, 1546, 1509, 1462, 1307, 1188, 1154, 1053, 971. MS (ESI$^+$, CH_3CN): *m/z* 382.22 $[M+H]^+$. ^{1}H-NMR (200 MHz, $CDCl_3$, ppm): δ 7.44 (d, 2H, ^3J = 7.9 Hz, $H_{3,5}$-C_6H_4), 7.22 (d, 2H, ^3J = 8.0 Hz, $H_{2,6}$-C_6H_4), 5.97 (s, 2H, $H_{2,6}$-BODIPY), 3.50 (s, 2H, $CH_2N(CH_3)_2$), 2.55 (s, 6H, BODIPY-$(CH_3)_2$), 2.26 (s, 6H, $N(CH_3)_2$), 1.39 (s, 6H, BODIPY-$(CH_3)_2$). ^{13}C-NMR (50.33 MHz, $CDCl_3$, ppm) δ 14.49, 14.60, 45.79, 64.48, 121.67, 127.59, 129.73, 132.49, 133.60, 140.00, 142.04, 142.62, 154.75. ^{11}B-NMR (160.47 MHz, $CDCl_3$, ppm) δ -0.17 (t, 1B, $J_{B\text{-}F}$ = 33.0 Hz). ^{19}F-NMR (188.09 MHz, $CDCl_3$, ppm) δ -146.37 (q, 2F, $J_{F\text{-}B}$ = 32.6 Hz).

5.2.33 Synthesis of COP-1[116]

USC-SP-126-02

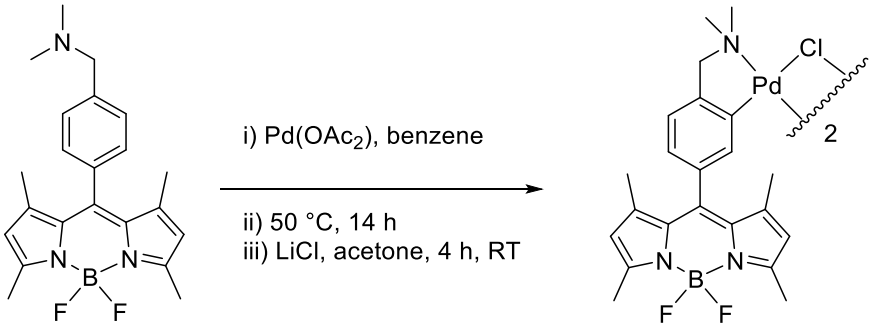

45

$C_{22}H_{26}BF_2N_3$

381 g/mol

46

$C_{44}H_{50}B_2Cl_2F_4N_6Pd_2$

1044 g/mol

A 10 mL glass vial was charged with compound **45** (120 mg, 0.32 mmol) and palladium(II) acetate (67 mg, 0.30 mmol) together with benzene (8 mL). The reaction mixture was sonicated for 1 min and the vial was immediately wrapped with aluminium foil and heated at 50 °C for 14 h under stirring. After cooling to room temperature, *n*-hexane (6 mL) was added which gave an orange precipitate. The solid was collected by filtration and was dissolved in a saturated solution of lithium chloride in acetone. The reaction mixture was stirred at room temperature for 4 h protected from light and then solvent was removed in vacuo. The residue was then dissolved in dichloromethane (30 mL) and filtered through a pad of Celite. The solvent was removed in vacuo to give an orange solid product. The NMR peaks reported below correspond to the predominant isomer as reported by Chang *et al*.

Yield: 98% (125 mg, 0.23 mmol). Elemental analysis (%): calc. for $C_{44}H_{50}B_2Cl_2F_4N_6Pd_2$: calc. for C 50.60, H 4.82, N 8.04; found: C 50.84, H 5.18, N 7.89. MS (ESI^+, CH_3CN): *m/z* 1008.20 $[M\text{-}Cl+H]^+$. IR (ATR, $\tilde{\upsilon}/cm^{-1}$) 2922, 1543, 1507, 1463, 1302, 1187, 1149, 1050, 969. ^{1}H-NMR (200 MHz, $CDCl_3$, ppm): δ 7.04 (s, 1H, H_2-C_6H_3), 6.97 (d, 1H, ^3J = 7.6 Hz, H_5-C_6H_3), 6.87 (d, 1H, ^3J = 7.6 Hz, H_6-C_6H_3), 5.97 (s, 2H, $H_{2,6}$-BODIPY), 3.98 (s, 2H, $CH_2N(CH_3)_2$), 2.84 (s, 6H, BODIPY-$(CH_3)_2$), 2.54 (s, 6H, $N(CH_3)_2$), 1.46 (s, 6H, BODIPY-$(CH_3)_2$). ^{13}C-NMR (50.33 MHz, $CDCl_3$, ppm) δ 14.69, 53.01, 73.20, 121.12, 121.93, 124.23, 131.52, 131.69, 131.89, 143.51, 143.53, 144.10, 147.78, 155.07. ^{11}B-NMR (96.30 MHz,

$CDCl_3$, ppm) δ 0.79 (t, 1B, $J_{B\text{-}F}$ = 33.3 Hz), ^{19}F (188.09 MHz, $CDCl_3$, ppm) δ -146.33 (m, 4F).

6 References

[1] D. Seebach, *Angew. Chem. Int. Ed. Engl.* **1990**, *29*, 1320-1367.

[2] R. H. Fish, G. Jaouen, *Organometallics* **2003**, *22*, 2166-2177.

[3] G. Jaouen, A. Vessieres, I. S. Butler, *Acc. Chem. Res.* **1993**, *26*, 361-369.

[4] L. Ronconi, P. J. Sadler, *Coord. Chem. Rev.* **2007**, *251*, 1633-1648.

[5] U. Schatzschneider, N. Metzler-Nolte, *Angew. Chem. Int. Ed.* **2006**, *45*, 1504-1507.

[6] T. Storr, K. H. Thompson, C. Orvig, *Chem. Soc. Rev.* **2006**, *35*, 534-544.

[7] C. Orvig, M. J. Abrams, *Chem. Rev.* **1999**, *99*, 2201-2204.

[8] M. J. Clarke, *Met. Ions Biol. Syst.* **1980**, *11*, 231.

[9] G. Sava, E. Alessio, A. Bergamo, G. Mestroni, in *Tpoics in Biological Inorganic Chemistry,* Vol. 1 (Eds.: M. Clarke, P. Sadler), Springer-Verlag, Berlin, **1999**, p. 143-169.

[10] M. Galanski, V. B. Arion, M. A. Jakupec, B. K. Keppler, *Curr. Pharm. Des.* **2003**, *9*, 2078-2089.

[11] M. J. Clarke, F. Zhu, D. R. Frasca, *Chem. Rev.* **1999**, *99*, 2511-2534.

[12] M. J. Clarke, S. Bitler, D. Rennert, M. Buchbinder, A. D. Kelman, *J. Inorg. Biochem.* **1980**, *12*, 79-87.

[13] W. H. Ang, E. Daldini, C. Scolaro, R. Scopelliti, L. Juillerat-Jeannerat, P. J. Dyson, *Inorg. Chem.* **2006**, *45*, 9006-9013.

[14] C. A. Vock, A. K. Renfrew, R. Scopelliti, L. Juillerat-Jeanneret, P. J. Dyson, *Eur. J. Inorg. Chem.* **2008**, *10*, 1661-1671.

[15] R. E. Morris, R. E. Aird, P. del Socorro Murdoch, H. Chen, J. Cummings, N. D. Hughes, S. Parsons, A. Parkin, G. Boyd, D. I. Jodrell, P. J. Sadler, *J. Med. Chem.* **2001**, *44*, 3616-3621.

[16] F. Wang, H. Chen, S. Parsons, I. D. H. Oswald, J. E. Davidson, P. J. Sadler, *Chem. Eur. J.* **2003**, *9*, 5810-5820.

[17] O. Novakova, H. Chen, O. Vrana, A. Rodger, P. J. Sadler, V. Brabec, *Biochemistry* **2003**, *42*, 11544-11554.

[18] H.-K. Liu, F. Wang, J. A. Parkinson, J. Bella, P. J. Sadler, *Chem. Eur. J.* **2006**, *12*, 6151-6165.

[19] G. Gasser, N. Metzler-Nolte, *Curr. Opin. Chem. Biol.* **2012**, *16*, 84-91.

[20] A. Casini, C. Gabbiani, F. Sorrentino, M. P. Rigobello, A. Bindoli, T. J. Geldbach, A. Marrone, N. Re, C. G. Hartinger, P. J. Dyson, L. Messori, *J. Med. Chem.* **2008**, *51*, 6773-6781.

[21] M. Guo, Z. Guo, P. J. Sadler, *J. Biol. Inorg. Chem.* **2001**, *6*, 698-707.

[22] M. Guo, H. Sun, H. J. McArdle, L. Gambling, P. J. Sadler, *Biochemistry* **2000**, *39*, 10023-10033.

[23] A. Riccardi, C. Ferlini, D. Meco, R. Mastrangelo, G. Scambia, R. Riccardi, *Eur. J. Cancer.* **1999**, *35*, 86-90.

[24] G. Jaouen, S. Top, A. Vessieres, G. Leclercq, M. J. McGlinchey, *Curr. Med. Chem.* **2004**, *11*, 2505-2517.

[25] A. Nguyen, A. Vessières, E. A. Hillard, S. Top, P. Pigeon, G. Jaouen, *Chimia* **2007**, *61*, 716-724.

[26] E. Hillard, A. Vessières, L. Thouin, G. Jaouen, C. Amatore, *Angew. Chem. Int. Ed.* **2006**, *45*, 285-290.

[27] H. Bregman, D. S. Williams, G. E. Atilla, P. J. Carroll, E. Meggers, *J. Am. Chem. Soc.* **2004**, *126*, 13594-13595.

[28] D. S. Williams, G. E. Atilla, H. Bregman, A. Arzoumanian, P. S. Klein, E. Meggers, *Angew. Chem. Int. Ed. Engl.* **2005**, *44*, 1984-1987.

[29] D.-L. Ma, H.-Z. He, K.-H. Leung, D. S.-H. Chan, C.-H. Leung, *Angew. Chem. Int. Ed.* **2013**, *52*, 7666-7682.

[30] H. D. Stoeffler, N. B. Thornton, S. L. Temkin, K. S. Schanze, *J. Am. Chem. Soc.* **1995**, *117*, 7119-7128.

[31] V. Wing-Wah Yam, K. Kam-Wing Lo, K.-K. Cheung, R. Yuen-Chong Kong, *Dalton Trans.* **1997**, 2067-2072.

[32] S. P. Foxon, T. Phillips, M. R. Gill, M. Towrie, A. W. Parker, M. Webb, J. A. Thomas, *Angew. Chem. Int. Ed.* **2007**, *46*, 3686-3688.

[33] S. C. Rasmussen, M. M. Richter, E. Yi, H. Place, K. J. Brewer, *Inorg. Chem.* **1990**, *29*, 3926-3932.

[34] C. Stinner, M. D. Wightman, S. O. Kelley, M. G. Hill, J. K. Barton, *Inorg. Chem.* **2001**, *40*, 5245-5250.

[35] E. W. Price, C. Orvig, *Chem. Soc. Rev.* **2014**, *43*, 260-290.

[36] D. Zeng, C. J. Anderson, *Chem. Commun.* **2013**, *49*, 2697-2699.

[37] G. Jaouen, *Bioorganometallics*, Wiley-VCH Verlag, Weinheim, **2006**.

[38] P. D. Acton, P. T. Meyer, P. D. Mozley, K. Plossl, H. F. Kung, *Eur. J. Nucl. Med.* **2000**, *27*, 1714-1718.

[39] H. F. Kung, M.-P. Kung, S.-P. Wey, K.-J. Lin, T.-C. Yen, *Nucl. Med. Biol.* **2007**, *34*, 787-789.

[40] S. K. Meegalla, K. Plössl, M.-P. Kung, D. A. Stevenson, Mu, S. Kushner, L. M. Liable-Sands, A. L. Rheingold, H. F. Kung, *J. Med. Chem.* **1998**, *41*, 428-436.

[41] R. Alberto, *J. Organomet. Chem.* **2007**, *692*, 1179-1186.

[42] R. Alberto, R. Schibli, A. Egli, A. P. Schubiger, U. Abram, T. A. Kaden, *J. Am. Chem. Soc.* **1998**, *120*, 7987-7988.

[43] R. Alberto, K. Ortner, N. Wheatley, R. Schibli, A. P. Schubiger, *J. Am. Chem. Soc.* **2001**, *123*, 3135-3136.

[44] R. Alberto, R. Schibli, A. P. Schubiger, U. Abram, H. J. Pietzsch, B. Johannsen, *J. Am. Chem. Soc.* **1999**, *121*, 6076-6077.

[45] R. Schibli, R. La Bella, R. Alberto, E. Garcia-Garayoa, K. Ortner, U. Abram, P. A. Schubiger, *Bioconjugate Chem.* **2000**, *11*, 345-351.

[46] G. Gasser, K. Jäger, M. Zenker, R. Bergmann, J. Steinbach, H. Stephan, N. Metzler-Nolte, *J. Inorg. Biochem.* **2010**, *104*, 1133-1140.

[47] N. Metzler-Nolte, *Chimia* **2007**, *61*, 736-741.

[48] J. Caddy, U. Hoffmanns, N. Metzler-Nolte, *Z. Naturforsch. B* **2007**, *62*, 460.

[49] U. Hoffmanns, N. Metzler-Nolte, *Bioconjugate Chem.* **2005**, *17*, 204-213.

[50] K. Splith, W. Hu, U. Schatzschneider, R. Gust, I. Ott, L. A. Onambele, A. Prokop, I. Neundorf, *Bioconjugate Chem.* **2010**, *21*, 1288-1296.

[51] R. Wang, *The Evolution of Gasotransmitter Biology and Medicine*, (Ed.: R. Wang), Humana Press, Totowa, **2004**.

[52] J. Haldane, *J. Physiol.* **1895**, *18*, 201-217.

[53] T. Sjöstrand, *Scand. J. Clin. Lab. Invest.* **1949**, *1*, 201-214.

[54] T. SjöStrand, *Acta Physiol. Scand.* **1951**, *22*, 137-141.

[55] T. Sjöstrand, *Acta Physiol. Scand.* **1952**, *26*, 328-333.

[56] T. Yoshida, S. Takahashi, G. Kikuchi, *J. Biochem.* **1974**, *75*, 1187-1191.

[57] M. D. Maines, A. Kappas, *Proc. Natl. Acad. Sci. USA.* **1974**, *71*, 4293-4297.

[58] L. Wu, R. Wang, *Pharmacol. Rev.* **2005**, *57*, 585-630.

[59] J. Alam, K. Igarashi, S. Immenschuh, S. Shibahara, R. M. Tyrrell, *Antioxid. Redox Signal.* **2004**, *6*, 924-933.

[60] S. W. Ryter, J. Alam, A. M. Choi, *Physiol. Rev.* **2006**, *86*, 583-650.

[61] M. D. Maines, G. M. Trakshel, R. K. Kutty, *J. Biol. Chem.* **1986**, *261*, 411-419.

[62] W. J. Wilkinson, P. J. Kemp, *J. Physiol.* **2011**, *589*, 3055-3062.

[63] C. Taillé, J. El-Benna, S. Lanone, J. Boczkowski, R. Motterlini, *J. Biol. Chem.* **2005**, *280*, 25350-25360.

[64] L. E. Otterbein, F. H. Bach, J. Alam, M. Soares, H. Tao Lu, M. Wysk, R. J. Davis, R. A. Flavell, A. M. K. Choi, *Nature Med.* **2000**, *6*, 422-428.

[65] B. Brüne, V. Ullrich, *Mol. Pharmacol.* **1987**, *32*, 497-504.

[66] T. L. Poulos, *Curr. Opin. Struct. Biol.* **2006**, *16*, 736-743.

[67] B. Wedel, P. Humbert, C. Harteneck, J. Foerster, J. Malkewitz, E. Böhme, G. Schultz, D. Koesling, *Proc. Natl. Acad. Sci. USA.* **1994**, *91*, 2592-2596.

[68] N. G. Abraham, A. Kappas, *Pharmacol. Rev.* **2008**, *60*, 79-127.

[69] B. S. Zuckerbraun, T. R. Billiar, S. L. Otterbein, P. K. Kim, F. Liu, A. M. Choi, F. H. Bach, L. E. Otterbein, *J. Exp. Med.* **2003**, *198*, 1707-1716.

[70] A. Rich, G. Farrugia, J. L. Rae, *Am. J. Physiol.* **1994**, *267*, C435-C442.

[71] S. Hou, S. H. Heinemann, T. Hoshi, *Physiology* **2009**, *24*, 26-35.

[72] R. Motterlini, L. E. Otterbein, *Nature Rev. Drug Discov.* **2010**, *9*, 728-743.

[73] R. Motterlini, J. E. Clark, R. Foresti, P. Sarathchandra, B. E. Mann, C. J. Green, *Circ. Res.* **2002**, *90*, e17-e24.

[74] R. Motterlini, P. Sawle, S. Bains, J. Hammad, R. Alberto, R. Foresti, C. J. Green, *FASEB J.* **2004**, *18*, 284-286.

[75] R. Alberto, R. Motterlini, *Dalton Trans.* **2007**, 1651-1660.

[76] T. S. Pitchumony, B. Spingler, R. Motterlini, R. Alberto, *Chimia* **2008**, *62*, 277-279.

[77] T. S. Pitchumony, B. Spingler, R. Motterlini, R. Alberto, *Org. Biomol. Chem.* **2010**, *8*, 4849-4854.

[78] T. R. Johnson, B. E. Mann, I. P. Teasdale, H. Adams, R. Foresti, C. J. Green, R. Motterlini, *Dalton Trans.* **2007**, 1500-1508.

[79] Y. Tayem, T. R. Johnson, B. E. Mann, C. J. Green, R. Motterlini, *Am. J. Physiol. Renal Physiol.* **2006**, *290*, F789-F794.

[80] A. Levina, A. Mitra, P. A. Lay, *Metallomics* **2009**, *1*, 458-470.

[81] U. Schatzschneider, *Brit. J. Pharmacol.* **2014**, doi: 10.1111/bph.12688.

[82] I. J. S. Fairlamb, A.-K. Duhme-Klair, J. M. Lynam, B. E. Moulton, C. T. O'Brien, P. Sawle, J. Hammad, R. Motterlini, *Bioorg. Med. Chem. Lett.* **2006**, *16*, 995-998.

[83] I. J. S. Fairlamb, J. M. Lynam, B. E. Moulton, I. E. Taylor, A. K. Duhme-Klair, P. Sawle, R. Motterlini, *Dalton Trans.* **2007**, 3603-3605.

[84] F. Zobi, O. Blacque, R. A. Jacobs, M. C. Schaub, A. Y. Bogdanova, *Dalton Trans.* **2012**, *41*, 370-378.

[85] C. C. Romao, W. A. Blattler, J. D. Seixas, G. J. L. Bernardes, *Chem. Soc. Rev.* **2012**, *41*, 3571-3583.

[86] J. D. Seixas, A. Mukhopadhyay, T. Santos-Silva, L. E. Otterbein, D. J. Gallo, S. S. Rodrigues, B. H. Guerreiro, A. M. L. Goncalves, N. Penacho, A. R. Marques, A. C. Coelho, P. M. Reis, M. J. Romao, C. C. Romao, *Dalton Trans.* **2013**, *42*, 5985-5998.

[87] U. Schatzschneider, *Eur. J. Inorg. Chem.* **2010**, 1451-1467.

[88] U. Schatzschneider, *Inorg. Chim. Acta* **2011**, *374*, 19-23.

[89] B. E. Mann, *Organometallics* **2012**, *31*, 5728-5735.

[90] F. Zobi, *Future Med. Chem.* **2013**, *5*, 175-188.

[91] S. Romanski, B. Kraus, U. Schatzschneider, J.-M. Neudörfl, S. Amslinger, H.-G. Schmalz, *Angew. Chem. Int. Ed.* **2011**, *50*, 2392-2396.

[92] S. Romanski, H. Rücker, E. Stamellou, M. Guttentag, J.-M. Neudörfl, R. Alberto, S. Amslinger, B. Yard, H.-G. Schmalz, *Organometallics* **2012**, *31*, 5800-5809.

[93] S. Romanski, B. Kraus, M. Guttentag, W. Schlundt, H. Rucker, A. Adler, J.-M. Neudorfl, R. Alberto, S. Amslinger, H.-G. Schmalz, *Dalton Trans.* **2012**, *41*, 13862-13875.

[94] R. D. Rimmer, A. E. Pierri, P. C. Ford, *Coord. Chem. Rev.* **2012**, *256*, 1509-1519.

[95] J. Niesel, A. Pinto, H. W. Peindy N'Dongo, K. Merz, I. Ott, R. Gust, U. Schatzschneider, *Chem. Commun.* **2008**, 1798-1800.

[96] K. Meister, J. Niesel, U. Schatzschneider, N. Metzler-Nolte, D. A. Schmidt, M. Havenith, *Angew. Chem. Int. Ed.* **2010**, *49*, 3310-3312.

[97] P. C. Kunz, W. Huber, A. Rojas, U. Schatzschneider, B. Spingler, *Eur. J. Inorg. Chem.* **2009**, *35*, 5358-5366.

[98] M. A. Gonzalez, M. A. Yim, S. Cheng, A. Moyes, A. J. Hobbs, P. K. Mascharak, *Inorg. Chem.* **2011**, *51*, 601-608.

[99] M. A. Gonzalez, S. J. Carrington, N. L. Fry, J. L. Martinez, P. K. Mascharak, *Inorg. Chem.* **2012**, *51*, 11930-11940.

[100] R. Kretschmer, G. Gessner, H. Görls, S. H. Heinemann, M. Westerhausen, *J. Inorg. Biochem.* **2011**, *105*, 6-9.

[101] C. S. Jackson, S. Schmitt, Q. P. Dou, J. J. Kodanko, *Inorg. Chem.* **2011**, *50*, 5336-5338.

[102] P. Agostinis, K. Berg, K. A. Cengel, T. H. Foster, A. W. Girotti, S. O. Gollnick, S. M. Hahn, M. R. Hamblin, A. Juzeniene, D. Kessel, M. Korbelik, J. Moan, P. Mroz, D. Nowis, J. Piette, B. C. Wilson, J. Golab, *Cancer J. Clin.* **2011**, *61*, 250-281.

[103] K. Szaciłowski, W. Macyk, A. Drzewiecka-Matuszek, M. Brindell, G. Stochel, *Chem. Rev.* **2005**, *105*, 2647-2694.

[104] N. Lane, *Sci. Am.* **2008**, *18*, 80-87.

[105] H. Pfeiffer, A. Rojas, J. Niesel, U. Schatzschneider, *Dalton Trans.* **2009**, 4292-4298.

[106] G. Dörrdelmann, H. Pfeiffer, A. Birkner, U. Schatzschneider, *Inorg. Chem.* **2011**, *50*, 4362-4367.

[107] H. Maeda, *Bioconjugate Chem.* **2010**, *21*, 797-802.

[108] H. Maeda, K. Greish, J. Fang, *Adv. Polym. Sci.* **2006**, *193*, 103-121.

[109] Y. Matsumura, H. Maeda, *Cancer Res.* **1986**, *46*, 6387-6392.

[110] P. R. Gil, W. J. Parak, *ACS Nano* **2008**, *2*, 2200-2205.

[111] P. Govender, B. Therrien, G. S. Smith, *Eur. J. Inorg. Chem.* **2012**, 2853-2862.

[112] P. Govender, S. Pai, U. Schatzschneider, G. S. Smith, *Inorg. Chem.* **2013**, *52*, 5470-5478.

[113] Y. Lee, J. Kim, *Anal. Chem.* **2007**, *79*, 7669-7675.

[114] H. J. Vreman, R. J. Wong, T. Kadotani, D. K. Stevenson, *Anal. Biochem.* **2005**, *341*, 280-289.

[115] J. Wang, J. Karpus, B. S. Zhao, Z. Luo, P. R. Chen, C. He, *Angew. Chem. Int. Ed.* **2012**, *51*, 9652-9656.

[116] B. W. Michel, A. R. Lippert, C. J. Chang, *J. Am. Chem. Soc.* **2012**, *134*, 15668-15671.

[117] A. E. Pierri, A. Pallaoro, G. Wu, P. C. Ford, *J. Am. Chem. Soc.* **2012**, *134*, 18197-18200.

[118] R. B. Merrifield, *J. Am. Chem. Soc.* **1963**, *85*, 2149-2154.

[119] L. A. Carpino, G. Y. Han, *J. Am. Chem. Soc.* **1970**, *92*, 5748-5749.

[120] W. König, R. Geiger, *Chem. Ber.* **1970**, *103*, 788-798.

[121] N. Metzler-Nolte, U. Schatzschneider, *Bioinorganic Chemistry: A Practical Course.*, *Vol. 49*, WILEY-VCH Verlag, Weinheim, **2010**.

[122] H. C. Kolb, M. G. Finn, K. B. Sharpless, *Angew. Chem. Int. Ed.* **2001**, *40*, 2004-2021.

[123] V. V. Rostovtsev, L. G. Green, V. V. Fokin, K. B. Sharpless, *Angew. Chem. Int. Ed.* **2002**, *41*, 2596-2599.

[124] C. W. Tornøe, C. Christensen, M. Meldal, *J. Org. Chem.* **2002**, *67*, 3057-3064.

[125] V. Hong, S. I. Presolski, C. Ma, M. G. Finn, *Angew. Chem. Int. Ed.* **2009**, *48*, 9879-9883.

[126] J. E. Hein, V. V. Fokin, *Chem. Soc. Rev.* **2010**, *39*, 1302-1315.

[127] I. S. Carrico, B. L. Carlson, C. R. Bertozzi, *Nature Chem. Biol.* **2007**, *3*, 321-322.

[128] E. M. Sletten, C. R. Bertozzi, *Angew. Chem. Int. Ed.* **2009**, *48*, 6974-6998.

[129] J. Kalia, R. T. Raines, *Angew. Chem. Int. Ed.* **2008**, *47*, 7523-7526.

[130] A. Dirksen, T. M. Hackeng, P. E. Dawson, *Angew. Chem. Int. Ed.* **2006**, *45*, 7581-7584.

[131] S. Ulrich, D. Boturyn, A. Marra, O. Renaudet, P. Dumy, *Chem. Eur. J.* **2014**, *20*, 34-41.

[132] K. D. Roberts, J. N. Lambert, N. J. Ede, A. M. Bray, *J. Pept. Sci.* **2004**, *10*, 659-665.

[133] H. C. Hang, C. R. Bertozzi, *Acc. Chem. Res.* **2001**, *34*, 727-736.

[134] T. S. Zatsepin, D. A. Stetsenko, M. J. Gait, T. S. Oretskaya, *Bioconjugate Chem.* **2005**, *16*, 471-489.

[135] S. Trofimenko, *Polyhedron* **2004**, *23*, 197-203.

[136] D. L. Reger, R. F. Semeniuc, M. D. Smith, *J. Organomet. Chem.* **2003**, *666*, 87-101.

[137] A. J. Atkin, J. M. Lynam, B. E. Moulton, P. Sawle, R. Motterlini, N. M. Boyle, M. T. Pryce, I. J. S. Fairlamb, *Dalton Trans.* **2011**, *40*, 5755-5761.

[138] S. McLean, B. E. Mann, R. K. Poole, *Anal. Biochem.* **2012**, *427*, 36-40.

[139] C. G. Hatchard, C. A. Parker, *Proc. R. Soc. Lond. A* **1956**, *235*, 518-536.

[140] K. Splith, I. Neundorf, W. Hu, H. W. P. N'Dongo, V. Vasylyeva, K. Merz, U. Schatzschneider, *Dalton Trans.* **2010**, *39*, 2536-2545.

[141] I. Neundorf, J. Hoyer, K. Splith, R. Rennert, H. W. Peindy N'Dongo, U. Schatzschneider, *Chem. Commun.* **2008**, 5604-5606.

[142] H. W. P. N'Dongo, I. Neundorf, K. Merz, U. Schatzschneider, *J. Inorg. Biochem.* **2008**, *102*, 2114-2119.

[143] M. Boyce, C. R. Bertozzi, *Nature Methods* **2011**, *8*, 638-642.

[144] J. J. J. M. Donners, G. A. Silva, H. A. Behanna, S. G. Anthony, Northwestern University, US Pat. 7544661 B2, **2009**.

[145] M. B. Sporn, A. B. Roberts, *Cell Regul.* **1990**, *1*, 875-882.

[146] A. B. Roberts, M. A. Anzano, L. M. Wakefield, N. S. Roche, D. F. Stern, M. B. Sporn, *Proc. Natl. Acad. Sci. USA.* **1985**, *82*, 119-123.

[147] I. Y. Kim, H. J. Ahn, D. J. Zelner, J. W. Shaw, S. Lang, M. Kato, M. G. Oefelein, K. Miyazono, J. A. Nemeth, J. M. Kozlowski, C. Lee, *Clin. Cancer Res.* **1996**, *2*, 1255-1261.

[148] Y. Guo, S. C. Jacobs, N. Kyprianou, *Int. J. Cancer.* **1997**, *71*, 573-579.

[149] H. Pfeiffer, T. Sowik, U. Schatzschneider, *J. Organomet. Chem.* **2013**, *734*, 17-24.

[150] R. D. Rimmer, H. Richter, P. C. Ford, *Inorg. Chem.* **2009**, *49*, 1180-1185.

[151] D. Peer, J. M. Karp, S. Hong, O. C. Farokhzad, R. Margalit, R. Langer, *Nature Nanotechnol.* **2007**, *2*, 751-760.

[152] S. El Kazzouli, N. El Brahmi, S. Mignani, M. Bousmina, M. Zablocka, J. P. Majoral, *Curr. Med. Chem.* **2012**, *19*, 4995-5010.

[153] Y. Matsumura, H. Maeda, *Cancer Res.* **1986**, *46*, 6387-6392.

[154] J. E. Clark, P. Naughton, S. Shurey, C. J. Green, T. R. Johnson, B. E. Mann, R. Foresti, R. Motterlini, *Circ. Res.* **2003**, *93*, e2-e8.

[155] G. R. Fulmer, A. J. M. Miller, N. H. Sherden, H. E. Gottlieb, A. Nudelman, B. M. Stoltz, J. E. Bercaw, K. I. Goldberg, *Organometallics* **2010**, *29*, 2176-2179.

[156] G. Sheldrick, *Acta Crystallogr. A* **2008**, *64*, 112-122.

[157] O. V. Dolomanov, L. J. Bourhis, R. J. Gildea, J. A. K. Howard, H. Puschmann, *J. Appl. Cryst.* **2009**, *42*, 339-341.

[158] L. J. Bourhis, O. V. Dolomanov, R. J. Gildea, J. A. K. Howard, H. Puschmann, **2013**, In preparation.

[159] S. I. Kirin, F. Noor, N. Metzler-Nolte, W. Mier, *J. Chem. Educ.* **2007**, *84*, 108-111.

[160] E. Kaiser, R. L. Colescott, C. D. Bossinger, P. I. Cook, *Anal. Biochem.* **1970**, *34*, 595-598.

[161] H. J. Kuhn, S. E. Braslavskyi, R. Schmidt, *Pure Appl. Chem.* **1989**, *61*, 187-210.

[162] E. A. Jaffe, R. L. Nachman, C. G. Becker, C. R. Minick, *J. Clin. Invest.* **1973**, *52*, 2745-2756.

[163] F. Neese, *WIREs Comput. Mol. Sci.* **2012**, *2*, 73-78.

[164] A. Schäfer, H. Horn, R. Ahlrichs, *J. Chem. Phys.* **1992**, *97*, 2571-2577.

[165] F. Weigend, R. Ahlrichs, *Phys. Chem. Chem. Phys.* **2005**, *7*, 3297-3305.

[166] D. L. Reger, J. D. Elgin, R. F. Semeniuc, P. J. Pellechia, M. D. Smith, *Chem. Commun.* **2005**, 4068-4070.

[167] D. L. Reger, B. Reinecke, M. D. Smith, R. F. Semeniuc, *Inorg. Chim. Acta.* **2009**, *362*, 4377-4388.

[168] S. Pai, M. Hafftlang, G. Atongo, C. Nagel, J. Niesel, S. Botov, H.-G. Schmalz, B. Yard, U. Schatzschneider, *Dalton Trans.* **2014**, *43*, 8664-8678.

[169] S. Pai, K. Radacki, U. Schatzschneider, *Eur. J. Inorg. Chem.* **2014**, 2886-2895.

7 Appendices

Table A1: Crystallographic data for 16 and 19

Compound	16	19
Empirical formula	$C_{18}H_{14}F_6IMnN_5O_3P$	$C_{21}H_{22}BrIMnN_5O_4$
Formula weight	675.15	670.19
Temperature (K)	113(2)	113(2)
λ Mo-$K\alpha$ (Å)	0.71073	0.71073
Dimensions (mm)	0.30 × 0.25 × 0.15	0.30 × 0.10 × 0.10
Crystal system	Monoclinic	Triclinic
Space group	P2(1)/n	P-1
a (Å)	14.7315(7)	9.8908(3)
b (Å)	11.1201(3)	11.9141(4)
c (Å)	15.6814(7)	12.1870(3)
α (°)	90	98.487(2)
β (°)	116.031(6)	110.618(3)
γ (°)	90	106.055(3)
V (Å^3)	2308.27(19)	1242.87(6)
Z	4	2
ρ_{calc} (g cm^{-3})	1.943	1.791
μ (mm^{-1})	2.059	3.417
$2\Theta_{max}$ (°)	25.00	25.00
Reflections measured	7728	13673
Unique refl. / [$I > 2\sigma(I)$]	4066 / 3435	4376 / 3727
Data completeness	0.999	0.998
Variables	316	302
R ($I \geq 2\sigma(I)$)	0.0301	0.0200
wR ($I \geq 2\sigma(I)$)	0.0643	0.0460
Largest difference map peak/hole in e Å^{-3}	0.802 / -0.463	0.593 / -0.291
Goodness of fit (GOF)	1.026	0.954

Table A2: Crystallographic data for 26 and 20

Compound	26	20
Empirical formula	$C_{19}H_{17}F_6MnN_5O_4P$	$C_{20}H_{17}F_6MnN_5O_3P$
Formula weight	579.28	575.29
Temperature (K)	100(2)	100
λ Mo-K_α (Å)	0.71073	0.71073
Dimensions (mm)	0.14 × 0.12 × 0.05	0.54 × 0.31 × 0.12
Crystal system	Monoclinic	Monoclinic
Space group	*P*2(1)/n	P1 21/c 1
a (Å)	15.0215(14)	13.8840(6)
b (Å)	9.2082(11)	14.3060(6)
c (Å)	16.4618(14)	11.6373(5)
α (°)	90	90
β (°)	91.226(5)	99.146(2)
γ (°)	90	90
V (Å^3)	2276.5(4)	2282.07(17)
Z	4	4
ρ_{calc} (g cm^{-3})	1.690	1.6743
μ (mm^{-1})	0.737	0.732
$2\Theta_{max}$ (°)	26.02	26.00
Reflections measured	41218	36746
Unique refl. / [$I > 2\sigma(I)$]	4492 / 3560	4453 / 3388
Data completeness	1.000	1.000
Variables	307	324
R ($I \geq 2\sigma(I)$)	0.0424	0.0377
wR ($I \geq 2\sigma(I)$)	0.0972	0.1159
Largest difference map peak/hole in e Å^{-3}	0.839 / -0.681	0.6272 / -0.6742
Goodness of fit (GOF)	1.066	1.0253

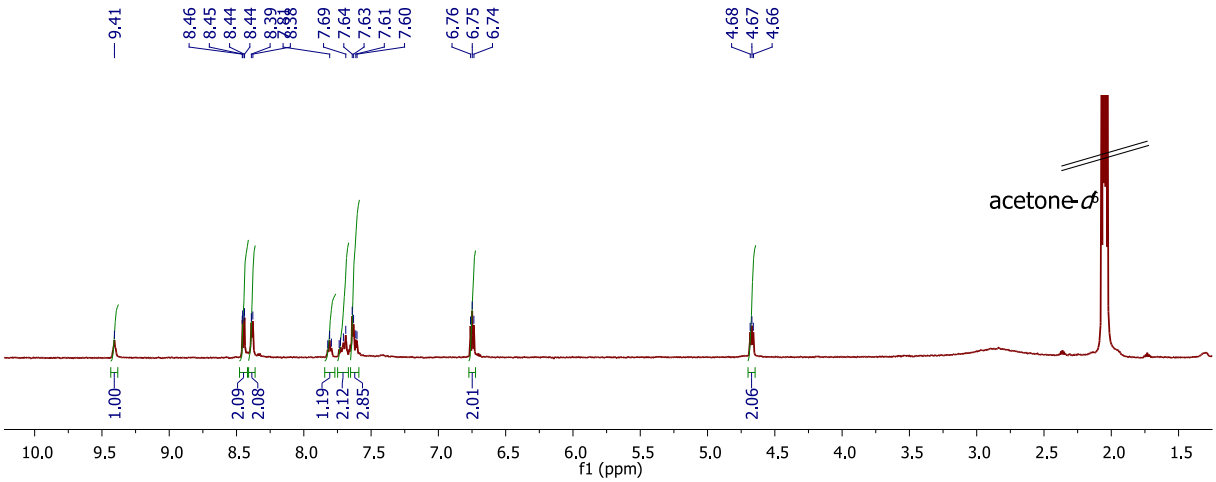

Fig. A1: 400 MHz ^{1}H NMR spectrum of [Mn(bpea$^{N=CHC_6H_5}$)(CO)$_3$]PF$_6$ **15** in acetone d_6.

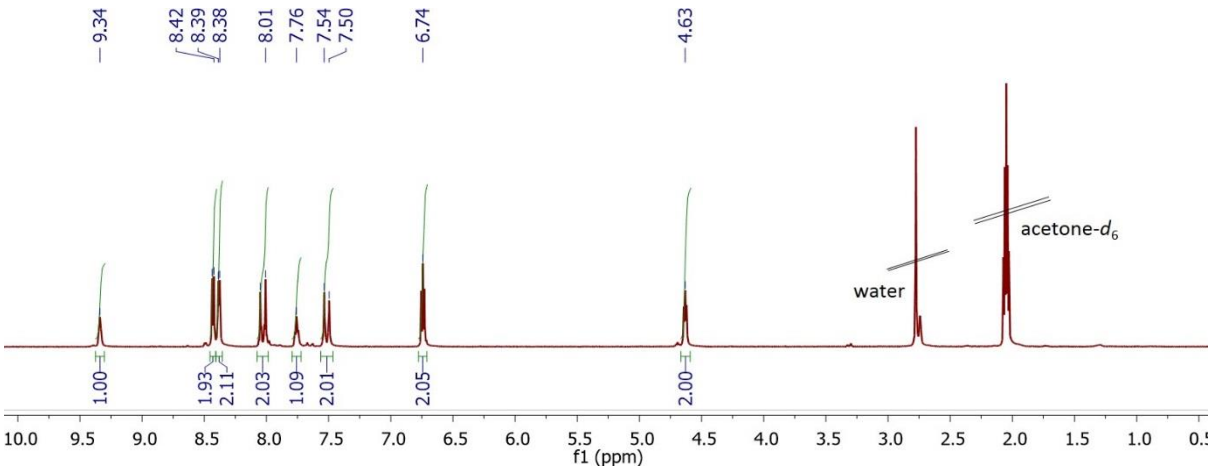

Fig. A2: 400 MHz ^{1}H NMR spectrum of [Mn(bpea$^{N=CHC_6H_4I}$)(CO)$_3$]PF$_6$ **16** in acetone d_6.

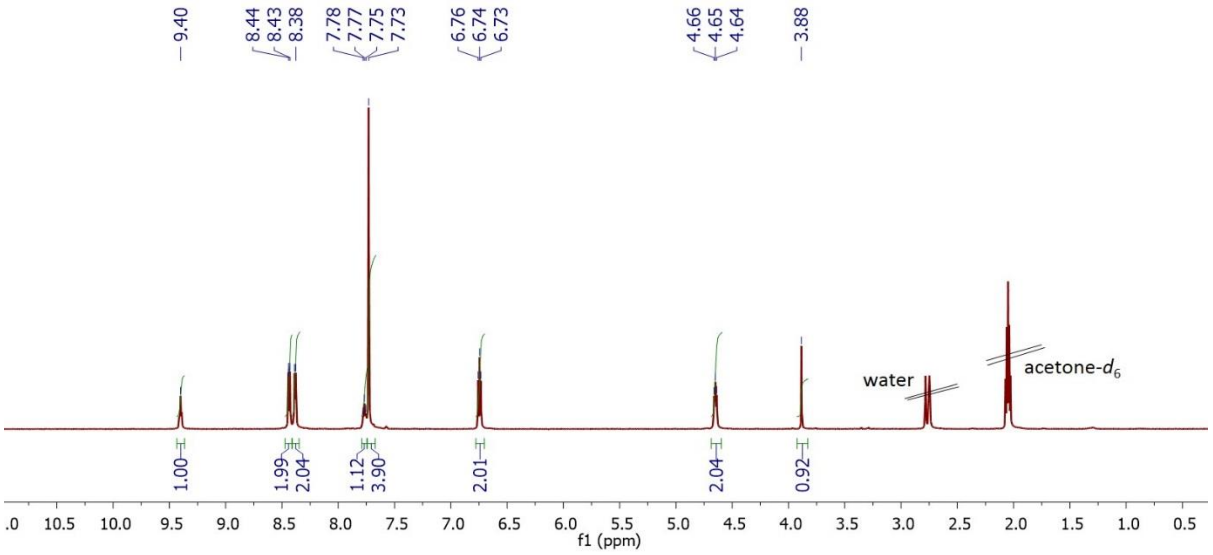

Fig. A3: 400 MHz ^{1}H NMR spectrum of [Mn(bpea$^{N=CHC6H4C\equiv CH}$)(CO)$_3$]PF$_6$ **17** in acetone d_6.

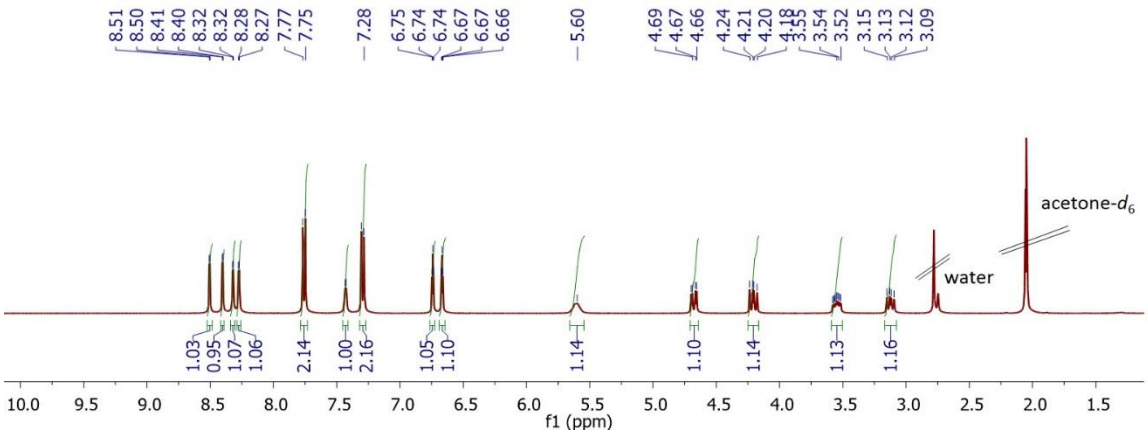

Fig. A4: 400 MHz ^{1}H NMR spectrum of [Mn(bpea^{NHCH2C6H4I})(CO)$_3$]PF$_6$ **19** in acetone-d_6.

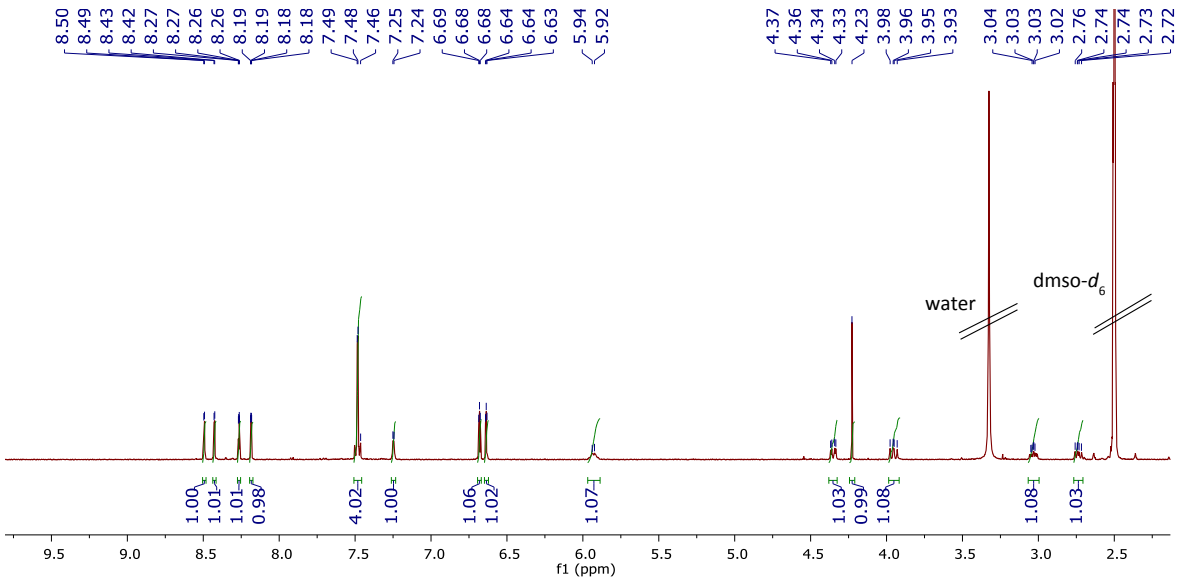

Fig. A5: 500 MHz ^{1}H NMR spectrum of [Mn(bpea$^{NHCH2C6H4C\equiv CH}$)(CO)$_3$]PF$_6$ **20** in dmso-d_6.

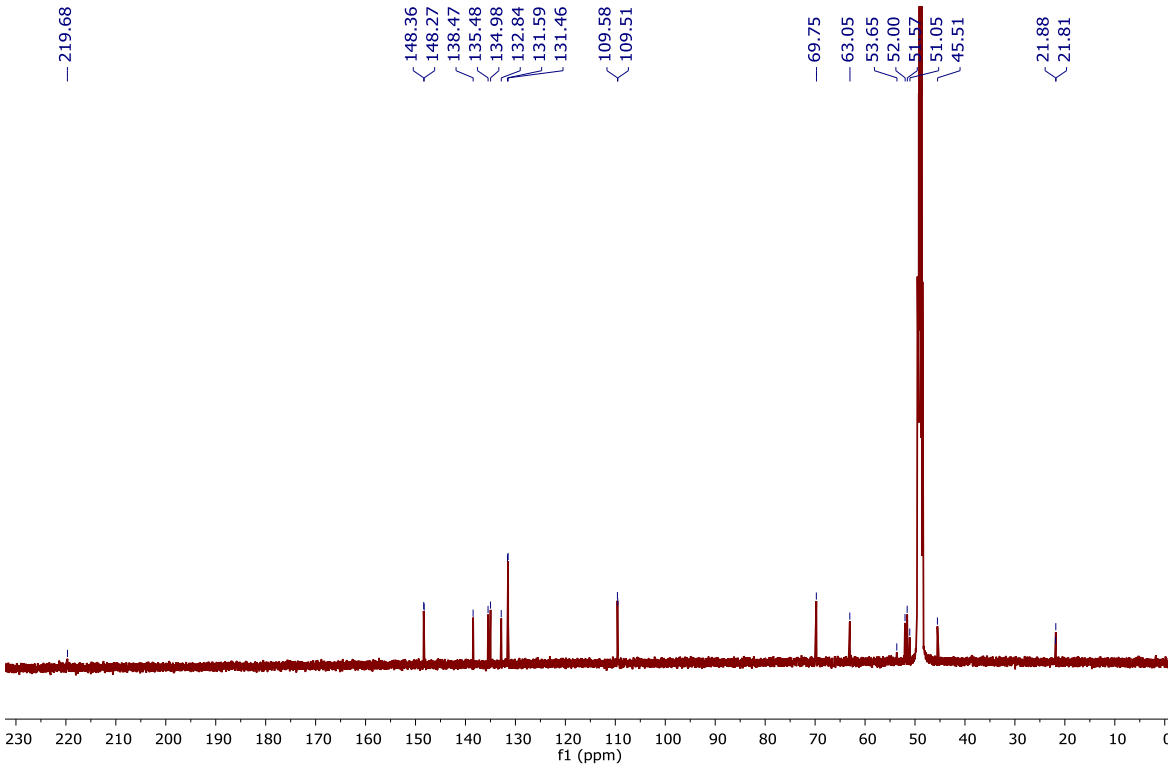

Fig. A6: 500 MHz ^{13}C NMR spectrum of [DAB-G1-PPI-(Mn(bpea^{NHCH2C6H4CH2NH})(CO)$_3$)$_4$](CF$_3$COO)$_4$ **40** in MeOD.

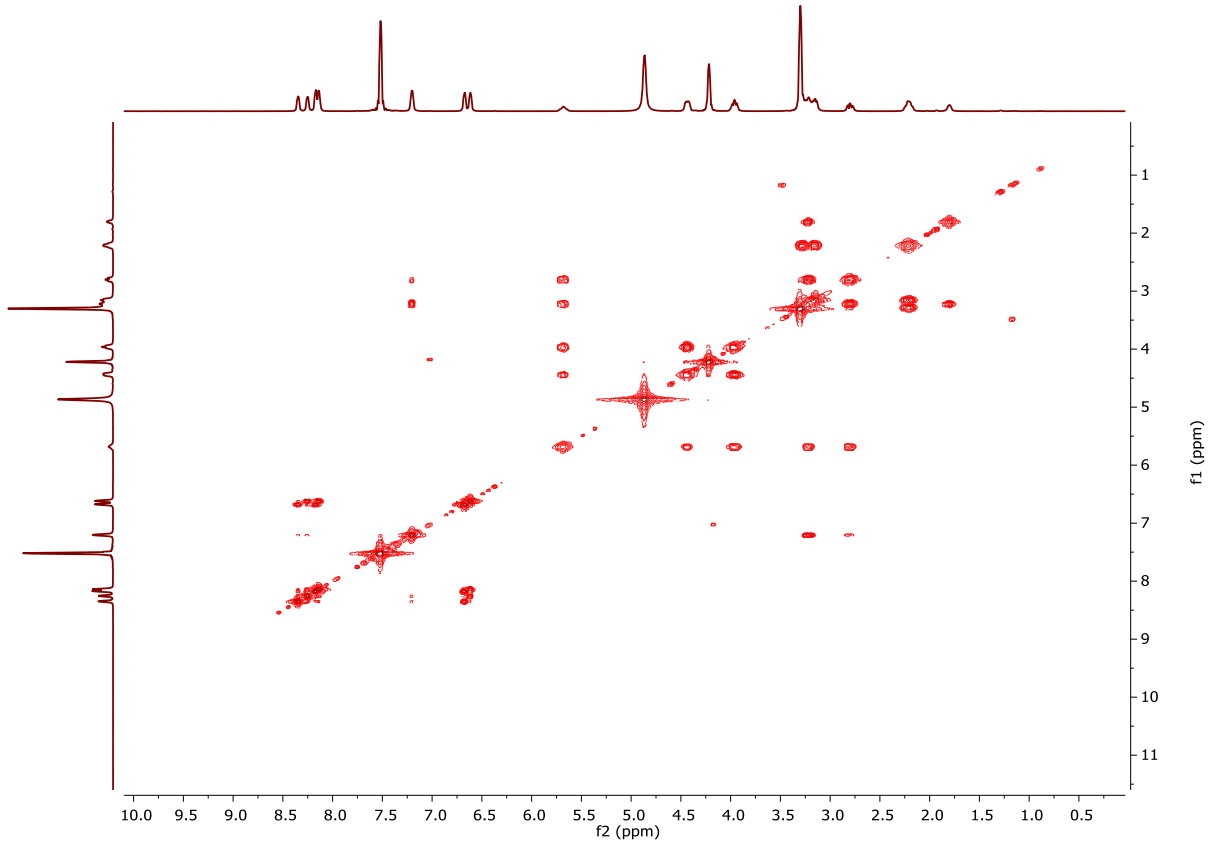

Fig. A7: 500 MHz ^{1}H-^{1}H COSY spectrum of [DAB-G1-PPI-(Mn(bpea^{NHCH2C6H4CH2NH})(CO)$_3$)$_4$](CF$_3$COO)$_4$ **40** in MeOD.

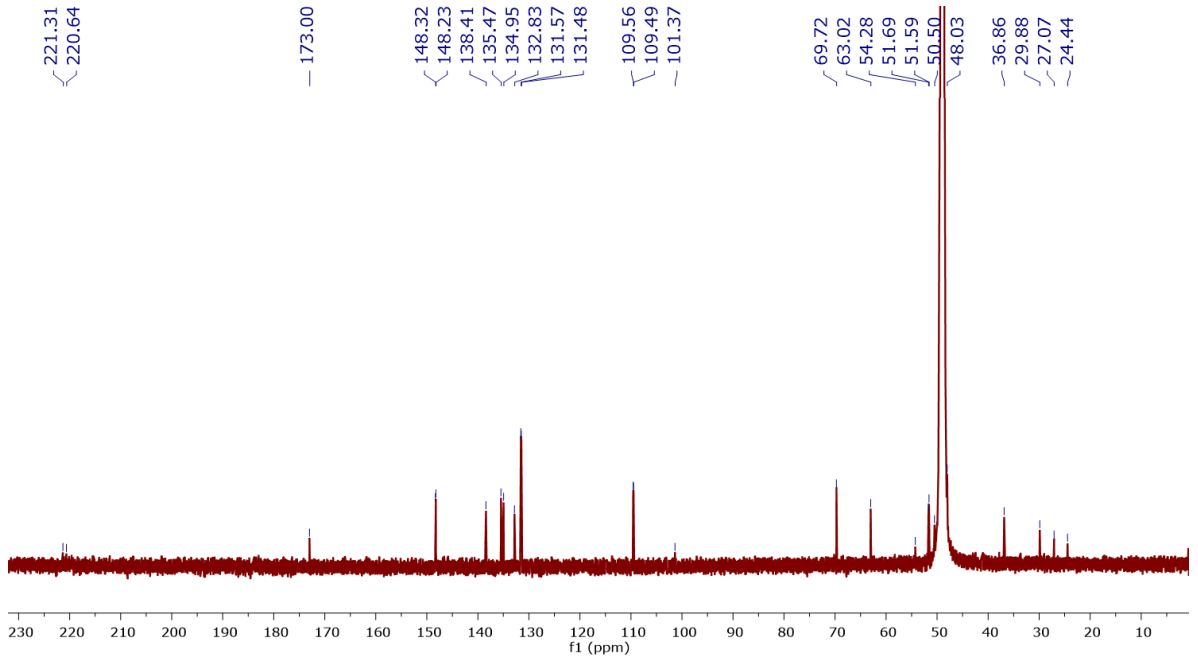

Fig. A8: 500 MHz ^{13}C NMR spectrum of [PAMAM-G0-(Mn(bpea^{NHCH2C6H4CH2NH})(CO)$_3$)$_4$](CF$_3$COO)$_4$ **41** in MeOD.

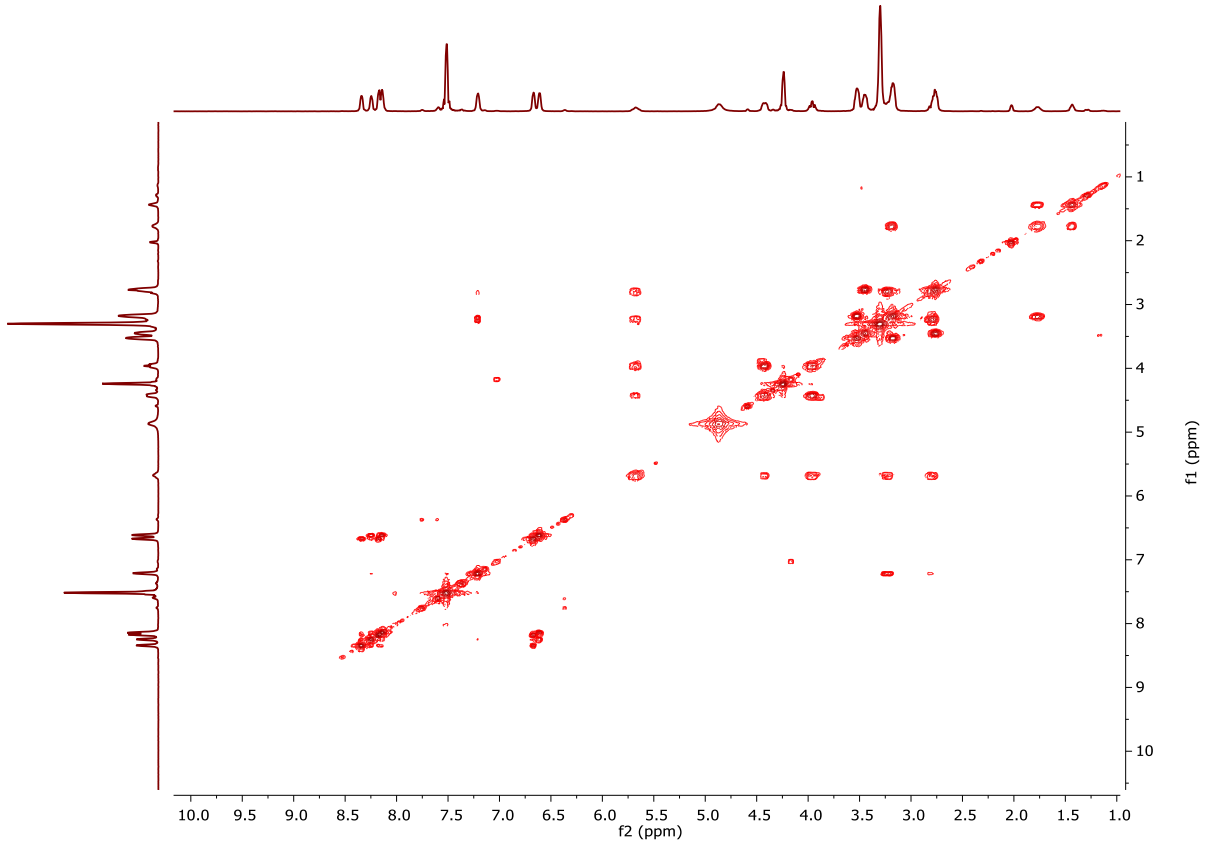

Fig. A9: 500 MHz ^{1}H-^{1}H COSY spectrum of [PAMAM-G0-(Mn(bpea^{NHCH2C6H4CH2NH})(CO)$_3$)$_4$](CF$_3$COO)$_4$ **41** in MeOD.

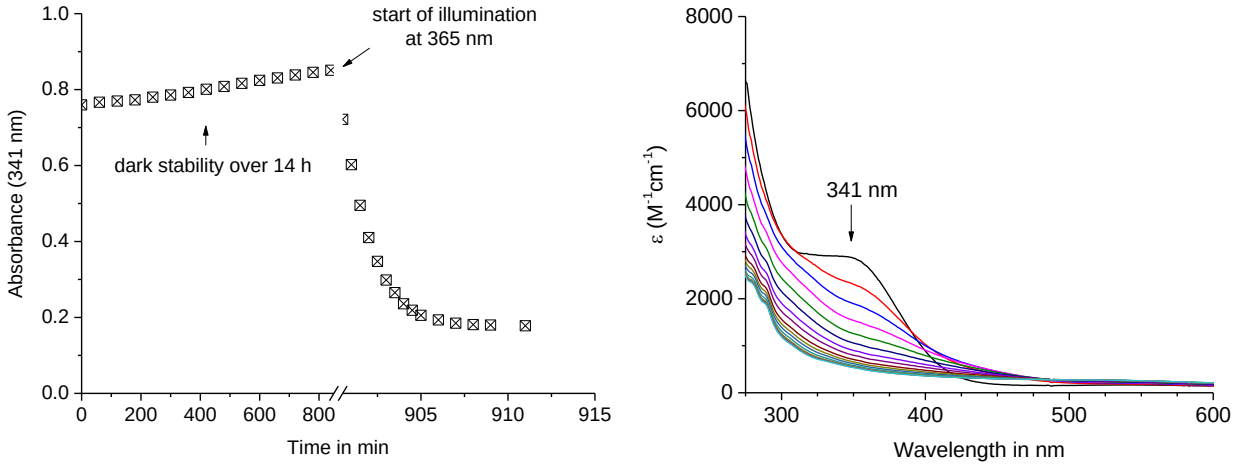

Fig. A10: Absorption changes at 341 nm of **15** in DMSO upon incubation in the dark for 14 h and subsequent photolysis with an UV lamp at 365 nm (left). UV/Vis spectral changes of **15** (0.3 mM) upon photolysis with increasing illumination time, 0-600 s (right).

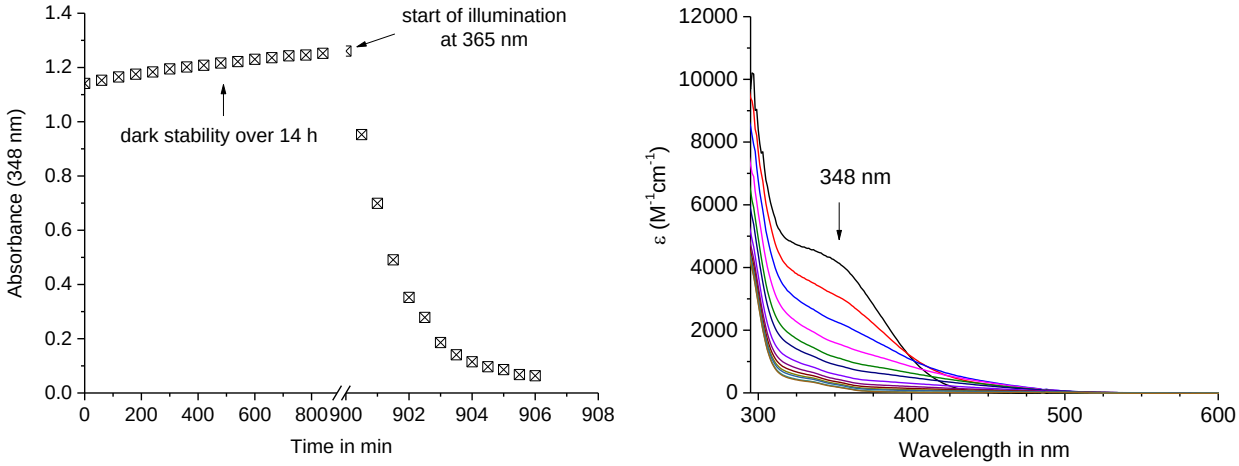

Fig. A11: Absorption changes at 348 nm of **16** in DMSO upon incubation in the dark for 14 h and subsequent photolysis with an UV lamp at 365 nm (left). UV/Vis spectral changes of **16** (0.3 mM) upon photolysis with increasing illumination time, 0-420 s (right).

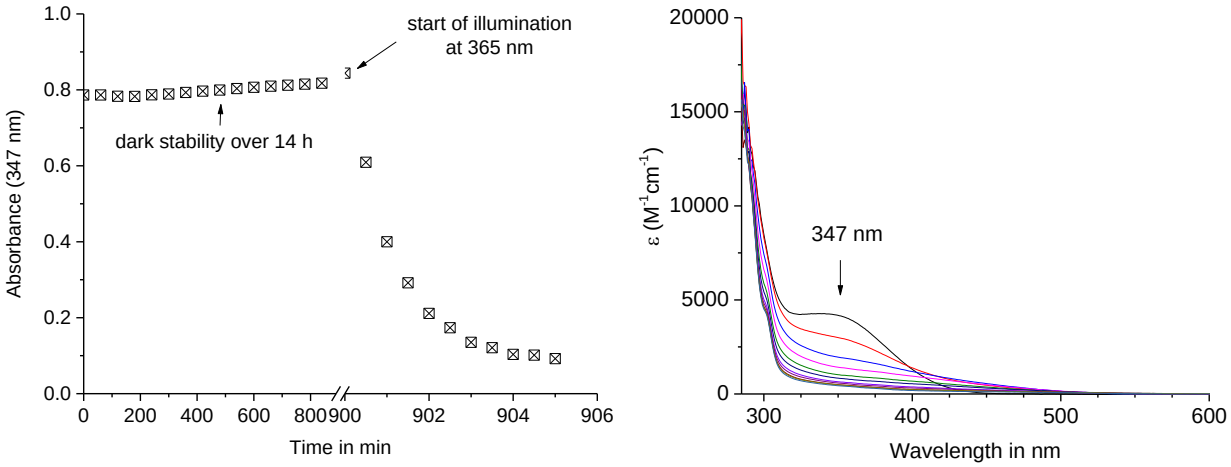

Fig. A12: Absorption changes at 347 nm of **17** in DMSO upon incubation in the dark for 14 h and subsequent photolysis with an UV lamp at 365 nm (left). UV/Vis spectral changes of **17** (0.2 mM) upon photolysis with increasing illumination time, 0-300 s (right).

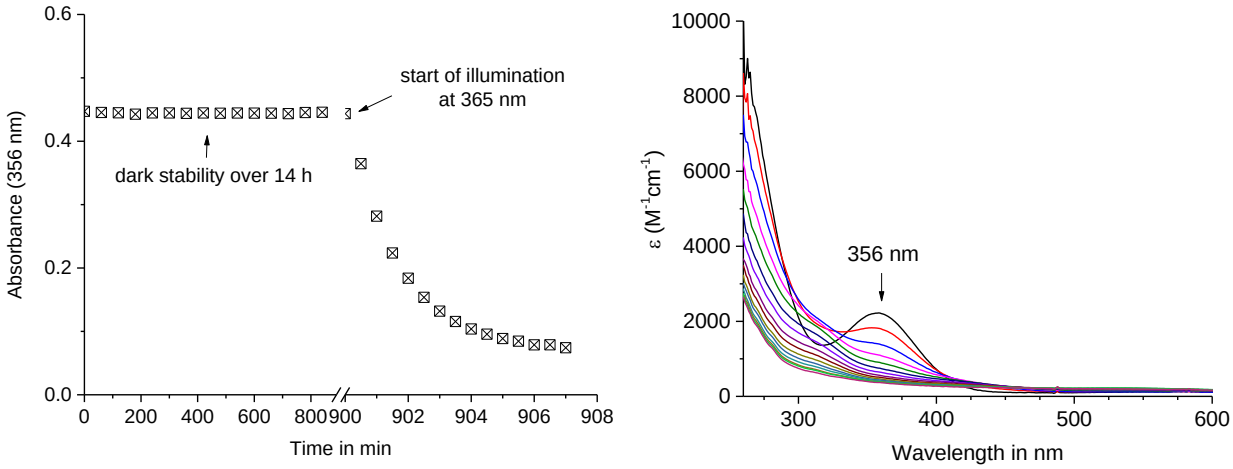

Fig. A13: Absorption changes at 356 nm of **19** in DMSO upon incubation in the dark for 14 h and subsequent photolysis with an UV lamp at 365 nm (left). UV/Vis spectral changes of **19** (0.2 mM) upon photolysis with increasing illumination time, 0-420 s (right).

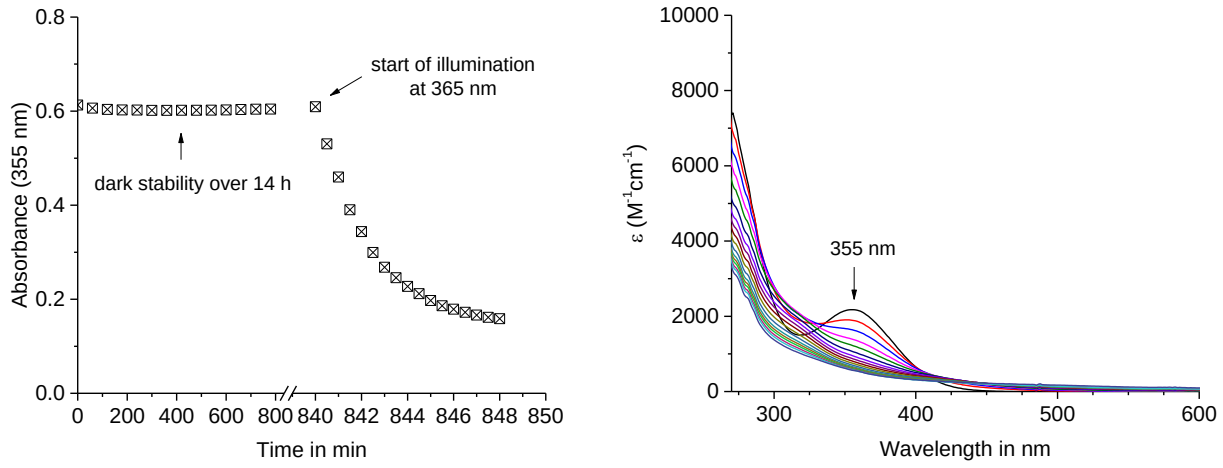

Fig. A14: Absorption changes at 355 nm of **20** in DMSO upon incubation in the dark for 14 h and subsequent photolysis with an UV lamp at 365 nm (left). UV/Vis spectral changes of **20** (0.3 mM) upon photolysis with increasing illumination time, 0-480 s (right).

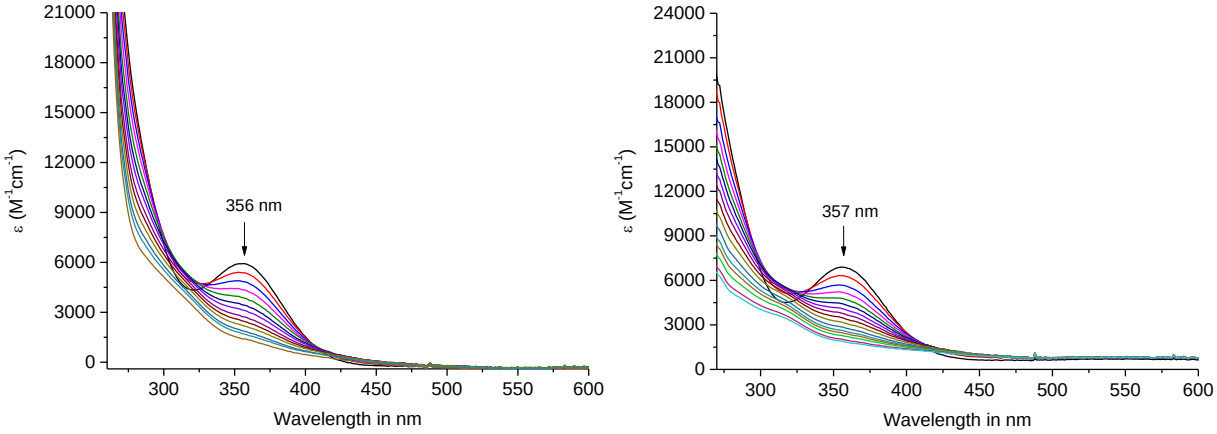

Fig. A15: UV/Vis spectral changes of **40** (left, 0.06 mM) and **41** (right, 63 mM) in DMSO/PBS (10:90% v/v) upon photolysis with an UV lamp at 365 nm and increasing illumination time of 0-240 s and 0-300 s, respectively.

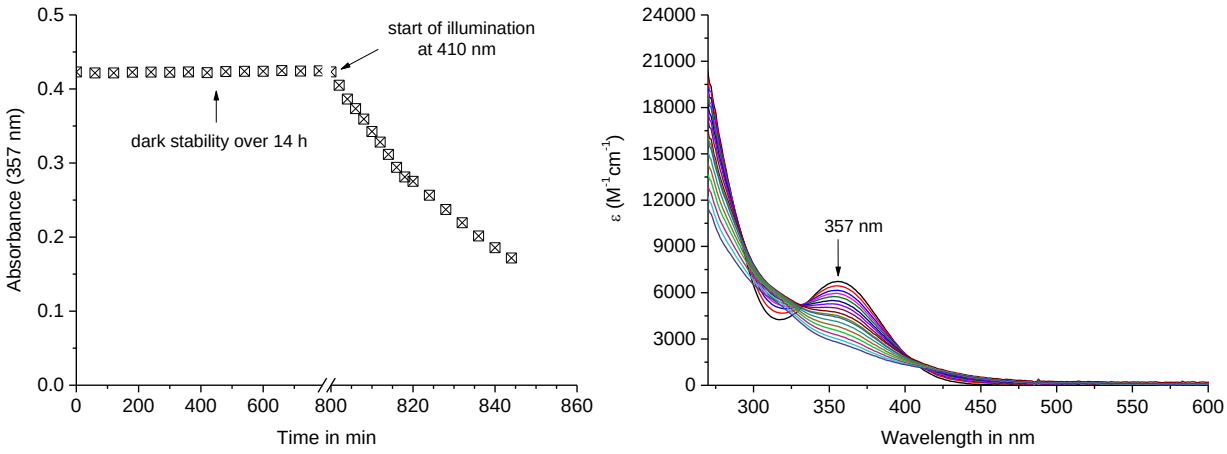

Fig. A16: Absorption changes at 357 nm of **41** in DMSO/PBS (10:90% v/v) upon incubation in the dark for 14 h and subsequent photolysis with a LED cluster at 410 nm (left). UV/Vis spectral changes of **41** (63 mM) upon photolysis with increasing illumination time, 0-44 min (right).

Selbständigkeitserklärung

Hiermit erkläre ich an Eides statt, dass ich die Doktorarbeit

„Synthesis of manganese tricarbonyl PhotoCORM conjugates – from small molecules to peptides and dendrimers“

selbständig angefertigt und keine anderen als die von mir angegebenen Quellen und Hilfsmittel benutzt habe. Die deutsche Version der Zusammenfassung wurde aus der englischen Version von Prof. Dr. Ulrich Schatzschneider übersetzt da ich kein Deutsch spreche.

Ich erkläre außerdem, dass diese Arbeit weder in gleicher oder anderer Form bereits in einem anderen Prüfungsverfahren vorgelegen hat.

Ich habe früher außer den mit dem Zulassungsgesuch urkundlich vorgelegten Graden keine weiteren akademischen Grade erworben oder zu erwerben versucht.

Würzburg, den

_____

(Sandesh Pai)